DOCTORAATSPROEFSCHRIFT

2009 | Faculteit Wetenschappen

Design, Synthesis and Characterization of Functionalized Poly(p-Phenylene Vinylene) Copolymers: The Development of a Universal Method towards Advanced Conjugated Polymers for Device Applications

Proefschrift voorgelegd tot het behalen van de graad van
Doctor in de Wetenschappen, richting scheikunde, te verdedigen door:

Jan DUCHATEAU

Promotor: prof. dr. Thomas Cleij
Copromotor: prof. dr. Dirk Vanderzande

universiteit hasselt
INSTITUUT VOOR
MATERIAALONDERZOEK

D/2009/2451/57

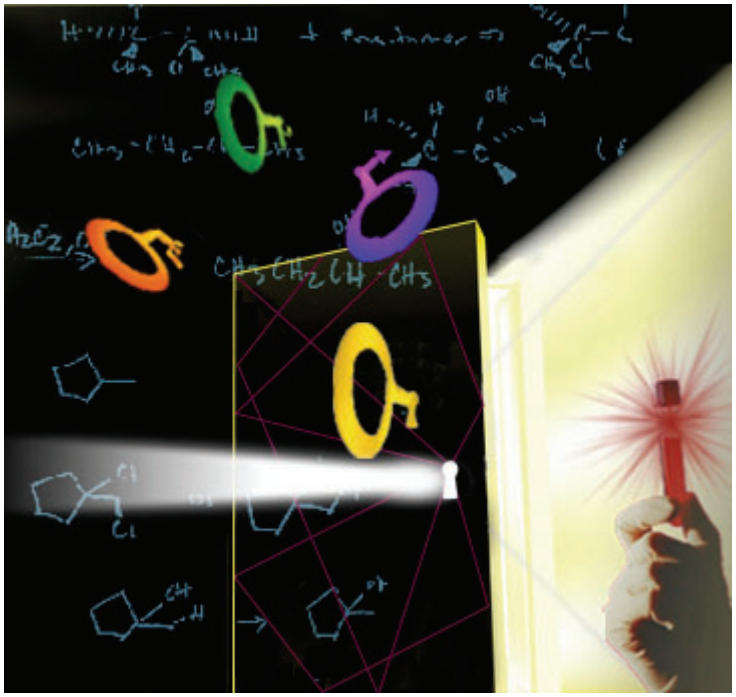

“Klasse zonder karakter is eigenlijk geen klasse,
maar een talent dat vervliegt in de wind”

Prof. Rik Torfs

Table of contents

Chapter 5 Grafting onto PPV derivatives

Chapter 6 Towards the post-polymerization functionalization of PPV derivatives with natural and artificial receptors

Chapter 1

General introduction

Chapter 1 includes a general introduction to the field of conjugated polymers. Since the focus of this work is on poly(para-phenylene vinylene) (PPV) and its derivatives, this class of conjugated polymers is discussed in somewhat more detail. Introduction of functional groups into (conjugated) polymers, including PPV, leads to materials with a broad range of possible applications. As will be presented in the aim and outline of this work, a platform PPV polymer is synthesized from which further functionalization is possible with virtually any group via a straightforward procedure. In addition, some applications are further highlighted.

1.1. Conjugated polymers

Conjugated polymers consist of alternating single (σ bonds) and double bonds (π bonds). The π electrons present in these polymers are highly delocalized and have a considerable polarizability. This plays an important role in the electrical and optical properties of these systems. However, the alternating single and double bonds make the polymer chains rather stiff. As a result, conjugated polymers are often not readily soluble and processable, unless side groups are introduced onto the backbone. Examples within this class of polymers are poly(acetylene), poly(pyrrole), poly(thiophene), poly(ethylenedioxythiophene), poly(*para*-phenylene) and poly(*para*-phenylene vinylene). Their chemical structures are shown in Figure 1-1.

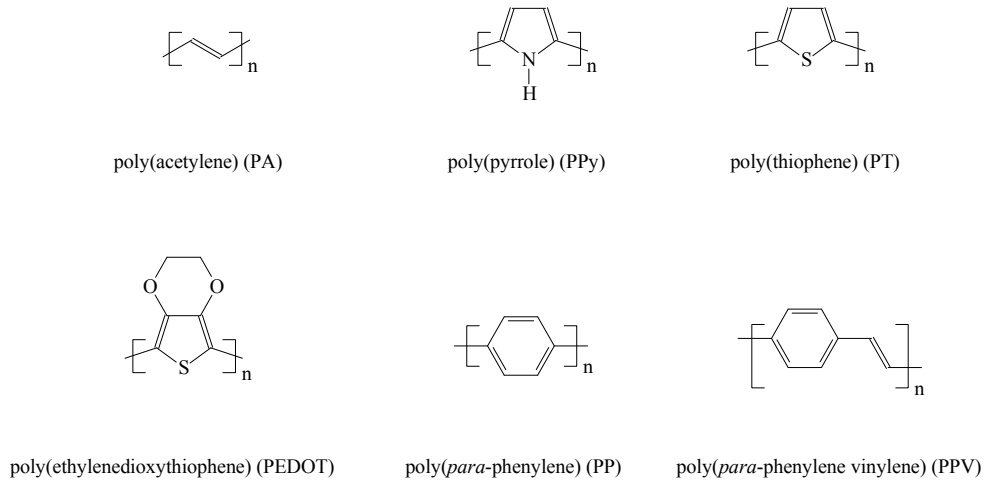

Figure 1-1 Examples of conjugated polymers

A summary on the polymerization chemistry towards these different classes of conjugated polymers can be found in many review articles and specialized books.[1-9]

1.1.1. Electrical and optical properties of conjugated polymers

Conjugation of the polymer is not the only condition to induce conductivity in polymers. In addition, charge carriers *i.e.* electrons and holes, need to be injected into the polymer. These charge carriers can be generated by processes like electrical stimulation, photo-excitation, charge injection or chemical doping. The generated electrons or holes can move along the backbone of the polymer (intrachain mobility) and even move between conjugated parts of different chains (interchain "hopping").

The electrical properties of conjugated polymer are determined by their electronic structure. Molecular orbital theory[10] can give some useful information on the changes in the electronic structure upon the creation of

charge carriers. Overlap of adjacent atomic p_z-orbitals yields lower energy bonding (π) and higher energy bonding (π^*) molecular orbitals. When many π molecular orbitals are spaced together in a given range of energy, they can generate a virtually continuous, occupied valence band. The π^* molecular orbitals generate in the same way an unoccupied conduction band. The energy spacing between the highest occupied molecular orbital (HOMO) and the lowest unoccupied molecular orbital (LUMO) is called the band gap (E_g). This is schematically represented in Figure 1-2. The HOMO and LUMO levels and thus the band gap, can be varied by modification of, for example, side groups[11], steric hindrance and π conjugation length.

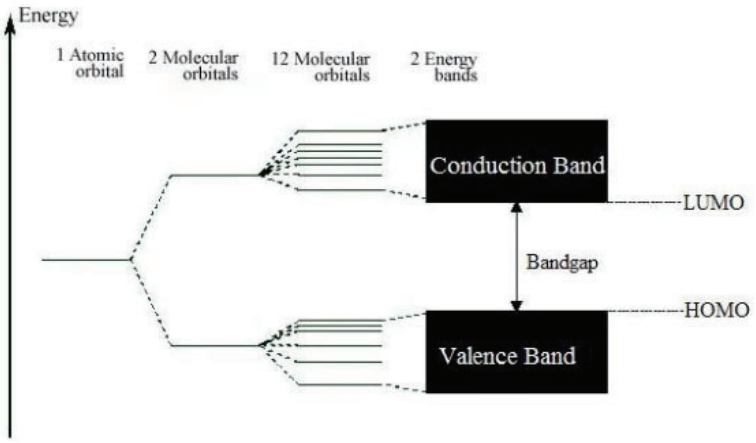

Figure 1-2 Band structure in an electronically conducting polymer[10]

E_g for conjugated polymers ranges from 0.5 to 4 eV. By synthesizing the appropriate chemical structures, the desired band gap can be obtained. This band gap determines the electronic and optical properties of the conjugated polymer to a substantial degree.

As a result of their electronic properties, conjugated polymers have also important optical properties, such as electroluminescence and photoluminescence.[12] Both phenomena are closely related and are depicted in Figures 1-3 and 1-4 using a conjugated polymer as an active material. In both cases identical excited states are involved.[13-15]

Electroluminescence is the generation of light by electrical excitation. This process is schematically represented in Figure 1-3. From the cathode, electrons are injected in the LUMO to form radical anions (negative polarons). From the anode, holes are injected in the HOMO to form radical cations (positive polarons). Injecting of holes is done by extracting electrons from the HOMO. Under influence of an applied electric field, the resulting charges migrate within the polymer film. In the film, electrons and holes recombine and form excitons. Decay of these excitons to the ground state can lead to emission of light.

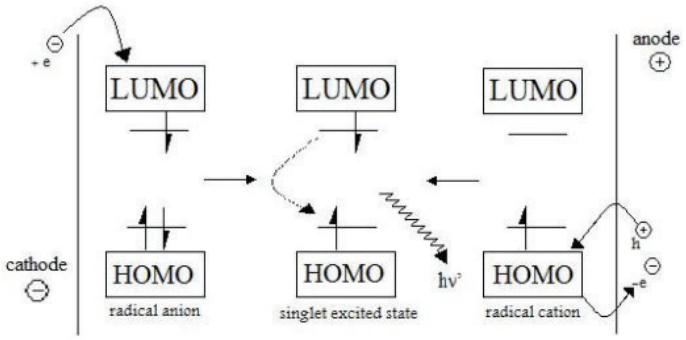

Figure 1-3 Schematic representation of electroluminescence in conjugated polymers[12]

Photoluminescence is a comparable process, which is depicted in Figure 1-4. An incident photon can excite an electron from the HOMO into the LUMO of a fluorescent polymer. The partial delocalization causes the formation of two new energy states, each filled with an electron of opposite spin (singlet excited state). Decay of this exciton to the ground state can be radiative or non-radiative. Photoluminescence is the radiative decay of this exciton and occurs at a longer wavelength than the wavelength of the absorbed photon.

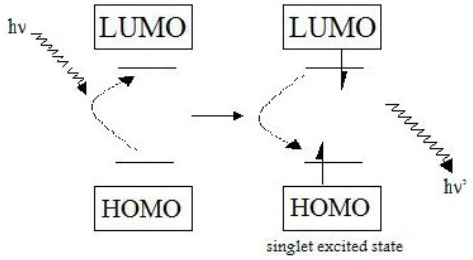

Figure 1-4 Schematic representation of photoluminescence in conjugated polymers[12]

1.1.2. Applications of conjugated polymers

In the late 70's, the rediscovery of conjugated polymers like poly(acetylene), poly(aniline) and poly(pyrrole), ignited an intense investigation of the properties of these conducting materials. More than 30 years after the initial explosion of interest in conjugated polymers, the science and technology of these materials is still an exciting research area.

Conjugated polymers are unique materials, which combine the electronic and optical properties of semiconductors with the mechanical properties and processability of regular polymers. Organic and polymeric materials generally have the advantage of being lightweight, flexible, low-cost and straightforward to process. Nowadays, due to the wide variety in available synthetic methods, scientists are able to customize the properties of many conjugated polymers for a particular function. As a result, conjugated polymers are useful for a wide range of optical and electronic applications, such as polymer light emitting diodes (PLEDs)[12,16-21], field effect transistors (FETs)[22-27], photovoltaic (solar) devices[28-31], optical lasers[32-34], (bio)sensors[35-39], polymer batteries[40-44], capacitors[43], electrostatic discharge coatings[43-44], smart windows[42,44], mechanical actuators[45] and photodetectors[46-47]. Currently, after more than 30 years of research, one can see the commercialization of the first conjugated polymer applications.

In addition, the science of conjugated polymers continues to be of considerable interest for fundamental studies in physics and chemistry. Through the better understanding of structure-property relationships, increasingly sophisticated structures of conjugated polymers can be designed and assembled. For example, as a result of the reversible electrochemical properties of conjugated polymers, they can be oxidized and reduced, giving rise to an electrochemically induced change in properties. Such switchable properties form the basis for applications such as solar cells, sensors, transistors and re-chargeable batteries. The understanding of these molecular processes is continuously developing. This gives a scientist the opportunity to tune the molecular structure and assemble devices from the nano to the macro level.

Conjugated polymers can also act as a linker between the electronic and biological world. For example, one can chemically tune the properties of conjugated polymers to be biocompatible or biofunctional. In this way, one can envision that the sensing of biological systems can be enabled or that the polymers can be utilized to modify biological functions. However, in this area still a significant amount of research needs to be done to achieve fully controllable interactions between conjugated polymers and biological species.

1.2. Poly(*para*-phenylene vinylene)

Within the broad range of possible conjugated polymers, this work will only focus on the conjugated polymer poly(*para*-phenylene vinylene) (PPV) and many of its derivatives. PPV consists of phenylene rings that are connected in their *para* positions by vinylene bonds, as can be seen in Figure 1-1.

There has been a steadily growing interest in PPV and its derivatives, which is reflected in the large number of publications each year on the chemistry and physics of this versatile class of conjugated polymers. There are several reasons for this interest, *i.e.* it is a relatively stable conjugated polymer and can be synthesized in good purity and with a high molecular weight. In

addition, very good soluble precursor polymers can be obtained to form films and fibers. The optical band gap of parent PPV is around 2.5 eV resulting in a bright yellow fluorescence[12], which makes PPV useful in applications such as light emitting diodes and photovoltaic devices. Field effect transistors and (bio)sensors are examples of typical other applications in which PPV derivatives have already been used.[12,16-31,35-39]

The physical, electrical and optical properties of PPV can be varied over a wide range by the incorporation of functional groups. Even after more than 30 years since its first synthesis, there remains much to be learned about this interesting class of polymers.

1.2.1. Synthesis of poly(*para*-phenylene vinylene)

♦ Step-growth polymerization

From a synthetic point of view, two major but rather different approaches for making PPV derivatives are known. A first approach is the direct synthesis of the PPV polymer, in which the double bond between the aromatic rings is formed *in situ*. Step-growth polycondensation reactions, like Wittig[48-49], McMurry[50-51] and Knoevenagel[52-54], have been used to obtain PPV derivatives. More common are the transition-metal catalyzed coupling reactions, like the Heck[55-56], Stille[57-58] and Suzuki[59] reaction. These three reaction types all make use of palladium catalysts. Finally, PPV derivatives can also be synthesized electrochemically using different types of monomers[60-61]. An overview of these reactions is depicted in Scheme 1-1.

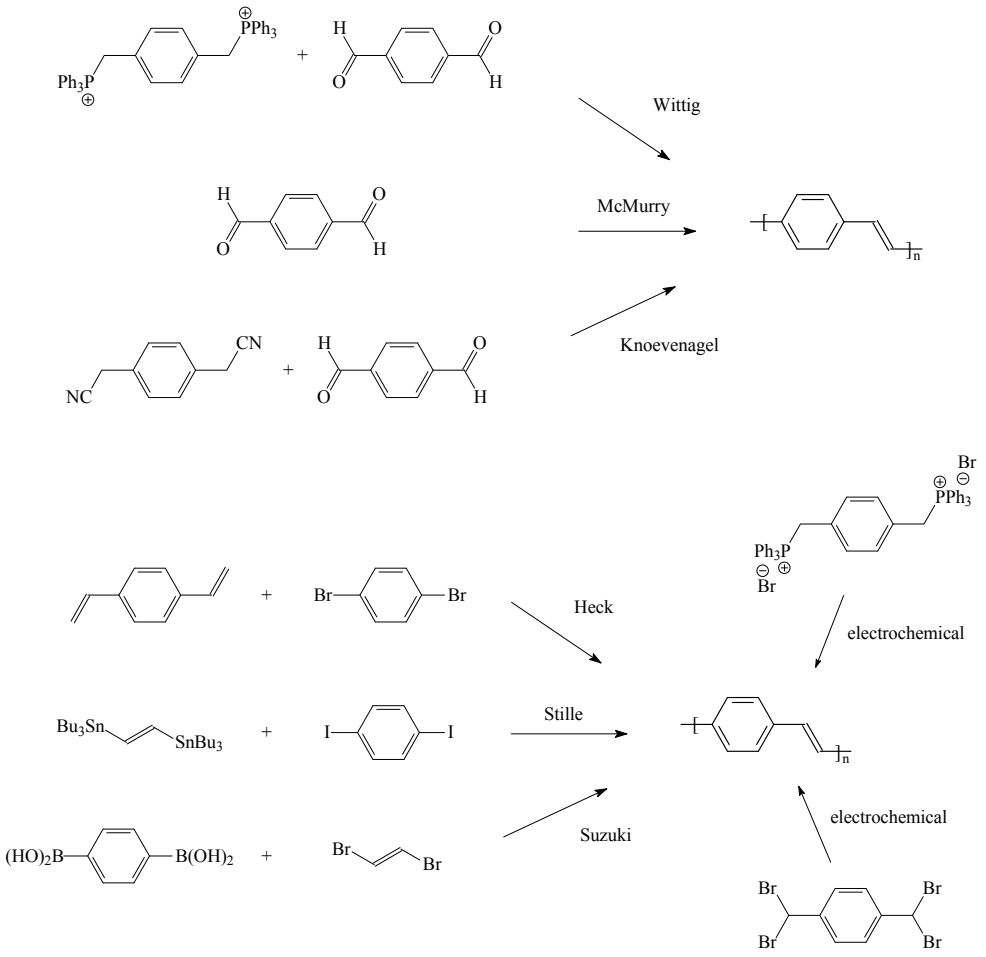

Scheme 1-1 Overview of typical direct routes towards PPV derivatives

However, these step-growth polymerization methods towards PPV derivatives often lead to insoluble, and therefore not processable, materials.[62-68] To make the polymers more soluble in common solvents, solubilizing side groups, such as phenyl rings and long alkyl or alkoxy chains, are attached onto the polymer backbone.[16,69-70] Although this may solve the solubility problems, these direct polymerization reactions only give polymers with low or moderate molecular weights. In addition, with these direct techniques, complex functionalization of PPV derivatives is not possible, although this is important for the development of advanced

functional polymers for a variety of devices such as (bio)sensors and solar cells with an improved performance.

♦ Precursor route polymerization

Another alternative approach to synthesize soluble, processable and functionalized PPV derivatives is the precursor approach. The most common precursor approaches towards poly(*para*-phenylene vinylene) polymers are the Gilch[71-73], Wessling-Zimmerman[74-79], xanthate[80-81], dithiocarbamate[82-85] and sulfinyl precursor routes.[86-88] The general principle for each precursor route is the same and can be found in Scheme 1-2.

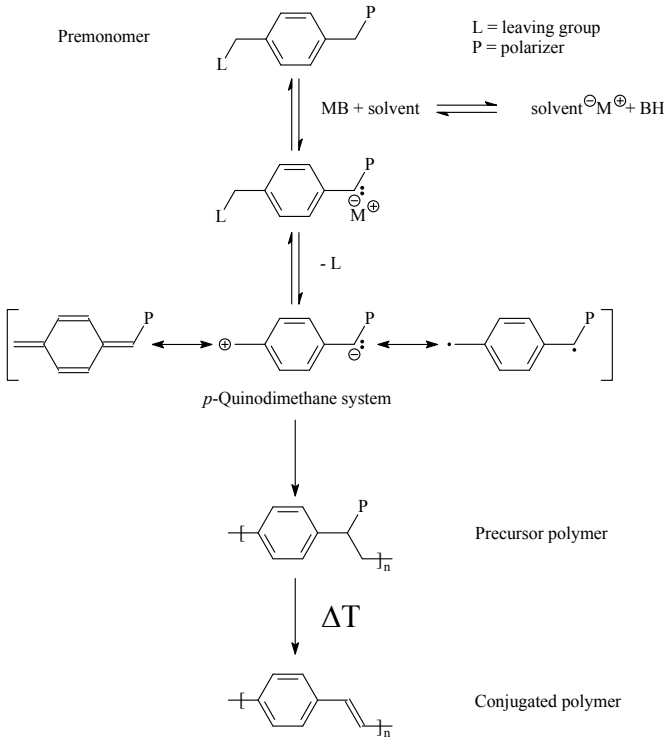

Scheme 1-2 General reaction scheme of the precursor routes towards PPV derivatives

The start of the polymerization mechanism involves proton abstraction of the premonomer under influence of a strong base, followed by 1,6-elimintation of the leaving group of the premonomer to give the reactive *p*-xylylene derivative. This *p*-xylylene or *p*-quinodimethane (*p*-QM) derivative is the actual monomer and is as such formed *in situ*. It can be represented using its three resonance forms.[89-91] This highly reactive *p*-QM intermediate will spontaneously polymerize to the precursor form of the polymer. Because of the presence of high molecular weight polymer at low monomer conversions, it is generally believed that the polymerization occurs *via* a radical chain mechanism.[71-72] In contrast, it can be assumed that the anionic polymerization mechanism results in low molecular weight material.[92] Depending on the premonomer structure and/or the polymerization conditions, the conjugated form of the polymer can be obtained immediately or by a subsequent thermal treatment of the precursor polymer.

Differentiation between the precursor routes towards PPV derivatives is the substituents on the premonomer, *i.e.* the leaving group (L) and the polarizer (P) and the polymerization conditions (reaction temperature and time, solvent, base). Leaving group (L) and polarizer (P) for the different routes are presented in Table 1-1.

Precursor route	**Leaving group (L)**	Polarizer (P)
Gilch	**Cl**	Cl
Wessling-Zimmerman	**$^{+}SR_2X^{-}$**	$^{+}SR_2X^{-}$
xanthate	**SC(S)OR**	SC(S)OR
dithiocarbamate	**$SC(S)NR_2$**	$SC(S)NR_2$
sulfinyl	**Cl, Br**	S(O)R

Table 1-1 Leaving group (L) and polarizer (P) for the different precursor routes towards PPV derivatives

From this table, it can be noticed that the premonomers for the Gilch, Wessling-Zimmerman, xanthate and dithiocarbamate precursor routes have the same functional group as the leaving group and the polarizer. This symmetrically substituted premonomer can cause unwanted side reactions such as branching, cross linking, gelation, solvent substitution or preliminary elimination.[84-85] Therefore our laboratory developed a new precursor route, the so-called sulfinyl precursor route, in which the leaving group and polarizer of the premonomer are different functional groups.[86-88] This chemical differentiation will result in an asymmetric premonomer, which allows full control over the entire polymerization procedure. The polarizer allows straightforward proton abstraction at the benzylic position next to the sulfinyl group. The R group of the polarizer guarantees good solubility of the formed precursor polymer. Another advantage of this polarizer is that it is stable at lower temperatures and can readily be removed at elevated temperatures to form the completely conjugated structure. Due to the steric and electronic properties of the sulfinyl *p*-QM system, formation of good head to tail additions of the premonomers is mostly guaranteed resulting in considerably fewer sp and sp^3 defects compared to the other precursor routes. Therefore the sulfinyl precursor route has been used to synthesize all the different PPV derivatives studied in this work.

1.2.2. The sulfinyl precursor route

Although at first sight the sulfinyl premonomer synthesis seems to be quite straightforward, this actually is the most challenging step. This is explained in **Chapter 2**, in which the synthesis of a sulfinyl premonomer with a functional group in the side chain, is described. After their synthesis, the sulfinyl premonomers are polymerized in a special designed setup. This polymerization setup is depicted in Figure 1-5. The premonomer solution (below) and the base solution (above) are purged with a flow of nitrogen and the reaction temperature is usually maintained at 30 °C. At standard polymerization conditions of PPV-type polymers, the concentration of the

premonomer is 0.02 M when the total amount of solvent (premonomer and base solution) is taken into account. After addition of the base solution to the premonomer, the reaction is stirred for one hour at 30 °C. Subsequently, the mixture is poured into ice water and extracted with dichloromethane or chloroform. After evaporation of the organic layers, the precursor polymer is precipitated in a cold non-solvent, collected and dried in vacuum.

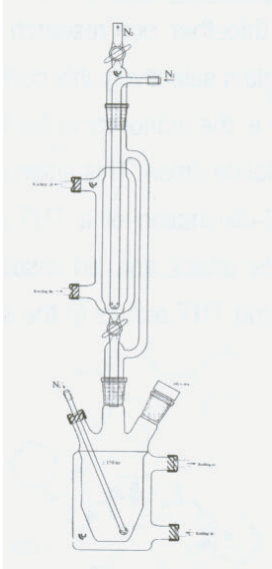

Figure 1-5 Polymerization setup used in the sulfinyl precursor route

Thermal elimination of the sulfinyl group will convert the precursor polymer into the corresponding conjugated polymer. The elimination process proceeds through a syn-elimination in which the intermediate is believed to have a planar structure. This process is depicted in Scheme 1-3. Only *trans*-vinylene bonds are formed due to steric hindrance in the transition sate, as can be seen in Scheme 1-3.

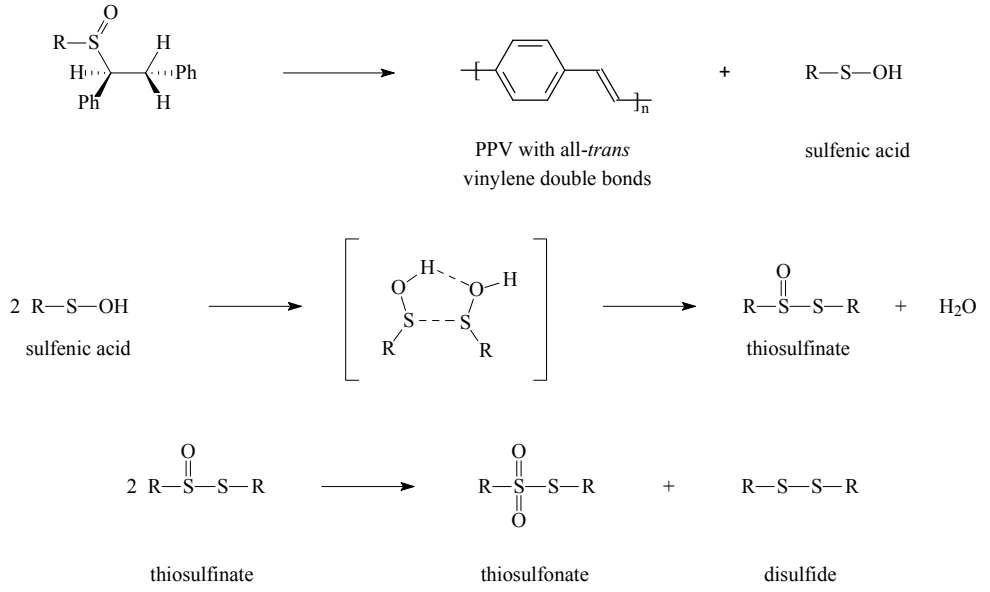

Scheme 1-3 Formation of *trans*-vinylene double bonds in PPV and possible reactions of the eliminated sulfenic acids

The elimination products are sulfenic acids, which will dimerize with the formation of a thiosulfinate molecule. Eventually, a disulfide and a thiosulfonate are formed *via* a disproportionation reaction involving two thiosulfinate molecules.[93-98]

1.3. Functionalization of polymers and their synthesis

1.3.1. Synthesis approaches for functionalization of polymers

There are two general methods for functionalizing (conjugated) polymers. A first approach is the introduction of the desired functionality at the monomer stage, after which the monomer is polymerized. This approach can give a

significant amount of restrictions with respect to the possible functional groups, which can be built in. For example, the functionalized monomers may not influence the polymerization reaction, since otherwise the achieved molecular weights may not be sufficiently high or in the worst case scenario the functionalization may even hamper the polymerization altogether. Another possible drawback is that the polymerization conditions transform or destroy the introduced functionalities. Finally, the synthesis of the monomer with the desired functionality can also be troublesome. In spite of these potential drawbacks, a review of the literature reveals that the above outlined approach is frequently utilized for the functionalization of (conjugated) polymers.

The second approach is called the post-polymerization functionalization method. In this approach the desired functionality is attached to a preformed (conjugated) polymer. This method gives the opportunity to attach a variety of functional groups to the same (conjugated) polymer platform. As a result, complex polymer structures can be formed starting from this platform. In this manner, the contribution of different functionalities to the polymer behavior can be studied. However, a drawback is the lack of a universal approach, leading to a wide variety of methods and functionalization procedures to obtain specific functional materials. In addition, complete functionalization can be troublesome. To avoid these drawbacks, a universal platform and methodology is needed, which allow for a wide variety of further functionalizations in a uniform manner. Both approaches are summarized in Figure 1-6.

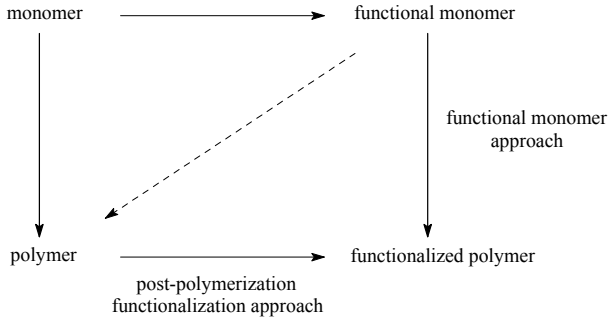

Figure 1-6 Different synthesis approaches for functionalization of polymers

In the current work, a combination of both approaches is applied. At first, a functional monomer is synthesized *i.e.* a monomer with an easy accessible and stable functional group for further functionalization. This functional monomer is then polymerized to form the 'functionalized' platform polymer (- - - - ➤ in Figure 1-6), which can undergo post-polymerization functionalization steps to obtain a large amount of different functionalized polymers, all starting from the same platform.

1.3.2. Functionalization of (conjugated) polymers

The approach of post-polymerization functionalization has been successfully used to functionalize common (non-conjugated) polymers. Examples include are the addition of a pyridyl disulfide functionality to poly(ethyleneglycol)[99], the addition of a drug to a polymer with acetal side chains *via* oxime linkages[100], the attachment of charged functionalities to polymers[101], introduction of functionalities for molecular recognition including molecular imprinted polymers (MIPs)[102-104], side chain functionalities for the creation of reactive membranes[105] and formation of copolymers *via* RAFT/MADIX (reversible addition fragmentation chain transfer/macromolecular design via the interchange of xanthates), ATRP (atom transfer radical polymerization) or "click" chemistry.[106-107] One can envision that similar modifications can be achieved for conjugated polymers.

Functionalization of conjugated polymer based materials is a powerful tool for tuning the properties of these materials. After all, the properties of functionalized conjugated polymers are not fully derived from their conjugated structure, but also strongly depend on their functional groups. In comparison to the functionalization of common polymers, functionalization of conjugated polymers is considerably more difficult, due to stability and solubility issues. Notwithstanding, various examples can be found in the literature. For example, poly(thiophene)s can be functionalized *via* post-polymerization functionalization or polymerization of the desired functional monomer. Poly(3-(6-bromohexyl)thiophene) has been post-polymerization

functionalized to form glycopoly(thiophene)s[108], the bromine function can be converted into an alcohol or into piperidinic moieties[109-110] and into different ester functionalities.[111] The bromine function in poly(3-bromo-4-hexylthiophene) can be transformed *via* a palladium catalyzed coupling reaction to form more complex structures.[112] Thiophene monomers with functional groups like epoxy and cyclic carbonate groups[113], vinylene-phenylene groups[114] or ethynylene-phenylene groups[115] and acrylic acid functions[116] can be polymerized into the polymeric form to obtain in this way functional poly(thiophene)s. Functionalized disubstituted poly(acetylene) polymers are synthesized *via* post-polymerization functionalization containing side chains with indolylazo moieties[117], strong green fluorescence molecules[118] and other chromophores.[119] Furthermore, also poly(3,4-ethylenedioxythiophene) (PEDOT) can efficiently be functionalized with tetrathiafulvalene (TTF) *via* the post-polymerization approach.[120] Finally, the azide-alkyne Huisgen cycloaddition, also called "click" chemistry, is a powerful tool for post-polymerization functionalization. This is illustrated on different polymers like poly(*p*-phenyleneethynylene)[121], poly(thiophene)[122], PEDOT[123] and poly(fluorene).[124-125] Sometimes both above mentioned approaches can be used to form functionalized polymers *e.g.* the synthesis of well-defined fluorescent conjugated fluorene based glycopolymers.[126]

1.3.3. Functionalization of poly(*para*-phenylene vinylene)

PPV derivatives can be functionalized by incorporation of functional side chains onto the phenyl units of the polymer backbone. Alternatively, functionalization is also possible at the vinylic carbons.[127-128] Introducing these chemical functionalities to PPV derivatives will offer a wide range of new material properties depending on the attached functional groups.

For example, PPV derivatives with polar ionic groups in the side chain have been reported in the literature. These derivatives are well soluble in polar solvents including water.[129-132] Decoration of PPV derivatives with sulphonate (SO_3^-)[133-136] and carboxylate (COO^-)[137-141] functional groups can

be useful for the application of PPV-type polymers in biological and chemical sensors. Besides functionalization with anionic functional groups, cationic groups, such as ammonium (NR_3^+)[142-145], can also be used to functionalize PPV and to obtain good sensor devices. At the same time, PPV derivatives with polar non-ionic groups in the side chain comprise also an important research domain. A 1,4-dialkoxybenzene moiety forms the base structure of the monomers, used for the synthesis of these functionalized PPV derivatives.[146-148] This 1,4-dialkoxybenzene base structure is also present in the frequently applied poly(2-methoxy-5-(3,7-dimethyloctyloxy)-1,4-phenylene vinylene), which is usually referred to as MDMO-PPV or OC_1C_{10}-PPV (Figure 1-7).

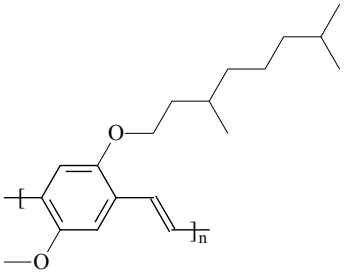

Figure 1-7 Chemical structure of MDMO-PPV

By replacing the branched C_{10}-alkyl side chain with an oligo(ethylene oxide) side chain, the PPV becomes polar. The resulting polar PPV derivatives have been used in several applications, such as sensors[149] and as an active layer in light emitting electrochemical cell devices.[150-159] PPV derivatives tailored with amine groups[160-161], bromine atoms[162], hydroxyl moieties[163], vinyl groups[164-165], nitroxide[166] and oxadiazole groups[167] have also been synthesized. All these derivatives have been functionalized *via* the first approach, *i.e.* by the synthesis and subsequent polymerization of a functional monomer.

Until now, only a limited number of investigations focusing on the post-polymerization functionalization for PPV derivatives have been reported in the literature. Examples include the deprotection of functional groups[168-169]

and grafting PPV derivatives with porphyrin rings.[170] Previously, in our group PPV derivatives have been post-polymerization functionalized *via* the Mitsunobu reaction.[171] Finally, it should be noted that also the end-groups of PPV derivatives can be functionalized, *e.g.* with methyl methacrylate, to form diblock copolymers.[172]

1.4. Aim and outline

1.4.1. Aim

The central aim of the research presented in this work is the synthesis and characterization of different novel functionalized conjugated polymers *via* the sulfinyl precursor route. In the past, this precursor route has already proven its versatility for several different monomer systems. Polymers made *via* the sulfinyl precursor route have enhanced properties as compared to polymers made *via* other available synthetic routes.

In this work, functionalities are incorporated onto the phenyl units of the polymer backbone and not onto the vinylic carbons. For the actual tailoring process of conjugated polymers a wide variety of methods can be found in literature. Hitherto, a significant drawback is the lack of a universal approach, leading to a wide variety of methods and functionalization procedures to obtain specific functional materials. To avoid this drawback, the aim of this work is to develop a universal platform and methodology, which allow for a wide variety of further functionalizations in a uniform manner. Within the wide range of available conjugated polymers, our focus is on the conjugated polymer poly(*para*-phenylene vinylene) (PPV) and its derivatives. Notwithstanding, a similar approach can maybe be utilized for a wide variety of other conjugated polymers.

A first major objective to achieve is the formation of a PPV derivative with functional groups. This polymer should be chemically stable and well soluble in common organic solvents to allow further reactions. From this

platform polymer, post-polymerization functionalization of the functional side chain of the PPV needs to be possible *via* a straightforward, optimized and efficient procedure to obtain the desired functional group. In this way, the new or other functional group is covalently linked to the backbone of the platform polymer.

In the current work, an improved method is developed, which has been tested and optimized first using a monomer model compound. The translation of this methodology to the platform polymer should give identical results. Although the functionalization of molecules is obviously much easier than functionalization of polymers, the synthesis of a versatile PPV derivative platform as well as the development of a universal functionalization methodology remain the main goals of this work. In the end, post-polymerization functionalization of PPV derivatives with virtually any functional group should be possible, allowing the development of many new and exciting applications. Not only from a fundamental scientific point of view this is an enormous challenge, but also from a practical point of view this is a worthwhile effort since one would be able to improve systems that have already proven to be useful in devices. For example, these new functionalized PPV derivatives can be used in the active layer of photovoltaic devices. Functionalization might lead to stabilization of the morphology and thus a better performance of these devices. Other possible applications are the use in advanced polymer based devices like (bio)sensors, by functionalizing the PPV derivatives with biological species to enable sensing.

1.4.2. Outline

In **Chapter 2**, a new platform copolymer is developed for further post-polymerization functionalization, which is done *via* an optimized procedure. This procedure was first tested and optimized for model compounds, after which it was used to functionalize the platform copolymer. In this way, PPV derivatives can be post-functionalized with a variety of functional groups *i.e.* vinyl groups, propenylphenyl groups, propynylphenyl groups,

methacrylate groups, ATRP initiator groups, dithiocarbamate initiator groups and propargyl groups. The latter group can be utilized for even further post-polymerization functionalization *via* "click" chemistry. No substantial degradation of the conjugated system occurs, even after consecutive post-polymerization functionalization reactions, which demonstrates the versatility of the developed universal functionalization methodology. **Chapter 3** focuses on the influence of the built-in of some of these functional groups in bulk heterojunction solar devices. The performance of these different solar cells is compared with a reference material and can be correlated with the nanoscale morphology of the active layer of these solar cells. In addition, their influence on the thermal stability of the active layers is investigated. Although improvements are observed, the efficiency of the resulting organic photovoltaic devices is limited due to, amongst others, the insufficient absorption of solar radiation by the active layer. A broadening of the absorption window of the active layer can be achieved by introducing phthalocyanine (Pc) molecules in PPV derivatives. **Chapter 4** deals with the covalent attachment of these Pc molecules to PPV derivatives *via* the optimized procedure, derived in **Chapter 2**, as well as two different "click" chemistry methods. Subsequently, these materials are tested in bulk heterojunction solar devices. In **Chapter 5**, two different procedures are investigated to graft PPV derivatives. Both, ATRP and benzyl dithiocarbamate photoiniferter polymerization belong to the class of "pseudo" living radical polymerization reactions. The compatibility of both polymerization reactions with PPV derivatives is studied and polymerization is initiated directly from the side chains of the PPV derivatives. Finally, **Chapter 6** presents some initial experiments to post-polymerization functionalize PPV derivatives with natural and artificial receptors. This dissertation is completed with some general conclusions, perspectives and **summaries** in English and in Dutch as well as a list of **publications**, **conference contributions** and **awards**. At the very end, some **words of thanks** are presented.

1.5. References

[1] Feast, W. J.; Tsibouklis, J.; Pouwer, K. L.; Groendaal, L.; Meijer, E. W. *Polymer* **1996**, *37*, 5017.

[2] Chien, J. C. W. *Polyacetylene: chemistry, physics and material science*, Academic Press, Orlando, **1984**.

[3] Curran, S.; Stark-Hauser, A.; Roth, S. *Organic conductive molecules and polymers*, John Wiley & Sons, New York, **1997**, vol 2.2.

[4] Rodriguez, J.; Grande H. J.; Othero, T. F. *Handbook of organic and conductive molecules and polymers*, John Wiley & Sons, New York, **1997**, vol 2, 505.

[5] Mc Cullough, R. D. *Adv. Mat.* **1998**, *10*, 93.

[6] Kovacic, P.; Jones, M. B. *Chem Rev.* **1987**, *87*, 357.

[7] Roncali, J. *Chem. Rev.* **1992**, *92*, 711.

[8] Roncali, J. *Chem. Rev.* **1997**, *97*, 173.

[9] Kiebooms, R. ; Menon, R.; Lee, K. *Handbook of advanced electronic and photonic materials and devices*, Academic Press **2001** vol. 8,1.

[10] Shriver, D. F.; Atkins, P. W.; Langford, C. H. *Inorganic Chemistry – second edition*, Oxford University Press, **1994**, 91.

[11] Cornil, J.; Dos Santos, D. A.; Beljonne, D.; Brédas, J. L. *J. Phys. Chem.* **1995**, 99.

[12] Friend, R. H.; Gymer, R. W.; Holmes, A. B.; Burroughes, J. H.; Marks, R. N.; Taliani, C.; Bradley, D. C.; Dos Santos, D. A.; Brédas, J. L.; Lögdlund, M.; Salaneck, W. R. *Nature* **1999**, *397*, 121.

[13] Bradley D. D. C. et al. *Synth. Met.* **1991**, *41*, 3135.

[14] Friend, R. H.; Bradley, D. D. C.; Holmes, A. B. *Physics World* **1992**, 42.

[15] Yang, Y. *Mrs. Bulletin* **1997**, 31.

[16] Braun, D.; Heeger, A. J. *Appl. Phys. Lett.* **1991**, *58*, 1982.

[17] Burn, P. L.; Holmes, A. B.; Kraft, A.; Bradley, D. D. C.; Brown, A. R.; Friend, R. H.; Gymer, R. W. *Nature*, **1992**, *356*, 47.

[18] Bradley, D. D. C. *Synthetic Metals* **1993**, *54*, 401.

[19] May, P. *Physics World* **1995**, *8*, 52.

[20] Salbeck, J. *Ber. Bunsenges. Phys. Chem.* **1996**, *100*, 1666.
[21] Kraft, A.; Grimsdale, A. C.; Holmes, A. B. *Angew. Chem. Int. Ed.* **1998**, *37*, 402.
[22] Roth, S. *One-dimensional metals* **1995**, Weinheim VCH, 209-231.
[23] Sirringhaus, H.; Tessler, N.; Friend, R. H. *Science* **1998**, *280*, 1741.
[24] Horowitz, G. *Adv. Mat.* **1998**, *10*, 365.
[25] Bao, Z. *Adv. Mat.* **2000**, *12*, 227.
[26] Dimitrakopoulos, C. D.; Malenfant, R. L. *Adv. Mat.* **2002**, *14*, 99.
[27] Scgeinert, S.; Paasch, G. *Phys. Stat. Sol.* **2004**, *201*, 1263.
[28] Rostalski, J.; Meissner D. *Solar Energy Materials & Solar Cells* **2000**, *61*, 87.
[29] Brabec, J. C.; Sariciftci, N. S.; Hummelen, J. C. *Adv. Funct. Mater.* **2001**, *11*, 15.
[30] Hoppe, H.; Sariciftci, N. S. *J. Mater. Res.* **2004**, *19*, 1924.
[31] Hoppe, H.; Niggeman, M.; Winder C.; Kraut, J.; Heisgen, R.; Hinsch, A.; Meissner, D.; Sariciftci, N. S. *Adv. Funct. Mater.* **2004**, *14*, 1005.
[32] Schwartz, B.; Diaz-Garcia, M.; Hilde, F.; Andersson, M.; Pei, Q.; Heeger, A. *Polym. Prepr.* **1997**, *38*, 325.
[33] Tessler, N. *Adv. Mater.* **1999**, *11*, 363.
[34] McGehee, M.; Heeger, A. *Adv. Mater*. **2000**, *12*, 1655.
[35] Mac Diarmid, A. G.; Zhang, W. J.; Huang, Z.; Wang, P.-C.; Huang, F.; Xie, S. *Polymer Prepr.* **1997**, *11*, 333.
[36] Heeger, P. S.; Heeger, A. J. *Proc. Natl. Acad. Sci.* **1999**, *96*, 12219.
[37] Chen, L.; McBranch, W.; Wang, H.; Helgeson, R.; Wudl, F.; Whitten, D. G. *Proc. Natl. Acad. Sci.* **1999**, *96*, 12287.
[38] Tyler McQuade, D.; Pullen, A. E.; Swager, T. M. *Chem. Rev.* **2000**, *100*, 2537.
[39] Gerard, M.; Chaubey, A.; Malhotra, B. D. *Biosensors and Bioelectronics* **2002**, *17*, 345.
[40] Nigrey, P.; MacInnes, D.; Nairns, D.; MacDiarmid, A.; Heeger, A. *J. Electrochem. Soc.* **1981**, *128*, 1651.
[41] Wirsén, A. *"Electroactive Polymer Materials"*, Technomic publishing AG, Switzerland, **1987**.
[42] Kanatzidis, M. G. *C & EN* **1990**, *3*, 36.

[43] Miller, J. *Adv. Mater.* **1993**, *5*, 671.
[44] Roth, S. *"One-Dimensional Metals"*, Weinheim VCH, **1995**, 209.
[45] Lu, W.; Fadeev, A. G.; Qi, B.; Smela, E.; Mattes, B. R.; Ding, J.; Spinks, G. M.; Mazurkiewicz, J.; Zhou, D.; Wallace, G. G.; MacFarlane, D. R.; Forsyth, S. A.; Forsyth, M. *Science*, **2002**, *297*, 983.
[46] Yu, G.; Wang, J.; McElvain, J.; Heeger, A. J. *Adv. Mater.* **1998**, *10*, 1431.
[47] Miyasaki, S.; Itami, S.; Araki, T. *Rev. Sci. Instrum.* **1998**, *69*, 3751.
[48] McDonald, R. N.; Campbell, T. W.; J. *Am. Chem. Soc.* **1960**, *82*, 4669.
[49] Hörhold, H.-H.; Opfermann, J. *Makromol. Chem.* **1970**, *131*, 105.
[50] Rehahn, M.; Schlüter, A.-D. *Makromol. Chem. Rapid Commun.* **1990**, *11*, 375.
[51] Stalmach, V.; Kolsharm, H.; Brehm, I.; Meier, M. *Liebigs Ann.* **1996**, 1449.
[52] Lenz, R. W.; Handlovits, C. E. *J. Org. Chem.* **1960**, *25*, 813.
[53] Staring, E. G. J.; Demandt, R. C. J. E.; Braun, D.; Rikken, G. L. J.; Kessener, Y. A. R. R.; Venhuizen, A. H. J.; Knippenberg, M. M. F.; Bouwmans, M. *Synth. Met.* **1995**, *71*, 2179.
[54] Moratti, S. C.; Bradley, D. D. C.; Friend, R. H.; Greenham, N. C.; Holmes, A. B. *Polym. Prep.* **1994**, *35*, 214.
[55] Heck, R. F. *Org. React.* **1982**, *27*, 345.
[56] Greiner, A.; Heitz, W. *Makromol. Chem. Rapid Commun.* **1988**, *9*, 581.
[57] Babudri, F.; Cieco, S. R.; Farinola, G. M.; Naso, F.; Bolognesi, A.; Porzio, W. *Macromol. Rapid Commun.* **1996**, *17*, 905.
[58] Bao, Z.; Chan, W. K.; Yu, L. *J. Am. Chem. Soc.* **1995**, *117*, 12426.
[59] Koch, F.; Heitz, W. *Macromol. Chem. Phys.* **1997**, *198*, 1531.
[60] Chang, W. P.; Whang, W. T.; Lin, P. W. *Polymer* **1996**, *37*, 1513.
[61] Nishihara, H.; Tateishi, M.; Aramaki, K.; Ohsawa, T.; Kimura, O. *Chem. Lett.* **1987**, 539.
[62] Heitz, W.; Brügging, W.; Freund, L.; Gailberger, M.; Greiner, A.; Jung, H.; Kampschulte, U.; Niesser, N.; Osan, F.; Schmidt, H. W.; Wicker, M. *Makromol. Chem.* **1988**, *189*, 119.

[63] Martelock, H.; Greiner, A.; Heitz, W. *Makromol. Chem.* **1991**, *192*, 967.
[64] Greiner, A.; Martelock, H.; Noll, A.; Siegfried, N.; Heitz, W. *Polymer*, **1991**, *32*, 1857.
[65] Remmers, M.; Schulze, M.; Wegner, G. *Macromol. Rapid Commun.* **1996**, *17*, 239.
[66] Cooke, A. W.; Wagener, K. B. *Macromolecules* **1990**, *24*, 1404.
[67] Rehahn, M.; Schlüter, A. D. *Chem. Lett.* **1987**, *11*, 375.
[68] Hanack, M.; Segura, J. L.; Spreitzer, H. S. *Adv. Mater.* **1996**, *8*, 663.
[69] Wudl, F.; Sardanov, G. *US Patent* 5, 189, 136, **1993**.
[70] Becker, H.; Spreitzer, H.; Kreuder, W.; Kluge, E.; Schenk, H.; Parker, I.; Cao, Y. *Adv. Mater.* **2000**, *12*, 42.
[71] Gilch, H. G.; Wheelwright, W. L. *J. Polym. Sci.: A* **1966**, *4*, 1337.
[72] Louwet, F.; Vanderzande, D.; Gelan, J.; Mullens, J. *Macromolecules* **1995**, *28*, 1330.
[73] Becker, H.; Spreitzer, H.; Ibrom, K.; Kreuder, W. *Macromolecules* **1999**, *32*, 4925.
[74] Wessling, R. A.; Zimmerman, R. G. *U.S. Pat.* **1968** 3 401 152; 3 404 132; **1970** 3 532 643; **1972** 3 706 677.
[75] Wessling, R. A. *J. Polym. Sci., Polym. Symp.* **1985**, *72*, 55.
[76] Garay, R. G.; Myrian, N. S.; Montani, R. S.; Hernandez, S. A. *Designed Monomers and Polymers* **2000**, *3*, 231.
[77] Shah, H. V.; McGhie, A. R.; Arbuckle, G. A. *Thermochimica acta* **1996**, *287*, 319.
[78] Hsieh, B. R.; Antoniadis, H.; Abkowitz, M. A.; Stolka, H. *Polym. Prep.* **1992**, *33*, 414.
[79] Lahti, P. M.; Sarker, A.; Garay, R. O.; Lenz, R. W.; Karasz, F. E. *Polymer* **1994**, *35*, 1312.
[80] Son, S.; Dodabalapur, A.; Lovinger, A. J.; Galvin, M. E. *Science* **1995**, *269*, 376.
[81] Son, S.; Lovinger, A. J.; Galvin, M. E. *Polym. Mater. Sci. and Engin.* **1995**, *72*, 567.
[82] Henckens, A.; Lutsen, L.; Vanderzande, D.; Knipper, M.; Manca, J.; Aernouts, T.; Poortmans J. *Proc. Spie-Int. Soc. Opt. Eng.* **2004**, *5464*, 52.

[83] Henckens, A.; Duyssens, I.; Lutsen, L.; Vanderzande, D.; Cleij, T. J. *Polymer* **2006**, *47*, 123.
[84] Garay, R. G.; Lenz, R. W. *Makromol. Chem. Suppl.* **1989**, *15*, 1.
[85] Yamada, S.; Tokito, S.; Tsutsui, T.; Saito, S. *J. Chem. Soc. Chem. Commun.* **1987**, 1448.
[86] van Breemen, A. J. J. M.; Issaris, A. C. J.; de Kok, M. M.; Van Der Borght, M. J. A. N.; Adriaensens, P. J.; Gelan, J. M. J. V.; Vanderzande, D. J. M. *Macromolecules* **1999**, *32*, 5728.
[87] Lutsen, L. J.; van Breemen, A. J.; Kreuder, W.; Vanderzande, D. J. M.; Gelan, J. M. J. V. *Helv. Chim. Acta* **2000**, *83*, 3113.
[88] Lutsen, L.; Adriaensens, P.; Becker, H.; van Breemen, A. J.; Vanderzande, D. J. M.; Gelan, J. *Macromolecules* **1999**, *32*, 6517.
[89] Hiberty, P. C.; Karafiloglou, P. *Theoret. Chim. Acta (Berl.)* **1982**, *61*, 171.
[90] Döhnert, D.; Koutecky, J. *J. Am. Chem. Soc.* **1980**, *102*, 1789.
[91] Flynn, C. R.; Michl, J. *J. Am. Chem. Soc.* **1974**, *96*, 3280.
[92] Vanderzande, D. J. M.; Hontis, L.; Palmaerts, A.; Van Den Berghe, D.; Wouters, J.; Lutsen, L.; Cleij, T. *Proc. Of SPIE* **2005**, *5937*, 116.
[93] Kesters, E.; Lutsen, L.; Vanderzande, D.; Gelan, J.; Nguyen, T. P.; Molinié, P. *Thin Solid Films* **2002**, *120*, 403.
[94] Kesters, E.; Vanderzande, D.; Lutsen, L.; Penxten, H.; Carleer, R. *Macromolecules* **2005**, *38*, 1141.
[95] Durst, T.; Jones, D. N. *Comprehensive Organic Chemistry volume 3* Oford Pergamon **1979**, *121*.
[96] Trost, B. M.; Salzmann, T. N.; Hiroi, K. J. *J. Am. Chem. Soc.* **1976**, *98*, 4887.
[97] Trost, B. M. *Acc. Chem. Res.* **1978**, *11*, 453.
[98] Paptai, S. *The Chemistry of Sulphones and Sulphoxides*, John Wiley & Sons Ltd., Chichester, UK **1988**.
[99] Boyer, C.; Liu, J.; Wong, L.; Tippett, M.; Bulmus, V.; Davis, T. P. *Journal of Polymer Science: Part A: Polymer Chemistry* **2008**, *46*, 7207.
[100] Li, R. C.; Broyer, R. M.; Maynard, H. D. *Journal of Polymer Science: Part A: Polymer Chemistry* **2006**, *44*, 5004.
[101] Decher, G. *Science* **1997**, *277*, 1232.

[102] Boal, A. K.; Ilhan, F.; DeRouchey, J. E.; Thurn-Albrecht, T.; Russel, T. P.; Rotello, V. M. *Nature* **2000**, *404*, 2202.
[103] Duffy, D. J.; Das, K.; Hsu, S. L.; Penelle, J.; Rotello, V. M.; Stidham, H. D. *J. Am. Chem. Soc.* **2002**, *124*, 8290.
[104] Das, K.; Penelle, J.; Rotello, V. M. *Langmuir* **2003**, *19*, 3921.
[105] Tripp, J. A.; Stein, J. A.; Svec, F.; Frechet, J. M. J. *Org. Lett.* **2000**, *2*, 195.
[106] Wang, J.; Kara, S.; Long, T. E.; Ward, T. C. *J. Polym. Sci., Polym. Chem.* **2000**, *38*, 3742.
[107] Quémener, D.; Le Hellaye, M.; Bissett, C.; Davis, T. P.; Barner-Kowollik C., Stenzel, M. H. *Journal of Polymer Science: Part A: Polymer Chemistry* **2008**, *46*, 155.
[108] Xue, C.; Luo, F.-T.; Liu, H. *Macromolecules* **2007**, *40 (19)*,6863.
[109] Lanzi, M.; Costa-Bizzarri, P.; Paganin, L.; Cesari, G. *Reactive & Functional Polymers* **2007**, *67*, 329.
[110] Lanzi, M.; Costa-Bizzarri, P.; Paganin, L.; Cesari, G. *Synthetic Metals* **2007**, *157*, 719.
[111] Lanzi, M.; Costa-Bizzarri, P.; Paganin, L.; Cesari, G. *European Polymer Journal* **2007**, *43*, 72.
[112] Li, Y.; Vamvounis, G.; Yu, J.; Holdcroft, S. *Macromolecules* **2001**, *34*, 3130.
[113] Li, G.; Koßmehl, G.; Kautek, W.; Plieth, W.; Melsheimer, J.; Dolbhofer, K.; Hunnius, W.-D.; Zhu, H. *Macromol. Chem. Phys.* **1999**, *200*, 450.
[114] Hou, J.; Huo, L.; He, C.; Yang, C.; Li, Y. *Macromolecules* **2006**, *39*, 594.
[115] Zhou, E.; Hou, J.; Yang, C.; Li, Y. *Journal of Polymer Science: Part A: Polymer Chemistry* **2006**, *44*, 2206.
[116] Peng, H.; Soeller, C.; Travas-Sejdic, J. *Sensors* **2007**, *28-31*, 1124.
[117] Li, Z.; Li, Q.; Qin, A.; Dong, Y.; Lam, J. W. Y.; Dong, Y.; Ye, C.; Qin, J.; Zhong Tang, B. *Journal of Polymer Science: Part A: Polymer Chemistry* **2006**, *44*, 5672.
[118] Zeng, Q.; Lam, J. W. Y.; Jim, C. K. W.; Qin, A.; Qin, J.; Li, Z.; Zhong Tang, B. *Journal of Polymer Science: Part A: Polymer Chemistry* **2008**, *46*, 8070.

[119] Sukwattanasinitt, M.; Lee, D.-C.; Kim, M.; Wang, X.; Li, L.; Yang, K.; Kumar, J.; Tripathy, S. K.; Sandman, D. J. *Macromolecules* **1999**, *32*, 7361.

[120] Besbes, M.; Trippé, G.; Levillain, E.; Mazari, M.; Le Derf, F.; Perepichka, I. F.; Derdour, A.; Gorgues, A.; Sallé, M.; Roncali, J. *Adv. Mater.* **2001**, *13*, 1249.

[121] Englert, B. C.; Bakbak, S.; Bunz, U. H. F. *Macromolecules* **2005**, *38*, 5868.

[122] Benanti, T. L.; Kalaydjian, A.; Venkataraman, D. *Macromolecules* **2008**, *41*, 8312.

[123] Bu, H.-B.; Götz, G.; Reinold, E.; Vogt, A.; Schmid, S.; Blanco, R.; Segura, J. L.; Bäuerle, P. *Chem. Commun.* **2008**, *11*, 1320.

[124] Li, B.-L.; Liu, Z.-T.; He, Y.-M.; Pan, J.; Fan, Q.-H. *Polymer* **2008**, *49*, 1527.

[125] Li, Z.; Zeng, Q.; Yu, G.; Li, Z.; Ye, C.; Liu, Y.; Qin, J. *Macromol. Rapid Commun.* **2008**, *29*, 136.

[126] Xue, C.; Donuru, V. R. R.; Liu, H. *Macromolecules* **2006**, *39*, 5747.

[127] Greenham, N. C.; Moratti, S. C.; Bradley, D. D. C.; Friend, R. C.; Holmes, A. B. *Nature* **1993**, *365*, 628.

[128] Kaul, S. N.; Fernande, J. E. *Macromolecules* **1990**, *23*, 2875.

[129] Pinto, M. R.; Schanze, K. S. *Synthesis* **2002**, *9*, 105.

[130] McGehee, M. D.; Miller, E. K.; Moses, D.; Heeger, A. J. *Advances in Synthetic Metals. Twenty Years of progress in Science and Technology*; Bernier, P.; Lefrant, S.; Bidan, G. Eds.; Amsterdam **1999**, *98*.

[131] Chen, L.; Xu, S.; McBranch, D.; Whitten, D. *J. Am. Chem. Soc.* **2000**, *122*, 9302.

[132] Shi, S.; Wudl, F. *Macromolecules* **1999**, *23*, 2119.

[133] Wang, J.; Wang, D.; Miller, E. K.; Moses, D.; Bazan, G. C.; Heeger, A. J. *Macromolecules* **2000**, *33*, 5153.

[134] Gaylord, B. S.; Wang, S.; Heeger, A. J.; Bazan, G. C. *J. Am. Chem. Soc.* **2002**, *124*, 5942.

[135] Fan, C.; Plaxco, K. W.; Heeger, A. J. *J. Am. Chem. Soc.* **2001**, *123*, 6417.

[136] Ramachandran, G.; Smith, T. A.; Gómez, D.; Ghiggino, K. P. *Synth. Met.* **2005**, *152*, 17.
[137] Peng, Z.; Xu, B.; Zhang, J.; Pan, Y. *Chem. Commun.* **1999**, 1855.
[138] Fujii, A.; Sonoda, T.; Yoshino, K. *Jpn. J. Appl. Phys.* **2000**, *39*, L249.
[139] Fujii, A.; Sonoda, T.; Fujisawa, T.; Ootaka, R.; Yoshino, K. *Synth. Met.* **2001**, *119*, 189.
[140] Gin, D.; Yonezawa, K. *Synth. Met.* **2001**, *121*, 1291.
[141] Wagaman, M. W.; Grubbs, R. H. *Macromolecules* **1997**, *30*, 3978.
[142] Li, H.; Xiang, C.; Li, Y.; Xiao, S.; Fang, H.; Zhu, D. *Synth. Met.* **2003**, *135-136*, 483.
[143] Chen, X.; Wudl, F. *Polym. Prepr.* **2002**, *43*, 19.
[144] Li, H.; Li, Y.; Zhai, J.; Cui, G.; Liu, H.; Xiao, S.; Liu, Y.; Lu, F.; Jiang, L.; Zhu, D. *Chem. Eur. J.* **2003**, *9*, 6031.
[145] Fan, Q.-L.; Zhang, G.-W.; Lu, X.-M.; Chen, Y.; Huang, Y.-Q.; Zhou, Y.; Chan, H. S. O. Lai, Y.-H.; Xu, G.-Q.; Huang, W. *Polymer* **2005**, *46*, 11165.
[146] Momii, T.; Tokito, S.; Tsutsui, T.; Saito, S. *Chem. Lett.* **1988**, 1201.
[147] Delmotte, A.; Biesemans, M.; Raier, H.; Gielen, M.; Meijer, E. W. *Synth. Met.* **1993**, *58*, 325.
[148] Jin, J.; Park, C. K.; Shim, H. K. *Polymer* **1994**, *35*, 480.
[149] Holzer, L.; Winkler, B.; Wenzl, F. P.; Tasch, S.; Dai, L.; Mau, A. W. H.; Leising, G. *Synth. Met.* **1999**, *100*, 71.
[150] Garay, R. O.; Mayer, B.; Karasz, F. E.; Lenz, R. W. *J. Polym. Sci. Part A Polym. Chem.* **1995**, *33*, 525.
[151] Carvalho, L. M.; Santos, L. F.; Guimaraes, F. E. G.; Gonçalves, D.; Gomes, A. S.; Faria, R. M. *Synth. Met.* **2001**, *119*, 361.
[152] Huang, C.; Huang, G.; Guo, J.; Huang, W.; Kang, E. T.; Yang, C.-Z. *Polym. Prepr.* **2002**, *43*, 574.
[153] Tasch, S.; Holzer, L.; Wenzl, F. P.; Gao, J.; Winkler, B.; Dai, L.; Mau, A. W. H.; Sotgiu, R.; Sampietro, M.; Scherf, U.; Müllen, K.; Heeger, A. J.; Leising, G. *Synth. Met.* **1999**, *102*, 1046.
[154] Hwang, D. H.; Chuah, B. S.; Li, X.-C.; Kim, S. T.; Moratti, S. C.; Holmes, A. B. *Macromol. Symp.* **1997**, *125*, 111.

[155] Morgado, J.; Friend, R. H.; Cacialli, F.; Chuah, B. S.; Rost, H.; Moratti, S. C.; Holmes, A. B. *Synth. Met.* **2001**, *122*, 111.
[156] He, G.; Yang, C.; Wang, R.; Li, Y. *Displays* **2000**, *21*, 69.
[157] Huang, C.; Huang, W.; Guo, J.; Yang, C.-Z.; Kang, E.-T. *Polym.* **2001**, *42*, 3929.
[158] Xiang, D.; Shen, Q.; Zhang, S.; Jiang, X. *J. Appl. Polym. Sci.* **2003**, *88*, 1350.
[159] Morgado, J.; Cacialli, F.; Friend, R. H.; Chuah, B. S.; Rost, H.; Holmes, A. B. *Macromolecules* **2001**, *34*, 3094.
[160] Liang, Z.; Mindaugas, R.; Li, K.; Manias, E.; Wang, Q. *Chem. Mater.* **2003**, *15*, 2699.
[161] Liang, Z.; Wang, Q. *Langmuir* **2004**, *20*, 9600.
[162] Benvenho, A. R. V.; Lessmann, R.; Hümmelgen, I. A.; Mello, R. M. Q.; Li, R. W. C.; Bazito, F. F. C.; Gruber, J. *Mater. Chem. Phys.* **2006**, *95*, 176.
[163] Benjamin, I.; Hong, H.; Avny, Y.; Davidov, D.; Neumann, R. *J. Mater. Chem.* **1998**, *8*, 919.
[164] Sun, H.; Liu, Z.; Hu, Y.; Wang, L.; Ma, D.; Jing, X.; Wang, F. *Journal of Polymer Science: Part A: Polymer Chemistry* **2004**, *42*, 2124.
[165] Yang, C.; Hou, J.; Zhang, B.; Zhang, S.; He, C.; Fang, H.; Ding, Y.; Ye, J.; Li, Y. *Macromol. Chem. Phys.* **2005**, *206*, 1311.
[166] Iraqi, A.; Mlynski, A.; Heard, A.; Walton, J. C.; Crayston, J. A. *Synthetic Metals* **1997**, *84*, 333.
[167] Wen, S.; Pei, J.; Zhou, Y.; Xue, L.; Xu, B.; Li, Y.; Tian, W. *Journal of Polymer Science: Part A: Polymer Chemistry* **2009**, *47*, 1003.
[168] Liang, Z.; Cabarcos, O. M.; Allara, D. L.; Wang, Q. *Adv. Mater.* **2004**, *16*, 823.
[169] Chan, E. W. L.; Lee, D. C.; Ng, M. K.; Wu, G. H.; Lee, K. Y. C.; Yu, L. P. *J. Am. Chem. Soc.* **2002**, *124*, 12238.
[170] Feng, J.; Zhang, Q.; Li, W.; Li, Y.; Yang, M.; Cao, Y. *Journal of Applied Polymer Science* **2008**, *109*, 2283.
[171] Van Severen, I.; Motmans, F.; Lutsen, L.; Cleij, T. J.; Vanderzande, D. *Polymer* **2005**, *46*, 5466.

[172] Qu, G.; Jiang, F.; Zhang, S.; Usuda, S. *Materials letters* **2007**, *61*, 3421.

Chapter 2

Synthesis of a platform copolymer (MDMO-CPM)-PPV for further post-polymerization functionalization

Chapter 2 presents the synthesis of a carboxylic acid-functionalized PPV derivative, copolymer (MDMO-CPM)-PPV, via the sulfinyl precursor route. Post-polymerization functionalization of this platform copolymer is done using an optimized DCC/DMAP-esterification method. This DCC/DMAP method is first optimized on a model compound. The method allows for the synthesis of complex ester-functionalized PPV-type copolymers bearing vinyl groups, propenylphenyl groups, propynylphenyl groups, methacrylate groups, atom transfer radical polymerization initiator groups, dithiocarbamate initiator groups and propargyl groups. The latter group can be utilized to perform "click" chemistry.

2.1. Introduction

As was already mentioned in **Chapter 1**, the properties of the conjugated PPV-type polymers synthesized *via* the sulfinyl precursor route are significantly improved as compared to those made with other precursor routes. This is a result of the fact that an asymmetric premonomer is formed, which allows full control over the entire polymerization procedure, although

it should be noted that the synthesis of the premonomers is more complex. Notwithstanding, in view of the enhanced purity of the conjugated polymers, the sulfinyl precursor route is used to synthesize all the different PPV derivatives made in this work.

This chapter describes the synthesis and characterization of a PPV derivative containing a functional group, which can be post-polymerization functionalized with virtually any other functional group. For this initial functional group to be directly attached to the PPV derivative, we have chosen for a carboxylic acid function. This carboxylic acid can react with a large number of other types of functional groups, which opens a broad window of opportunities for the post-polymerization functionalization step. Literature reports on PPV derivatives containing carboxylic acid functionalities are scarce and the starting (pre)monomers are usually not sulfinyl premonomers.[1-6] Only one example of a PPV derivative with carboxylic acid functionalities in the side-chain prepared *via* the sulfinyl precursor route has been reported in the literature.[7] This polymer was prepared in our group and the particular sulfinyl premonomer is also one of the two premonomers used for the new platform copolymer. It should be noted that this sulfinyl premonomer is bearing a methylester group, a protection group for the carboxylic acid, to avoid solubility problems and interference with the polymerization conditions of the sulfinyl precursor route. After synthesizing the conjugated PPV derivative, these methylester groups can be hydrolyzed to form the desired carboxylic acid groups. This deprotection can be seen as the first post-polymerization functionalization reaction. The homopolymer of this sulfinyl ester premonomer, after deprotection of the methylester group, is called poly(1,4-(2-(5-carboxypentyloxy)-5-methoxy phenylene) vinylene) (CPM-PPV) (Figure 2-1).

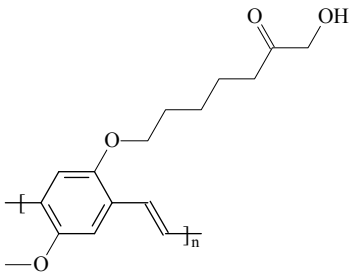

Figure 2-1 Chemical structure of poly(1,4-(2-(5-carboxypentyloxy)-5-methoxy phenylene) vinylene) (CPM-PPV)

To avoid possible solubility problems and especially to lower the amount of functionalities in the platform polymer, copolymers have been synthesized. This is important since the number of carboxylic acid functionalities in the homopolymer is too high to achieve a fully quantitative post-polymerization functionalization. This is especially the case when attaching large and complex functional molecules to the polymer. In addition, any unreacted carboxylic acid functions on the backbone of the PPV may cause unwanted interactions with other (bio)molecules. To this end, the sulfinyl premonomer of MDMO-PPV is chosen as a comonomer since MDMO-PPV (Figure 1-10) is one of the best studied representatives of the class of PPV-type materials and is therefore often used in polymer research and development. A copolymer was synthesized starting from the MDMO sulfinyl premonomer and the ester functionalized sulfinyl premonomer in a feed ratio of 9/1. This platform copolymer has an optimal composition to obtain sufficient solubility in a variety of common organic solvents. A higher built-in ratio of carboxylic acid groups results in a reduced solubility, which can hamper further functionalization in a reproducible manner.

As was already mentioned in **Chapter 1**, for the actual tailoring process of conjugated polymers a wide variety of methods can be found in the literature. Hitherto, a significant drawback is the lack of a universal approach, leading to a wide variety of methods and functionalization procedures to obtain specific functional materials. To avoid this drawback, after synthesizing a new platform copolymer, a methodology is optimized,

which allows for a wide variety of further functionalizations of this platform copolymer (MDMO-CPM)-PPV in a uniform manner. As mentioned above, the side-chains of (MDMO-CPM)-PPV consist of branched C_{10}-alkylchains and alkyl chains with carboxylic acid groups in a ratio of 9:1.

2.2. Synthesis and characterization of the sulfinyl premonomers

2.2.1. Synthesis and characterization of the MDMO sulfinyl premonomer

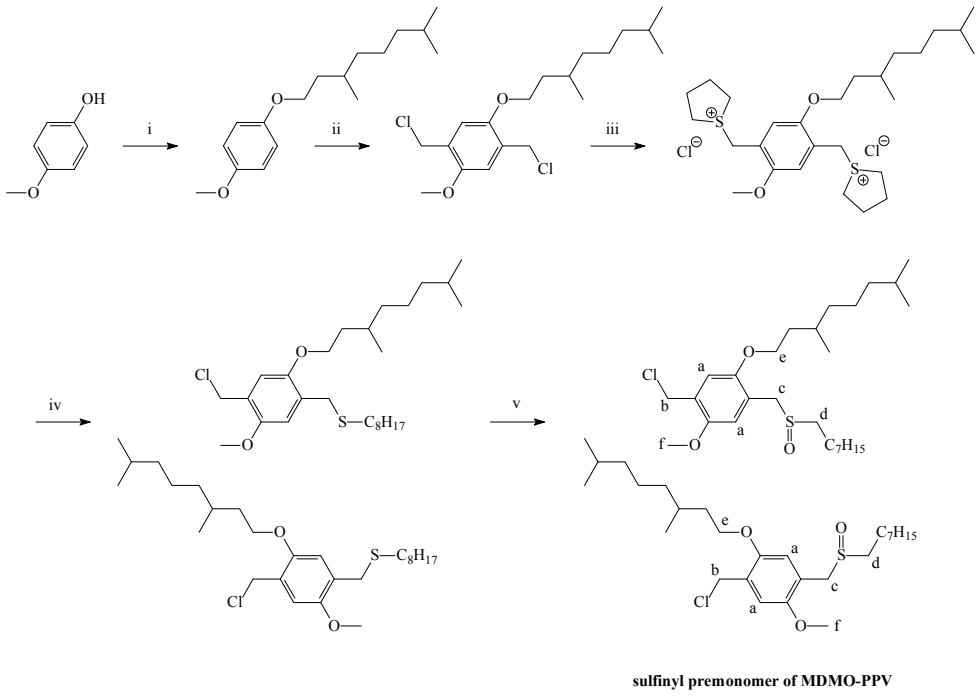

Scheme 2-1 Synthesis of the MDMO sulfinyl premonomer (i: NaO*t*Bu, 3,7-dimethyloctylchloride, NaI_{cat}, EtOH (reflux); ii: *p*-CH_2O, Ac_2O, HCl, 75 °C; iii: THT, MeOH, 50 °C; iv: $C_8H_{17}SH$, NaO*t*Bu, MeOH; v: H_2O_2, TeO_2, HCl_{cat}, 1,4-dioxane)

The synthesis of the MDMO sulfinyl premonomer, which is in reality a mixture of two compounds, *i.e.* 2-octylsulfinylmethyl-5-chloromethyl-1-(3,7-dimethyloctyloxy)-4-methoxybenzene and 5-octylsulfinylmethyl)-2-chloromethyl-1-(3,7-dimethyloctyloxy)-4-methoxybenzene, is presented in Scheme 2-1. The experimental details, used for synthesis of this premonomer, and the spectroscopic properties are identical to those reported in the literature.[8,9] The final sulfinyl premonomer of MDMO-PPV is obtained in excellent purity as can be seen in Figure 2-2, in which the ^{1}H-NMR spectrum is depicted. The most important peaks are correlated with the chemical structure of the sulfinyl premonomer of MDMO-PPV (Scheme 2-1).

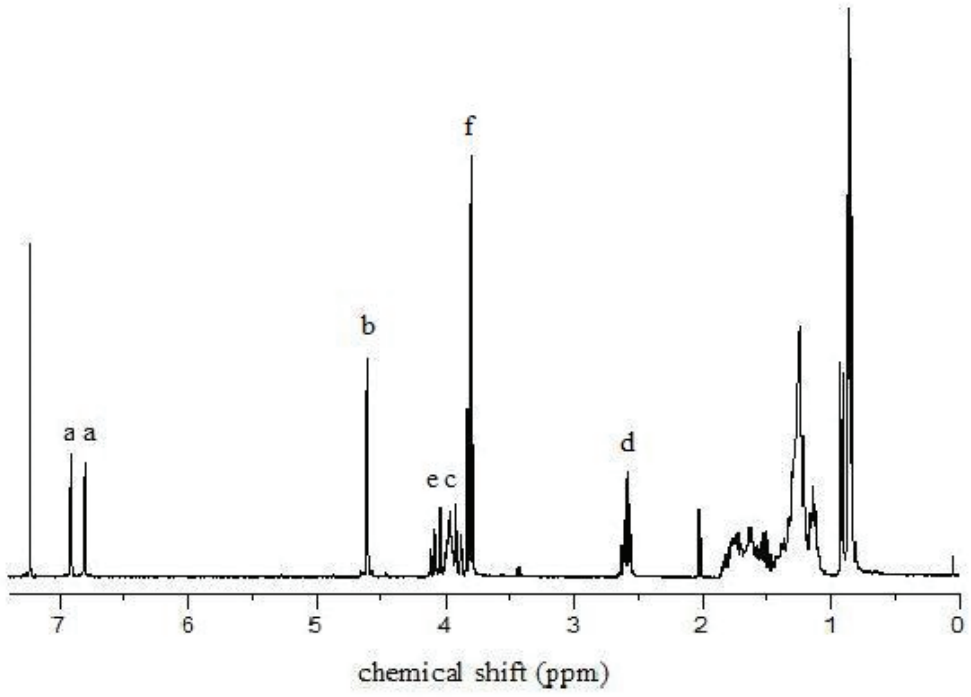

Figure 2-2 ^{1}H-NMR spectrum of the sulfinyl premonomer of MDMO-PPV recorded in $CDCl_3$ and assignment of the most important peaks

2.2.2. Synthesis and characterization of the ester sulfinyl premonomer

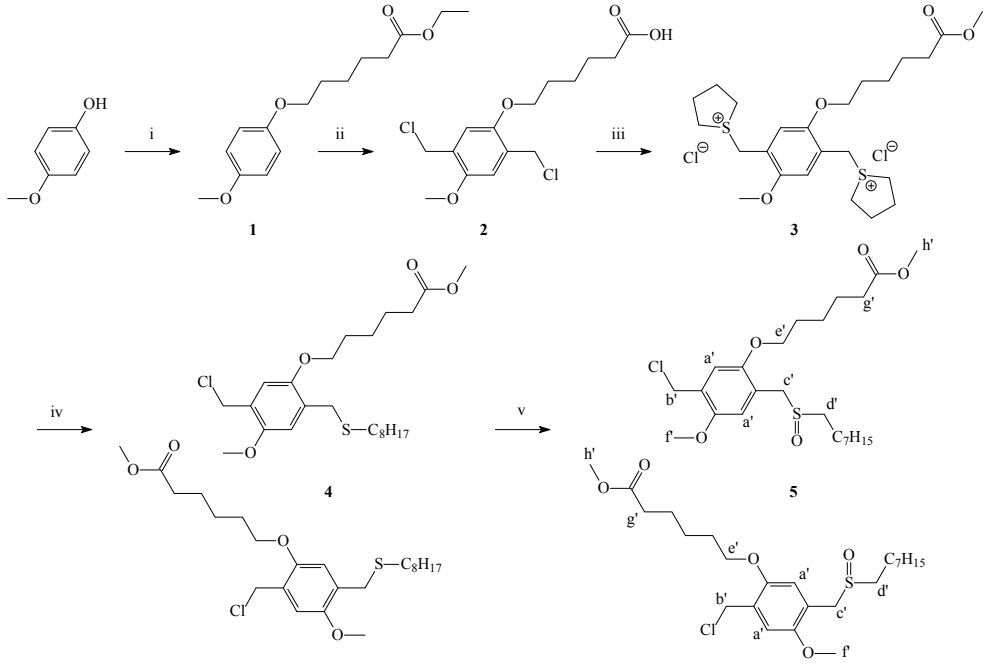

Scheme 2-2 Synthesis of the ester sulfinyl premonomer **5** (i: NaO*t*Bu, ethyl 6-bromohexanoate, NaI_{cat}, EtOH (reflux); ii: *p*-CH_2O, Ac_2O, HCl, 60 °C; iii: THT, MeOH, 50 °C; iv: $C_8H_{17}SH$, NaO*t*Bu, MeOH; v: H_2O_2, TeO_2, HCl_{cat}, 1,4-dioxane)

The ester functionalized premonomer **5**, *i.e.* the mixture of 6-(5-chloromethyl-4-methoxy-2-octylsulfinylmethyl-phenoxy)-hexanoic acid methyl ester and 6-(2-chloromethyl-4-methoxy-5-octylsulfinylmethyl-phenoxy)-hexanoic acid methyl ester, as well as all intermediates **1**, **2**, **3** and **4** are prepared *via* a modified literature procedure (Scheme 2-2).[7]

Premonomer **5** is prepared in a five step reaction according to Scheme 2-2. Starting with a Williamson etherification between 4-methoxyphenol and

ethyl-6-bromohexanoate, ester **1** is obtained, which is chloromethylated using concentrated HCl and formaldehyde in acetic anhydride giving **2**, according to a literature procedure.[6] Because of the acid conditions in this reaction, ester **1** converts into the corresponding carboxylic acid **2**. Subsequently, the bissulphonium salt **3** is synthesized by stirring **2** and THT in MeOH.[10] Under these reaction conditions, not only the bissolphonium salt **3** is formed, but also the carboxylic acid function of **2** is converted into the corresponding methyl ester **3**. The mono-substituted thio-ether **4** is formed by reaction of the symmetrical bissulfonium salt **3** with an equimolar amount of an alkylthiolate anion, followed by azeotropic removal of tetrahydrothiophene. As can be seen in Scheme 2-2, compound **4** is obtained as a mixture of regio-isomers in a ratio of 1/1. Finally, selective mono-oxidation should give the desired ester sulfinyl premonomer **5**, also in a 1/1 mixture of regio-isomers. Since this is the most crucial step in the premonomer synthesis, several literature procedures have been tested. Transformation of sulfide **4** into sulfoxide **5** has been tested with periodic acid (H_5IO_6) in acetonitrile[11], with aqueous H_2O_2 in phenol[12] and with aqueous H_2O_2 in 1,4-dioxane catalyzed with TeO_2 and HCl.[7] Purification of the first reaction is not possible due to the formation of a large amount of side-products, which cannot be separated from the desired product. The second reaction did not give any formation of the sulfoxide, only compound **4** is present in the reaction mixture. The conditions of the last reaction are most suitable and the ester sulfinyl premonomer **5** is obtained in excellent purity after two column chromatography purifications in CH_2Cl_2/MeOH 19/1 and EtOAc. The ^{1}H-NMR spectrum of **5** is presented in Figure 2-3 and the most important peaks are correlated with the chemical structure **5** (Scheme 2-2).

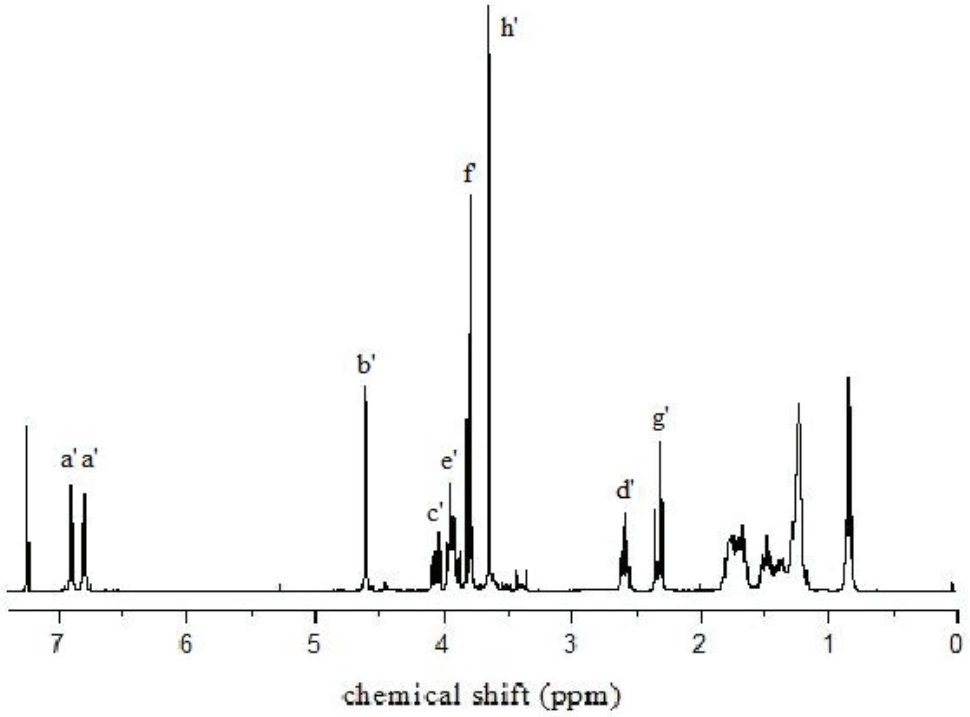

Figure 2-3 ^{1}H-NMR spectrum of the ester sulfinyl premonomer **5** recorded in $CDCl_3$ and assignment of the most important peaks

2.3. Synthesis and characterization of the platform copolymer (MDMO-CPM)-PPV

After both monomers, *i.e.* the sulfinyl premonomer of MDMO-PPV and the ester sulfinyl premonomer, are obtained in good purity, the polymerization towards the platform copolymer (MDMO-CPM)-PPV *via* the sulfinyl precursor route can be started.

Although both monomers are a mixture of regio-isomers (Scheme 2-1 and 2-2), for reasons of simplicity only one isomer is depicted in the general scheme of the synthesis of the platform copolymer (Scheme 2-3).

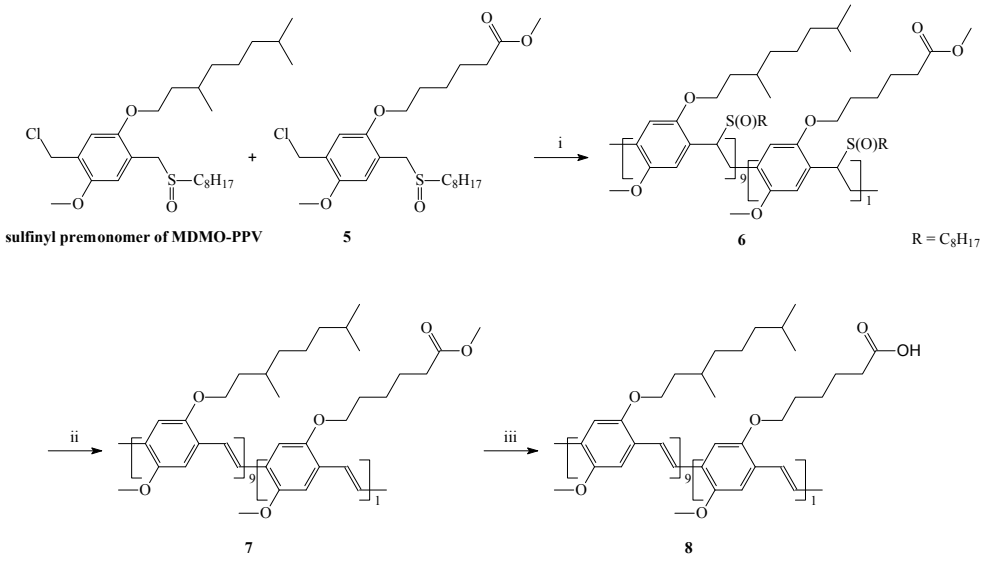

Scheme 2-3 Synthesis of the copolymer (MDMO-CPM)-PPV **8** *via* the sulfinyl precursor route (i: NaO*t*Bu, 2-BuOH, 30 °C; ii: toluene (reflux); iii: KO*t*Bu, H_2O, 1,4-dioxane (reflux))

2.3.1. Synthesis of the precursor copolymer

The copolymerization is performed in *sec*-BuOH according to the standard procedure of the sulfinyl precursor route (Scheme 2-3).[9] Polymerization takes place in a special designed setup (Figure 1-7). The premonomer solution (MDMO and ester in a feed-ratio of 9/1) and the base solution (NaO*t*Bu) are purged with a flow of nitrogen. After addition of the base solution, the polymerization reaction is allowed to proceed for 1h and the reaction temperature is maintained at 30 °C. The concentration of the premonomer is 0.02 M when the total amount of solvent (premonomer and base solution) is taken into account. Subsequently, the polymerization

mixture is poured into ice water, after which the resulting mixture is extracted with dichloromethane. After separation of the layers and evaporation under reduced pressure of the organic layer, the crude precursor polymer is obtained, which is used without further purification. An analytical SEC measurement of **6** is performed *versus* polystyrene standards using THF as the eluent. The observed molecular weight M_w is 1.5 x 10^5 g/mol (PD = 3.6), which confirms that a high molecular weight polymer is obtained (Table 2-1). FT-IR spectroscopy confirms that the ester side groups are not affected by the polymerizations conditions, since the signal at 1730 cm^{-1} remains unaffected. This observation is corroborated by ^{1}H-NMR spectroscopy data, which show that the singlet of the methyl ester group at 3.6 ppm remains visible.

Copolymer	M_w (g/mol)	PD = M_w/M_n	λ_{max} in THF (nm)
6	1.5 x 10^5	3.6	301
7	5.4 x 10^5	2.5	510
8	2.7 x 10^5	3.2	507

Table 2-1 Polymerization results for the precursor ester-functionalized copolymer **6**, the ester-functionalized conjugated copolymer **7** and the carboxylic acid-functionalized copolymer **8**. SEC measurements were performed *versus* polystyrene standards using THF as the eluent

2.3.2. Thermal conversion of the precursor copolymer to the conjugated structure

Thermal conversion of the precursor copolymer **6** gives the corresponding conjugated copolymer **7** after a two-step elimination procedure and purification in refluxing toluene (Scheme 2-3).[7] This conversion is readily visible with solution UV-Vis spectroscopy. Whereas the λ_{max} of the precursor copolymer **6** is 301 nm, the corresponding conjugated copolymer **7** has a red shifted λ_{max} at 510 nm (Table 2-1, Figure 2-4).

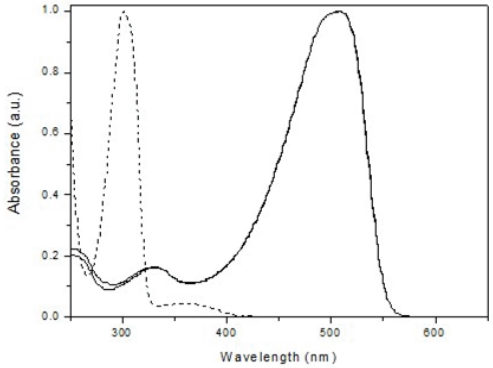

Figure 2-4 Solution UV-Vis absorption spectra of copolymers **6** (dashed), **7** (solid) and **8** (solid) in THF (the spectra of **7** and **8** are virtually indistinguishable from each other)

This elimination process of the sulfinyl groups of **6** in a thin film has been monitored by *in situ* UV-Vis absorption spectroscopy using a dynamic heating program of 2 °C/min from ambient temperature up to 146 °C under a continuous N_2 flow (Figure 2-5).

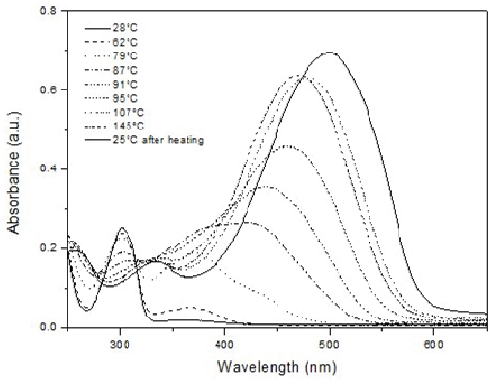

Figure 2-5 Thin film UV-Vis absorption spectroscopy of the gradual formation of the conjugated copolymer **7**

At room temperature, the thin film of **6** exhibits a strong absorbance with a maximum at λ_{max} = 301 nm. Upon heating, a new absorption band appears, which is associated with the conjugated system. At increasing temperatures, this band exhibits a gradual red shift (λ_{max} = 469 nm at 110 °C). After cooling down to room temperature, λ_{max} is even more red shifted to 510 nm as a result of a reversible thermochromic effect.[13] When the absorbance at this maximum wavelength is monitored *versus* temperature, it becomes evident that the conjugated structure starts to develop around 75 °C (Figure 2-6) and is complete around 110 °C. At temperatures above 110 °C, the absorption intensity at 510 nm starts to decrease as a result of the thermochromic effect.[13]

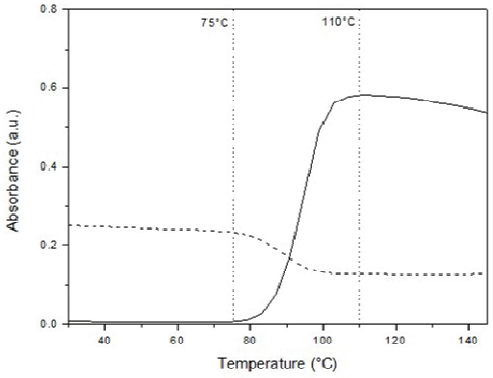

Figure 2-6 Absorbance at 301 nm (dashed) and 510 nm (solid) as a function of temperature

The observed molecular weight, M_w, for precursor copolymer **6** is 1.5 x 10^5 g/mol. The corresponding conjugated copolymer **7** has a somewhat higher M_w of 5.4 x 10^5 g/mol (Table 2-1). This apparent increase in molecular weight measured in THF solution using polystyrene standards can be explained by the significant differences in hydrodynamic volume, flexibility and polarity of the conjugated copolymer, as compared to the precursor copolymer. In reality, it can be assumed that a small decrease of the molecular weight occurs upon formation of the conjugated structure due to

the elimination of sulfinyl groups. Notwithstanding, the observed M_w values confirm that high molecular weight conjugated polymers are obtained.

Copolymer **7** is composed of the MDMO sulfinyl premonomer and the ester sulfinyl premonomer **5** in a feed-ratio of 9/1. The actual built in ratio can be determined *via* ^{1}H-NMR spectroscopy. The signals at 0.99 ppm are assigned to the CHC*H*$_3$ groups in the MDMO part of copolymer **7**. The triplet at 2.35 ppm originates from the C*H*$_2$COOCH$_3$ in the ester part of the copolymer. It is found that the ratio of the two comonomers built in is *circa* 9 % ester monomer and *circa* 91 % MDMO-monomer, which is in good agreement with the feed-ratio.

2.3.3. Hydrolysis of the ester function towards the platform copolymer (MDMO-CPM)-PPV

Hydrolysis of the ester group of copolymer **7**, using a base (KO*t*Bu in H_2O), gives copolymer **8** in excellent yield. Purification of **8** is not done by precipitating in a non-solvent, as described in the literature[7], but only *via* an extraction with 1 N HCl. This new procedure avoids that **8** becomes insoluble in any solvent, which is the case when the literature procedure was followed. Purification by extraction, makes the platform copolymer (MDMO-CPM)-PPV soluble in common organic solvents like $CHCl_3$, CH_2Cl_2 and THF.

The almost quantitative conversion could readily be observed using IR spectroscopy, in which the ν_{C-O} of the ester at 1733 cm^{-1} is shifted to a value of 1709 cm^{-1} for the corresponding carboxylic acid (Figure 2-7). This is also confirmed *via* ^{1}H-NMR spectroscopy, where the peak of the methylester CH$_2$COOC*H*$_3$ at 3.63 ppm has completely disappeared for copolymer **8**. The UV-Vis absorption spectrum of copolymer **8** is almost identical to that of copolymer **7** (Table 2-1, Figure 2-4), indicating that no significant degradation of the conjugated system occurs upon hydrolyzing the ester functionalities. The M_w value for **8** is 2.7 x 10^5 g/mol, which is also in the same order of magnitude as copolymer **7** (Table 2-1).

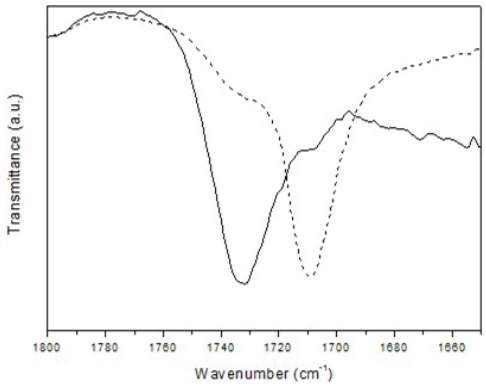

Figure 2-7 Thin film FT-IR spectroscopy of the conjugated copolymers with ester function **7** (solid) and with carboxylic acid function **8** (dashed)

2.3.4. Study of the thermal stability of the platform copolymer (MDMO-CPM)-PPV

To obtain more information about the thermal stability of the conjugated system of **8**, an *in situ* UV-Vis heating experiment is performed. To this end, a thin film of **8** is heated using a dynamic heating program at 2 °C/min from ambient temperature up to 120 °C and subsequently cooled down to room temperature. In the next run, the sample is heated to 140 °C and subsequently cooled down. This sequence is repeated up to 240 °C (Figure 2-8). After each heating ramp, the film of **8** is cooled down to 25 °C and a UV-Vis absorption spectrum is taken at that temperature (Figure 2-9).

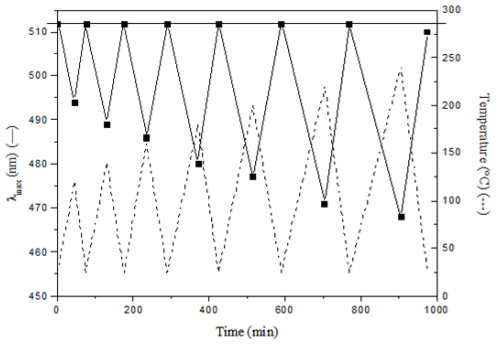

Figure 2-8 Plot demonstrating the dynamic heating program (dashed) and the absorption maximum as a function of time and temperature (solid)

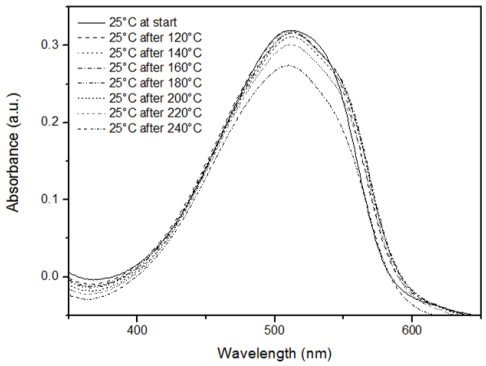

Figure 2-9 Individual thin film UV-Vis absorption spectra of **8** at room temperature after using a dynamic heating program

The absorption maximum (λ_{max}) measured of **8** in film at room temperature is 512 nm. By heating **8** the effective conjugation length decreases *e.g.* when **8** is heated up to 120 °C, the λ_{max} is shifted from 512 nm to 496 nm. However, after subsequent cooling to 25 °C, the conjugated system is fully recovered and again a λ_{max} of 512 nm is observed. This thermochromic effect can also be observed during the heating at higher temperatures. Up to temperatures of 220 °C, the original λ_{max} is fully recovered upon cooling to 25 °C. In contrast, after heating at a temperature of 240 °C, a small blue-

shift (λ_{max} = 510 nm) is observed after cooling to 25 °C. This demonstrates that the heating process is no longer reversible, indicating that the onset of degradation of the conjugated system occurs around this temperature. Apparently, the effect on the thermal stability of the 9 % built in carboxylic acid functionalizations is negligible, since a similar stability is observed as was previously found for MDMO-PPV.[8]

In conclusion, copolymer **8** is an excellent platform for further functionalization steps. In addition, it is soluble in common organic solvents like $CHCl_3$, CH_2Cl_2 and THF. Post-functionalization of the carboxylic acid groups of copolymer **8** can therefore be investigated.

2.4. Post-polymerization functionalization of the platform copolymer (MDMO-CPM)-PPV towards complex ester-functionalized PPV-type copolymers

2.4.1. Possible ways of post-polymerization functionalization of the platform copolymer (MDMO-CPM)-PPV

Functionalization of the carboxylic acid function can be done in several possible ways. Especially the formation of an amide bond is an interesting option to introduce functionality (Scheme 2-3). This chemical bond has several advantages. For example, it is resistant towards hydrolysis (*i.e.* it is chemically stable) in a broad range of conditions. This robustness can be of importance in applications like (bio)sensors. An amide bond is generally obtained by reaction of a carboxylic acid with an amine. Since a very broad range of amines is available (commercially or by synthesis), post-polymerization functionalization of PPV derivatives with a wide variety of different molecules should be possible.

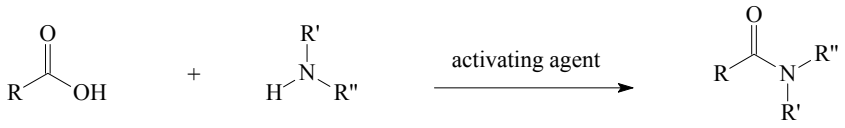

Scheme 2-3 Formation of an amide bond from a carboxylic acid with the use of an activating agent

One of the most widely used reagents for such a functionalization is 1-ethyl-3-(3-dimethylaminopropyl) carbodiimide (EDC) (Figure 2-10). EDC is water soluble allowing for aqueous coupling reactions, which is very interesting to link biomolecules. Examples can be found in the literature, such as the linking of DNA to films of poly(ethylene-co-acrylic-acid)[14] and the anchoring of an enzyme to polypyrrole films modified with acrylic acid.[15] Notwithstanding, EDC has also some drawbacks. During the reaction, a reactive intermediate is formed, which is sensitive to hydrolysis. This can be troublesome, since when performing the reaction in water, hydrolysis can occur, which gives back the acid. In order to circumvent this drawback another reagent has been reported in the literature, *i.e.* 4-(4,6-dimethoxy-1,3,5-triazin-2-yl)-4-methylmorpholinium chloride (DMT-MM) (Figure 2-10).[16]

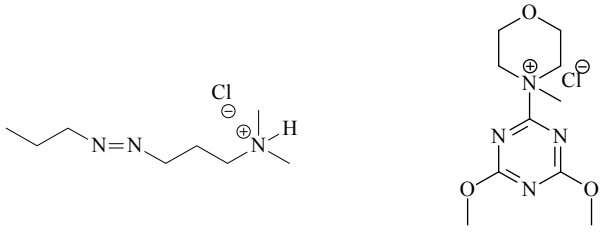

EDC DMT-MM

Figure 2-10 Chemical structure of 1-ethyl-3-(3-dimethylaminopropyl) carbodiimide (EDC) and 4-(4,6-dimethoxy-1,3,5-triazin-2-yl)-4-methylmorpholinium chloride (DMT-MM)

This reagent is also water soluble and the reaction is not affected by water. While this reagent has proven its efficiency in synthesizing amides, it is only very recently that it was applied to post-polymerization functionalization of poly-acrylic acid polymers.[17] Indeed, good and reproducible results are obtained by using DMT-MM for functionalization of a model compound with allyl and propargyl amine. However, translating this procedure to the conjugated polymer gave no full functionalization of the carboxylic acid and also no reproducible results, even at reaction times of well over 100 hours.

2.4.2. DCC/DMAP-esterification method

As an alternative to the amide bond, the formation of an ester bond has been used to introduce functionality into PPV derivatives (Scheme 2-4). This ester bond is made by reaction between a carboxylic acid and an alcohol. Also in this case, a very broad range of alcohols are commercially available or by synthesis and post-polymerization functionalization of PPV derivatives can be done with a wide variety of different molecules.

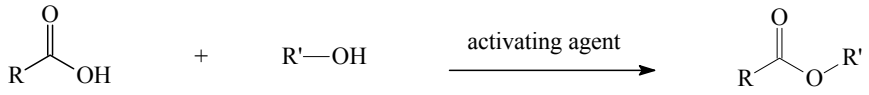

Scheme 2-4 Formation of an ester bond from a carboxylic acid with the use of an activating agent

The formation of an ester bond by reaction between a carboxylic acid and an alcohol can be performed in several different ways. A well known method is the Steglich esterification.[18,19] This coupling reaction is a mild one pot esterification method. The carboxylic acid groups are converted *in situ* by N,N-dicyclohexylcarbodiimide (DCC) to an anhydride functionality that can react with an alcohol to the corresponding ester. This reaction takes place at

room temperature and under neutral conditions. Addition of a catalytic amount of N,N-dimethyl-4-aminopyridine (DMAP) accelerates the DCC-activated esterification of carboxylic acids with alcohols to such an extent that formation of side products is suppressed. The so-called DCC/DMAP-esterification method gives good yields, even at room temperature. The DCC/DMAP-esterification method or Steglich esterification is schematically represented in Scheme 2-5.

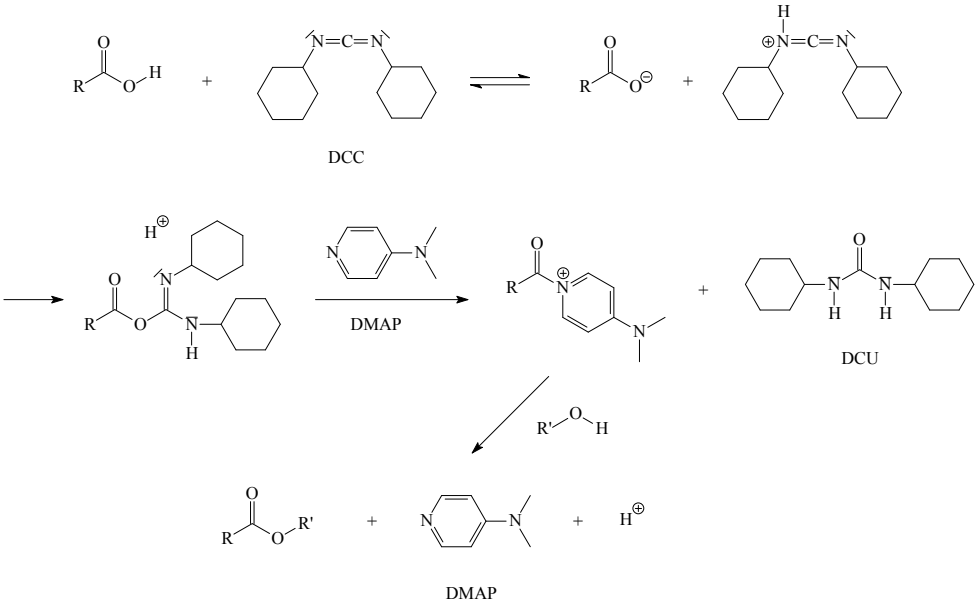

Scheme 2-5 Schematic representation of the DCC/DMAP-esterification method

2.4.3. Optimizing of the DCC/DMAP-esterification method for the functionalization of a model compound

With copolymer **8** being readily available, post-polymerization functionalizations become possible. However, since the optimization of the reaction conditions on a conjugated polymer is not straightforward due to

synthetic and analytical limitations, first a model compound is prepared on which the reaction conditions are tested. Model compound **9** is obtained *via* a simple hydrolysis of the ester group of **1** using a base (KO*t*Bu in H_2O) (Scheme 2-6). The carboxylic acid function of **9** readily reacts with alcohol-functionalized molecules *via* an optimized DCC/DMAP-method to the corresponding esters. These esterification reactions are conducted in dry CH_2Cl_2 under nitrogen atmosphere. To a solution of **9** and the respective alcohol-functionalized reagent, DCC and DMAP are added as effective esterification promoting reagents. The reaction is allowed to proceed for 1 h at 0 °C and for an additional 24 h at room temperature. Dicyclohexylurea (DCU) is filtered off and purification of the crude product is done by column chromatography.

The model compound reaction is tested with six hydroxyl-bearing compounds giving **10**, **11**, **12**, **13**, **14** and **17** (Scheme 2-6). Alcohol **16** is synthesized by a reduction of 4-chloromethyl benzoic acid with $BH_3 \cdot THF$.[20] The propargyl group of **14** can be used to attach a desired molecule, with an azide group, *via* "click" chemistry. The working principle and all the different components of the "click" method are discussed in **Chapter 4**. This "click" method is tested with an azide-functionalized reagent, *i.e.* azidomethyl phenyl sulfide, to form compound **15** with the help of PMDETA and Cu(I)Br (Scheme 2-6). Compound **17**, containing an ATRP initiator group, is also further functionalized to form compound **18**, containing a benzyl dithiocarbamate initiator group (Scheme 2-6). Purification of **15** and **17** is also done by column chromatography. Compounds **9**, **10**, **11**, **12**, **13**, **14**, **15**, **16**, **17** and **18** are all characterized with ^{1}H-NMR, ^{13}C-NMR, FT-IR and mass spectroscopy and are pure.

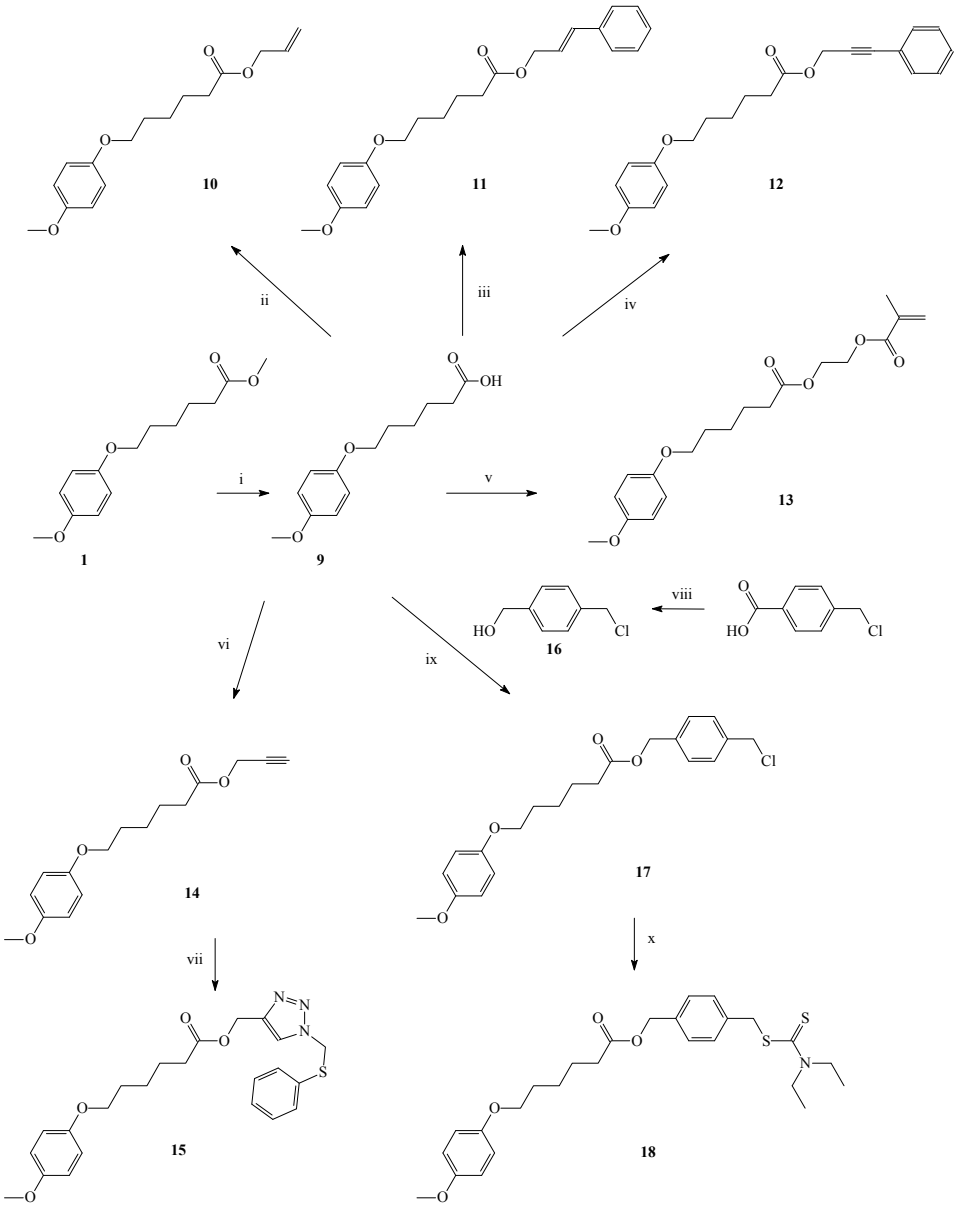

Scheme 2-6 Synthesis of model compound **9** and further functionalizations towards compounds **10**-**18** (i: KO*t*Bu, H_2O, MeOH, 50 °C; ii: "DCC, DMAP, CH_2Cl_2", allylalcohol; iii: "…", cinnamyl alcohol; iv: "…", 3-phenyl-2-propyn-1-ol; v: "…", 2-hydroxyethyl-methacrylate; vi: "…", propargylalcohol; vii: PMDETA, Cu(I)Br, azidomethyl phenyl sulfide, THF; viii: $BH_3 \cdot THF$, THF; ix: "…"; x: sodium diethyldithiocarbamate trihydrate, THF)

In this way, model compound **9** is functionalized with a vinyl group (**10**), a propenylphenyl group (**11**), a propynylphenyl group (**12**), an acrylate group (**13**), a propargyl group (**14**), allowing the introduction of "click" chemistry (**15**) and finally an ATRP and benzyl dithiocarbamate initiator group is introduced (**17** and **18**), which allow for further grafting. The next step is to translate this procedure of functionalization to the platform copolymer (MDMO-CPM)-PPV **8**.

2.4.4. Translation of the optimized DCC/DMAP-esterification reaction for post-polymerization functionalization of the platform copolymer (MDMO-CPM)-PPV towards complex ester-functionalized PPV-type copolymers

The introduction of different functional groups is optimized for the conversion of model compound **9** to **10**, **11**, **12**, **13**, **14**, **15**, **17** and **18**. Subsequently, the reaction is translated to the platform copolymer (MDMO-CPM)-PPV **8**. These esterification reactions also take place in dry CH_2Cl_2 under nitrogen atmosphere and protected from light. To a solution of **8** and the respective alcohol-functionalized reagent, DCC and DMAP are added drop wise. The reaction is allowed to proceed for 1 h at 0 °C and for an additional 24 h at room temperature. The solutions are precipitated drop wise in a non-solvent. The functionalized copolymers **19**, **20**, **21**, **22**, **23** and **25** (Scheme 2-7) are filtered off, washed and dried under reduced pressure. "Click" chemistry is also tested on copolymer **23**. Azidomethyl phenyl sulfide is "clicked" to the propargyl group of **23** with the help of PMDETA and Cu(I)Br to form copolymer **24** (Scheme 2-7). Copolymer **25**, containing an ATRP initiator group, is also further functionalized to form copolymer **26**, containing a benzyl dithiocarbamate initiator group (Scheme 2-7). Purification of **24** and **26** is also done by precipitating in a non-solvent, filtering off, washing and drying under reduced pressure.

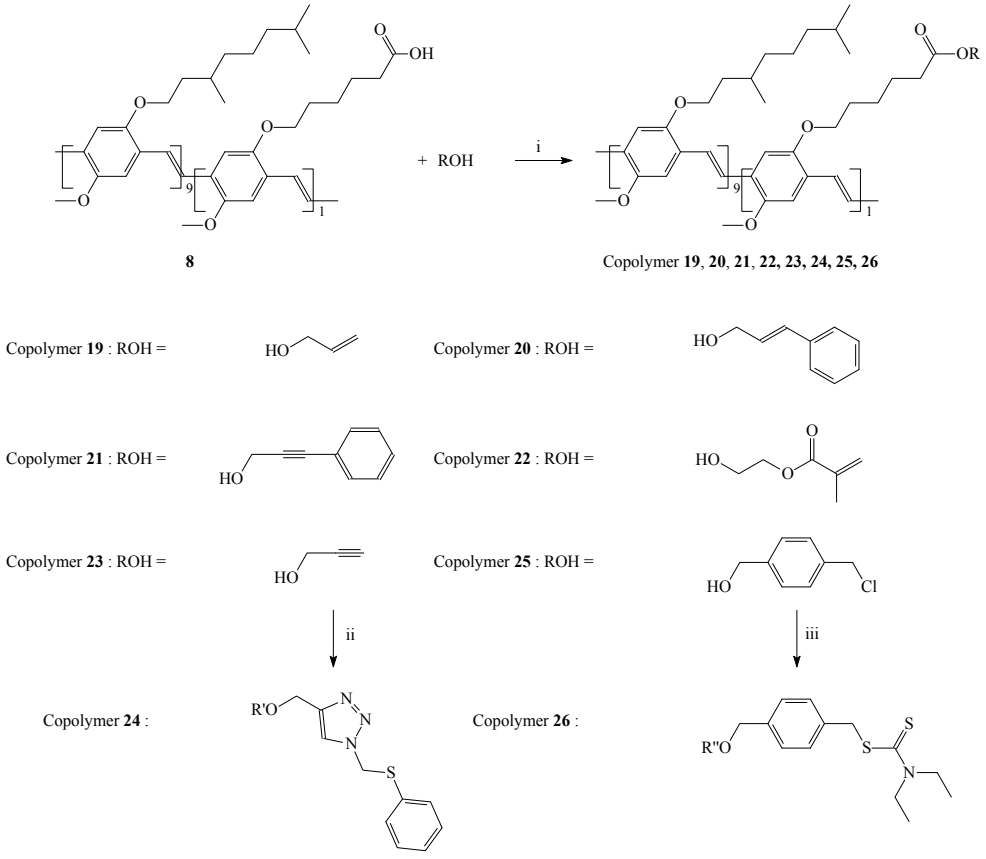

Scheme 2-7 Synthesis of **19-26** *via* the optimized DCC/DMAP-procedure (i: DCC, DMAP, CH_2Cl_2; ii: PMDETA, Cu(I)Br, azidomethyl phenyl sulfide, THF; iii: sodium diethyldithiocarbamate trihydrate, THF)

The successful conversions on the conjugated copolymer are clearly visible in the ^{1}H-NMR spectra. All the characteristic peaks for the attached substituents, which are present in the model compound functionalization, are also present in the post-polymerization functionalized copolymers **19**, **20**, **21**, **22**, **23**, **24**, **25** and **26**. The integration of the signals is consistent with a quantitative conversion of the carboxylic acid to the corresponding ester.

The different functionalizations of platform copolymer **8** are further confirmed by FT-IR spectroscopy (Figure 2-11). The carbonyl vibration at 1709 cm^{-1} of the carboxylic acid shifts to higher frequency due to the formation of the ester bond. FT-IR spectra corroborate the full conversion of the carboxylic acid functionalities.

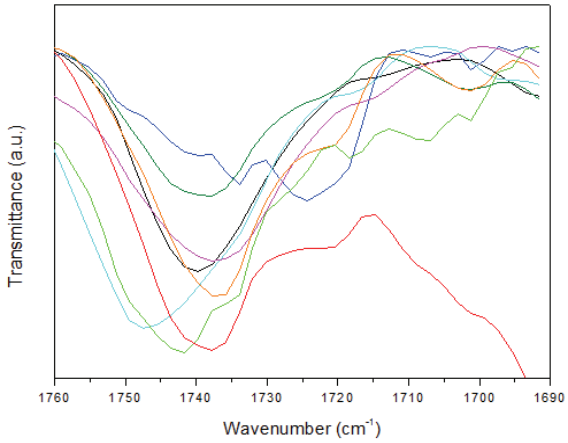

Figure 2-11 FT-IR spectra of copolymers **19**, **20**, **21**, **22**, **23**, **24**, **25** and **26**

To investigate the effect of the post-polymerization functionalization procedures on the physical properties of the functionalized copolymers, the molecular weights of the different copolymers **19-26** are compared (Table 2-2).

Copolymer	M_w (g/mol)	PD = M_w/M_n	λ_{max} in THF (nm)
6	1.5×10^5	3.6	301
7	5.4×10^5	2.5	510
8	2.7×10^5	3.2	507
19	2.4×10^5	4.3	504
20	4.5×10^5	5.8	508
21	3.0×10^5	4.9	511
22	4.6×10^5	5.6	508
23	3.8×10^5	5.2	507
24	3.6×10^5	3.7	509
25	3.1×10^5	4.7	507
26	3.2×10^5	4.6	507

Table 2-2 Polymerization results for the precursor ester-functionalized copolymer **6**, the ester-functionalized conjugated copolymer **7**, the carboxylic acid-functionalized copolymer **8** and the post-polymerization functionalized copolymers **19**, **20**, **21**, **22**, **23**, **24**, **25** and **26**. SEC measurements were performed *versus* polystyrene standards using THF as eluent

The observed M_w values in THF solution using polystyrene standards range from 2.4×10^5 g/mol to 4.6×10^5 g/mol, which is comparable to the platform copolymer (MDMO-CPM)-PPV **8** which has a M_w value of 2.7×10^5 g/mol. Apparently, no significant decrease in the average molecular weight occurs during the substitution reactions. It should be noted that there is a moderate increase in the polydispersity upon functionalization. Whereas copolymer **8** has a polydispersity value of 3.2, for copolymers **19-26** the polydispersity values range between 3.7-5.8, reflecting a broadening of the molecular weight distributions.

The quality of the conjugated system is further confirmed using UV-Vis measurements in THF for all copolymers prepared. As can be seen in Table 2-2, the peak positions (λ_{max}) of the π-π^* transitions of the post-functionalized copolymers **19-26** are all positioned between 503 and 511 nm. This is the same spectral region as the transition observed for

copolymer **8** (λ_{max} = 507 nm). In addition to the peak positions, also the shapes of the UV-Vis absorption spectra are identical (Figure 2-12).

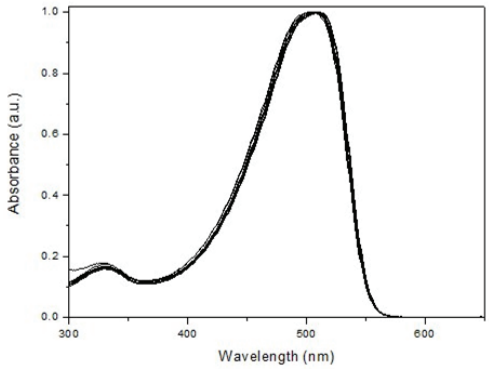

Figure 2-12 Solution UV-Vis absorption spectra of the carboxylic acid-functionalized copolymer **8** and all post-polymerization functionalized copolymers **19**, **20**, **21**, **22**, **23**, **24**, **25** and **26** in THF (all solid) (no significant changes are observed upon functionalization)

Apparently, the post-polymerization procedures have no significant impact on the quality of the conjugated system, further confirming the suitability of our approach as a general method to obtain advanced functional conjugated polymers for device applications.

2.5. Motivation for the selected post-polymerization functionalizations

A variety of functional groups has been introduced. The functional groups have been selected in such a way, that the resulting functional PPV-derivatives can be applied in a variety of optical and electronic applications

in the future. This section intends to give a brief overview of the potential application areas of these novel functional conjugated polymers.

Introducing vinyl groups into PPV derivatives (**19**) presents an alternative way to obtain cross-linkable polymeric materials. The vinyl group shows more flexible characteristics and can be cross-linked by photo-irradiation with or without initiators, or simply by heating. It has been reported that the introduction of vinyl groups in the side chain of PPV changes the electrochemical behavior compared with other PPV derivatives. For example, this post-treatable conjugated copolymer can be used to make multilayer light-emitting diodes or photovoltaic cells.[21,22] In addition to the vinyl groups, a number of similar functionalities with application potential have been introduced onto copolymer **8**. Examples of such a functionalities are propenylphenyl (**20**) and propynylphenyl groups (**21**). These types of groups can be cross-linked by UV irradiation and/or thermal treatment, allowing a potential fixation of device morphology. This in turn can improve the stability of these devices, which for example can be useful to obtain stabilized hole-transporting layers in light-emitting devices.[23-26]

Another example of an interesting functionality, which has been introduced, is an acrylate group (**22**). By introducing an ultrathin layer of poly(methyl methacrylate) (PMMA) between a hole injection layer, polyethylenedioxythiophenne:polystyrenesulfonate (PEDOT:PSS) and an emitting layer, PPV, the electroluminescence efficiency for polymer light-emitting diodes can improve significantly.[27-30] This improvement in device performance is due to the decrease of hole injection and the promotion of electron injection, which creates a better balanced distribution of the charge carriers within the emitting layer. To increase the stability of this device configuration, a covalent bond between the conjugated polymer and the PMMA may be desirable. Covalently linking the PMMA layer on the PPV can be done by attaching a methacrylate group to copolymer **8**. This group can participate in a radical polymerization reaction with other methacrylate monomers to form a PMMA layer.

By functionalizing copolymer **8** with a propargyl group (**23**), “click” chemistry can be used to attach a desired molecule with an azide group to

the conjugated copolymer. In this way the conjugated copolymer can be covalently linked with a wide variety of functional organic molecules.[31-35] In addition, it may introduce the possibility of connecting two polymers with each other, to obtain block copolymers.[35]

Copolymers **19**, **20**, **21**, **22** and **23** have been used in the preparation of solar cells. In this way the influence of the functional groups on the optical and electronic properties can be tested as compared to the base polymer MDMO-PPV. This study is described in **Chapter 3**. Copolymer **23**, with a propargyl group, is also used to attach phthalocyanine molecules to PPV-derivatives. The results of this study are outlined in **Chapter 4**.

The final two examples introduce the possibility to graft polymer chains onto the PPV backbone. Grafting of the PPV backbone can be done by introducing initiator groups into the side-chain of the PPV. Two types of initiator groups have been introduced, *i.e.* ATRP initiator groups (**25**) and benzyl dithiocarbamate initiator groups (**26**). Both groups can initiate polymerizations, which belong to the class of "pseudo" living radical polymerizations. Hence, a controlled radical reaction can be started directly at the substituents of the PPV chain. This gives the opportunity to functionalize the PPV with different oligomeric or polymeric side chains,[28,35-37] which can be used to develop advanced materials for chemical sensing, drug delivery, catalysis and micropatterning.[38-40] A typical ATRP initiator group was introduced to copolymer **8** in a straightforward manner, giving copolymer **25** with chloromethylphenyl groups. Subsequently, the chloromethyl groups of **25** have also been converted to dithiocarbamate initiator groups, giving copolymer **26**. Both copolymers **25** and **26** are potentially capable of initiating "living" polymerizations, which is discussed in detail in **Chapter 5**.

2.6. Conclusions

In conclusion, a new copolymer (MDMO-CPM)-PPV **8** has been developed, which can be used as a platform for further post-polymerization functionalization. Copolymer **8** is prepared *via* the sulfinyl precursor route from the MDMO sulfinyl premonomer as well as the ester sulfinyl premonomer **5** in a ratio of 9/1. After a double thermal conversion of the precursor copolymer **6**, the conjugated copolymer **7** is quantitatively hydrolyzed to the platform copolymer **8**. This copolymer is soluble in common organic solvents, such as $CHCl_3$, CH_2Cl_2 and THF. It has been fully characterized using different analytical techniques. Post-polymerization functionalization of the acid group of copolymer **8** is done *via* an optimized DCC/DMAP-procedure with the desired alcohol. This procedure is first tested and optimized for model compounds, after which it is utilized to functionalize copolymer **8**. In this way, copolymer **8** is post-functionalized with a variety of functional groups, which can be regarded as representative examples. PPV-copolymers are prepared with vinyl groups, propenylphenyl groups, propynylphenyl groups, methacrylate groups, ATRP initiator groups, benzyl dithiocarbamate initiator groups and propargyl groups. The latter group can be utilized to do "click" chemistry, which is demonstrated with an azide-functionalized reagent, *i.e.* azidomethyl phenyl sulfide.

In all cases, FT-IR and ^{1}H-NMR are consistent with a quantitative conversion of the functional groups. Furthermore, spectroscopic data and SEC measurements indicate that no substantial degradation of the conjugated system occurs even after consecutive post-polymerization functionalization reactions. This demonstrates the versatility of the developed universal functionalization methodology, which is not only of interest to functionalize PPV-type materials, but can also be utilized on other conjugated polymer systems. This allows for the development of many new and exciting applications, some of which are demonstrated in the next chapters.

2.7. Experimental section

2.7.1. Chemical and optical characterization

NMR spectra were recorded with a Varian Inova Spectrometer (^{1}H-NMR 300 MHz, ^{13}C-NMR 75 MHz). Analytical Size Exclusion Chromatography (SEC) was performed using a Spectra series P100 (Spectra Physics) pump equipped with a pre-column (5 μm, 50 x 7.5 mm, guard, Polymer Labs) and two mixed-B columns (10 μm, 2 x 300 x 7.5 mm, Polymer Labs) and a Refractive Index detector (Shodex) at 40 °C. THF was used as the eluent at a flow rate of 1.0 mL/min. Molecular weight distributions are given relative to polystyrene standards. Gas chromatography/mass spectrometry (GC/MS) analyses were carried out on TSQ-70 and Voyager mass spectrometers (Thermoquest); the capillary column was a Chrompack Cpsil5CB or Cpsil8CB. DIP-MS measurements were performed at a heating rate of 10 °C/min up to 600 °C. In this technique the material is brought directly on the heating element of the probe as a thin film and this enables to study the products that are liberated in the high vacuum (4 x 10^{-4} Pa) inside the spectrometer. Liberated products were ionized by electron impact. FT-IR spectra were collected with a Perkin Elmer Spectrum One FT-IR spectrometer (nominal resolution 4 cm^{-1}, summation of 16 scans). UV-Vis measurements were performed on a Cary 500 UV-Vis-NIR spectrophotometer (scan rate 600 nm/min, continuous run from 200 to 800 nm).

2.7.2. Chemicals

Unless stated otherwise, all reagents and chemicals were obtained from commercial sources and used without further purification. PMDETA was distilled under vacuum. Cu(I)Br was purified by stirring in acetic acid for 24 h, to reduce Cu(II) to Cu(I). Subsequently, Cu(I)Br was filtered off and

washed with ethanol and diethyl ether to remove Cu(II)Br_2 and acetic acid, after which it was dried in a vacuum oven at 75 °C. The MDMO premonomer was synthesized as described elsewhere.[8,9]

2.7.3. Synthesis

- **Ester sulfinyl premonomer**

6-(4-methoxy-phenoxy)-hexanoic acid ethyl ester 1. A mixture of 4-methoxyphenol (46.36 g, 373.5 mmol), NaO*t*Bu (43.07 g, 448.2 mmol) and EtOH (375 mL) was stirred for 1 h at room temperature under N_2 atmosphere, after which ethyl 6-bromohexanoate (32.1 g, 448.2 mmol) and NaI (1.5 g, 10 mmol) were added. The resulting solution was stirred for 4 h at reflux temperature and then overnight at 50 °C under N_2 atmosphere. The reaction was quenched with water (400 mL), and extracted with CH_2Cl_2 (3 x 200 mL). The combined organic extracts were dried over anhydrous $MgSO_4$. Evaporation of the solvent under reduced pressure gave the crude product as a brown oil. The pure product was obtained, by column chromatography (SiO_2, eluent CH_2Cl_2/MeOH 95/5) and afterwards mixed-solvent crystallizations from MeOH and hexane, as a colorless oil (78.6 g, 79 % yield). ^{1}H-NMR ($CDCl_3$): δ = 6.80 (s,4H), 4.10 (q,2H), 3.88 (t,2H), 3.74 (s,3H), 2.30 (t,2H), 1.75 (m, 2H), 1.67 (m, 2H), 1.47 (m, 2H), 1.23 (t, 3H).

6-(2,5-bis-chloromethyl-4-methoxy-phenoxy)-hexanoic acid 2. To a stirred mixture of **1** (20 g, 75.6 mmol) and *p*-formaldehyde (6.2 g, 207 mmol) at 0 °C under N_2 atmosphere, concentrated HCl (48.03 g, 487.5 mmol) was added drop wise. Subsequently, acetic anhydride (76.56 g, 756 mmol) was added at such a rate that the temperature did not exceed 70 °C. After the addition was complete, the resulting solution was stirred at 60 °C for 10 h after which it was cooled down to room temperature and poured into water (200 mL). The resulting precipitate was filtered off, redissolved in CH_2Cl_2 (200 mL) and dried over anhydrous $MgSO_4$. Evaporation of the

solvent under reduced pressure gave the crude product. The pure carboxylic acid was obtained by crystallization from EtOAc as a white solid (22.42 g, 89 % yield). ^{1}H-NMR ($CDCl_3$): δ = 6.89+6.88 (2s, 2H), 4.61+4.60 (2s, 4H), 3.97 (t, 2H), 3.83 (s, 3H), 2.39 (t, 2H), 1.81 (m, 2H), 1.72 (m, 2H), 1.58 (m, 2H).

Bis-tetrahydrothiophenium salt of 6-(2,5-bis-chloromethyl-4-methoxy-phenoxy)-hexanoic acid methyl ester 3. To a solution of **2** (22.24 g, 69.9mmol) in MeOH (220 mL) tretrahydrothiophene (23.598 g, 267.6mmol) was added. The mixture was allowed to react for 24 h at 50 °C, after which the total volume was reduced to 100 mL by evaporation at room temperature. Subsequently the product was precipitated in cold diethyl ether (1 L) after which the bissulfonium salt was filtered off and washed with cold diethyl ether. The resulting pure product was a white solid (22.84 g, 65 % yield). ^{1}H-NMR (D_2O): δ = 7.12+7.11 (2s, 2H), 4.44+4.43 (2s, 4H), 4.03 (t, 2H), 3.80 (s, 3H), 3.57 (s, 3H), 3.40 (m, 8H), 2.32 (t, 2H), 2.24 (m, 8H), 1.75 (m, 2H), 1.59 (m, 2H), 1.42 (m, 2H).

6-(5-chloromethyl-4-methoxy-2-octylsulfanylmethyl-phenoxy)-hexanoic acid methyl ester and 6-(2-chloromethyl-4-methoxy-5-octylsulfanylmethyl-phenoxy)-hexanoic acid methyl ester 4. A mixture of *n*-octane thiol (1.346 g, 9.2 mmol) and NaO*t*Bu (0.884 g, 9.2 mmol) in MeOH (50 mL) was stirred for 30 min at room temperature after which a clear solution was obtained. This solution was added drop wise to a solution of **3** (5 g, 9.2 mmol) in MeOH (150 mL) under N_2 atmosphere. The reaction mixture was stirred for 2 h after which it was concentrated under reduced pressure at 40 °C. Subsequently, *n*-octane (125 mL) was added and evaporated again to remove the tetrahydrothiophene. This sequence was repeated three times. After removal of the solvents under reduced pressure, the residue was redissolved in CH_2Cl_2 (125 mL) and the organic layer was extracted with water (3 x 150 mL). The organic layer was dried over anhydrous $MgSO_4$. Evaporation of the solvent gave the crude product, as a yellow oil. ^{1}H-NMR ($CDCl_3$): δ = 6.90+6.88+6.84+6.82 (4s, 2H), 4.61+4.60 (2s, 2H), 3.94 (m, 2H), 3.83+3.81 (2s, 3H), 3.69+3.68 (2s, 2H), 3.65 (s, 3H), 2.44 (t, 2H), 2.33 (t, 2H), 1.79 (m, 2H), 1.71 (m, 2H), 1.52 (m, 2H), 1.23-1.30 (m, 12H), 0.85 (t, 3H). Because of the instability of **4**, the

oxidation of the sulfanyl-group towards **5** was done without further purification.

6-(5-chloromethyl-4-methoxy-2-octylsulfinylmethyl-phenoxy)-hexanoic acid methyl ester and 6-(2-chloromethyl-4-methoxy-5-octylsulfinylmethyl-phenoxy)-hexanoic acid methyl ester 5. An aqueous (35 wt%) solution of H_2O_2 (1.55 g, 16 mmol) was added drop wise to a mixture of **4** (3.68 g, 8 mmol) and TeO_2 (0.0768 g, 0.5 mmol) in dioxane (75 mL). To this solution, 3 droplets of concentrated HCl were added. As soon as all **4** was consumed (TLC, CH_2Cl_2/MeOH 19/1), 200 mL of a saturated $Na_2S_2O_3$-solution was added to quench the reaction. The reaction mixture was extracted with $CHCl_3$ (3 x 100 mL) after which the combined organic extracts were dried over anhydrous $MgSO_4$. Evaporation of the solvent under reduced pressure gave the crude product. The pure product was obtained by column chromatography (SiO_2, eluent CH_2Cl_2/MeOH 19/1), followed by another column chromatography (SiO_2, eluent EtOAc) as a white-yellow solid (1/1 mixture of regio-isomers; 2.36 g, 54 % yield). ^{1}H-NMR ($CDCl_3$): δ = 6.90+6.89+6.81+6.80 (4s, 2H), 4.61+4.60 (2s, 2H), 4.10+4.07+4.05+4.02 (2dd, 2H), 3.94 (m, 2H), 3.82+3.80 (2s, 3H), 3.65 (s, 3H), 2.60 (m, 2H), 2.33 (t, 2H), 1.65-1.80 (m, 6H), 1.18-150 (m, 12H), 0.85 (t, 3H).

♦ Platform copolymer (MDMO-CPM)-PPV (n/m = 9)

Precursor copolymer 6 (n/m = 9) towards (MDMO-CPM)-PPV. The molar monomer feed ratio of the copolymerization reaction was 1 equivalent of sulfinyl monomer **5** to 9 equivalents of the MDMO sulfinyl monomer. A thermostatic flask (30 °C) was charged with a mixture of sulfinyl monomer **5** (0.047 g, 0.1 mmol) and the MDMO sulfinyl monomer (0.438 g, 0.9 mmol) in 2-BuOH (30 mL). NaO*t*Bu (0.125 g, 1.3 mmol), dissolved in the same solvent (20 mL), was added in one portion *via* a thermostatic funnel after both solutions were purged with N_2. Polymerization was allowed to proceed for 1 h at 30 °C. The reaction was terminated by pouring the reaction mixture in a well stirred amount of ice water (250 mL). After

extraction with CH_2Cl_2 (3 x 150 mL), the combined organic layers were evaporated under reduced pressure giving the crude the precursor copolymer **6**. ^{1}H-NMR ($CDCl_3$): δ = 7.0-6.3, 4.5, 4.1-3.5, 3.4, 2.5-2.2, 1.9-1.1, 0.9; FT-IR (NaCl, cm^{-1}): 2954, 2922, 2856, 1730 (ν_{C-O}), 1505, 1464, 1408, 1384, 1366, 1327, 1261, 1217, 1044, 870; SEC (THF) M_w = 1.50 x 10^5 g/mol (PD = M_w/M_n = 3.6). UV-Vis λ_{max} = 301 nm (THF).

Ester-functionalized copolymer 7 (n/m = 9). A stirred solution of copolymer **6 (n/m = 9)** (0.475 g) in toluene (50 mL) was purged with N_2 for 30 min, after which the elimination reaction was allowed to proceed at 110 °C and stirred for 3 h. Subsequently, toluene was evaporated under reduced pressure and **7** was redissolved in THF (30 mL). The resulting red solution was precipitated drop wise in cold MeOH (400 mL). The resulting red copolymer was filtered off, washed with cold MeOH and redissolved in toluene (50 mL). The elimination procedure was repeated after which pure **7** was filtered off, washed with cold MeOH and dried at room temperature under reduced pressure as a red, fibrous polymer (0.244 g, 85 % yield). ^{1}H-NMR ($CDCl_3$): δ = 7.6-7.4, 7.2-7.1, 4.1-3.8, 3.63, 2.4-2.3, 1.9-0.6; FT-IR (NaCl, cm^{-1}): 2958, 2922, 2851, 1733 (ν_{C-O}), 1504, 1464, 1413, 1384, 1353, 1259, 1205, 1094, 1030, 968, 860, 800; SEC (THF) M_w = 5.4 x 10^5 g/mol (PD = M_w/M_n = 2.5). UV-Vis λ_{max} = 510 nm (THF).

(MDMO-CPM)-PPV 8 (n/m = 9). A solution of copolymer **7 (n/m = 9)** (0.244 g, 0.085 mmol ester functionalities) and dioxane (50 mL) was heated to reflux temperature after which a solution of KO*t*Bu (0,094 g, 0.85 mmol) in water (1 mL) was added at reflux temperature. After 4 h stirring at reflux temperature, CH_2Cl_2 (150 mL) was added to the reaction mixture and extracted with 1 N HCl-solution (100 mL). The organic layer was evaporated under reduced pressure giving copolymer **8**. The resulting red copolymer was dried at room temperature under reduced pressure (0.230 g, 95 % yield). ^{1}H-NMR ($CDCl_3$): δ = 7.6-7.4, 7.2-7.1, 4.1-3.8, 2.4-2.3, 1.9-0.6; FT-IR (NaCl, cm^{-1}): 3059, 2954, 2923, 2855, 1709 (ν_{C-O}), 1505, 1464, 1414, 1383, 1353, 1259, 1205, 1095, 1035, 968, 857, 801; SEC (THF) M_w = 2.7 x 10^5 g/mol (PD = M_w/M_n = 3.2). UV-Vis λ_{max} = 507 nm (THF).

♦ Model compound and functionalization *via* the optimized DCC/DMAP-esterification method

6-(4-methoxy-phenoxy)-hexanoic acid 9. A solution of **1** (4 g, 15 mmol) and MeOH (200 mL) was heated to 50 °C after which a solution of KO*t*Bu (4.213 g, 37.5 mmol) in water (4 mL) was added. After overnight stirring at 50°C the reaction mixture was cooled down to room temperature and a 1 N HCl-solution was added until pH 6. Water was added and the reaction mixture was extracted with CH_2Cl_2 (3 x 150 mL). The combined organic extracts were dried over anhydrous $MgSO_4$. Evaporation of the solvent under reduced pressure gave the crude product. The pure carboxylic acid was obtained by crystallization from hexane as a white solid (3.26 g, 65 % yield). ^{1}H-NMR ($CDCl_3$): δ = 6.80 (s, 4H), 3.89 (t, 2H), 3.74 (s, 3H), 2.37 (t, 2H), 1.64-1.80 (m, 4H), 1.50 (m, 2H); ^{13}C-NMR ($CDCl_3$): δ = 179.4, 153.5, 152.9, 115.2, 114.4, 68.1, 64.0, 55.5, 33.7, 28.9, 25.4, 24.3; Mass (GC-MS, EI): 238 $[M+1]^+$, 124 $[M+1]^+$ - $C_7O_2H_{10}$, 109 $[M+1]^+$ - $C_7O_2H_{10}$ - CH_3; FT-IR (NaCl, cm^{-1}): 3041, 3014, 2949, 2901, 2872, 2838, 1721, 1701 (ν_{C-O}), 1591, 1513, 1475, 1456, 1449, 1428, 1407, 1392, 1307, 1249, 1223, 1232, 1203, 1174, 1109, 1051, 1038, 1008, 908, 825.

6-(4-methoxy-phenoxy)-hexanoic acid allyl ester 10. 9 (0.5 g, 2.1 mmol) was dissolved in dry CH_2Cl_2 (20 mL) and cooled down to 0 °C. The alcohol-functionalized reagent, *i.e.* allylalcohol (0.304 g, 5.25 mmol) and N,N'-dicyclohexylcarbodiimide (DCC) (0.476 g, 2.31 mmol) were added. Subsequently 4-(N,N'-dimethylamino)pyridine (DMAP) (0.050 g, 0.42 mmol) in dry CH_2Cl_2 was added drop wise over a period of 15 minutes under N_2 atmosphere. The reaction was allowed to proceed for 1 h at 0°C and for an additional 24 h at room temperature. Filtering off dicyclohexylurea (DCU) gave the crude product. The pure product was obtained by column chromatography (SiO_2, eluent CH_2Cl_2) as a yellow oil (0.455 g, 78 % yield). ^{1}H-NMR ($CDCl_3$): δ = 6.80 (s, 4H), 5.90 (m, 1H), 5.29 (dq, 1H), 5.21 (dq, 1H), 4.55 (dt, 2H), 3.88 (t, 2H), 3.74 (s, 3H), 2.35 (t, 2H), 1.64-1.80 (m, 4H), 1.49 (m, 2H); ^{13}C-NMR ($CDCl_3$): δ = 173.1, 153.5, 152.9, 132.1, 118.0, 115.2, 114.4, 68.1, 64.8, 55.5, 33.9, 28.9, 25.5, 24.5; Mass (GC-MS, EI): 278 $[M+1]^+$, 155 $[M+1]^+$ - $C_7O_2H_7$, 124 $[M+1]^+$ -

$C_9O_2H_{14}$, 109 $[M+1]^+$ - $C_9O_2H_{14}$ - CH_3; FT-IR (NaCl, cm^{-1}): 2994, 2943, 2868, 2834, 1738 (ν_{C-O}), 1648 ($\nu_{C=C}$), 1591, 1510, 1466, 1442, 1383, 1232, 1162, 1107, 1039, 990, 932, 825.

6-(4-methoxy-phenoxy)-hexanoic acid prop-2-enyl ester or cinnamyl 6-(4-methoxyphenoxy) hexanoate 11. 11 was prepared following the DCC/DMAP-procedure described for **10** using 3-phenyl-2-propene-1-ol (cinnamyl alcohol) (0.704 g, 5.25 mmol) as the alcohol-functionalized molecule. The pure product was obtained by column chromatography (SiO_2, eluent CH_2Cl_2) as a yellow oil (0.639 g, 86 % yield). ^{1}H-NMR ($CDCl_3$): δ = 7.24-7.39 (m, 5H), 6.80 (s, 4H), 6.63 (ds, 1H), 6.27 (dt, 1H), 4.71 (dd, 2H), 3.88 (t, 2H), 3.74 (s, 3H), 2.37 (t, 2H), 1.66-1.81 (m, 4H), 1.50 (m, 2H); ^{13}C-NMR ($CDCl_3$): δ = 172.9, 153.2, 152.6, 135.7, 133.7, 128.1, 127.6, 126.1, 122.7, 114.9, 114.1, 67.7, 64.4, 55.2, 33.7, 28.5, 25.2, 24.2; Mass (GC-MS, EI): 354 $[M+1]^+$, 124 $[M+1]^+$ - $C_{15}O_2H_{18}$, 117 $[M+1]^+$ - $C_{13}O_4H_{17}$, 109 $[M+1]^+$ - $C_{15}O_2H_{18}$ - CH_3; FT-IR (NaCl, cm^{-1}): 3647, 3447, 3027, 3000, 2936, 2868, 2834, 2543, 2473, 2319, 2060, 1955, 1880, 1851, 1732 (ν_{C-O}), 1592, 1578, 1505, 1470, 1385, 1353, 1236, 1108, 1036, 969, 824, 745, 693.

6-(4-methoxy-phenoxy)-hexanoic acid 3-phenylprop-2-ynyl ester 12. 12 was prepared following the DCC/DMAP-procedure described for **10** using 3-phenyl-2-propyn-1-ol (0.693 g, 5.25 mmol) as the alcohol-functionalized molecule. The pure product was obtained by column chromatography (SiO_2, eluent CH_2Cl_2) as a white-yellow solid (0.604 g, 82 % yield). ^{1}H-NMR ($CDCl_3$): δ = 7.42 (m, 2H), 7.30 (m, 3H), 6.80 (s, 4H), 4.89 (d, 2H), 3.88 (t, 2H), 3.74 (s, 3H), 2.40 (t, 2H), 1.65-1.81 (m, 4H), 1.50 (m, 2H); ^{13}C-NMR ($CDCl_3$): δ = 169.8, 150.5, 150.0, 128.7, 125.6, 125.1, 118.9, 112.2, 111.4, 83.2, 79.8, 65.0, 52.6, 49.5, 30.8, 25.8, 22.4, 21.4; Mass (GC-MS, EI): 352 $[M+1]^+$, 124 $[M+1]^+$ - $C_{15}O_2H_{16}$, 115 $[M+1]^+$ - $C_{13}O_4H_{17}$, 109 $[M+1]^+$ - $C_{15}O_2H_{16}$ - CH_3; FT-IR (NaCl, cm^{-1}): 3655, 3463, 3055, 2937, 2968, 2834, 2473, 2337, 2237, 2118 ($\nu_{\equiv CH}$), 2061, 1978, 1887, 1732 (ν_{C-O}), 1593, 1572, 1510, 1471, 1455, 1385, 1349, 1233, 1107, 1033, 955, 825, 758, 692.

6-(4-methoxy-phenoxy)-hexanoic acid 2-(2-methyl-acryloyloxy)-ethyl ester 13. 13 was prepared following the DCC/DMAP-procedure described for **10** using 2-hydroxyethyl-methacrylate (0.682 g, 5.25 mmol) as the

alcohol-functionalized molecule. The pure product was obtained by column chromatography (SiO_2, eluent CH_2Cl_2) as a yellow oil (0.672 g, 91 % yield). ^{1}H-NMR ($CDCl_3$): δ = 6.80 (s, 4H), 6.10 (dd, 1H), 5.56 (dd, 1H), 4.32 (m, 4H), 3.88 (t, 2H), 3.74 (s, 3H), 2.35 (t, 1H), 1.92 (s, 3H), 1.63-1.78 (m, 4H), 1.48 (m, 2H); ^{13}C-NMR ($CDCl_3$): δ = 173.4, 167.1, 153.7, 153.1, 135.9, 126.0, 115.3, 114.6, 68.2, 62.4, 61.9, 55.7, 34.0, 29.0, 25.6, 24.6, 18.2; Mass (GC-MS, EI): 350 $[M+1]^+$, 124 $[M+1]^+$ - $C_{12}O_4H_{18}$, 113 $[M+1]^+$ - $C_{13}O_4H_{17}$, 109 $[M+1]^+$ - $C_{12}O_4H_{18}$ - CH_3; FT-IR (NaCl, cm^{-1}): 3045, 2947, 2867, 2834, 1740 (ν_{C-O}), 1722 (ν_{C-O}), 1637, 1591, 1509, 1464, 1455, 1377, 1320, 1297, 1232, 1155, 1107, 1039, 945, 825.

6-(4-methoxy-phenoxy)-hexanoic acid prop-2-ynyl ester 14. 14 was prepared following the DCC/DMAP-procedure described for **10** using propargylalcohol (0.304 g, 5.25 mmol) as the alcohol-functionalized molecule. The pure product was obtained by column chromatography (SiO_2, eluent CH_2Cl_2) as a white-yellow solid (0.429 g, 74 % yield). ^{1}H-NMR ($CDCl_3$): δ = 6.80 (s, 4H), 4.65 (d, 2H), 3.88 (t, 2H), 3.74 (s, 3H), 2.44 (t, 1H), 2.37 (t, 2H), 1.65-1.80 (m, 4H), 1.49 (m, 2H); ^{13}C-NMR ($CDCl_3$): δ = 172.6, 153.5, 152.9, 115.2, 114.4, 77.6, 74.6, 68.0, 55.5, 51.6, 33.7, 28.8, 25.4, 24.4; Mass (GC-MS, EI): 276 $[M+1]^+$, 153 $[M+1]^+$ - $C_7O_2H_7$, 124 $[M+1]^+$ - $C_9O_2H_{12}$, 109 $[M+1]^+$ - $C_9O_2H_{12}$ - CH_3; FT-IR (NaCl, cm^{-1}): 3286 ($\nu_{\equiv CH}$), 2997, 2942, 2867, 2834, 2118 ($\nu_{\equiv CH}$), 1742 (ν_{C-O}), 1591, 1510, 1466, 1442, 1381, 1232, 1155, 1107, 1037, 937, 825.

6-(4-methoxy-phenoxy)-hexanoic acid 1-phenylsulfanylmethyl-1H-[1,2,3] triazol-4-ylmethyl ester 15. 14 (0.250 g, 0.90 mmol) was dissolved in degassed THF (25 mL) under N_2 atmosphere. The azide-functionalized reagent, *i.e.* azidomethyl phenyl sulfide (0.297 g, 1.80 mmol) and distilled N,N,N',N'',N''-pentamethyldiethylenetriamine (PMDETA) (0.016 g, 0.09 mmol) were added. The solution was again degassed for 5 min and purified Cu(I)Br (0.013 g, 0.09 mmol) was added under a continuous N_2 flow. After overnight stirring at 50 °C the reaction mixture was filtered over Al_2O_3 and washed with THF and CH_2Cl_2. The pure product was obtained by column chromatography (SiO_2, eluent CH_2Cl_2) as a white solid (0.246 g, 62 % yield). ^{1}H-NMR ($CDCl_3$): δ = 7.57 (s, 1H), 7.28 (s, 5H), 6.77 (s, 4H), 5.56 (s, 2H), 5.14 (s, 2H), 3.84 (t, 2H), 3.72 (s, 3H), 2.31 (t, 2H), 1.59-1.78 (m,

4H), 1.44 (m, 2H); ^{13}C-NMR ($CDCl_3$): δ = 173.2, 153.6, 153.1, 143.4, 132.1, 131.8, 129.5, 128.7, 123.3, 115.4, 114.6, 68.1, 57.4, 55.6, 53.7, 33.9, 28.9, 25.6, 24.5; Mass (GC-MS, EI): 441 $[M+1]^+$, 318 $[M+1]^+$ - $C_7O_2H_7$, 176 $[M+1]^+$ - $C_7O_2H_7$ - $C_8O_2H_{14}$, 123 $[M+1]^+$ - $C_{16}O_2N_3SH_{20}$, 109 $[M+1]^+$ - $C_{16}O_2N_3SH_{20}$ - CH_2; FT-IR (NaCl, cm^{-1}): 3001, 2942, 2867, 2834, 1735 (ν_{C-O}), 1584, 1510, 1466, 1440, 1390, 1232, 1158, 1108, 1044, 825.

4-chloromethyl benzyl alcohol 16. 4-chloromethyl benzoic acid (2 g, 11.76 mmol) was dissolved in dry THF (40 mL), under N_2 atmosphere, and cooled down to 0 °C. 1N BH_3·THF (19.52 mL, 19.52 mmol) was added drop wise under N_2 atmosphere. The reaction was allowed to proceed for 1 h at room temperature. Water was added to quench the reaction at 0 °C and the reaction mixture was extracted with diethyl ether (3 x 150 mL). The combined organic extracts were dried over anhydrous $MgSO_4$. Evaporation of the solvent under reduced pressure gave the crude product. The pure product was obtained by column chromatography (SiO_2, eluent EtOAc) as a white solid (0.691 g, 38 % yield). ^{1}H-NMR (CD_3OD): δ = 7.36 (dd, 4H), 4.62 (s, 2H), 4.60 (s, 2H); ^{13}C-NMR (CD_3OD + $CDCl_3$): δ = 142.2, 137.4, 129.3, 127.7, 64.4, 46.4; Mass (GC-MS, EI): 156 $[M+1]^+$, 121 $[M+1]^+$ - Cl, 107 $[M+1]^+$ - Cl - CH_2, 91 $[M+1]^+$ - Cl - CH_2 - O; FT-IR (NaCl, cm^{-1}): 3217, 1444, 1421, 1262, 1195, 1025, 1013, 844, 834.

6-(4-methoxy-phenoxy)-hexanoic acid 4-chloromethyl-benzyl ester 17. **17** was prepared following the DCC/DMAP-procedure described for **10** using **16** (0.820 g, 5.25 mmol) as the alcohol-functionalized molecule. The pure product was obtained by column chromatography (SiO_2, eluent CH_2Cl_2) as a white-yellow solid (0.564 g, 67 % yield). ^{1}H-NMR ($CDCl_3$): δ = 7.34 (dd, 4H), 6.79 (s, 4H), 5.10 (s, 2H), 4.56 (s, 2H), 3.87 (t, 2H), 3.74 (s, 3H), 2.37 (t, 2H), 1.65-1.78 (m, 4H), 1.48 (m, 2H); ^{13}C-NMR ($CDCl_3$): δ = 170.2, 150.5, 149.9, 134.3, 133.2, 125.6, 125.4, 112.2, 111.4, 65.0, 62.4, 42.7, 27.8, 25.9, 22.5, 21.5; Mass (GC-MS, EI): 376 $[M+1]^+$, 139 $[M+1]^+$ - $C_{13}O_4H_{17}$, 124 $[M+1]^+$ - $C_{14}O_2ClH_{17}$, 109 $[M+1]^+$ - $C_{14}O_2ClH_{17}$ - CH_3; FT-IR (NaCl, cm^{-1}): 2997, 2945, 2867, 2834, 1736 (ν_{C-O}), 1591, 1508, 1465, 1443, 1384, 1352, 1289, 1232, 1158, 1107, 1038, 977, 825.

6-(4-methoxy-phenoxy)-hexanoic acid 4-((N,N-diethyldithiocarbamate)methyl)-benzyl ester 18. A mixture of **17** (0.200 g, 0.53 mmol), sodium diethyldithiocarbamate trihydrate (0.120 g, 0.53 mmol) in THF (20 mL) was stirred overnight at room temperature. Evaporation of the solvent under reduced pressure gave the crude product. The pure product was obtained by column chromatography (SiO_2, eluent CH_2Cl_2) as a yellow oil (0.156 g, 60 % yield). ^{1}H-NMR ($CDCl_3$): δ = 7.34 (dd, 4H), 6.79 (s, 4H), 5.06 (s, 2H), 4.52 (s, 2H), 4.01 (q, 2H), 3.86 (t, 2H), 3.73 (s, 3H), 3.71 (q, 2H), 2.37 (t, 2H), 1.65-1.78 (m, 4H), 1.48 (m, 2H), 1.24 (2t, 6H); ^{13}C-NMR ($CDCl_3$): δ = 194.9, 173.4, 153.7, 153.1, 136.2, 135.2, 129.5, 128.7, 115.4, 114.6, 68.2, 65.8, 55.7, 49.5, 46.7, 41.7, 34.2, 29.0, 25.6, 24.7, 12.5, 11.6; Mass (DIP-MS, EI): 489 $[M+1]^+$, 340 $[M+1]^+$ - $C_5S_2NH_{11}$, 148 $[M+1]^+$ - $C_{21}O_4H_{25}$, 124 $[M+1]^+$ - $C_5S_2NH_{11}$ - $C_{14}O_2H_{16}$; FT-IR (NaCl, cm^{-1}): 3453, 3044, 2935, 2870, 2833, 2059, 1738 (ν_{C-O}), 1732, 1615, 1591, 1508, 1488, 1465, 1443, 1417, 1380, 1355, 1269, 1233, 1158, 1206, 1107, 1070, 1038, 1010, 985, 918, 825.

♦ **Post-polymerization functionalization of the platform copolymer (MDMO-CPM)-PPV *via* the optimized DCC/DMAP-esterification method**

Allyl ester of (MDMO-CPM)-PPV 19 (n/m = 9). (MDMO-CPM)-PPV **8 (n/m = 9)** (0.050 g, 0.018 mmol carboxylic acid functionalities) was dissolved in dry CH_2Cl_2 (12 mL) and cooled down to 0 °C. The alcohol-functionalized reagent, *i.e.* allylalcohol (0.002 g, 0.022 mmol) and N,N'-dicyclohexylcarbodiimide (DCC) (0.004 g, 0.022 mmol) were added. Subsequently 4-(N,N'-dimethylamino)pyridine (DMAP) (0.003 g, 0.022 mmol) in dry CH_2Cl_2 was added drop wise over a period of 15 minutes under N_2 atmosphere. The reaction was allowed to proceed for 1 h at 0 °C and for an additional 24 h at room temperature after which the solution was precipitated drop wise in cold MeOH (200 mL). The resulting red copolymer was filtered off, washed with cold MeOH and dried at room temperature under reduced pressure as a red, fibrous polymer (0.045 g, 88 %

yield). ^{1}H-NMR ($CDCl_3$): δ = 7.6-7.4, 7.2-7.1, 6.0-5.8, 5.3-5.2, 4.55, 4.1-3.8, 2.4-2.3, 1.8-0.6; FT-IR (NaCl, cm^{-1}): 3059, 2954, 2926, 2868, 1738 (ν_{C-O}), 1651, 1505, 1464, 1414, 1384, 1353, 1259, 1158, 1092, 1037, 968, 859; SEC (THF) M_w = 2.4 x 10^5 g/mol (PD = M_w/M_n = 4.3). UV-Vis λ_{max} = 504 nm (THF).

Prop-2-enyl ester or cinnamyl ester of (MDMO-CPM)-PPV 20 (n/m = 9). Copolymer **20** was prepared following the DCC/DMAP-procedure described for copolymer **19** using 3-phenyl-2-propene-1-ol (cinnamyl alcohol) (0.003 g, 0.022 mmol) as the alcohol-functionalized molecule. After precipitation in cold MeOH (200 mL), the resulting red copolymer was filtered off, washed with cold MeOH and dried at room temperature under reduced pressure as a red, fibrous polymer (0.047 g, 88 % yield). ^{1}H-NMR ($CDCl_3$): δ = 7.6-7.4, 7.36, 7.33, 7.2-7.1, 6.61, 6.25, 4.68, 4.2-3.8, 2.39, 1.9-076; FT-IR (NaCl, cm^{-1}): 3058, 2953, 2927, 2868, 1735 (ν_{C-O}), 1504, 1464, 1413, 1384, 1351, 1259, 1204, 1092, 1035, 968, 859, 800; SEC (THF) M_w = 4.5 x 10^5 g/mol (PD = M_w/M_n = 5.8). UV-Vis λ_{max} = 508 nm (THF).

3-phenylprop-2-ynyl ester of (MDMO-CPM)-PPV 21 (n/m = 9). Copolymer **21** was prepared following the DCC/DMAP-procedure described for copolymer **19** using 3-phenyl-2-propyn-1-ol (0.003 g, 0.022 mmol) as the alcohol-functionalized molecule. After precipitation in cold MeOH (200 mL), the resulting red copolymer was filtered off, washed with cold MeOH and dried at room temperature under reduced pressure as a red, fibrous polymer (0.041 g, 79 % yield). ^{1}H-NMR ($CDCl_3$): δ = 7.6-7.4, 7.28, 7.2-7.1, 4.88, 4.2-3.8, 2.42, 1.9-076; FT-IR (NaCl, cm^{-1}): 3058, 2954, 2926, 2868, 1743 (ν_{C-O}), 1505, 1464, 1414, 1384, 1352, 1259, 1205, 1092, 1034, 969, 860, 801; SEC (THF) M_w = 3.0 x 10^5 g/mol (PD = M_w/M_n = 4.9). UV-Vis λ_{max} = 511 nm (THF).

2-(2-methyl-acryloyloxy)-ethyl ester of (MDMO-CPM)-PPV 22 (n/m = 9). Copolymer **22** was prepared following the DCC/DMAP-procedure described for copolymer **19** using 2-hydroxyethyl-methacrylate (0.003 g, 0.022 mmol) as the alcohol-functionalized molecule. After precipitation in cold MeOH (200 mL), the resulting red copolymer was filtered off, washed

with cold MeOH and dried at room temperature under reduced pressure as a red, fibrous polymer (0.050 g, 96 % yield). ^{1}H-NMR ($CDCl_3$): δ = 7.6-7.4, 7.2-7.1, 6.10, 5.55, 4.30, 4.1-3.8, 2.4-2.3, 1.90, 1.8-0.6; FT-IR (NaCl, cm^{-1}): 3059, 2954, 2926, 2868, 1739 (ν_{C-O}), 1724 (ν_{C-O}), 1505, 1464, 1414, 1384, 1353, 1256, 1158, 1092, 1037, 968, 859; SEC (THF) M_w = 4.6 x 10^5 g/mol (PD = M_w/M_n = 5.6). UV-Vis λ_{max} = 508 nm (THF).

Prop-2-ynyl ester of (MDMO-CPM)-PPV 23 (n/m = 9). Copolymer **23** was prepared following the DCC/DMAP-procedure described for copolymer **19** using propargylalcohol (0.002 g, 0.022 mmol) as the alcohol-functionalized molecule. After precipitation in cold MeOH (200 mL), the resulting red copolymer was filtered off, washed with cold MeOH and dried at room temperature under reduced pressure as a red, fibrous polymer (0.045 g, 89 % yield). ^{1}H-NMR ($CDCl_3$): δ = 7.6-7.4, 7.2-7.1, 4.65, 4.1-3.8, 2.43, 2.4-2.3, 1.8-0.6; FT-IR (NaCl, cm^{-1}): 3058, 2954, 2927, 2868, 1745 (ν_{C-O}), 1505, 1464, 1414, 1384, 1352, 1258, 1158, 1092, 1037, 969, 860; SEC (THF) M_w = 3.8 x 10^5 g/mol (PD = M_w/M_n = 5.2). UV-Vis λ_{max} = 507 nm (THF).

1-Phenylsulfanylmethyl-1H-[1,2,3] triazol-4-ylmethyl ester of (MDMO-CPM)-PPV 24 (n/m = 9). Copolymer **23** (0.035 g, 0.013 mmol triple bond functionalities) was dissolved in THF (10 mL) under N_2 atmosphere. The azide-functionalized reagent, *i.e.* azidomethyl phenyl sulfide (0.004 g, 0.025 mmol) and distilled N,N,N',N'',N''-pentamethyldiethylenetriamine (PMDETA) (0.0002 g, 0.001 mmol) were added. The solution was purged with N_2 for 5 min and purified Cu(I)Br (0.0002 g, 0.001 mmol) was added under a continuous N_2 flow. After overnight stirring at 50 °C the reaction mixture was filtered over Al_2O_3 and washed with THF and CH_2Cl_2. Subsequently, the total volume was reduced to 15 mL by evaporation under reduced pressure and the resulting red solution was precipitated drop wise in cold MeOH (200 mL). The resulting red copolymer was filtered off, washed with cold MeOH and dried at room temperature under reduced pressure as a red, fibrous polymer (0.036 g, 96 % yield). ^{1}H-NMR ($CDCl_3$): δ = 7.58, 7.55-7.4, 7.30, 7.2-7.1, 5.53, 5.13, 4.1-3.8, 2.4-2.3, 1.8-0.6; FT-IR (NaCl, cm^{-1}): 3059, 2955, 2925, 2868, 1739 (ν_{C-O}), 1505, 1464, 1414, 1385, 1353,

1260, 1158, 1093, 1033, 969, 862; SEC (THF) M_w = 3.6 x 10^5 g/mol (PD = M_w/M_n = 3.7). UV-Vis λ_{max} = 509 nm (THF).

4-chloromethyl benzyl ester of (MDMO-CPM)-PPV 25 (n/m = 9). Copolymer **25** was prepared following the DCC/DMAP-procedure described for copolymer **19** using 4-chloromethyl benzyl alcohol **16** (0.003 g, 0.022 mmol) as the alcohol-functionalized molecule. After precipitation in cold MeOH (200 mL), the resulting red copolymer was filtered off, washed with cold MeOH and dried at room temperature under reduced pressure as a red, fibrous polymer (0.047 g, 95 % yield). ^{1}H-NMR ($CDCl_3$): δ = 7.6-7.4, 7.31, 7.2-7.1, 5.06, 4.52, 4.1-3.8, 2.4-2.3, 1.8-0.6; FT-IR (NaCl, cm^{-1}): 3059, 2954, 2926, 2868, 1736 (ν_{C-O}), 1505, 1464, 1414, 1384, 1353, 1259, 1158, 1093, 1037, 969, 858; SEC (THF) M_w = 3.1 x 10^5 g/mol (PD = M_w/M_n = 4.7). UV-Vis λ_{max} = 507 nm (THF).

4-((N,N-diethyldithiocarbamate)methyl)-benzyl ester of (MDMO-CPM)-PPV 26 (n/m = 9). A mixture of copolymer **25** (0.035 g, 0.013 mmol 4-chloromethyl benzyl functionalities), sodium diethyldithiocarbamate trihydrate (0.002 g, 0.009 mmol) in THF (10 mL) was stirred for 48 h at room temperature. After precipitation in cold MeOH (200 mL), the resulting red copolymer was filtered off, washed with cold MeOH and dried at room temperature under reduced pressure as a red, fibrous polymer (0.034 g, 89 % yield). ^{1}H-NMR ($CDCl_3$): δ = 7.6-7.4, 7.31, 7.2-7.1, 5.04, 4.49, 4.1-3.8, 3.72, 2.4-2.3, 1.8-0.6; FT-IR (NaCl, cm^{-1}): 3059, 2954, 2927, 2868, 1738 (ν_{C-O}), 1505, 1464, 1414, 1384, 1353, 1259, 1158, 1093, 1035, 969, 860; SEC (THF) M_w = 3.2 x 10^5 g/mol (PD = M_w/M_n = 4.6). UV-Vis λ_{max} = 507 nm (THF).

2.8. References

[1] Benjamin, I.; Hong, H.; Avny, Y.; Davidov, D.; Neumann, R. *J. Mater. Chem.* **1998**, *8*, 919.

[2] Fujii, A.; Sonoda, T.; Yoshino, K. *Jpn. J. Appl. Phys.* **2000**, *39*, L249.

[3] Fujii, A.; Sonoda, T.; Fujisawa, T.; Ootaka, R.; Yoshino, K. *Synth. Met.* **2001**, *119*, 189.

[4] Sonoda, T.; Fujisawa, T.; Fujii, A.; Yoshino, K. *Appl. Phys. Let.* **2000**, *76*, 3227.

[5] Peng, Z.; Xu, B.; Zhang, J.; Pan, Y. *Chem. Commun.* **1999**, 1855.

[6] Wagaman, M. W.; Grubbs, R. H. *Macromolecules* **1997**, *30*, 3978.

[7] Van Severen, I.; Motmans, F.; Lutsen, L.; Cleij, T. J.; Vanderzande D. *Polymer* **2005**, *46*, 5466.

[8] Lutsen, L. J.; van Breemen, A. J.; Kreuder, W.; Vanderzande, D. J. M.; Gelan, J. M. J. V. *Helv. Chim. Acta* **2000**, *83*, 3113.

[9] Lutsen, L. J.; Adriaensens, P.; Becker, H.; van Breemen, A. J.; Vanderzande, D. J. M.; Gelan, J. M. J. V. *Macromolecules* **1999**, *32*, 6517.

[10] van Breemen, A. J.; Issaris, A. C. J.; De Kok, M. M.; Van Der Borght, M. A. N.; Adriaensens, P. J.; Gelan, J. M. J. V.; Vanderzande, D. J. M. *Macromolecules* **1999**, *32*, 5728.

[11] Kim, S. S.; Nehru, K.; Kim, S. S.; Kim, D. W.; Jung, H. C. *Synthesis* **2002**, *17*, 2484.

[12] Xu, W. L.; Li, Y. Z.; Zhang, Q. S.; Zhu, H. S. *Synthesis* **2004**, *2*, 227.

[13] Kesters, E.; Vanderzande, D.; Lutsen, L.; Penxten, H.; Carleer, R. *Macromolecules* **2005**, *38*, 1141.

[14] Zhang, P.; Fawcett, N. C.; Evans, J. A.; Hurt, T.; Harvey, K. G.; Craven, R. C. *Analytical Biochemistry* **2000**, *282*, 218.

[15] Cen, L.; Neoh, K. G.; Kang, E. T. *Biosensors and Bioelectronics* **2003**, *18*, 363.

[16] Kunishima, M.; Kawachi, C.; Hioki, K.; Terao, K.; Tani, S. *Tetrahedron Letters* **2001**, *57*, 1551.

[17] Thompson, K.; Michielsen, S. *J. Polym. Sci. Part A: Chemistry* **2006**, *44*, 126.

[18] Steglich, W.; Höfle, G. *Angew. Chem., Int. Ed. Engl.* **1969**, *8*, 981.

[19] Neises, B.; Steglich, W. *Angew. Chem., Int. Ed. Engl.* **1978**, *17*, 522.

[20] Yoon, N. M.; Pak, C. S.; Brown, H. C.; Krishnamurthy, S.; Stocky, T. P. *J. Org. Chem.* **1973**, *38*, 2786.
[21] Sun, H.; Liu, Z.; Hu, Y.; Wang, L.; Ma, D.; Jing, X.; Wang, F. *J. Polym. Sci., Part A: Polym. Chem.* **2004**, *42*, 2124.
[22] Yang, C.; Hou, J.; Zhang, B.; Zhang, S.; He, C.; Fang, H.; Ding, Y.; Ye, J.; Li, Y. *Macromol. Chem. Phys.* **2005**, *206*, 1311.
[23] Li, X.-C.; Yong, T.-M.; Grüner, J.; Holmes, A. B.; Moratti, S. C.; Cacialli, F.; Friend, R. H. *Synthetic Metals* **1997**, *84*, 437.
[24] Kato, M.; Hirayama, T.; Matsuda, H.; Minami, N.; Okada, S.; Nakanishi H. *Macromol. Rapid. Commun.* **1994**, *15*, 741.
[25] Lee, C.; Kang, Y.; Hyun Jung, S.; Kim, J.-S.; Lee, J. *Opt. Mater.* **2002**, *21*, 337.
[26] Barentsen, H. M.; van Dijk, M.; Kimkes, P.; Zuilhof, H.; Sudhölter, E. J. R. *Macromolecules* **1999**, *32*, 1753.
[27] Jung, H. J.; Park, Y. J.; Choi, S. H.; Hong, J.-M.; Huh, J.; Cho, J. H.; Kim, J. H.; Park, C. *Langmuir* **2007**, *23*, 2184.
[28] Qu, G.; Jiang, F.; Zhang, S.; Usuda, S. *Mater. Lett.* **2007**, *61*, 3421.
[29] Xu, D.; Deng, Z.; Li, X.; Chen, Z.; Liang, C. *Appl. Surf. Sci.* **2007**, *253*, 3378.
[30] Morgado, J.; Friend, R. H.; Cacialli, F. *Synth. Met.* **2000**, *114*, 189.
[31] Li, B.-L.; Liu, Z.-T.; He, Y.-M.; Pan, J.; Fan, Q.-H. *Polymer* **2008**, *49*, 1527.
[32] Li, Z.; Zeng, Q.; Yu, G.; Li, Z.; Ye, C.; Liu, Y.; Qin, J. *Macromol. Rapid Commun.* **2008**, *29*, 136.
[33] Campidelli, S.; Ballesteros, B.; Filoramo, A.; Diaz Diaz, D.; de la Torre, G.; Torres, T.; Aminur Rahman, G. M.; Ehli, C.; Kiessling D.; Werner, F.; Guldi, D. M.; Cioffi, C.; Prato, M.; Bourgoin, J.-P. *J. Am. Chem. Soc.* **2008**, *130*, 11503.
[34] Feng, J.; Zhang, Q.; Li, W.; Li, Y.; Yang, M.; Cao, Y. *J. Appl. Polym. Sci.* **2008**, *109*, 2283.
[35] Quémener, D.; Le Hellaye, M.; Bissett, C.; Davis, T. P.; Barner-Kowollik, C.; Stenzel, M. H. *J. Polym. Sci., Part A: Polym. Chem.* **2008**, *46*, 155.
[36] Luo, N.; Hutchison, J. B.; Anseth, K. S.; Bowman, C. N. *J. Polym. Sci., Part A: Polym. Chem.* **2002**, *40*, 1885.
[37] Nagesh, K.; Ramakrishnan, S. *Synth. Met.* **2005**, *155*, 320.
[38] Pérez-Moral, N.; Mayes, A. G. *Macromol. Rapid Commun.* **2007**, *28*, 2170.
[39] Sellergren, B.; Rückert, B.; Hall, A. J. *Adv. Mater.* **2002**, *14*, 1204.
[40] Peppas, N. A.; Ward, J. H. *Adv. Drug Delivery Rev.* **2004**, *56*, 1587.

Chapter 3

Influence of 10 % 'built-in' functional groups in MDMO-PPV on plastic solar cells

Bulk heterojunction photovoltaic devices exhibit a considerably improved interfacial area between donor and acceptor as compared to layered devices. However, the price paid is the complex nanoscale morphology of the blend, which is difficult to optimize and control. This nanoscale morphology is strongly dependent on device processing parameters. In addition, molecular (polymer) structure is also of significant importance, since a good control of the nanoscale morphology can potentially be achieved by adding functional groups. This chapter focuses on the impact of the presence of functional groups on the formation of the nanoscale morphology of the active layer in bulk heterojunction photovoltaic devices. To this end, the donor, MDMO-PPV, has been 'modified' with 10 % of different functional groups.

3.1. Introduction

As has been pointed out in **Chapter 1** and the references cited therein, conjugated polymers, and thus PPV derivatives, are extremely useful for a wide range of electronic applications, such as photovoltaic (solar) devices.

In this chapter, the history of plastic solar cells is discussed together with the different organic solar cell concepts. One of the key problems in this field of research is the morphology of the active layer. Obtaining a good control of this morphology can potentially be achieved by adding functional groups to a conjugated polymer. This is demonstrated in this chapter for PPV derivatives.

A selection of functional groups has been tested in solar cells. In addition, the impact of these functional groups onto the thermal stability has been investigated. The selected functional groups are vinyl groups, propenylphenyl groups, propynylphenyl groups, acrylate groups and propargyl groups. These functional groups have been introduced in copolymers based on MDMO-PPV, with only 10 % of the repeating units containing a functional group. The synthetic details of these copolymers are described in **Chapter 2**. This chapter focuses on the application of these copolymers in organic photovoltaics.

3.2. Brief history of plastic solar cells

The discovery of the photovoltaic (PV) effect can be attributed to Becquerel. When he illuminated platinum electrodes, covered with silver bromide or silver chloride, in an aqueous solution, he discovered a photocurrent. Actually, this is not a PV effect but rather a photo electrochemical effect.[1,2] The first real reports on photoconductivity are made by Smith and Adams, in 1873 and 1876, respectively, working on selenium.[3,4] Pochettino[5], in 1906 and Volmer[6], in 1913, observed photoconductivity in anthracene. This was the first time that the PV effect was seen in an organic compound. In the late 1950s and 1960s the potential use of organic materials as photoreceptors in imaging systems was recognized.[7] The commercial potential of these photoconductive materials have encouraged the research into this subject. In 1960, Bube discovered that various dyes, such as methylene blue, had semi-conducting properties.[8] Later, these dyes where among the first organic materials to exhibit the PV effect.[9,10] The PV effect

was also observed in many biological molecules such as carotenes, chlorophylls as well as other porphyrins and phthalocyanines. Despite many improvements and optimizations, the performance of organic PVs does not yet match that of inorganic solar cells. The first inorganic solar cell was developed at Bell Laboratories in 1954.[11] This inorganic solar cell was based on Si and had an efficiency of 6 %. Over the years the efficiency has become 24 % for crystalline Si solar cells.[12]

In the past 30 years, the demand for solar energy has grown consistently with growth rates of 20-25 % per year. Fifty years of research and innovation have significantly reduced the price of Si PVs. However, despite the effort of further reducing the price of Si based PVs, the complex production technology involved, hampers a much wider application of this technology. Hence, alternative PV technologies are needed to optimally use the energy provided by the sun. Organic semiconductors are potentially a considerably less expensive alternative to the Si-based inorganic semiconductors. These organic semiconductors have also other advantages, such as straightforward roll to roll processing and flexibility. During the last years, especially the use of conjugated polymeric materials for the active layer of organic PVs has been investigated.

3.3. Different organic solar cell concepts

The underlying principle of a photovoltaic (PV) solar cell is basically the reverse of the principle of an organic light emitting diode (OLED). In OLEDs, electrons are injected at the low work function electrode (cathode), while positive holes are injected at the high work function electrode (anode). At some point in the organic material, the negative electron and the positive hole meet each other and recombine with light emission as a consequence. The reverse occurs in a PV cell. When light is absorbed an electron from the highest occupied molecular orbital (HOMO) is promoted to the lowest unoccupied molecular orbital (LUMO) by formation of an exciton. After exciton dissociation, the electron can reach the low work function electrode

(anode) and the hole the high work function electrode (cathode). The general built-up of both, OLED and PV cell, is depicted in Figure 3-1.

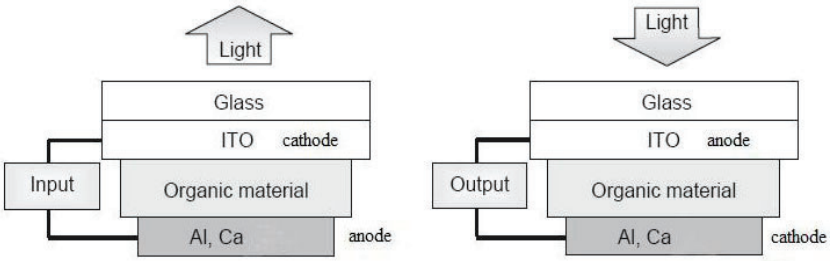

Figure 3-1 General built-up of organic light emitting diode (OLED) (left) and photovoltaic (PV) cell (right)[13]

Almost all current organic photovoltaic solar cells have a planar layered structure. In this way the organic active layer(s) is (are) sandwiched between two different electrodes. One of them has to be transparent, for transmission of the incoming sunlight. A transparent conductive oxide, such as indium tin oxide (ITO), is often used. The other electrode is usually a metal such as aluminum. Even though calcium has a better work function, aluminum is more stable in air as compared to calcium.

3.3.1. Single layer devices

The first organic photovoltaic devices were single organic layers sandwiched between two metal electrodes of different workfunctions.[14,15] The two different workfunctions generate an electric field, which drives electrons and holes to respectively anode and cathode. However, this electric field is typically not strong enough to separate electron and hole. Instead, the exciton diffuses within the organic layer or it recombines. Since exciton diffusion lengths for most organic solar cells are below 10 nm[16], only those excitons generated in a small region within less than 10 nm from the contacts contribute to the photocurrent. As a consequence, such single

layer devices have small efficiencies and are only used to study specific device properties.[17-19]

3.3.2. Heterojunction devices

The general principle behind heterojunction devices is to use two organic materials with different electron affinities and ionization potentials. In this manner exciton (electron and hole) dissociation will be favored, since the electron will be accepted by the organic material with the largest electron affinity and the hole by the organic material with the lowest ionization potential.

The schematic structure of a bulk heterojunction photovoltaic device is depicted in Figure 3-2. In general, such a device has a transparent cathode through which the light can enter the photovoltaic device. The organic solar cell consists of at least four different layers on top of the glass substrate. First of all, the anode is placed on top of the glass. Most of the time this is ITO due to its transparency. Therefore, glass coated with ITO is commercially available. A layer of the conductive polymer mixture poly(3,4-ethylenedioxythiophene):poly(styrenesulfonate) (PEDOT:PSS) is placed in between the anode and the active layer. This layer has the function of a hole transporter and an electron blocker. It also smoothens out the ITO surface, seals the active layer from oxygen and prevents the diffusion of ITO into the active layer, which can lead to unwanted traps. Subsequently, on top of the PEDOT:PSS layer, the active layer is deposited. This layer serves for light absorption, exciton generation, exciton dissociation and charge carrier transport. It consists of a donor and an acceptor. On top of the active layer, the cathode is deposited, which is typically aluminum. Most of the time, a very thin layer of lithium fluoride (5-10 Å) is placed in between the active layer and the cathode. Lithium fluoride does not react with anything else. It serves only as a protecting layer between the aluminum and the organic components of the device.

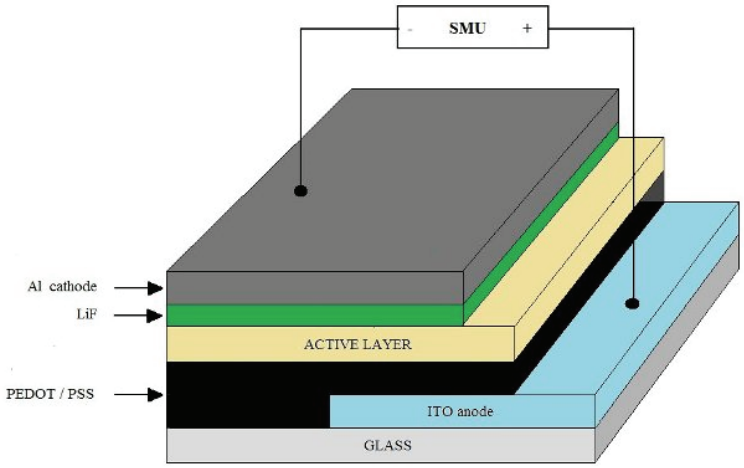

Figure 3-2 Schematic structure of a bulk heterojunction photovoltaic device[13]

In a typical bulk heterojunction photovoltaic device six processes occur during the conversion of solar energy into electrical energy (Figure 3-3). When light is absorbed by the donor, an electron is promoted from the HOMO to the LUMO forming an exciton (a). This formed exciton moves towards a donor/acceptor interface (b). Due to a more thermodynamic favorable state, the electron transfers from the donor to the acceptor (c). Electron and hole are now on different materials, but remain strongly bound by Coulomb interactions (d). Dissociation into free carriers (electron and hole) takes place (e) after which electron and hole can move through respectively acceptor and donor (f). In order to achieve charge separation, an electrical field is applied, which is provided by the asymmetrical workfunctions of the two electrodes. The free electrons must be transported *via* acceptor pathways towards the anode while the free holes must be transported *via* donor pathways towards the cathode. Eventually, electrons and holes can be used in an external circuit and will give rise to a photocurrent.

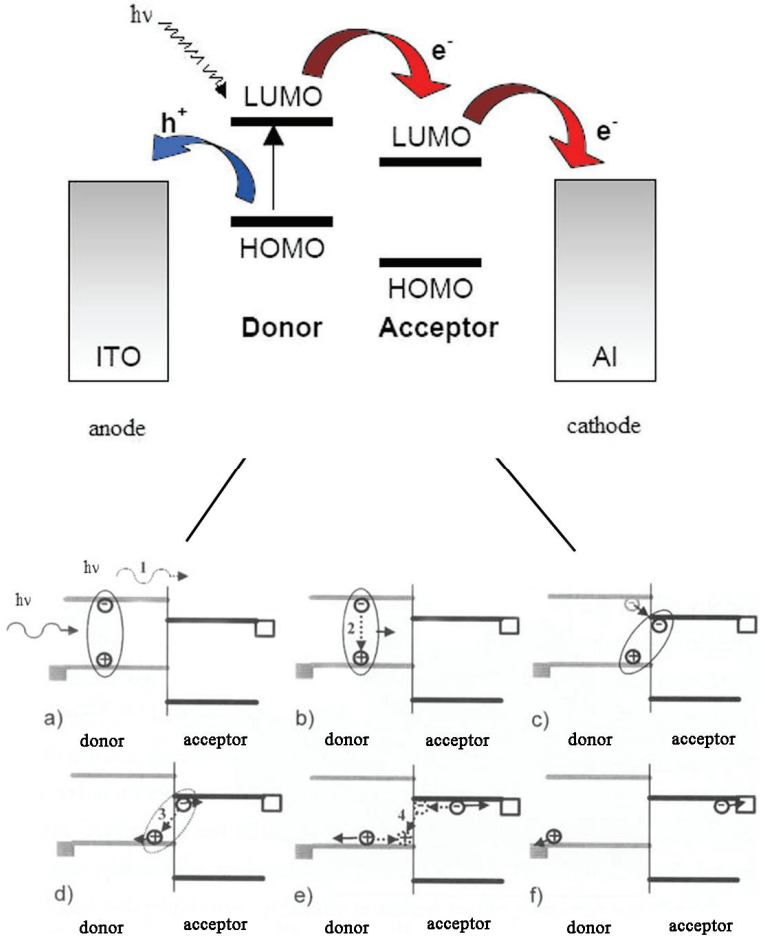

Figure 3-3 Schematic drawing of the working principle of a bulk heterojunction photovoltaic device[13]

Not all the light that is falling onto the photovoltaic device is converted into a photocurrent. There can be a large number of alternative processes, which usually limit the efficiency of a device (Figure 3-3). For example, not all the incoming photons are absorbed by the active layer (1). This is a result of the limited band gap and thickness of the active layer. In addition, excitons, which are created too far from the donor/acceptor interface, will decay (2). Finally, recombination of the bound electron hole can occur (3) and

recombination of free charges during transportation to the electrodes can also occur (4).

♦ **Bilayer heterojunction devices**

In a bilayer heterojunction device, the donor and acceptor are stacked, giving a planar interface at which the charge separation occurs.[20-22] The bilayer is sandwiched between two electrodes, which are responsible for extracting the charge carriers. The bilayer heterojunction device structure is schematically depicted in Figure 3-4.

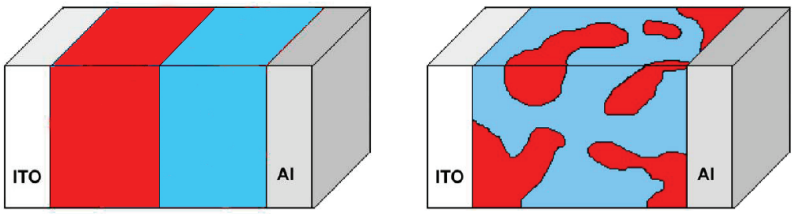

Figure 3-4 Schematic representation of a bilayer (left) and bulk (right) heterojunction device (donor and acceptor)[13]

In 1986, the first bilayer heterojunction device was made by placing a layer of copper phthalocyanine and a layer of a 3,4,9,10-perylene tetracarboxylic bisbenzimidazole (PTCBI) between two electrodes. This device obtained a power conversion efficiency (PCE) of 0.95 %.[22] Later, also conjugate polymers were used in similar devices. In 1993, Sariciftci *et al.*, reported the ultra fast photo induced charge transfer from conjugated polymers to fullerenes.[23] A bilayer device has been made by evaporating C_{60} (Buckminsterfullerene) on top of a spin-cast poly(2-methoxy-5-(2'-ethyl-hexyloxy)-1,4-phenylene vinylene) (MEH-PPV).[24] In this device, MEH-PPV absorbs the light and transports holes to the ITO. C_{60}, with an electron affinity, which is 0.7 eV more than the conjugated polymer, accepts the electrons and transports them to aluminium. It has been shown that presence

of the C_{60} layer increased the photocurrent more than 20 fold.[25] The chemical structures of MEH-PPV and C_{60} are depicted in Figure 3-5.

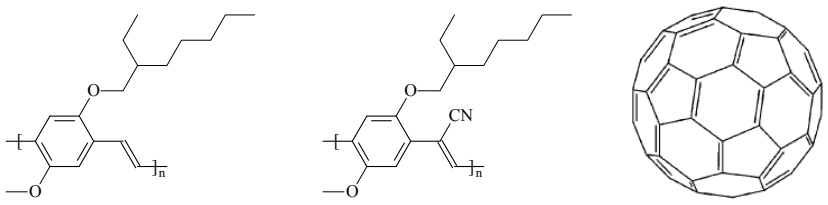

Figure 3-5 Chemical structure of poly(2-methoxy-5-(2'-ethyl-hexyloxy)-1,4-phenylene vinylene) (MEH-PPV), poly(2,5,2',5'-tetrahexyloxy-7,8'-dicyanodi-*p*-phenylenevinylene) (CN-PPV) and C_{60} (Buckminsterfullerene)

The development of bilayer heterojunction devices benefits the exciton dissociation and transportation of the formed charge carriers in comparison to a single layer device. At the same time, this device structure results in a decrease of the recombination probability of the carriers. However the donor/acceptor interface is still very small and only excitons near this interface can be dissociated.[22,25-31]

♦ Bulk heterojunction devices

Since exciton dissociation takes place at the donor/acceptor interface in heterojunction devices (Figure 3-4), the exciton should be formed within the diffusion length of the interface. Since typical diffusion lengths of excitons are in the range of 10 nm[16] and the film thickness of the active layer should be more than 100 nm in order to absorb most of the light, this will limit the efficiency of the above described bilayer devices. One possibility to overcome this problem is to make a blend of donor and acceptor. These bulk heterojunction devices have a large interface area and as result most excitons can reach the donor/acceptor interface.[32]

In 1994, Yu *et al.* made the first bulk heterojunction photovoltaic cell,[33] in which the active layer consisted of MEH-PPV and C_{60}. The cell showed a PCE of 2.9 %. One limitation of this approach is the relative low solubility of fullerenes in normal solvents. This problem was solved by Hummelen *et al.*[34] by synthesizing a number of C_{60}-derivatives with increased solubility, which allows to increase the amount of fullerene used for the production of the PV cells. Furthermore, it has also been shown that the actual synthetic route towards the PPV derivative influences the PCE.[35] Besides PPV derivatives, many other types of conjugated polymers, such as polythiophenes, have been used in fullerene bulk heterojunction devices, to obtain even higher efficiencies.[36-38]

In 1995, the first reports of polymer/polymer bulk heterojunction devices came independently from two research groups,[39,40] which both worked with the same PPV-derivatives: poly(2,5,2',5'-tetrahexyloxy-7,8'-dicyanodi-*p*-phenylenevinylene) (CN-PPV), depicted in Figure 3-5, as acceptor and MEH-PPV as donor. Since that time, a large number of studies have been done to find suitable polymer/polymer bulk heterojunction devices. However, the performances of this type of devices is rather low, due to the lack of good acceptor polymers.[41-44] Hence, the combination of conjugated polymers and fullerenes remains the most common approach towards the active layer in organic PV.

As a result, control of the morphology in bulk heterojunction devices is of considerable importance.[45,46] The degree of phase separation and domain size depend on the choice of solvent, speed of evaporation, solubility as well as the miscibility of donor and acceptor.

3.3.3. The I-V curve of a solar cell

The properties of photovoltaic devices can be represented by a graph of current I *versus* voltage V. In the dark, this I-V curve passes through the origin, since at that moment no current is flowing through the device and no potential is present. By exposing the photovoltaic device to light, the I-V

curve shifts downwards, as can be seen in Figure 3-6. The most important characteristic terms of organic photovoltaic devices can be found on this I-V curve.

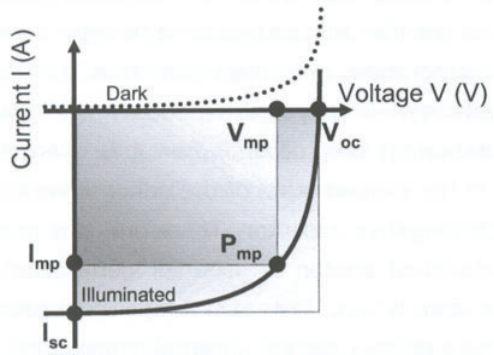

Figure 3-6 Typical I-V curve for a solar cell in the dark and under illumination (the most important photovoltaic parameters are indicated)[13]

Open-circuit voltage V_{oc}: The open-circuit voltage is the maximum possible voltage across a photovoltaic device. This is the voltage across the cell, in sunlight, when no current is flowing through the device.

Short-circuit current I_{sc}: The short-circuit current is the current that flows through an illuminated solar cell when there is no external resistance *i.e.* when the electrodes are simply connected or short-circuited. I_{sc} is the maximum current that a photovoltaic device is able to produce. Under an external load, the current will always be less than I_{sc}. The short-circuit current depends on a number of factors, such as the area of the solar cell. To remove the dependence of the solar cell area, it is more common to list the short-circuit current density (J_{sc} in mA/cm^2), rather than the short-circuit current (I_{sc} in mA).

Maximum power point: The maximum power point is the point (I_{mp},V_{mp}) on the I-V curve at which the maximum power is produced. Power P is the product of current I and voltage V. This is presented in Figure 3-6 as the

area of the rectangle formed between a point on the I-V curve and the axes I and V. The maximum power point is that point on the I-V curve at which the area of the resulting rectangle, I x V, is largest.

Fill factor FF: The fill factor of a photovoltaic device is the ratio of its actual maximum power output to its theoretical power output, if current and voltage would be at their maxima, I_{sc} and V_{oc}, respectively. This is a very important property used to measure photovoltaic device performance. It is a measure of the 'squareness' of the I-V curve. FF can be written down as follows

$$FF = \frac{I_{mp} \, x \, V_{mp}}{I_{sc} \, x \, V_{oc}}$$

Power conversion efficiency PCE or η_e: The power conversion efficiency is the ratio of power output to power input. PCE measures the amount of power produced by a photovoltaic device relative to the power available in the incident solar radiation P_{in}. P_{in} is the sum over all wavelengths, which usually has a value of 100 W/cm^2 when solar simulators are used. This is the most general way to define the efficiency of a photovoltaic device. PCE can be written down as follows

$$PCE = \frac{P_{out}}{P_{in}} = \frac{I_{mp} \, x \, V_{mp}}{P_{in}} = \frac{I_{sc} \, x \, V_{oc} \, x \, FF}{P_{in}}$$

Air mass AM: Air mass is the amount of atmosphere, though which sunlight has to travel to reach the earth's surface. This is abbreviated as AM x, in which x is the inverse of the cosine of the zenith angle of the sun. A typical value for photovoltaic device measurements is AM 1.5, which means that the sun is at an angle of about 48°. Furthermore, air mass describes the spectrum of radiation, but not the intensity of it. As was mentioned above, for photovoltaic device measurements, the intensity is commonly fixed at 100 W/cm^2.

3.4. Morphology of the active layer in bulk heterojunction devices

The requirement of an intimate intermixing of donor and acceptor in bulk heterojunction devices makes these devices very sensitive to their nanoscale morphology. This section focuses on the typical morphology of the active layer, consisting of PPV derivatives and fullerenes.

To achieve high efficiency devices, all generated excitons have to reach the donor/acceptor interface and dissociate. Subsequently, all created charges have to move to the respective electrodes. Photoluminescence quenching[20,47] and photocurrent modeling[20,21,48] indicate that only those excitons can be dissociated, which are generated in proximity to the donor/acceptor interface within less than the exciton diffusion length. To have the most intimate mixing, donor-acceptor dyads[49-53] and donor-acceptor polymers (double cables)[54,55] have been synthesized and used in organic solar devices. However, the PCE of these devices, consisting of covalently bonded donor-acceptor pairs, is rather low. This indicates the presence of loss mechanisms due to the recombination of electrons and holes and poor charge transport. Apparently, too intimate mixing results in the occurrence of too small mean free paths. Therefore, not only the relationship between molecular structure and device properties but also between nanoscale morphology and device properties will play a very important role in the preparation of good devices.

To this end, for example, the influence of the casting solvent and the casting method on the phase separation is extensively investigated in MDMO-PPV/PCBM layers.[35,46,56-66] PCBM or (6,6)-phenyl C_{61} butyric acid methyl ester, a soluble derivative of C_{60}, is frequently used in organic photovoltaics. The structure is depicted in Figure 3-7. These investigations include the fine tuning of the optimal ratio of MDMO-PPV and PCBM in devices.[56-66] The effect of the casting solvent is probably the most pronounced. The use of toluene as solvent in the MDMO-PPV/PCBM system leads to a coarser phase separation than is observed for chlorobenzene. This has been clearly demonstrated with atomic force microscopy (AFM)[56] and transmission

electron microscopy (TEM).[57] The large-scale phase separation (toluene) yields smaller photocurrents and unquenched photoluminescence can be detected.[46] This photoluminescence can be assigned to the large PCBM clusters in the film. In addition, the phase separation is too large for the dissociation of all generated excitons and this lowers the overall PCE. In contrast, when using chlorobenzene, no photoluminescence of PCBM is detected. The devices with the highest PCE are based on chlorobenzene as the solvent with a MDMO-PPV/PCBM ratio of 1/4.[35,56,63,64] The high PCBM ratio is needed for an efficient electron transport. This demonstrates that a minimum grain size of PCBM is necessary to guarantee enough pathways for the electrons. This requirement is in accordance with measurements on systems consisting of perylene derivatives.[65,66] Hence, it is of considerable importance to find the optimum in the domain size of the phase separation between donor and acceptor, since a balance between 'good' exciton dissociation and 'good' charge transport needs to be achieved.

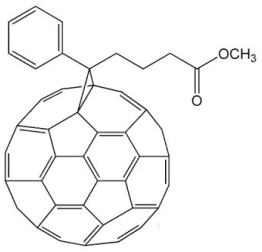

Figure 3-7 Chemical structure of (6,6)-phenyl C_{61} butyric acid methyl ester (PCBM)

Since the casting method also has an impact on the phase separation, further investigations have focused on the difference in the resulting morphology after drop-casting or spin-coating of the films.[59,60] Smaller PCBM domains are observed in spin-coated films than in drop-cast films. The reason for this is related to the faster evaporation rate during spin-coating as compared to drop-casting. While the slower evaporation in drop-casting allows the PCBM to coalesce into larger domains, spin-coating tends to freeze the blend, which results in smaller and more dispersed PCBM domains.

3.5. Solar cells of copolymers 19, 20, 21, 22 and 23

As mentioned above, the formation of a bulk heterojunction device significantly improves the interfacial area between donor and acceptor. However, the prize paid is the more complicated nanoscale morphology of the blend, which is difficult to optimize and to control. However, since the nanoscale morphology of the active layer of the photovoltaic devices also has a large impact on the mobility of the charge carriers, such control is very important. After all, mobility is not a material parameter but a device parameter. As discussed in the previous section, the morphology is strongly dependent on the device processing parameters. However, molecular (polymer) structure is obviously also of significant importance.

This chapter focuses on the impact of the presence of certain functional groups on the formation of the nanoscale morphology. To this end, the donor (MDMO-PPV) has been 'modified' with 10 % of functional groups, as described in **Chapter 2**.

3.5.1. Solar cell built-up

In order to study the effect of 10 % built-in functional groups in MDMO-PPV, bulk heterojunction devices have been made. The general built-up of the solar cell is as follows ITO/PEDOT:PSS/active layer/Ca/Al, in which the active layer consists of a PPV derivative as the donor and PCBM as the acceptor. The synthesized copolymers **19** (vinyl group), **20** (propenylphenyl group), **21** (propynylphenyl group), **22** (acrylate group) and **23** (propargyl group) are used as PPV derivatives and compared with the reference material MDMO-PPV. The chemical structures of the copolymers **19**, **20**, **21**, **22** and **23** are depicted in Figure 3-8. The side chains of the different copolymers differ only in 10 % with those of MDMO-PPV. **MDMO-PPV** has been synthesized via the sulfinyl precursor route.[67-69] All the properties

are similar to those reported in literature. The molecular weight according to size exclusion chromatography in THF is M_w = 3.4 x 10^5 g/mol (PD = M_w/M_n = 4.8). In addition, the **MDMO-PPV** displays the typical π-π* transition at λ_{max} = 510 nm (THF) in the UV-Vis absorption spectrum.

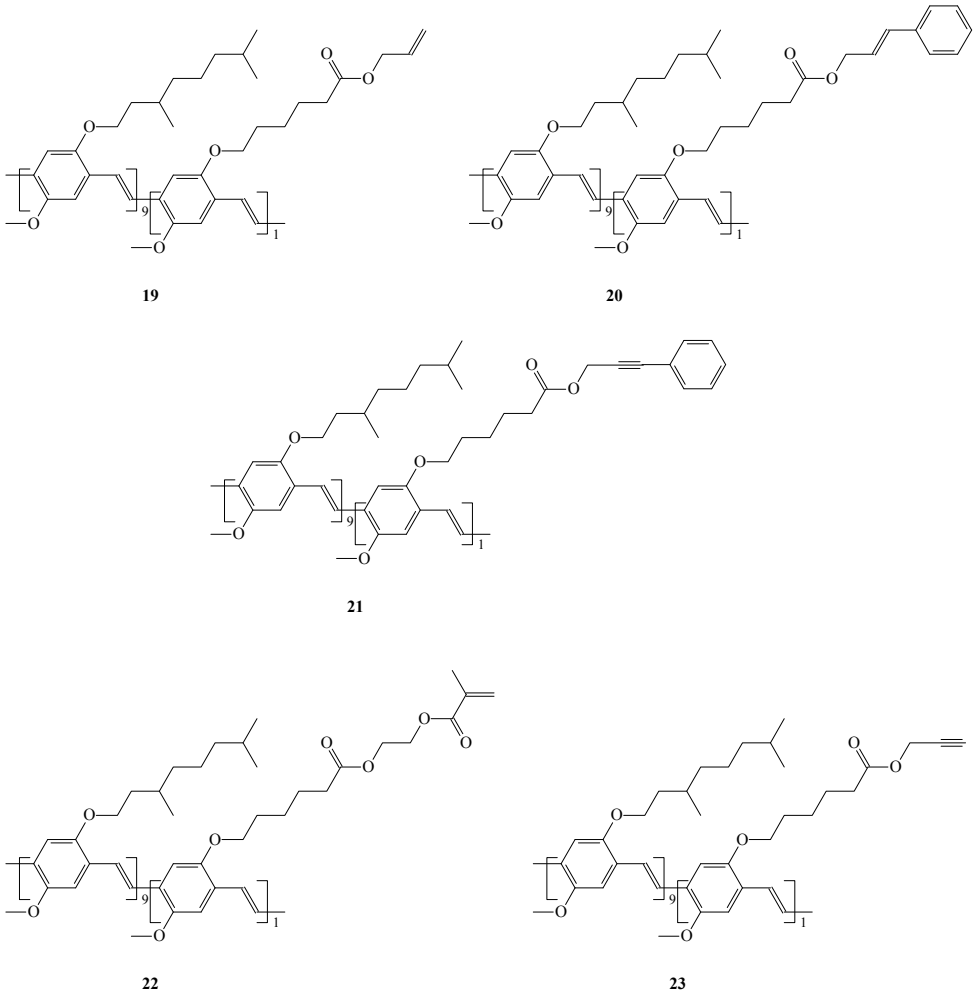

Figure 3-8 Chemical structure of copolymer **19** (vinyl group), **20** (propenylphenyl group), **21** (propynylphenyl group), **22** (acrylate group) and **23** (propargyl group)

In view of the existing literature on processing parameters (section 3.4.), the active layer has been spin-coated using chlorobenzene as the solvent. The 'active layer solution' consists of PPV derivative/PCBM in a ratio of 1/4. The thickness of the active layer of the different solar cells is between 80 nm and 120 nm. In Figure 3-9 a cartoon is depicted of the working principle of the above mentioned solar cells, with a PPV derivative as donor and PCBM as acceptor. It should be noted that all devices are illuminated under AM 1.5 conditions.

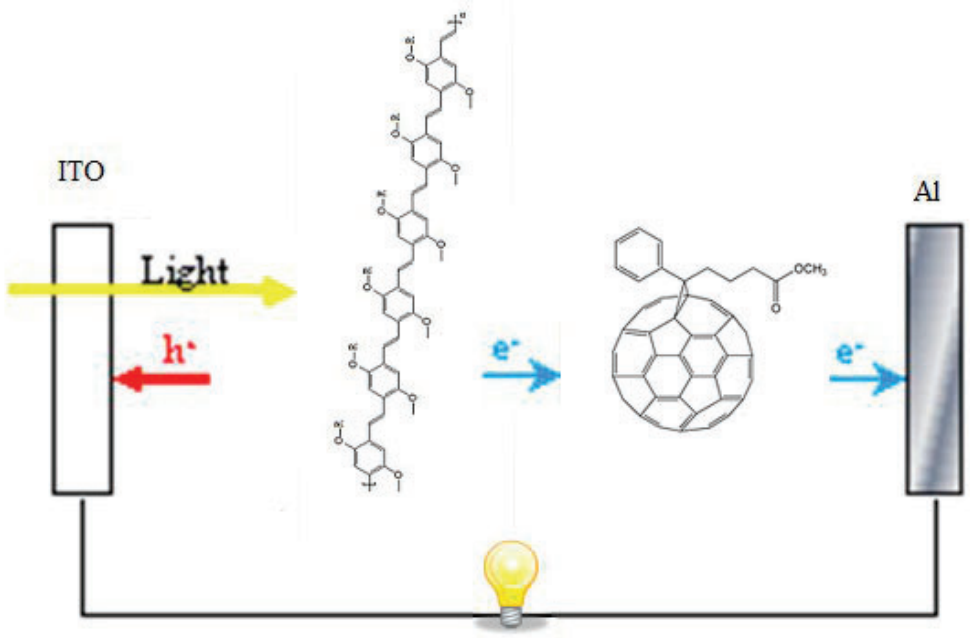

Figure 3-9 Cartoon of the working principle of a solar cell, with a PPV-derivative as donor and PCBM as acceptor

3.5.2. Influence of 10 % 'built-in' functional groups in MDMO-PPV on the solar cell performance

All the properties concerning the performance of the solar cells containing the novel copolymers are summarized in Table 3.1 and Figure 3.10.

Copolymer	J_{sc} (mA/cm^2)	V_{oc} (V)	FF (%)	PCE (%)
MDMO	3.37	0.77	0.58	1.53
19	3.06	0.80	0.40	1.00
20	3.77	0.79	0.56	1.65
21	3.41	0.62	0.49	1.06
22	3.10	0.81	0.32	0.81
23	4.22	0.80	0.59	2.00

Table 3-1 Solar cell performance for **MDMO-PPV**, copolymer **19**, **20**, **21**, **22** and **23**

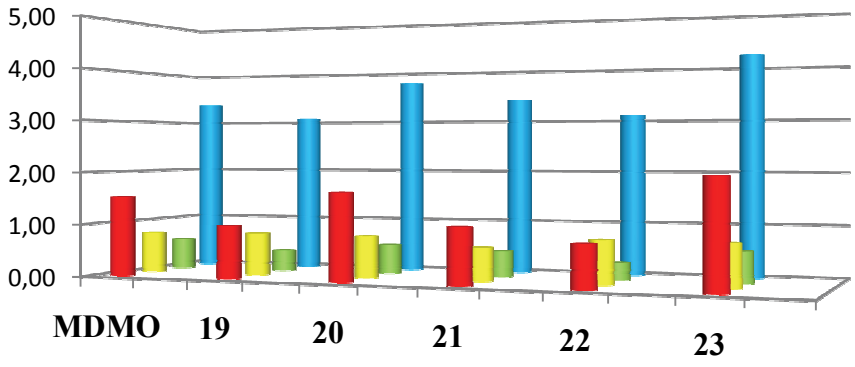

Figure 3-10 Representation of solar cell performance (PCE, V_{oc}, FF, J_{sc}) for **MDMO-PPV**, copolymer **19**, **20**, **21**, **22** and **23**

The open-circuit voltage depends on the energy levels of the used materials and to a lesser degree also on their interfaces.[70] From Table 3-1 and Figure 3-10 it can be concluded that the V_{oc} values of all the measured (co)polymers are in the same range. This is not surprising, since the V_{oc} depends especially on the HOMO and LUMO from respectively donor and acceptor.[71,72] The acceptor is in all cases PCBM and the donors are the different (co)polymers. Due to the same conjugated backbone of the studied (co)polymers, the HOMO level of all these polymers will be approximately have the same value. Thus, as can be expected, V_{oc} values are all in the same range, *i.e.* 0.77-0.81 V. Only for copolymer **21**, the V_{oc} is lower (0.62 V) than for the others. Although this can have a morphological reason, in this case charge carrier losses at the electrodes are a more likely cause of the lower V_{oc}.[73]

J_{sc} yields information about the charge separation and transport efficiency in the cell. Therefore J_{sc} values can often be correlated to the nanoscale morphology structure of the different active layers.[46,74-77] Figure 3-11 shows TEM pictures of the active layers of the different photovoltaic devices. Comparing with **MDMO-PPV**, the phase separation between the PPV-derivative and PCBM in copolymer **19**, **20** and **23** is somewhat better than observed for **MDMO-PPV**, *i.e.* a fine interpenetrating nanoscale morphology is observed. This results in a better J_{sc}, *i.e.* 3.77 mA/cm^2 for copolymer **20** and 4.22 mA/cm^2 for copolymer **23**, as compared to the J_{sc} for **MDMO-PPV** of 3.37 mA/cm^2 (Table 3-1 and Figure 3-10). J_{sc} for copolymer **19** is 3.06 mA/cm^2, which is somewhat lower than **MDMO-PPV**. This is not expected from TEM analysis and may, for example, be caused by the presence of impurities, which will lower the J_{sc} value (act as traps). For copolymers **21** and **22**, the phase separation is different, as can be seen in Figure 3-11. These PPV-derivatives and PCBM form almost one phase and insufficient phase separation is achieved for establishing well-defined transport pathways for electrons and holes. This increases the likelihood of recombination of the electrons and holes. As can be expected, this has a negative influence on the corresponding J_{sc} and FF values (Table 3-1 and Figure 3-10), which are in the same order of magnitude or even somewhat smaller than observed for **MDMO-PPV**. It is surprising to note that the nanoscale morphology of the different active layers is very much

influenced by the incorporation of 10 % functional groups in **MDMO-PPV**. The incorporated vinyl, propenylphenyl and propargyl groups form with PCBM smaller phases than MDMO does, but still leave enough phase separation for an efficient transport of charges. In contrast, propynylphenyl and acrylate groups form almost one phase with PCBM and not enough phase separation is present. However, unfortunately at this moment not yet a clear explanation for the observed differences in behavior can be given.

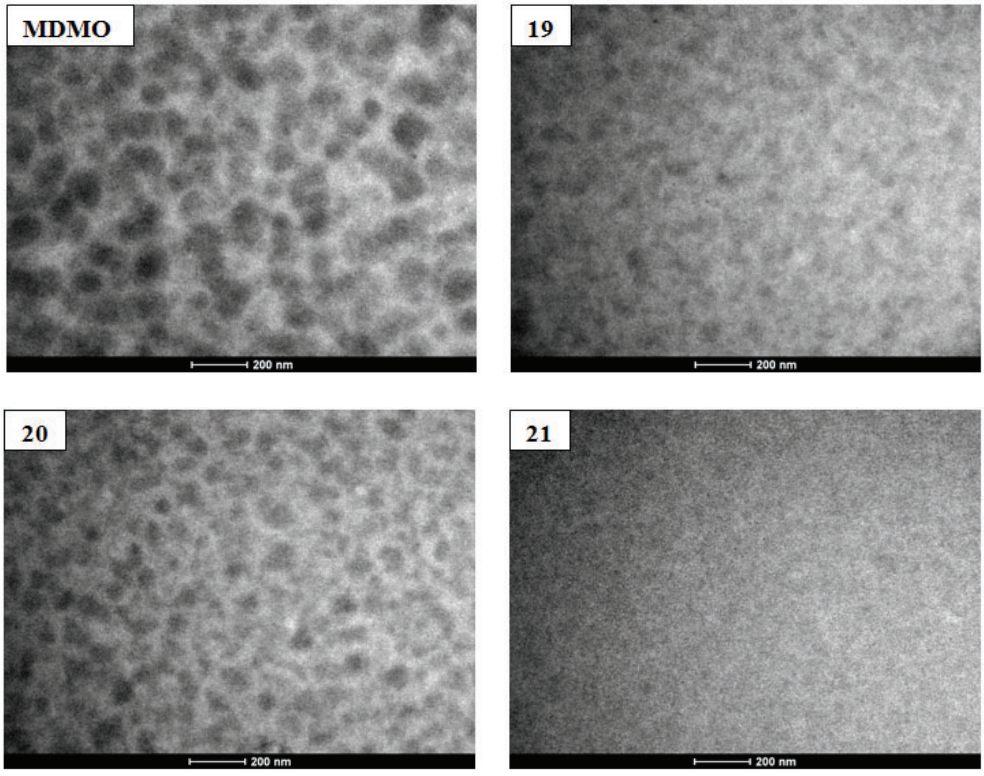

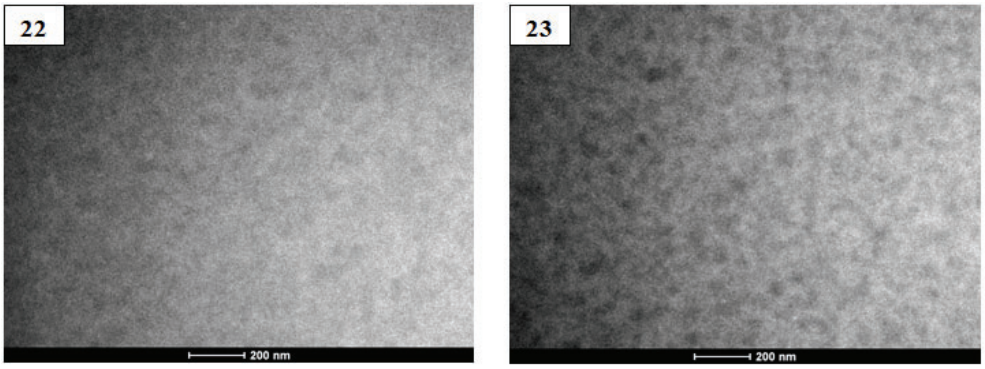

Figure 3-11 TEM pictures of the active layer of photovoltaic devices from **MDMO-PPV**, copolymer **19** (vinyl group), **20** (propenylphenyl group), **21** (propynylphenyl group), **22** (acrylate group) and **23** (propargyl group)

The FF is determined by the fraction of the electrons and holes that actually reach the electrodes.[78] There is a competition between charge carrier recombination and transport, as was discussed in section 3.3.2.. In organic solar cells, the FF is typically around 0.4-0.6. From Table 3-1 and Figure 3-10, all the FF values for the measured (co)polymers are in this range. The higher the FF, the better the quality of the device. The highest FFs are determined for **MDMO-PPV** and copolymers **20** and **23**.

V_{oc}, I_{sc} and FF determine the overall efficiency (PCE) of the photovoltaic device. There is a subtle interplay between these factors and they have to be resolved together to obtain high PCE organic photovoltaic devices. As compared to **MDMO-PPV**, the values of V_{oc}, I_{sc} and FF for copolymer **20** (propenylphenyl group) are in the same order of magnitude, which results in almost the same PCE for copolymer **20** (1.65 %) and **MDMO-PPV** (1.53 %). In addition, the V_{oc} and FF for copolymer **23** (propargyl group) are also in the same range as for **MDMO-PPV**. However, since the I_{sc} is much higher for copolymer **23** a better PCE (2.00 %) is observed. This improvement in PCE is mainly due an improved nanoscale morphology as is evident from the TEM analysis. A similar observation can be made for copolymer **20**, although the improvements for this copolymer are somewhat smaller.

3.6. Influence of 10 % 'built-in' functional groups in MDMO-PPV on the thermal stability of the morphology of the active layer in solar cells

The observation of an enhanced temperature controlled nanoscale morphology gives rises to the question how stable the bulk heterojunction devices are with respect to aging effects. Annealing experiments at high temperatures can result in micrometer sized PCBM aggregates, driven by the diffusion and crystallization of PCBM.[46,79,80] Thus, annealing results in morphological degradation due to the formation of too large PCBM domains. Hence, morphological stability in bulk heterojunction devices is of a great importance, as under operating conditions elevated temperatures can be expected. In this way, the optimal morphology of a bulk heterojunction device requires stable, nanometer sized interpenetrating donor and acceptor domains.

To study this aspect, the active layer of the six photovoltaic devices, described in section 3.5., have been investigated after annealing at a temperature of 100 °C for 15 and 30 minutes. After annealing, TEM pictures are taken to study the crystallization of PCBM.

The TEM pictures of all the active layers, before thermal annealing, are depicted in Figure 3-12 in the μm scale. It is evident that the structure of the active layer is for all copolymers essentially identical. After 15 minutes of thermal annealing at 100 °C, it can be observed that PCBM starts to crystallize in all samples (Figure 3-13). The black parts in these figures are identified as PCBM *via* their characteristic diffraction pattern. Crystallization of PCBM is the highest for the samples containing copolymers **19** and **22**. The samples with **MDMO-PPV** and copolymer **23** display the lowest amount of crystallized PCBM. This is better, since most of the phase separated regions, which are needed for transport of the charge carriers, remain available. In addition, the differences in crystal growth are

noteworthy. The shape of the formed PCBM crystals in the samples containing copolymers **19** and **22** (double bond at the end of the side chain) is very different as compared to the shape observed for the crystals in copolymers **20** and **21** (phenyl at the end of the side chain) as well as **MDMO-PPV** and copolymer **23**. In the presence of **MDMO-PPV** and copolymer **23**, small ellipsoid PCBM crystals are formed. The presence of triple bonds has apparently no effect on the formation of PCBM crystals. On the contrary, in the presence of copolymer **19** and **22** (double bond at the end of the side chain), spherulite-like PCBM crystals are formed. Meanwhile, in the presence of copolymer **20** and **21** (phenyl at the end of the side chain), rectangular-like PCBM crystals are visible. Apparently, the type of crystallization of PCBM is dependent on the different built-in functional groups in the PPV derivatives. This trend is further observed after thermal annealing for an additional 15 minutes (Figure 3-14). Also at this stage, the samples with **MDMO-PPV** and copolymer **23** exhibit the lowest amount of PCBM crystals. In addition, they have the most phase separation left between the corresponding PPV derivative and PCBM.

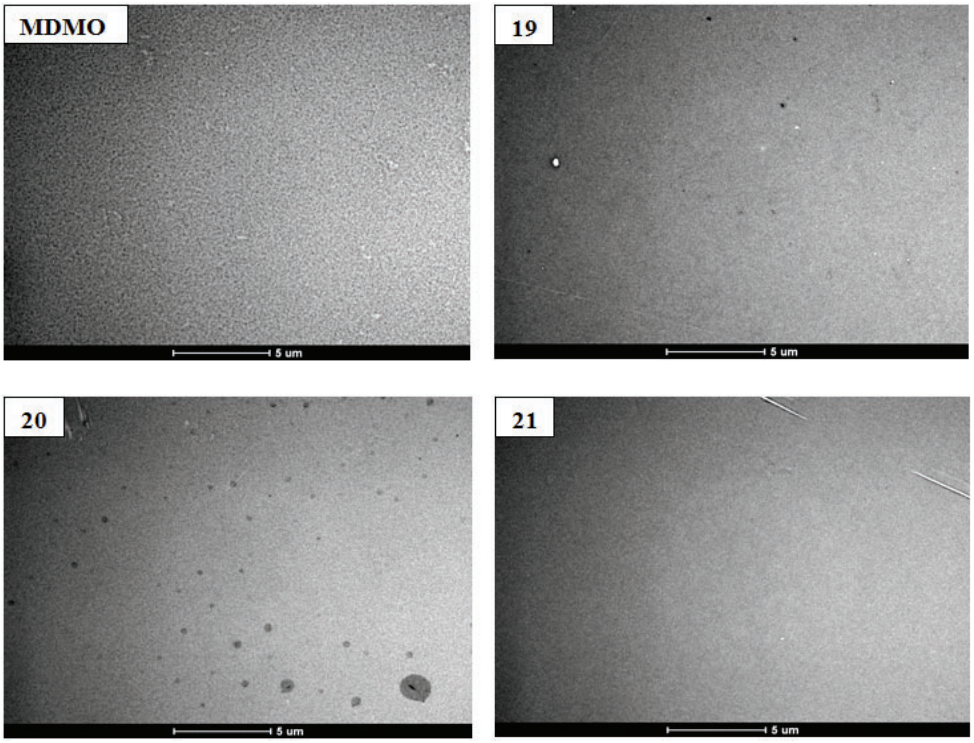

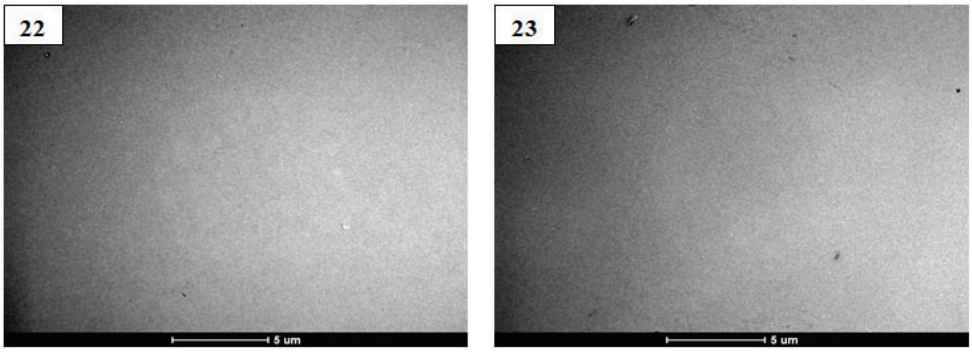

Figure 3-12 TEM pictures of the active layer of photovoltaic devices from **MDMO-PPV**, copolymer **19** (vinyl group), **20** (propenylphenyl group), **21** (propynylphenyl group), **22** (acrylate group) and **23** (propargyl group) before thermal treatment

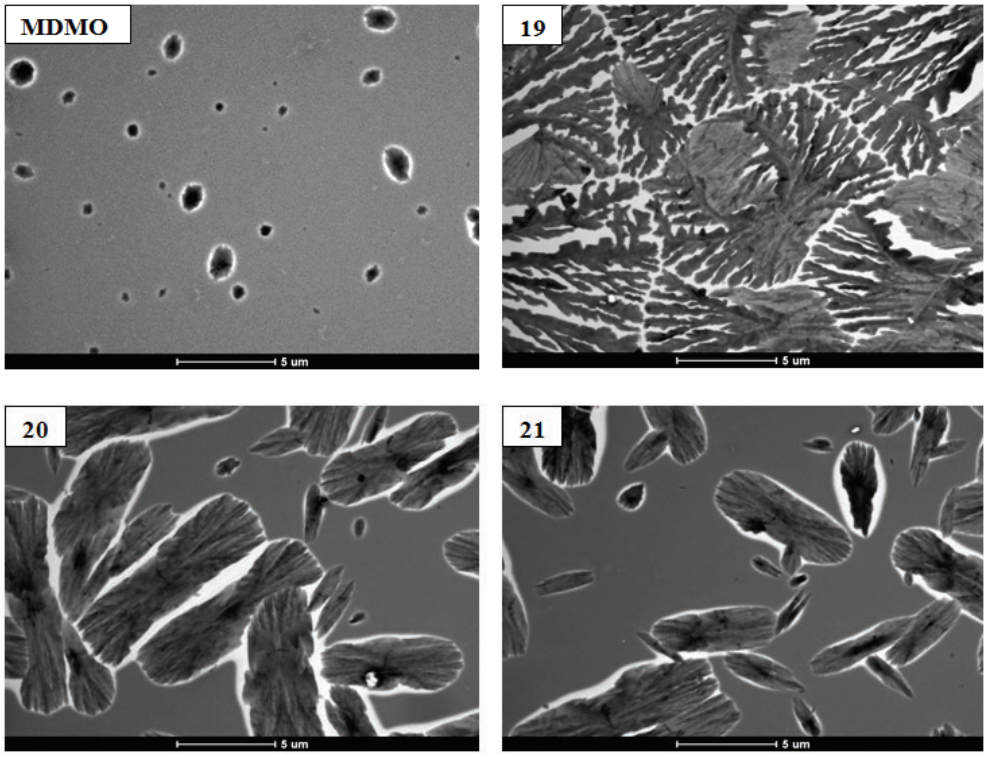

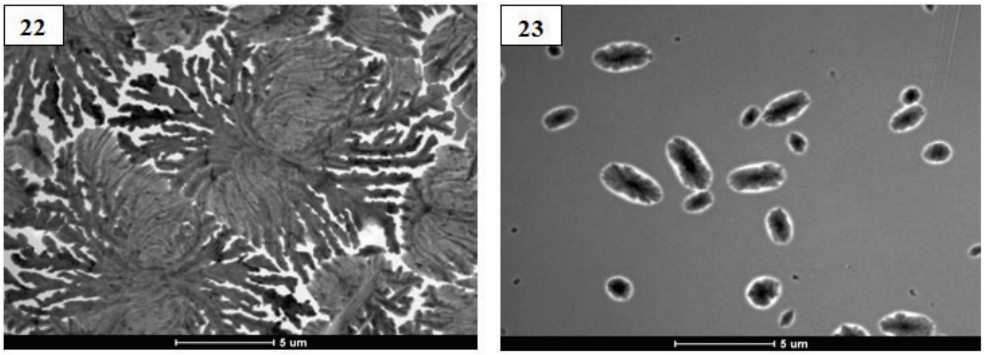

Figure 3-13 TEM pictures of the active layer of photovoltaic devices from **MDMO-PPV**, copolymer **19** (vinyl group), **20** (propenylphenyl group), **21** (propynylphenyl group), **22** (acrylate group) and **23** (propargyl group) after thermal treatment at 100 °C for 15 minutes

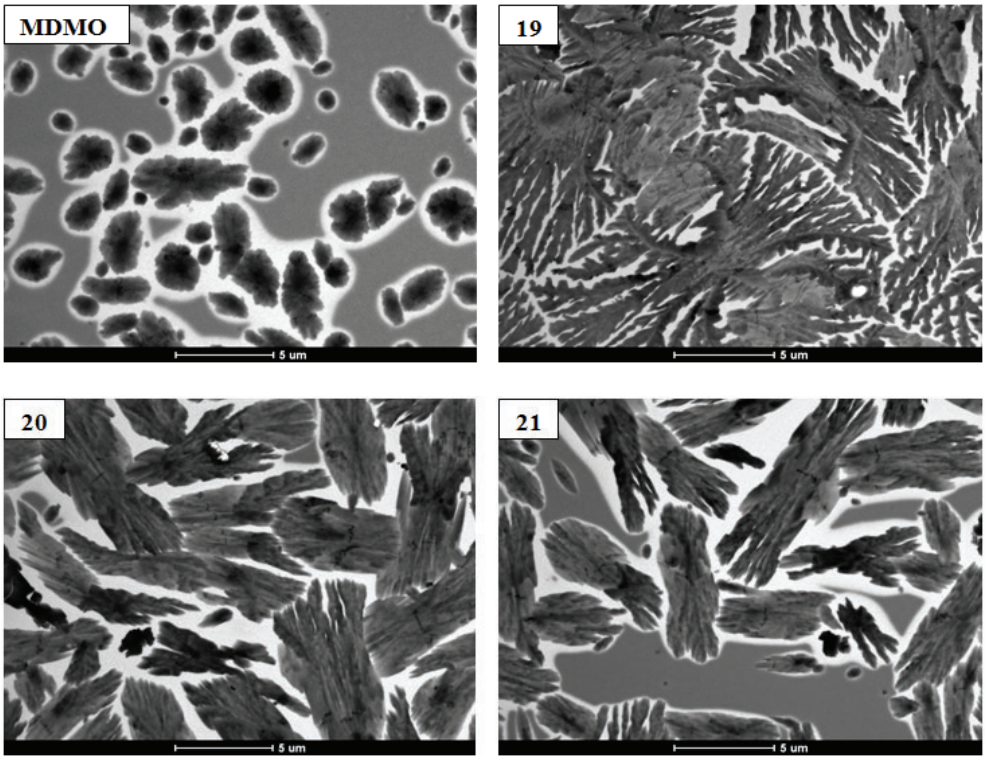

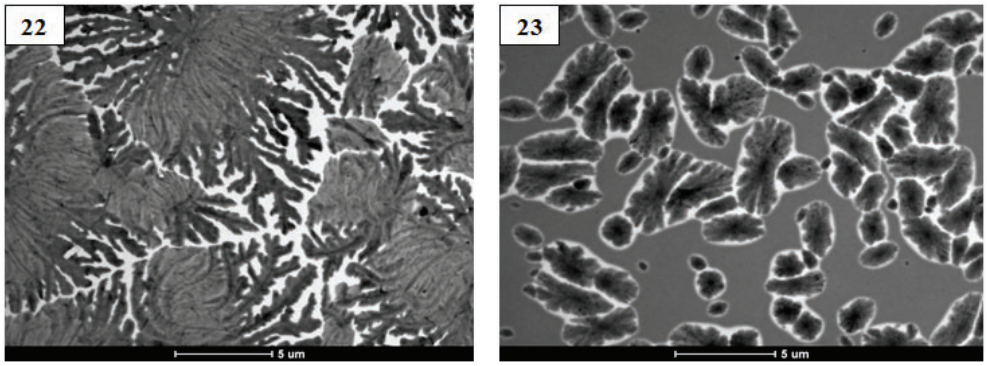

Figure 3-14 TEM pictures of the active layer of photovoltaic devices from **MDMO-PPV**, copolymer **19** (vinyl group), **20** (propenylphenyl group), **21** (propynylphenyl group), **22** (acrylate group) and **23** (propargyl group) after thermal treatment at 100 °C for 30 minutes

The same trend can be observed by comparing optical microscope pictures of all the active layers, before thermal annealing (Figure 3-15), after 15 minutes of thermal annealing at 100 °C (Figure 3-16) and after 30 minutes of thermal annealing at 100 °C (Figure 3-17). The differences in the formation of PCBM crystals are again clearly visible. In the presence of **MDMO-PPV** and copolymer **23**, small 'points' of PCBM crystals are observed. In contrast, in the presence of copolymer **19** and **22**, the same small PCBM crystals are visible as were observed in the TEM pictures, although they appear more connected with each other. Meanwhile, in the presence of copolymer **20** and **21**, needle-like PCBM crystals are found.

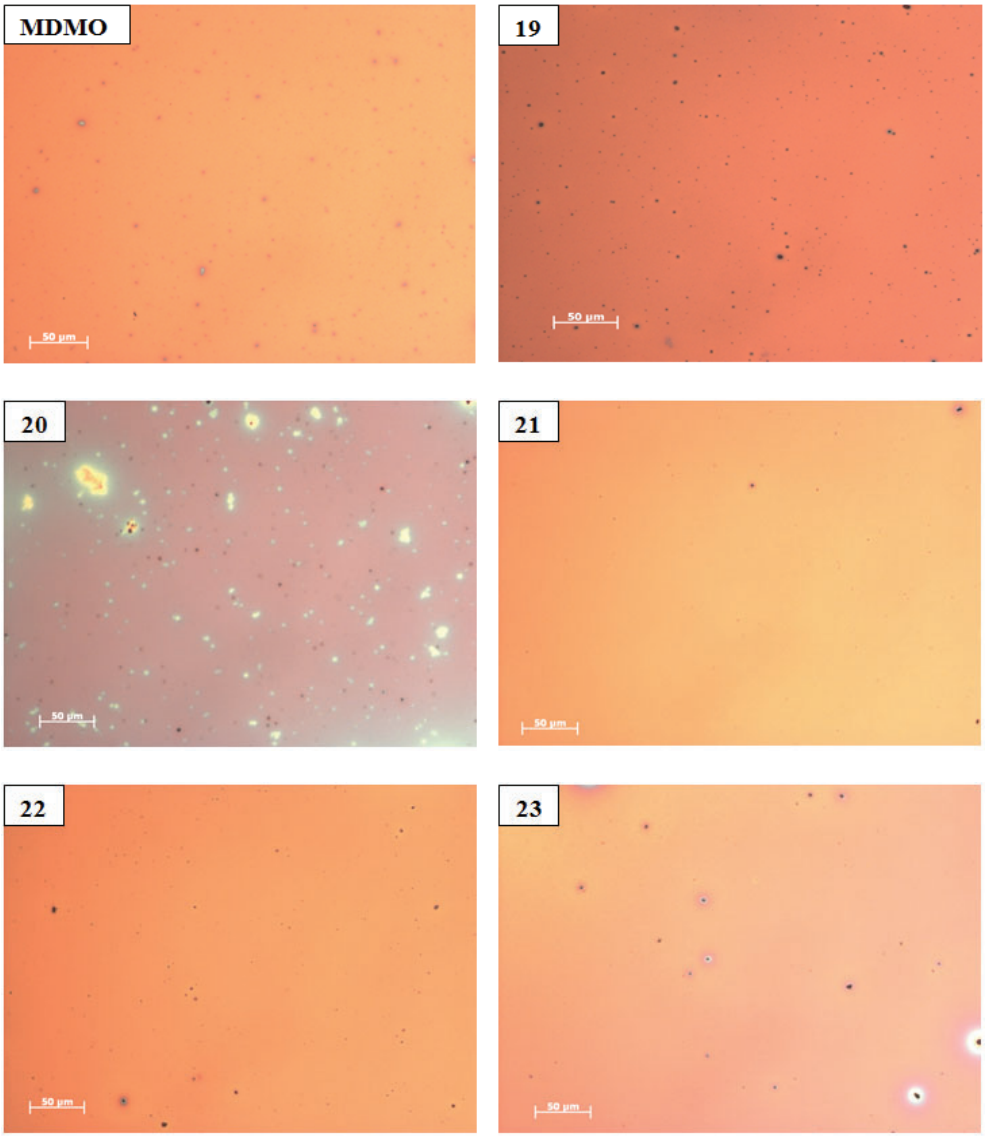

Figure 3-15 Optical microscope pictures of the active layer of photovoltaic devices from **MDMO-PPV**, copolymer **19** (vinyl group), **20** (propenylphenyl group), **21** (propynylphenyl group), **22** (acrylate group) and **23** (propargyl group) before thermal treatment

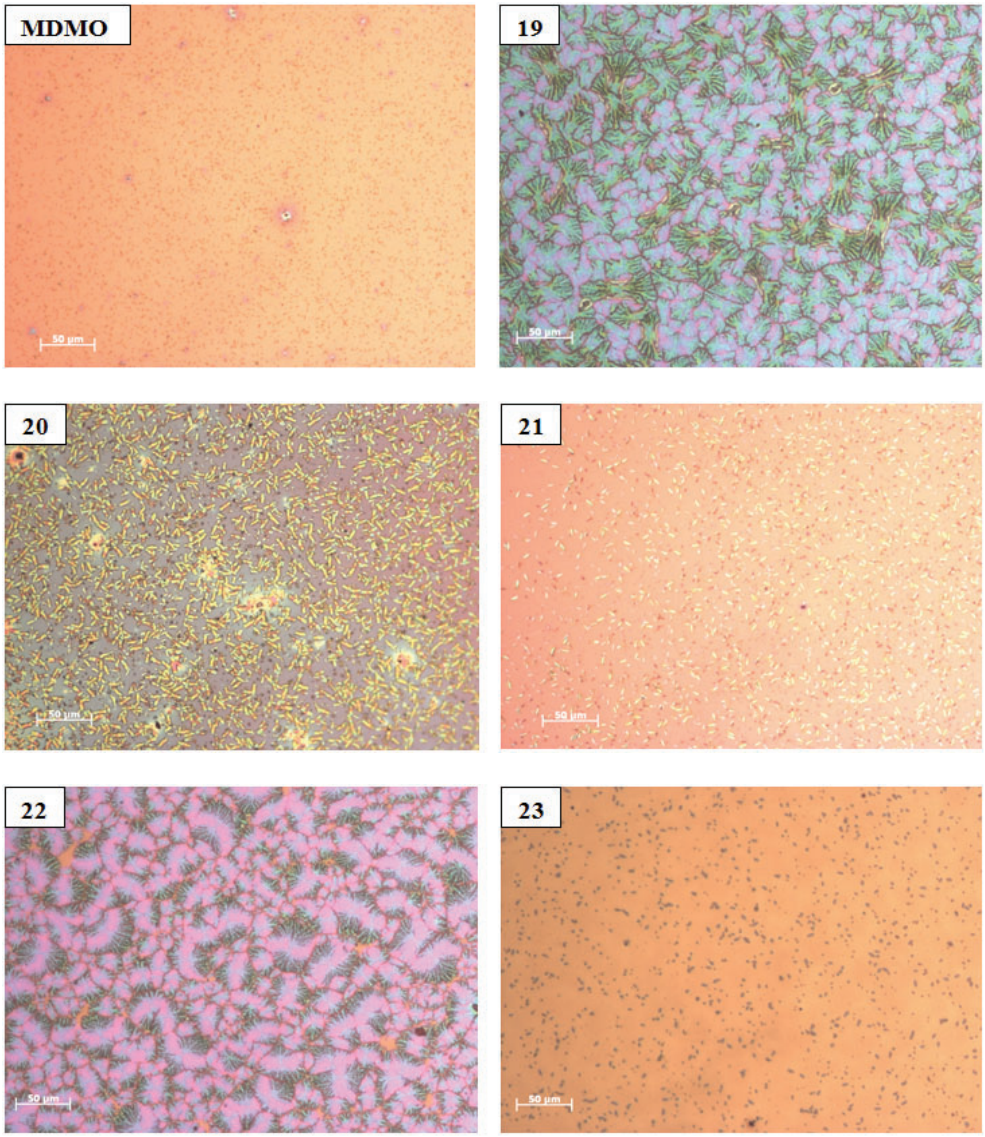

Figure 3-16 Optical microscope pictures of the active layer of photovoltaic devices from **MDMO-PPV**, copolymer **19** (vinyl group), **20** (propenylphenyl group), **21** (propynylphenyl group), **22** (acrylate group) and **23** (propargyl group) after thermal treatment at 100 °C for 15 minutes

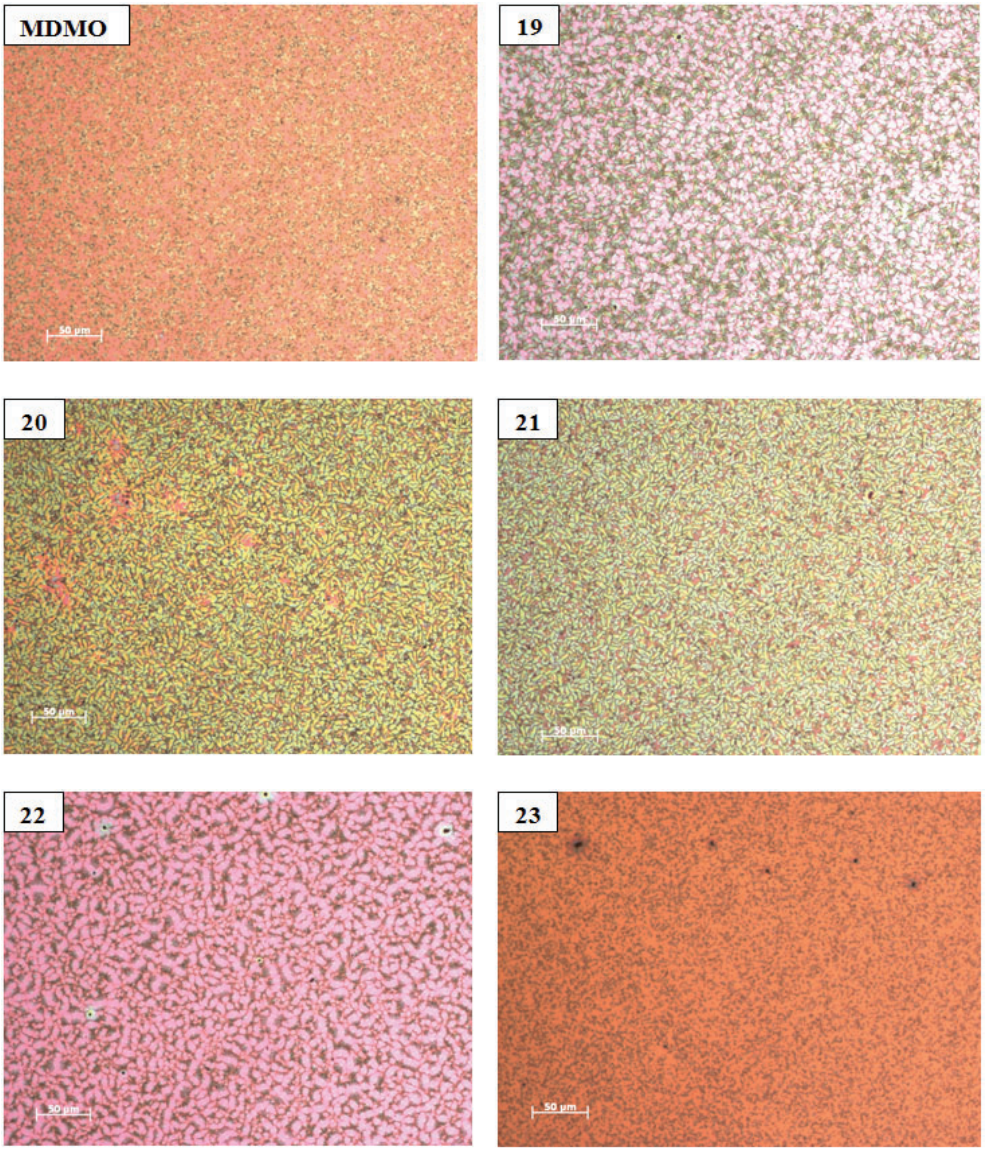

Figure 3-17 Optical microscope pictures of the active layer of photovoltaic devices from **MDMO-PPV**, copolymer **19** (vinyl group), **20** (propenylphenyl group), **21** (propynylphenyl group), **22** (acrylate group) and **23** (propargyl group) after thermal treatment at 100 °C for 30 minutes

3.7. Influence of 10 % 'built-in' functional groups in MDMO-PPV on the thermal characteristics

The solar cell performance for **MDMO-PPV** and copolymers **19**, **20**, **21**, **22** and **23** can be mainly correlated with the morphology of the active layer to a reasonable degree (section 3.5.2.). However, the origin of the differences in morphology remain unclear. To investigate whether a correlation exists with the thermal characteristics of the polymers, the glass transition temperature (T_g) of the different (co)polymers has been investigated. To this end, differential scanning calorimetry (DSC) and modulated temperature differential scanning calorimetry (MTDSC) have been performed on **MDMO-PPV**, copolymer **19**, **20**, **21**, **22** and **23**. The DSC measurements are depicted in Figure 3-18.

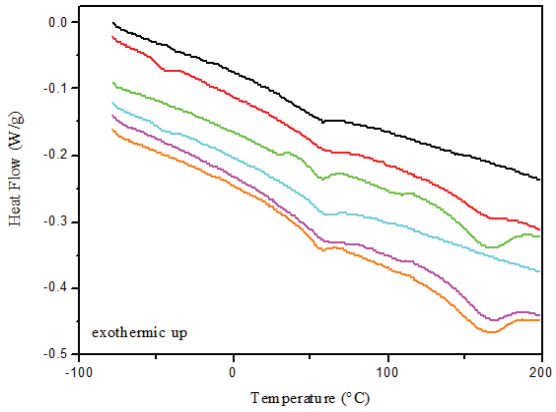

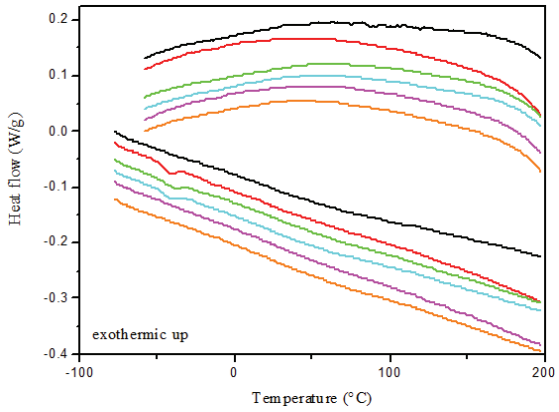

Figure 3-18 Differential scanning calorimetry (DSC) measurements of **MDMO-PPV**, copolymer **19**, **20**, **21**, **22** and **23** (top: first heating; bottom: first cooling and second heating)

In the first heating scan of a DSC experiment, usually multiple peaks are visible. There are several factors that can cause such peaks, *e.g.* remaining solvent, impurities, poor contact between sample and crucible. Only when the peaks are reproducible, they can be considered as real properties of the sample. Therefore the focus is on the second heating scans. In these scans, most of the peaks disappeared and no crystallization or melting is observed. It is clear that all observed (co)polymers are completely amorphous. Notwithstanding, there are some small peaks visible at about -40 °C for copolymers **19**, **20** and **21**, of which the physical origin remains unclear.

Since the T_g in the DSC measurements is not clearly visible, MTDSC measurements are performed to investigate the influence of 10 % 'built-in' functional groups in MDMO-PPV on the T_g. In MTDSC, temperature modulation is used, which makes the observation of the T_g more straightforward (Figure 3-19).

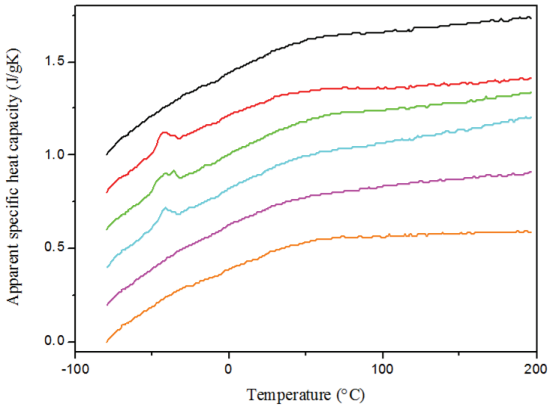

Figure 3-19 Modulated temperature differential scanning calorimetry (MTDSC) measurements of **MDMO-PPV**, copolymer **19**, **20**, **21**, **22** and **23**

For all the observed (co)polymers, a broad T_g can be seen at about 20 °C with a half-width of about 30 °C. Apparently, the 10 % 'built-in' functional groups only have a minor impact on the T_g and do not give rise to an additional T_g. Hence, it can be concluded that there is not a clear correlation between these (MT)DSC results and the corresponding solar cell performance. Evidently, the improved performance of **23** does not originate from a difference in thermal characteristics. It should be noted that also in MTDSC, the same small peaks are visible at about -40 °C for copolymers **19**, **20** and **21** of which the origin remains unclear (Figure 3-18).

In a series of final experiments the degradation temperature has been investigated *via* thermogravimetrical analysis (TGA) for **MDMO-PPV** and copolymers **19**, **20**, **21**, **22** and **23** (Figure 3-20).

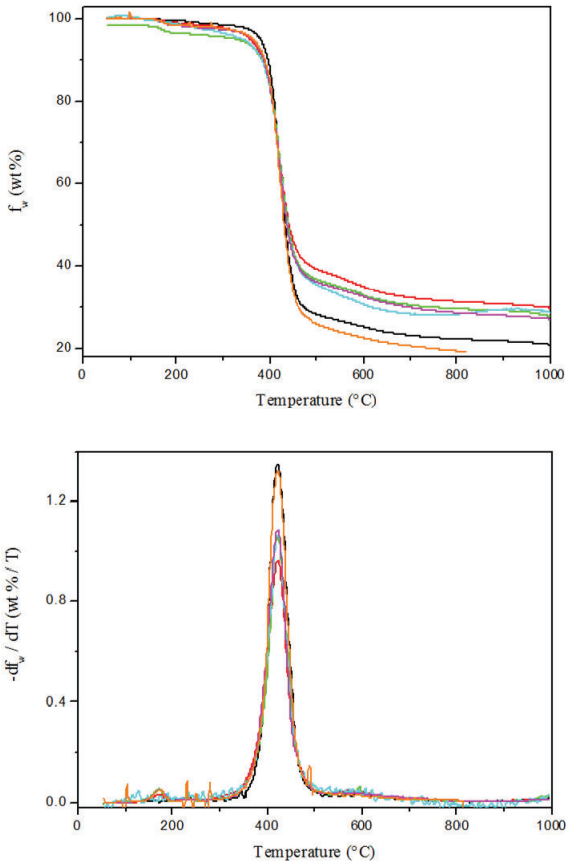

Figure 3-20 Thermogravimetrical analysis (TGA) of **MDMO-PPV**, copolymer **19**, **20**, **21**, **22** and **23** (top: TGA curve; bottom: derivative of TGA curve)

Similarly as observed for the (MT)DSC measurements, the 10 % 'built-in' functional groups have no distinct impact on the thermal stability of the different investigated PPV derivatives. For **MDMO-PPV**, copolymer **19**, **20**, **21**, **22** and **23** a major degradation occurs at *circa* 423 °C.

3.8. Conclusions

In the past 30 years, the demand for solar energy has steadily grown and currently a substantial amount of research is being done to develop efficient low cost photovoltaic devices. A promising class of new photovoltaics consists of organic solar cells, of which the bulk heterojunction devices are the best suitable. Control of the morphology in these devices is of considerable importance.[45,46] Obtaining a good nanoscale morphology results in an improvement of the interfacial area between donor (PPV derivative) and acceptor (PCBM). Studies into further improvement of the nanoscale morphology of the active layer in bulk heterojunction devices are presented in this chapter.

To this end, copolymers **19**, **20**, **21**, **22** and **23** have been synthesized. Their synthesis is described in **Chapter 2**. These copolymers can be regarded as MDMO-PPV, 'modified' with 10 % of functional groups. These functional groups are vinyl groups for copolymer **19**, propenylphenyl groups for copolymer **20**, propynylphenyl groups for copolymer **21**, acrylate groups for copolymer **22** and finally propargyl groups for copolymer **23**. The influence of this 10 % built-in of different functional groups is investigated in bulk heterojunction devices. All the results are compared with a reference material *i.e.* **MDMO-PPV**.

The performance of the solar cell, made by copolymer **23**, is found to be the best and even better than the reference material **MDMO-PPV**. This improvement can be correlated to the improved nanoscale morphology of blends containing copolymer **23** instead of **MDMO-PPV**. Focusing on the nanoscale morphology, the incorporation of vinyl, propenylphenyl and propargyl groups results in the formation of a finer interpenetrating network with PCBM as compared to **MDMO-PPV**. Notwithstanding, sufficient phase separation is left for an efficient transport of charges. In the case of propynylphenyl and acrylate groups, the mixing is so good that there is not enough phase separation left. Apparently in all cases, the introduced functional groups act as compatibilizers.

The thermal stability of active layers containing either copolymer **23** or **MDMO-PPV** is also comparable. Thermal annealing of the active layers lead to fast crystallization of PCBM in the samples containing copolymers **19** and **22**. The samples with **MDMO-PPV** and copolymer **23** display the lowest amount of crystallized PCBM. Also the formation of PCBM crystals is different, depending on the incorporated functional groups (double bond or phenyl).

The influence of the 10 % 'built-in' functional groups in MDMO-PPV on the T_g and thermal stability of these (co)polymers is almost negligible.

This leads to the final conclusion that copolymer **23**, with a propargyl group in the side-chain, is an excellent material to use in bulk heterojunction devices. Further optimization of the exact nature of the introduced functional groups as well as fine tuning of the copolymer composition, may lead to further improvements in the efficiency of the obtained solar cells.

3.9. Experimental section

3.9.1. Characterization

TEM pictures were obtained with a FEI Tecnai G2 Spirit Twin operating at 120kV. Analytical Size Exclusion Chromatography (SEC) was performed using a Spectra series P100 (Spectra Physics) pump equipped with a pre-column (5 μm, 50 x 7.5 mm, guard, Polymer Labs) and two mixed-B columns (10 μm, 2 x 300 x 7.5 mm, Polymer Labs) and a Refractive Index detector (Shodex) at 40 °C. THF was used as the eluent at a flow rate of 1.0 mL/min. Molecular weight distributions are given relative to polystyrene standards. UV-Vis measurements were performed on a Cary 500 UV-Vis-NIR spectrophotometer (scan rate 600 nm/min, continuous run from 200 to 800 nm).

3.9.2. Device preparation and measurement

The solar cells were prepared starting from indium tin oxide (ITO, 100 nm) coated glass plates, which were successively cleaned in a soap solution, demineralized water and acetone, each for 10 minutes in an ultrasonic bath. This was followed by cleaning in boiling isopropanol for 10 minutes. A 25 nm thick PEDOT:PSS layer (Bayer) was spin-coated on the clean glass/ITO substrates (40 seconds at 3000 RPM), after which the substrates were dried for 20 minutes on a hot plate at 120 °C. Subsequently, on top of the PEDOT:PSS layer, the active layer was spin coated. The active layer solution (PPV derivative/PCBM 1/4 in chlorobenzene at a concentration of 5 mg/mL of the PPV derivative) was spin coated in exactly the same conditions for each substrate (60 seconds at 3000 RPM). Finally, as a cathode, a metal top contact was evaporated, consisting of 20 nm calcium with 75 nm aluminum on top. All measurements were performed in a glove box, under nitrogen atmosphere. Current *versus* voltage characteristics were determined using a Newport class A solar simulator (model 91195A) calibrated with a silicon solar cell to give an AM 1.5 spectrum. The device current was registered using a Labview program, while sweeping a voltage across the device, going up from -0.1 V to a positive voltage of 1 V. The thickness of all spin coated (co)polymers, including the PEDOT:PSS layer were determined using a Dektak 3ST Surface Profile Measuring System.

DSC measurements, in both standard and modulated modes, were made on TA Instruments Q2000 DSC equipped with an RCS cooling accessory. Indium was employed for temperature calibration. The heat capacity was evaluated with respect to sapphire as a standard. Nitrogen with a flux of about 50 mL/min was used as a purge gas. Samples of *circa* 5 mg were sealed in TA Instruments Tzero aluminum crucibles. For the DSC measurements, the scan rate was 10 K/min. The stay time at the lower limit temperature of -90.0 °C was 10 min, while the stay time at the upper limit temperatures of 200.0 °C was 1 min. Three heating-cooling cycles were performed. For the MTDSC measurements, the modulation amplitude was 0.5 K with a period of 60 s. First, the samples were kept at 200.0 °C for 1 min. Subsequently, the samples were quenched in the DSC cell at about

100.0 K/min to -90.0 °C and then reheated to 200.0 °C at 2.5 K/min to observe the glass transition.

TGA measurements were performed on a TA Instruments Q5000 TGA. Platinum high-temperature Pan was used. Scan (heating) rate was 10.0 K/min. Nitrogen was used as purge gas at 10 mL/min for balance and 25 mL/min for sample.

3.10. References

[1] Becquerel, A. E. *Compt. Rend. Acad. Sci.* **1839**, *9*, 145.
[2] Becquerel, A. E. *Compt. Rend. Acad. Sci.* **1839**, *9*, 561.
[3] Smith, W. *Nature* **1873**, *7*, 303.
[4] Adams, W. G.; Day, R. E. *Proc. R. Soc. London* **1876**, *25*, 113.
[5] Pochettino, A. *Acad. Lincei Rend.* **1906**, *15*, 355.
[6] Volmer, M. *Ann. Physik* **1913**, *40*, 775.
[7] Borsenberger, P. M.; Weiss, D. S. *Organic Photoreceptors For Imaging Systems, New York* **1993**.
[8] Bube, R. H. *Photoconductivity of Solids, Wiley, New York* **1960**.
[9] Anthoe, S. *Rom. Rep. Phys.* **2002**, *53*, 427.
[10] Chamberlain G. A. *Sol. Cells* **1983**, *8*, 47.
[11] Chapin, D. M.; Fuller, C. S.; Pearson, G. L. *J. Appl. Phys.* **1954**, *25*, 676.
[12] Green, M. A.; Emery, K.; King, D. L.; Igari, S.; Warta, W. *Prog. Photovolt.: Res. Appl.* **2003**, *11*, 347.
[13] Spanggaard, H.; Krebs, F. C. *Solar Energy Materials & Solar Cells* **2004**, *83*, 125.
[14] Weinberger, B. R.; Aktar, M.; Gau, S. C. *Synth. Met.* **1982**, *4*, 187.
[15] Glenis, S.; Tourillon, G.; Garnier, F. *Thin Solid Films* **1986**, *139*, 221.
[16] Halls, J. J. M.; Pichler, K.; Friend, R. H. *Appl. Phys. Lett.* **1996**, *68*, 3120.
[17] Abdalla, T. A.; Mammo, W.; Workalemahu, B. *Synthetic Metals* **2004**, *213*, 144.
[18] Reis, F. T.; Mencaraglia, D.; Ould Saad, S.; Seguy, J.; Oukachmih, M.; Jolinat, P.; Destruel, P. *Journal Non Crystalline Solids* **2004**, *599*, 338.
[19] Sharma, G. D.; Sharma, S. K.; Roy, M. S. *Thin Solid Films* **2004**, *208*, 468.
[20] Peumans, P.; Yakimov, A.; Forrest, S. R. *J. Appl. Phys.* **2003**, *93*, 3693.

[21] Pettersson, L. A. A.; Roman, L. S.; Inganäs, O. *J. Appl. Phys.* **1999**, *86*, 487.
[22] Tang, C. W. *Appl. Phys. Lett.* **1986**, *48*, 183.
[23] Sariciftci, N. S.; Smilowitz, L.; Heeger, A. J. *Science* **1993**, *57*, 1474.
[24] Sariciftci, N. S.; Braun, D.; Zhang, C. *Appl. Phys. Lett.* **1993**, *62*, 585.
[25] F. T. Reis, F. T.; Mencaraglia, D.; Ould Saad, S.; Seguy, J.; Oukachmih, M.; Jolinat, P.; Destruel, P. *Journal Non Crystalline Solids* **2004**, *599*, 338.
[26] Halls, J. J. M.; Friend. R. H. *Synth. Met.* **1997**, *85*, 1307.
[27] Yonehara, H.; Pac. C. *Thin Solid Films* **1196**, *278*, 108.
[28] Sicot, L.; Fiovini, C.; Lorin, A.; Raimond, P.; Sentein, C.; Nunzi. J. M. *Sol. Ener. Mat. & Solar Cells* **2000**, *63*, 49.
[29] Tahahashi, K.; Kuraya, N.; Yamaguchi, T.; Komura, T.; Murata. K. *Sol. Ener. Mater. & Solar Cells* **2000**, *61*, 403.
[30] Pfeiffer, M.; Beyer, A. Ploinnings, B.; Nallau, A.; Fritz, T.; Leo, K.; Schlettwein, D.; Hiller, S.; Wohrle. D. *Sol. Ener. Mat. & Solar Cells* **2000**, *63*, 83.
[31] Drechsel, J.; Maenning, B.; Kozlowski, F.; Pfeiffer, M.; Leo, K. *Appl. Phys. Lett.* **2005**, *86*, 244102.
[32] Derouiche, H.; Bernède, J. C.; L'Hyver, J. *Dyes and Pigments* **2004**, *63*, 277.
[33] Yu, G.; Hummelen, J. C. *Science* **1995**, *270*, 1789.
[34] Hummelen, J. C.; Knight, B. W.; LePeq, F.; Wudl, F.; Yao, J.; Wilkins, C. L. *J. Org. Chem.* **1995**, *60*, 532.
[35] Munters, T.; Martens, T.; Goris, L.; Vrindts, V.; Manca, J.; Lutsen, L.; De Ceuninck, W.; Vanderzande, D.; De Schepper, L.; Gelan, J.; Sariciftci, N. S.; Brabec, C. J. *Thin Solid Film* **2002**, *403*, 247.
[36] Gebeheyu, D.; Padinger, F.; Fromherz, T.; Hummelen, J. C.; Sariciftci, N. S. *Int. J. Photoenergy* **1999**, *95*.
[37] Gamaioni, N.; Ridolfi, G.; Casalbore-Miceli, G.; Possamai, G.; Garlaschelli, L.; Maggini, M. *Sol. Ener. Mat. & Solar Cells* **2003**, *76*, 107.

[38] Schilinsky, P.; Waldauf, C.; Brabec, C. J. *Appl. Phys. Lett.* **2002**, *81*, 3885.
[39] Yu, G.; Heeger, A. J. *J. Appl. Phys.* **1995**, *78*, 4510.
[40] Halls, J. J. M.; Walsh, C. A.; Greenham, N. C.; Marseglia, E. A.; Friend, R. H.; Moratti, S. C.; Holmes, A. B. *Nature* **1995**, *376*, 498.
[41] Zhang, F. L.; Jonfronsen, M.; Johansson, D. M. *Synth. Met.* **2003**, *138*, 555.
[42] Breeze, A. J.; Schlesinger, Z.; Carter, S. A. *Sol. Ener. Mat. & Solar Cells* **2004**, 83, 263.
[43] Snaith, H. J.; Arias, A. C.; Morteani, A. C. *Nano. Lett.* **2002**, *2*, 1353.
[44] Halls, J. J. M.; Cornil, J.; dos Santos, D. A. *Phys. Rev. B* **1999**, *60*, 5721.
[45] Hoppe, H.; Sariciftci, N. S. *J. Mater. Chem.* **2006**, *16*, 45.
[46] Hoppe, H.; Niggerman, M.; Winder, C. *Adv. Funct. Mater.* **2004**, *14*, 1005.
[47] Haugeneder, A.; Neges, M.; Kallinger, C.; Spirkl, W.; Lemmer, U.; Feldmann, J.; Scherf, U.; Harth, E.; Gügel, A.; Müllen, K. *Phys. Rev. B* **1999**, *59*, 15346.
[48] Stübinger T.; Brütting, W. *J. Appl. Phys.* **2001**, *90*, 3632.
[49] Eckert, J.-F.; Nicoud, J.-F.; Nierengarten, J.-F.; Liu, S.-G.; Echegoyen,L.; Barigelletti, F.; Armaroli, N.; Ouali, L.; Krasnikov, V.; Hadziioannou, G. *J. Am. Chem. Soc.* **2000**, *122*, 7467.
[50] Dhanabalan, A.; Knol, J.; Hummelen, J. C.; Janssen, R. A. J. *Synth. Met.* **2001**, *119*, 519.
[51] Otsubo, T.; Aso, Y.; Takimiya, K. *J. Mater. Chem.* **2002**, *12*, 2565.
[52] Possamai, G.; Camaioni, N.; Ridolfi, G.; Franco, L.; Ruzzi, M.; Menna, E.; Casalbore-Miceli, G.; Fichera, A. M.; Scorrano, G.; Corvaja, C.; Maggini, M. *Synth. Met.* **2003**, *139*, 585.
[53] Loi, M. A.; Denk, P.; Hoppe, H.; Neugebauer, H.; Winder, C.; Meissner, D.; Brabec, C.; Sariciftci, N. S.; Gouloumis, A.; Vazquez, P.; Torres, T. *J. Mater. Chem.* **2003**, *13*, 700.
[54] Zhang, F.; Svensson, M.; Andersson, M. R.; Maggini, M.; Bucella, S.; Menna, E.; Inganäs, O. *Adv. Mater.* **2001**, *13*, 1871.

[55] Cravino, A.; Zerza, G.; Maggini, M.; Bucella, S.; Svensson, M.; Andersson, M. R.; Neugebauer, H.; Brabec, C. J.; Sariciftci, N. S. *Monatsh. Chem.* **2003**, *134*, 519.

[56] Shaheen, S.E.; Brabec, C.J.; Sariciftci, N.S.; Padinger, F.; Fromherz, T.; Hummelen, J.C. *Appl. Phys. Lett.* **2001**, *78*, 841.

[57] Martens, T.; D'Haen, J.; Munters, T.; Beelen, Z.; Goris, L.; Manca, J.; D'Olieslaeger, M.; Vanderzande, D.; De Schepper, L.; Andriessen, R. *Synth. Met.* **2003**, *138*.

[58] Martens, T.; D'Haen, J.; Manca, J. V.; D'Olieslaeger, M.; Vanderzande, D.; De Schepper L. *Physicalia Magazine* **2003**, *25*, 199.

[59] Martens, T.; D'Haen, J.; Munters, T.; Beelen, Z.; Goris, L.; Manca, J.; D'Olieslaeger, M.; Vanderzande, D.; De Schepper, L.; Andriessen, R. *Synth. Met.* **2002**, *138*, 243.

[60] Martens, T.; D'Haen, J.; Munters, T.; Goris, L.; Beelen, Z.; Manca, J.; D'Olieslaeger, M.; Vanderzande, D.; De Schepper, L.; Andriessen, R. *Materials Research Society Symposium Proceedings* **2002**, *725*, 169.

[61] Martens. T.; Munters, T.; Goris, L.; D'Haen, J.; Schouteden, K.; D'Olieslaeger, M.; Lutsen, L.; Vanderzande, D.; Geens, W.; Poortmans, J.; De Schepper, L.; Manca, J. V. *Appl. Phys. A* **2004**, *79*, 27.

[62] Hoppe, H.; Glatzel, T.; Niggemann, M.; Hinsch, A.; Lux-Steiner, M. C.; Sariciftci, N. S. *Nano Lett.* **2005**, *5*, 269.

[63] Kroon, J. M.; Wienk, M. M.; Verhees, W. J. H.; Hummelen, J. C. *Thin Solid Films* **2002**, *223*, 403.

[64] T. Aernouts, T.; Geens, W.; Portmans, J.; Heremans, P.; Borghs, S.; Mertens, R. *Thin Solid Films* **2002**, *297*, 403.

[65] Dittmer, J. J.; Lazzaroni, R.; Leclere, P.; Moretti, P.; Granström, M.; Petritsch, K.; Marseglia, E. A.; Friend, R. H.; Bredas, J. L.; Rost, H.; Holmes, A. B. *Sol. Ener. Mat. & Solar Cells* **2000**, *61*, 53.

[66] Dittmer, J. J.; Marseglia, E. A.; Friend, R. H. *Adv. Mater.* **2000**, *12*, 1270.

[67] Lutsen, L. J.; van Breemen, A. J.; Kreuder, W.; Vanderzande, D. J. M.; Gelan, J. M. J. V. *Helv. Chim. Acta* **2000**, *83*, 3113.

[68] Lutsen, L. J.; Adriaensens, P.; Becker, H.; van Breemen, A. J.; Vanderzande, D. J. M.; Gelan, J. M. J. V. *Macromolecules* **1999**, *32*, 6517.
[69] van Breemen, A. J. J. M.; Issaris, A. C. J.; de Kok, M. M.; Van Der Borght, M. J. A. N.; Adriaensens, P. J.; Gelan, J. M. J. V.; Vanderzande, D. J. M. *Macromolecules* **1999**, *32*, 5728.
[70] Hoppe, H.; Sariciftci, N. S. *J. Mater. Chem.* **2004**, *19*, 1924.
[71] Brabec, C. J.; Cravino, A.; Meissner, D.; Sariciftci, N. S.; Fromherz, T.; Minse, M.; Sanchez, L.; Hummelen, J. C. *Adv. Funct. Mater.* **2001**, *11*, 374.
[72] Scharber, M.; Mühlbacher, D.; Koppe, M.; Denk, P.; Waldauf, C.; Heeger, A. J.; Brabec, C. *Adv. Mater*. **2006**, *18*, 789.
[73] Mallairas, G. G.; Salem, J. R.; Brock, P. J.; Scott, J. C. *J. Appl. Phys.* **1998**, *84*, 1583.
[74] Van Duren, J.; Yang, X.; Loos, J.; Bulle-Lieuwma, C. W. T.; Sievel, A. B.; Hummelen, J. C.; Janssen, R. A. J. *Adv. Funct. Mater.* **2004**, *14*, 425.
[75] Hoppe, H.; Glatzel, T.; Niggemann, M.; Schwinger, W.; Schaeffler, F.; Hinsch, A.; Lux-Steiner, M.; Sariciftci, N. S. *Thin Solid Films* **2006**, *511-512*, 587.
[76] Gebeyehu, D.; Brabec, C. J.; Padinger, F.; Fromherz, T.; Hummelen, J. C.; Badt, D.; Schindler, H.; Sariciftci, N. S. *Synth. Met.* **2001**, *118*, 1.
[77] Martens, T.; D'Haen, J.; Munters, T.; Beelen, Z.; Goris, L.; Manca, J.; D'Olieslaeger, M.; Vanderzande, D.; De Schepper, L.; Andriessen, R. *Synth. Met.* **2003**, *138*, 243.
[78] Riedel, I.; Dyakonov, V. *Phys. Status Solidi A* **2004**, *201*, 1332.
[79] Bertho, S.; Haeldermans, I.; Swinnen, A.; Moons, W.; Martens, T.; Lutsen, L.; Vanderzande, D.; Manca, J.; Senes, A.; Bonfiglio, A. *Solar Energy Materials & Solar Cells* **2007**, *91*, 385.
[80] Bertho, S.; Janssen, G.; Cleij, T. J.; Conings, B.; Moons, W.; Gadisa, A.; D'Haen, J.; Goovaerts, E.; Lutsen, L.; Manca, J.; Vanderzande, D. *Solar Energy Materials & Solar Cells* **2008**, *92*, 753.

Chapter 4

Post-polymerization functionalization of PPV derivatives with phthalocyanines

This chapter focuses on two different post-polymerization functionalization methods for the attachment of bulky phthalocyanine molecules to PPV derivatives. These molecules can be attached to the conjugated polymer via their alcohol or azide functionalities. Analytical data of the functionalized polymers are consistent with an almost quantitative functional group substitution. In addition, these new phthalocyanine-functionalized PPV derivatives are tested in bulk heterojunction devices, in which they exhibit an improved overlap with the solar spectrum.

4.1. Introduction

Organic photovoltaic devices have already shown significant potential to convert solar energy into electricity in an effective manner. One of the main reasons for the currently still somewhat limited efficiency of this type of devices, is the insufficient absorption of the solar radiation by the active layer. This is schematically represented in Figure 4-1. MDMO-PPV absorbs strongly in the wavelength range 400 to 600 nm, whereas PCBM does the same at lower wavelengths. However, no absorption occurs at longer

wavelength, although a significant portion of the solar radiation falls in this spectral region.

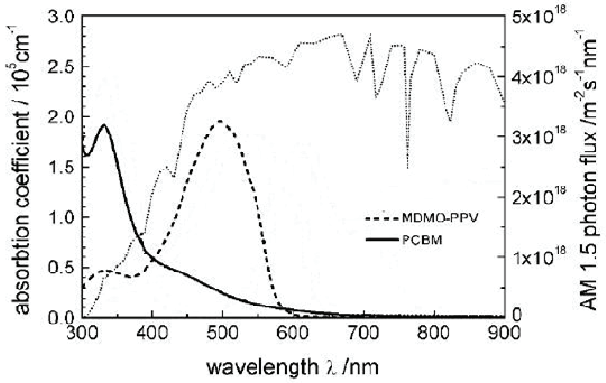

Figure 4-1 Optical absorption of MDMO-PPV (dashed) and PCBM (solid) as compared to the AM 1.5 solar spectrum (dotted)

One way to substantially increase the match with the AM 1.5 solar spectrum is to introduce low-bandgap materials with a strong absorption below 2 eV.[1-5] Another approach is to increase the absorption of the used fullerenes. For example, upon replacing C_{60}-PCBM with C_{70}-PCBM, an increased absorption in the visible range was observed.[6] In addition, new materials with high absorption wavelengths can be utilized for more efficient photon harvesting. For example, by using inorganic copper indium disulphide ($CuInS_2$) nanoparticles the spectral photocurrent was extended up to 900 nm.[7]

To improve the spectral match to the solar emission spectrum, from an organic point of view, phthalocyanines (Pc's) are interesting molecules. Pc's absorb strongly in the area in which the photon flux of the AM 1.5 solar spectrum peak is at a maximum. Since PPV derivatives absorb light with wavelengths ranging from 400-600 nm, the addition of Pc molecules absorbing in the 600-700 nm region will cause an increased absorption of energy from the sunlight (Figure 4-2). A material with a broader absorption

spectrum can potentially capture more energy from the sunlight, which will lead to a higher photocurrent in solar cells and an increased PCE.

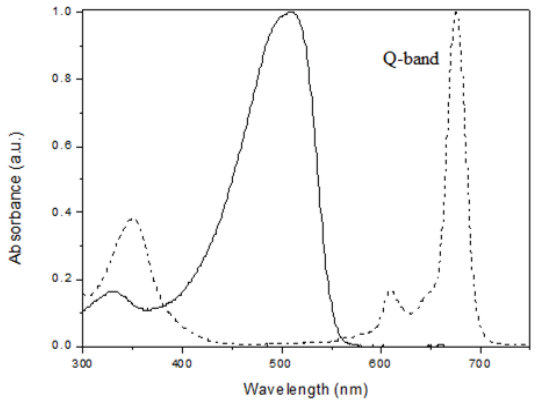

Figure 4-2 Solution UV-Vis absorption spectra of a PPV derivative (solid) and a typical phthalocyanine (dashed) in THF

As was already described in **Chapter 2**, various methods can be used to covalently link specific molecules to PPV derivatives. In this chapter, the optimized DCC/DMAP-esterification method and "click" chemistry are explored to link Pc molecules with PPV derivatives to obtain a material with a broader absorption spectrum. These new Pc-functionalized PPV derivatives are also tested in bulk heterojunction devices. A more detailed explanation of these devices can be found in **Chapter 3**.

4.2. What are phthalocyanines?

Phthalocyanines (Pc's), are two-dimensional 18 π-electron aromatic porphyrin analogues, consisting of four isoindole subunits linked together through nitrogen atoms.[8-12] The general chemical structure of a Pc is depicted in Figure 4-3.

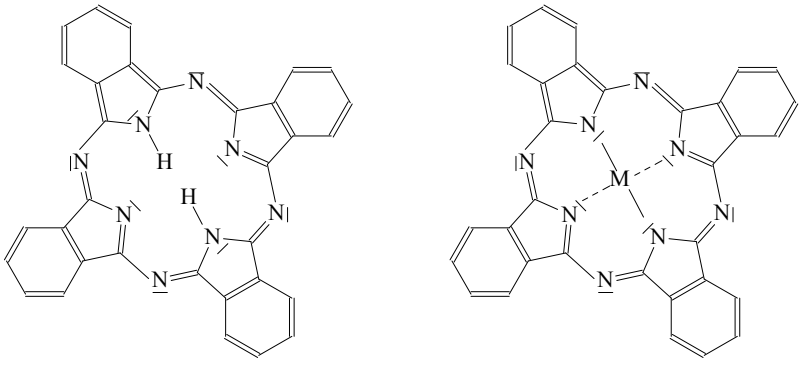

Figure 4-3 Chemical structure of a metal free phthalocyanine (Pc) molecule and a metallophthalocyanine (MPc) molecule

Phthalocyanines and their metallic derivatives (MPc's) are not only very useful for the preparation of dyes, but also of interest as new molecular materials for electronics and optoelectronics. Especially, their electronic delocalization makes them valuable in different fields of science and technology.[13] In addition, their chemical flexibility allows for the synthesis of a variety of related structures and thus, to tailor the physical, electronic and optical properties as desired. Furthermore, it is possible to incorporate a wide variety of metal atoms into a Pc, which offers additional opportunities to tailor their physical properties. Finally, Pc's are characterized by an outstanding stability and high polarizability. For applications, the control of the supramolecular organization of Pc's in the solid state is very important.[14-17]

The conjugated aromatic system of Pc's generates intense bands in their absorption spectra. The strongest absorption band in Pc's is the Q-band, which is positioned in the visible region of the absorption spectrum at a typical wavelength between 650 and 670 nm (Figure 4-2).[8,11] The high extinction coefficient (log ε is *circa* 5.2) is responsible for the green-blue color of Pc dyes. MPc's show a single Q-band, whereas for the

corresponding Pc's usually a split Q-band is visible as a result of their lower symmetry.[8,11] It is noteworthy that this observation is only valid for symmetrical substituted Pc's. For unsymmetrical Pc's, the breaking of the symmetry gives rise to the splitting of the Q-band.

Because of their blue and green colors, Pc's are used as photoconductors in xerography[18,19] and in optical data storage.[20] They are also interesting for applications in non-linear optics[21,22], molecular electronics[23], photodynamic cancer therapy[24,25], solar energy conversion[26-30], various catalytic processes[31,32], electrochromic and electroluminescent displays[33-35], chromatography[36-38] and as the active component in gas sensors.[39,40] Our focus is on the use of Pc's in solar cells due to their extended absorption in the near infrared region of the sunlight spectrum as well as excellent stability, high LUMO and relatively high hole mobility. More detailed information on Pc's, their properties and applications (*i.e.* their use in bulk heterojunction solar cells), can be found in literature.[41-46] The active layer of previously reported bulk heterojunction devices consist of Pc molecules as the donor and PCBM as the acceptor. In these devices, a complex nanoscale morphology of the blend is present, which is difficult to optimize and to control. This is the same difficulty as is observed with photovoltaics containing conjugated polymers (*cf.* section 3.4.). To overcome these morphological problems a substantial effort has been done in recent years to synthesize bipolar materials in which the donor and acceptor are covalently linked with each other like Pc-C_{60} dyads[47-60] and Pc covalently bonded with polynorbornene[61] and poly(thiophene).[62] Notwithstanding, the efficiency of the resulting solar cells remained rather low. However, in the above samples, the covalent linking of the Pc with poly(thiophene) was done *via* the monomer approach (*cf.* section 1.3.1.) and not *via* post-polymerization functionalization, which will be discussed in this chapter.

4.3. Post-polymerization functionalization of PPV derivatives with phthalocyanines

4.3.1. "Click" method

In **Chapter 2**, the propargyl group of copolymer **23** has been used to attach a molecule, with an azide group, *i.e.* azidomethyl phenyl sulfide, to the side chain of a conjugated polymer *via* "click" chemistry using PMDETA and Cu(I)Br. The same conditions are now tested to attach Pc molecules, with an azide group, to PPV derivatives. This reaction is first optimized on model compound **14**, as can be seen in Scheme 4-1. The "click" reaction is conducted in dry, degassed THF under nitrogen atmosphere. To a solution of **14** and Pc, with an azide function, pentamethyldiethylenetriamine (PMDETA) (Figure 4-4) and Cu(I)Br are added to form the catalyst system. The reaction is allowed to proceed for 12 h at 50 °C. Cu is removed by filtering over Al_2O_3 and purification of the crude product is done by column chromatography. Compound **27** has been characterized with ^{1}H-NMR and FT-IR and no impurities have been observed

Subsequently, this "click" reaction has been translated to copolymer **23**. The reaction is also performed in dry, degassed THF under nitrogen atmosphere and to preserve the conjugated polymers it is also protected from light. In a similar procedure as described for the model compound, to a solution of **23** and the Pc, with an azide function, PMDETA and Cu(I)Br are added. The reaction is allowed to proceed for 12 h at 50 °C. Cu is removed by filtering over Al_2O_3 and the solution is precipitated drop wise in a non-solvent. The Pc-functionalized copolymer **28 "click" Cu(I)Br** (Scheme 4-2) is filtered off, washed extensively with acetone, to remove the excess of Pc, and dried under reduced pressure.

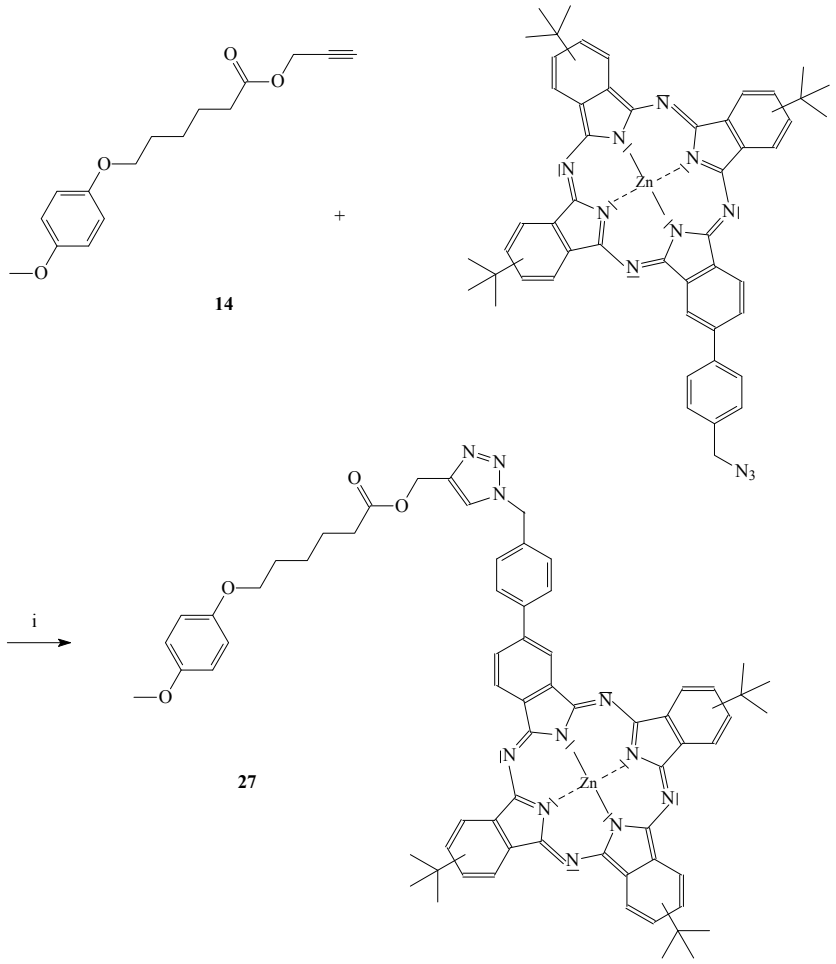

Scheme 4-1 Synthesis of **27** *via* "click" chemistry (i: PMDETA, Cu(I)Br, THF)

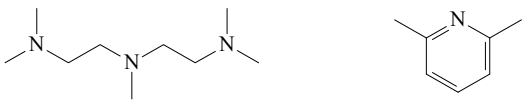

PMDETA 2,6-lutidine

Figure 4-4 Chemical structure of pentamethyldiethylenetriamine (PMDETA) and 2,6-lutidine

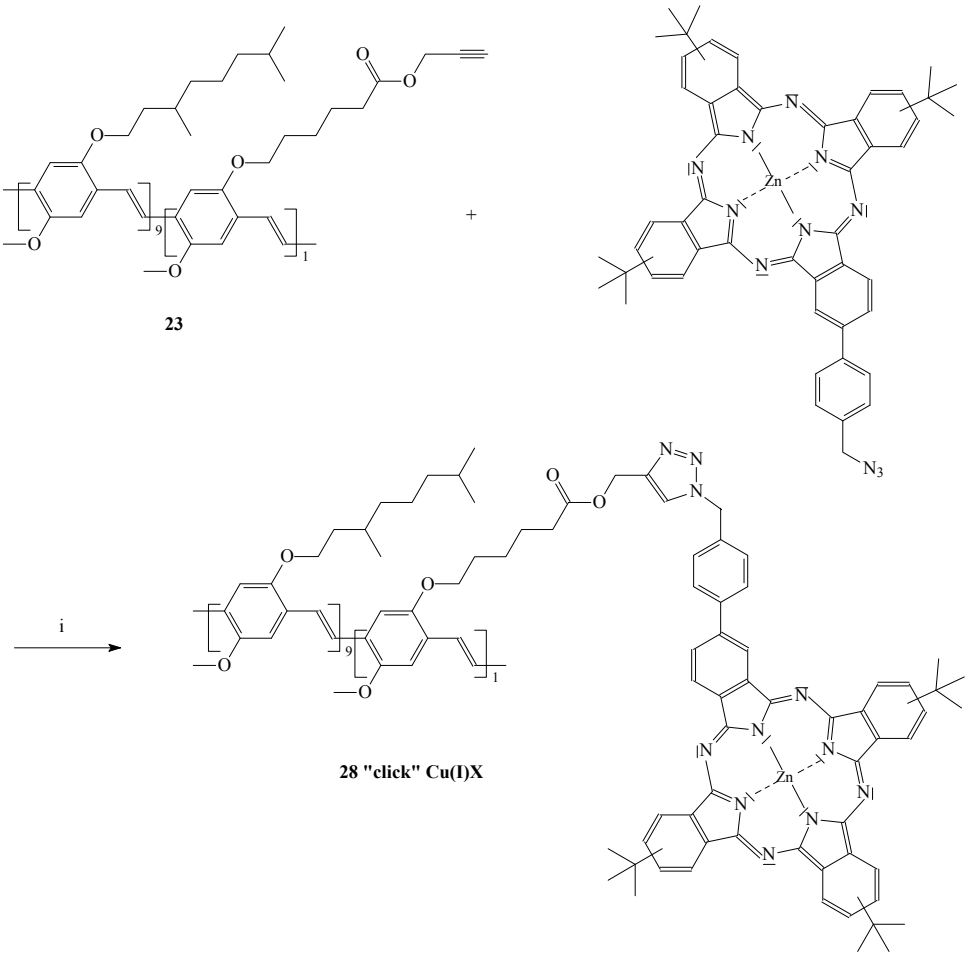

Scheme 4-2 Synthesis of **28 "click" Cu(I)X** *via* "click" chemistry (**X** = **Br** i: PMDETA, Cu(I)Br, THF or **X** = **I** i: 2,6-lutidine, Cu(I)I, THF)

The successful "click" reaction on the conjugated copolymer is clearly visible in ^{1}H-NMR spectroscopy. All the characteristic peaks for the attached Pc, which are present in the model compound, are also present in the post-polymerization functionalized copolymer **28 "click" Cu(I)Br**. The integration of the signals is consistent with a quantitative "click" reaction of the propargyl group with the azide functionality to form a 1,2,3 triazole ring.

The observed M_w value in THF solution using polystyrene standards is 3.0 x 10^5 g/mol, which is in the same order of magnitude as copolymer **23** which has a M_w value of 3.8 x 10^5 g/mol (Table 4-1). As was already observed in **Chapter 2**, no significant decrease in the average molecular weight occurs during the substitution reactions.

Copolymer	M_w (g/mol)	PD = M_w/M_n	λ_{max} in THF (nm)
8	2.7 x 10^5	3.2	507
23	3.8 x 10^5	5.2	507
28 "click" Cu(I)Br	3.0 x 10^5	4.0	509
28 "click" Cu(I)I	2.1 x 10^5	3.2	509
30 DCC	3.1 x 10^5	4.4	510

Table 4-1 Polymerization results for the carboxylic acid-functionalized copolymer **8** and the post-polymerization functionalized copolymers **23**, **28 "click" Cu(I)Br**, **28 "click" Cu(I)I** and **30 DCC**. SEC measurements were performed *versus* polystyrene standards using THF as eluent

The quality of the conjugated system and the success of the "click" reaction of the Pc to copolymer **23**, are further confirmed *via* UV-Vis measurements in THF solution. As can be seen in Table 4-1, the peak position (λ_{max}) of the π-π* transitions of copolymer **28 "click" Cu(I)Br** is positioned at 509 nm. This is the same spectral region as the transition observed for copolymer **23** (λ_{max} = 507 nm). In addition to the peak positions, also the shape of both UV-Vis absorption spectra is identical (Figure 4-5). In addition, in the UV-Vis absorption spectrum of the modified polymer the Q-band of the attached Pc is clearly visible at λ = 676 nm.

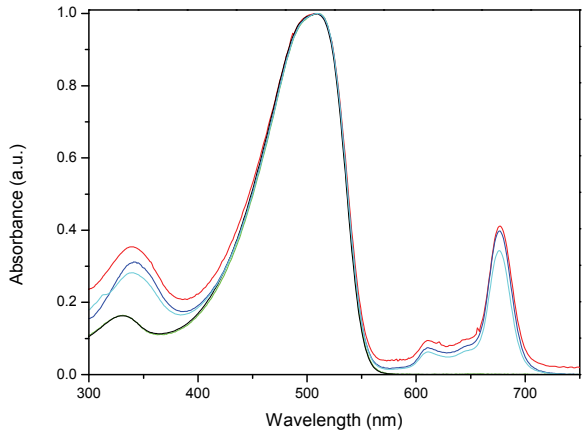

Figure 4-5 Solution UV-Vis absorption spectra of the carboxylic acid-functionalized copolymer **8** and the post-polymerization functionalized copolymers **23**, **28 "click" Cu(I)Br**, **28 "click" Cu(I)I** and **30 DCC** in THF (no significant changes are observed upon functionalization)

Due to the very poor solubility of copolymer **28 "click" Cu(I)Br** in chlorobenzene, which is the solvent of choice for spin-coating the active layer in solar cells, the same "click" reaction between copolymer **23** and an azide functionalized Pc has also been tested in different conditions *i.e.* with a different catalytic system and different work-up conditions.

This second "click" reaction also takes place in dry, degassed THF under nitrogen atmosphere and protected from light. To a solution of **23** and the Pc, with an azide function, 2,6-lutidine (Figure 4-4) and Cu(I)I are added. The reaction is allowed to proceed for 48 h at reflux temperature. Cu is removed by extraction with NH_4OH and H_2O and the solution is precipitated drop wise in a non-solvent. The Pc-functionalized copolymer **28 "click" Cu(I)I** (Scheme 4-2) is filtered off, washed extensively with acetone, to remove the excess of Pc, and dried under reduced pressure.

For this second method, the successful "click" reaction on the conjugated copolymer is also clearly visible in ^{1}H-NMR spectroscopy. The observed M_w value in THF solution using polystyrene standards is 2.1 x 10^5 g/mol, which remains reasonably comparable to copolymer **23** and copolymer **28 "click" Cu(I)Br** (Table 4-1). UV-Vis measurements in THF further confirm the quality of the conjugated system and the "click" of the Pc to copolymer **23**. The λ_{max} of copolymer **28 "click" Cu(I)I** is positioned at 509 nm, which is in the same spectral region as the transition observed for copolymer **23** and copolymer **28 "click" Cu(I)Br** (Table 4-1). The shapes of the UV-Vis absorption spectra are also identical and the Q-band of the attached Pc is clearly visible at λ = 676 nm, as can be seen in Figure 4-5.

From Figure 4-5 and Table 4-1, it can be concluded that both somewhat different methods to perform the "click" reaction have no significant impact on the quality of the conjugated system itself. This is in agreement with the results of the "click" reaction in **Chapter 2**. The main difference between both copolymers is the solubility in chlorobenzene. Copolymer **28 "click" Cu(I)I** is better soluble in chlorobenzene than copolymer **28 "click" Cu(I)Br**, due to the different reaction and work-up conditions.

4.3.2. Working principle of "click" method

When using the word "click" in this work, we refer to the azide-alkyne Huisgen cycloaddition. This is one of the most popular reactions within the "click" chemistry family. It is a 1,3-dipolar cycloaddition between an azide and an alkyne to give a 1,2,3-triazole. When using a Cu(I) catalyst, a 1,4-disubstituted-1,2,3-triazole is synthesized of which the substituents have their origin as side groups from respectively, the azide and the alkyne. The "click" reaction is schematically represented in Scheme 4-3.

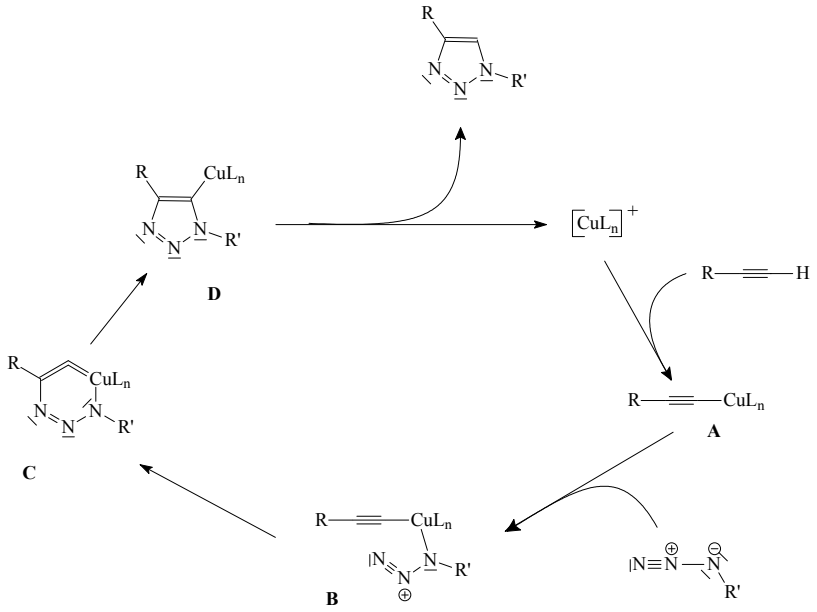

Scheme 4-3 Schematic representation of the "click" method

The Cu(I)-catalyzed cycloaddition between an azide and an alkyne proceeds through a stepwise mechanism. Coordination of the alkyne to $Cu(I)L_n$ takes place by replacing one ligand. In this Cu acetylide complex **A**, the azide replaces now one of the remaining ligands. The azide is bonded to the Cu acetylide complex **A** *via* the nitrogen adjacent to the carbon. Attack by the terminal N in **B** on C-2, in the acetylide, forms the six-membered Cu(III) intermediate **C**. Rearrangement of **C** gives **D**, which is transformed to the 1,4-disubstituted-1,2,3-triazole by proteolysis.

4.3.3. DCC/DMAP-esterification method

The same DCC/DMAP method, that has been used for the functionalizations described in **Chapter 2**, has also been utilized to attach Pc's to the PPV-type polymers, as an alternative method. In this way, both functionalization methods can be compared with each other to evaluate the best approach for

the attachment of large molecules to PPV derivatives. The DCC/DMAP method is first tested on model compound **9** (Scheme 4-4). The esterification reaction is conducted in dry CH_2Cl_2 under nitrogen atmosphere. To a solution of **9** and the Pc, with an alcohol function, DCC and DMAP are added as effective esterification promoting reagents. The reaction is allowed to proceed for 1 h at 0 °C and for an additional 24 h at room temperature. Dicyclohexylurea (DCU) is filtered off and purification of the crude product is done by column chromatography. The purity of compound **29** is confirmed with ^{1}H-NMR and FT-IR.

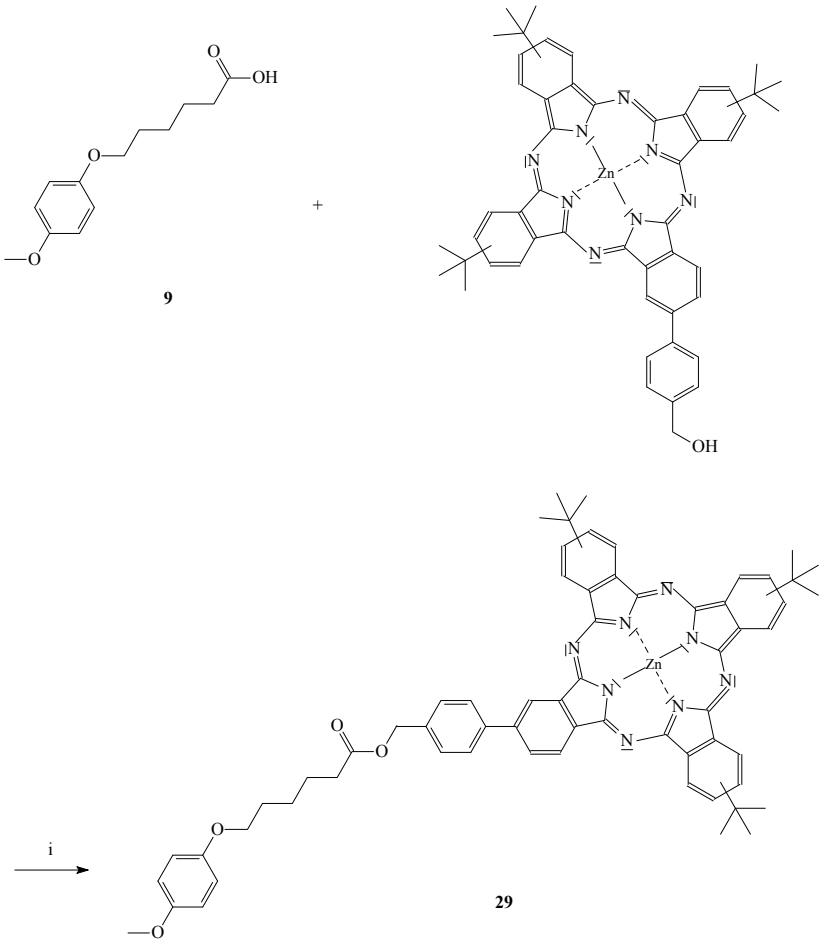

Scheme 4-4 Synthesis of **29** *via* the optimized DCC/DMAP-procedure (i: DCC, DMAP, CH_2Cl_2)

Subsequently, the reaction was translated to copolymer (MDMO-CPM)-PPV **8**. This esterification reaction also takes place in dry CH_2Cl_2 under nitrogen atmosphere and protected from light. To a solution of **8** and the Pc, with an alcohol function, DCC and DMAP are added drop wise. The reaction is allowed to proceed for 1 h at 0 °C and for an additional 24 h at room temperature. Subsequently, the solution is precipitated drop wise in a non-solvent. The Pc-functionalized copolymer **30 DCC** (Scheme 4-5) is filtered off, washed extensively with acetone, to remove the excess of Pc and dried under reduced pressure.

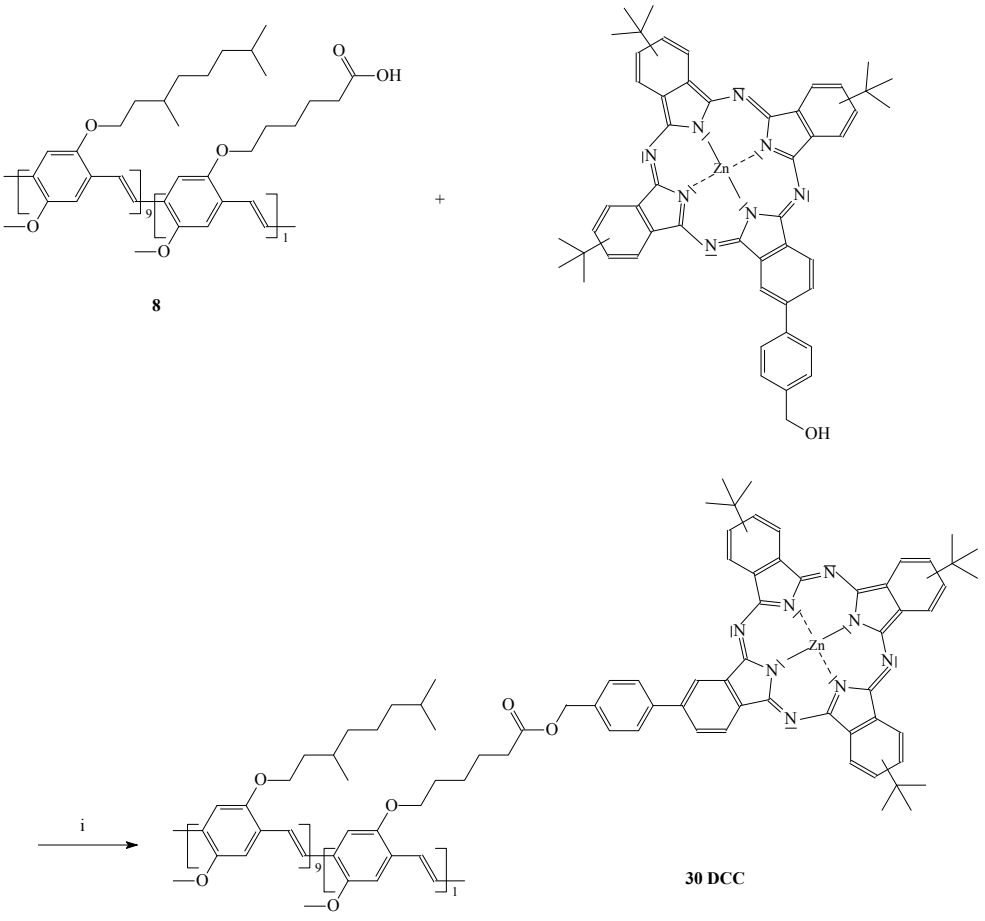

Scheme 4-5 Synthesis of **30 DCC** *via* the optimized DCC/DMAP-procedure (i: DCC, DMAP, CH_2Cl_2)

The successful conversion on the conjugated copolymer is clearly visible in ^{1}H-NMR spectroscopy. All the characteristic peaks for the attached Pc, which have also been observed in the model compound functionalization, are also present in the post-polymerization functionalized copolymer **30 DCC**. The integration of the signals is consistent with an almost quantitative conversion of the carboxylic acid to the corresponding ester. The functionalization of copolymer **8** is readily confirmed by FT-IR. The carbonyl vibration at 1709 cm^{-1} of the carboxylic acid shifts to higher frequency (1733 cm^{-1}) due to the formation of the ester bond.

The observed M_w value in THF solution using polystyrene standards is 3.1 x 10^5 g/mol, which is comparable to the platform copolymer (MDMO-CPM)-PPV **8** which has a M_w value of 2.7 x 10^5 g/mol (Table 4-1). This is in agreement with the findings of **Chapter 2**, that no significant decrease in the average molecular weight occurs during the DCC/DMAP substitution reactions. It should be noted that there is a moderate increase in the polydispersity upon functionalization. Whereas copolymer **8** has a polydispersity value of 3.2, for copolymer **30 DCC** the polydispersity is 4.4, reflecting a broadening of the molecular weight distribution.

The quality of the conjugated system and the successful attachment of the Pc to copolymer **8**, are further confirmed *via* UV-Vis measurements in THF. As can be seen in Table 4-1, the peak position (λ_{max}) of the π-π^* transitions of the post-functionalized copolymer **30 DCC** is positioned at 510 nm. This is the same spectral region as the transition observed for copolymer **8** (λ_{max} = 507 nm). In addition to the peak positions, also the shapes of the UV-Vis absorption spectra are identical (Figure 4-5). In Figure 4-5, also the Q-band of the attached Pc is clearly visible at λ = 676 nm. The height of this peak is directly related to the amount of Pc molecules present. Apparently, in copolymers **28 "click" Cu(I)I** and **28 "click" Cu(I)Br** slightly more Pc molecules are attached than in copolymer **30 DCC**. These results confirm that the DCC/DMAP method has no significant impact on the quality of the conjugated system, the same conclusion as can be found in **Chapter 2**. Notwithstanding, the degree of functionalization is somewhat higher with the "click" reactions.

4.4. Solar cells of copolymers 23, 28 “click” Cu(I)I and 30 DCC

After the linking of the Pc molecules to the PPV derivatives, the new synthesized materials possess a broader absorption window for sunlight (Figure 4-5). As a result, copolymers **28 “click” Cu(I)Br**, **28 “click” Cu(I)I** and **30 DCC** should match better with the AM 1.5 solar spectrum than copolymer **23**. Hence, it is of interest to test their performance in organic solar cells. Since copolymers **28 “click” Cu(I)Br** and **28 “click” Cu(I)I** have almost identical solution UV-Vis absorption spectra (Figure 4-4) and copolymer **28 “click” Cu(I)I** is much better soluble in chlorobenzene than copolymer **28 “click” Cu(I)Br**, only solar cells are made with copolymer **28 “click” Cu(I)I**.

4.4.1. Solar cell built-up

In order to study the effect of 10 % ‘built-in’ Pc groups in MDMO-PPV, bulk heterojunction devices have been made. The general built-up of the solar cell is as follows: ITO/PEDOT:PSS/active layer/LiF/Al, in which the active layer consists of the PPV derivative as the donor and PCBM as the acceptor. The synthesized copolymers **28 “click” Cu(I)I** and **30 DCC** are compared with the reference material, *i.e.* copolymer **23** (propargyl group). Copolymer **23** has already a good solar performance, as can be concluded from **Chapter 3**, and it was also the starting material for copolymer **28 “click” Cu(I)I**. The active layer is spin-coated using chlorobenzene as solvent. The ‘active layer solution’ consists of PPV derivative/PCBM in a ratio of 1/4. The thickness of the active layer is also investigated in function of the corresponding performance of the different solar cells. The devices are illuminated under AM 1.5 conditions.

4.4.2. Influence of phthalocyanine groups on the spectral response of the solar cells

To investigate whether the attached Pc molecules contribute to the sunlight absorbed by the solar cell, the spectral response of all solar cells has been measured. These spectral response curves are depicted in Figure 4-6, together with the solution UV-Vis absorption spectrum of copolymer **28 "click" Cu(I)I**.

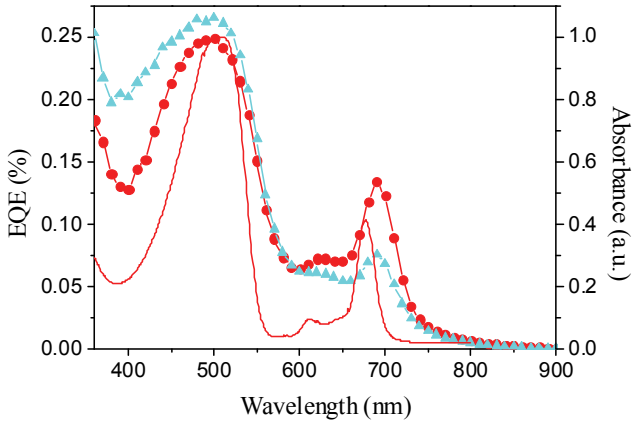

Figure 4-6 Solution UV-Vis absorption spectrum of copolymer **28 "click" Cu(I)I** in THF and spectral response curve of copolymers **28 "click" Cu(I)I** (●) and **30 DCC**

From Figure 4-6, a clear contribution of the attached Pc molecules is observed. The contribution of the PPV conjugated system is centered around 500 nm, whereas the contribution of the Pc is visible around approximately 700 nm. By comparing the spectral response curves of both copolymers **28 "click" Cu(I)I** and **30 DCC** with the solution UV-Vis absorption spectrum of copolymer **28 "click" Cu(I)I**, it becomes evident that the peak of the PPV backbone remains around 500 nm, whereas there is a clear red-shift of the peaks corresponding to the Pc's. This is a result of the interaction

between the individual Pc entities in the thin film. The absorption intensity of the Pc peak of copolymers **28 "click" Cu(I)I** and **30 DCC** is also different. To a lesser degree, this was already visible in Figure 4-5. Apparently, in copolymer **28 "click" Cu(I)I** more Pc molecules are attached than in copolymer **30 DCC**, which is directly reflected in the height of the Pc peaks at $\lambda = 676$ nm. This will in turn affect the spectral response curve.

It can be concluded that the absorption of the synthesized materials matches significantly better with the AM 1.5 solar spectrum, due to the covalent attachment of Pc's. In this way, more sunlight can be absorbed by these functionalized copolymers.

4.4.3. Influence of phthalocyanine groups on the solar cell performance

After establishing the contribution of the Pc's to the absorption of the solar cells, the actual performance of the solar cells has been investigated. V_{oc}, J_{sc}, FF and PCE for copolymer **23**, **28 "click" Cu(I)I** and **30 DCC**, in function of their active layer thickness, are summarized in Figure 4-7.

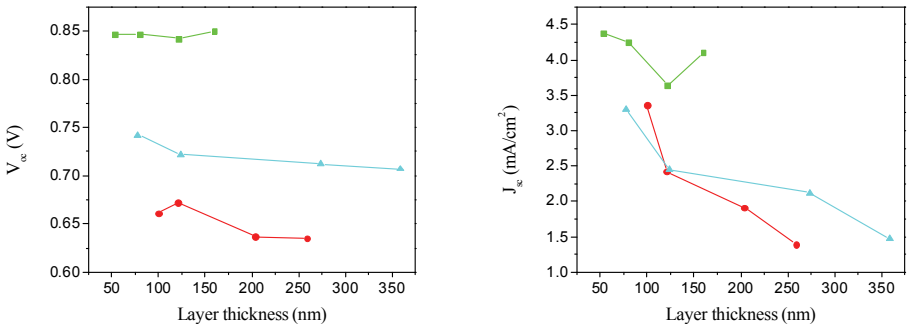

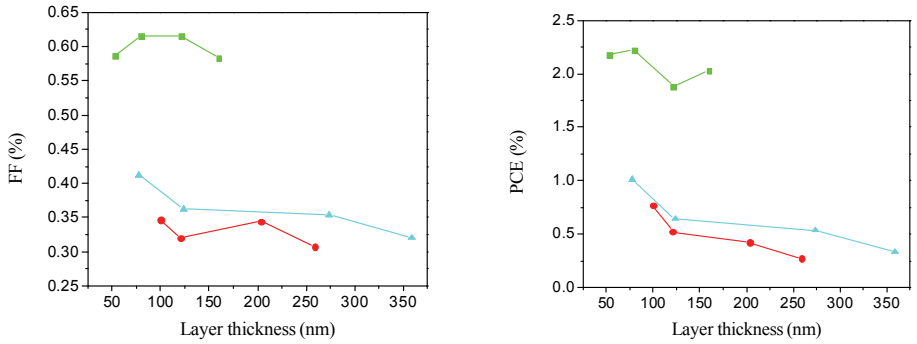

Figure 4-7 Solar cell performance of copolymers **23**, **28 "click" Cu(I)I** and **30 DCC**

Surprisingly, the values of V_{oc}, J_{sc}, FF and PCE for the two different (MDMO-Pc)-PPV functionalized copolymers are lower than those found for the reference copolymer **23**. Possibly, the poor solubility in chlorobenzene for both (MDMO-Pc)-PPV functionalized copolymers is an important reason. This low solubility has an immediate effect on the morphology of the active layer. All the measured solar cells exhibited a strong radial spreading over the sample, which indicates that poor quality thin films have been formed. Hence, it is not entirely surprising that this results in the observed inferior performance. Solubility studies and subsequent improvements may considerably improve the solar cell performance. In addition to the morphological problems, the presence of other traps or impurities could also be responsible for the lower solar cell performance, as compared to the reference copolymer **23**. The 'best' solar cells made with copolymer **28 "click" Cu(I)I** have a V_{oc} = 0.66 V, J_{sc} = 3.36 mA/cm^2, FF = 0.35 % and PCE = 0.77 %. The 'best' solar cells made with copolymer **30 DCC** have a V_{oc} = 0.74 V, J_{sc} = 3.30 mA/cm^2, FF = 0.41 % and PCE = 1.01 %. They both have an active layer thickness of less than 100 nm. Focusing on both (MDMO-Pc)-PPV derivatives, the solar cell performance of copolymer **30 DCC** is better compared with the performance of the solar cell made by copolymer **28 "click" Cu(I)I**. This can be explained by the fact that copolymer **30 DCC** is functionalized with less Pc molecules than

copolymer **28 "click" Cu(I)I** and is therefore slightly better soluble in chlorobenzene, which results in a somewhat better morphology of the active layer. In addition, the presence of residual "click" reagents, *i.e.* Cu, may potentially result in additional traps.

The above observations are valid for all studied layer thicknesses, although the thin devices perform better than the devices containing thicker active layers. Apparently, although a thicker layer potentially will lead to more light harvesting, this does not offset the impact of a decrease in transport properties.

As can be expected from the results obtained in **Chapter 3**, the solar cell made of the reference copolymer **23** has much better characteristics *i.e.* V_{oc} = 0.85 V, J_{sc} = 4.25 mA/cm^2, FF = 0.62 % and PCE = 2.22 %. These results are even better than those obtained in **Chapter 3** and compare well with the solar cells made by Shaheen *et al.*[63] (V_{oc} = 0.85 V, J_{sc} = 5.25 mA/cm^2, FF = 0.62 % and PCE = 2.50 %), which have MDMO-PPV/PCBM as the active layer.

4.5. Conclusions

One of the largest limitations of organic photovoltaic devices is the insufficient absorption of the solar radiation by the active layer. This mismatch with the AM 1.5 solar spectrum limits the efficiency of these devices. To overcome this problem, several possible improvements have been described in the literature,[1-7] but none of them gave satisfactory results. Since Pc's absorb strongly in the area where the photon flux of the AM 1.5 solar spectrum is at its maximum, the introduction of this type of molecules in PPV derivatives can lead to an increased absorption of energy from the sunlight. To accomplish a covalent connection between Pc molecules and PPV derivatives, two completely different methods have been tested. Both post-polymerization functionalization methods, the DCC/DMAP-esterification method as well as "click" chemistry, work well to obtain a good to almost quantitative conversion of the different functional groups of

the PPV derivatives. In addition, the spectroscopic data and SEC measurements indicate that no substantial degradation of the conjugated system occurs.

After the successful linking of the Pc molecules to the PPV derivatives, the new materials have been tested in bulk heterojunction devices. In the spectral response curve of the new solar cells, the contribution of the attached Pc's is clearly visible. In this way, the (MDMO-Pc)-PPV derivatives match substantially better with the AM 1.5 solar spectrum as compared to common other PPV derivatives. However, it appears that the built-in of Pc's has a negative influence on the performance of these solar cells. This can largely be explained by the poor morphology of the active layers. To improve the morphology of the active layers, one can attempt to synthesize Pc molecules, which are better soluble in solvents such as chlorobenzene. In this way, the Pc functionalized PPV derivatives are, most likely, also better soluble in chlorobenzene and a better morphology of the active layer can be obtained. In this way, not only the (MDMO-Pc)-PPV derivatives will match better with the AM 1.5 solar spectrum, but also the performance in photovoltaic devices can be improved.

4.6. Experimental section

4.6.1. Chemical and optical characterization

NMR spectra were recorded with a Varian Inova Spectrometer (^{1}H-NMR 300 MHz). Analytical Size Exclusion Chromatography (SEC) was performed using a Spectra series P100 (Spectra Physics) pump equipped with a pre-column (5 μm, 50 x 7.5 mm, guard, Polymer Labs) and two mixed-B columns (10 μm, 2 x 300 x 7.5 mm, Polymer Labs) and a Refractive Index detector (Shodex) at 40 °C. THF was used as the eluent at a flow rate of 1.0 mL/min. Molecular weight distributions are given relative to polystyrene standards. FT-IR spectra were collected with a Perkin Elmer

Spectrum One FT-IR spectrometer (nominal resolution 4 cm^{-1}, summation of 16 scans). UV-Vis measurements were performed on a Cary 500 UV-Vis-NIR spectrophotometer (scan rate 600 nm/min, continuous run from 200 to 800 nm).

4.6.2. Chemicals

Unless stated otherwise, all reagents and chemicals were obtained from commercial sources and used without further purification. PMDETA was distilled under vacuum. Cu(I)Br was purified by stirring in acetic acid for 24 h, to reduce Cu(II) to Cu(I). Subsequently, Cu(I)Br was filtered off and washed with ethanol and diethyl ether to remove $Cu(II)Br_2$ and acetic acid, after which it was dried in a vacuum oven at 75 °C.

4.6.3. Synthesis

- **"Click" method**

Model compound - Pc "click" Cu(I)Br 27. 14 (0.013 g, 0.045 mmol) was dissolved in dry, degassed THF (5 mL) under N_2 atmosphere. The azide-functionalized reagent, *i.e.* Pc-azide (0.078 g, 0.09 mmol) and distilled N,N,N',N'',N''-pentamethyldiethylenetriamine (PMDETA) (0.002 g, 0.009 mmol) were added. The solution was again degassed for 5 min and purified Cu(I)Br (0.0013 g, 0.009 mmol) was added under a continuous N_2 flow. After overnight stirring at 50 °C the reaction mixture was filtered over Al_2O_3 and washed with THF and CH_2Cl_2. The pure product was obtained by column chromatography (SiO_2, eluent THF/hexane 1/1) as a dark blue solid (0.036 g, 71 % yield). ^{1}H-NMR (THF-d_8): δ = 9.45 (m, 3H), 9.24 (m, 3H), 8.25 (m, 6H), 7.93 (s, 1H), 7.62 (dd, 2H), 6.77 (s, 4H), 6.74 (dd, 2H), 5.70 (s, 2H), 5.06 (s, 2H), 3.84 (t, 2H), 3.62 (s, 3H), 2.31 (t, 2H), 1.84 (t, 27H),

1.59-1.78 (m, 4H), 1.44 (m, 2H); FT-IR (NaCl, cm^{-1}): 3066, 2955, 2866, 2555, 2236, 1741 (ν_{C-O}), 1613, 1510, 1488, 1466, 1442, 1392, 1363, 1330, 1280, 1256, 1231, 1183, 1152, 1091, 1047, 920, 827, 763, 748.

(MDMO-Pc)-PPV 28 "click" Cu(I)Br (n/m = 9). Copolymer **23** (0.050 g, 0.018 mmol triple bond functionalities) was dissolved in dry, degassed THF (10 mL) under N_2 atmosphere. The azide-functionalized reagent, *i.e.* Pc-azide (0.031 g, 0.036 mmol) and distilled N,N,N',N'',N''-pentamethyldiethylenetriamine (PMDETA) (0.0003 g, 0.0018 mmol) were added. The solution was purged with N_2 for 5 min and purified Cu(I)Br (0.0003 g, 0.0018 mmol) was added under a continuous N_2 flow. After stirring overnight at 50 °C the reaction mixture was filtered over Al_2O_3 and washed with THF and CH_2Cl_2. Subsequently, the total volume was reduced to 15 mL by evaporation under reduced pressure and the resulting dark blue solution was precipitated drop wise in cold MeOH (200 mL). The resulting dark red-blue copolymer was filtered off, washed extensively with cold MeOH and acetone and dried at room temperature under reduced pressure, giving a dark red-blue, fibrous polymer (0.060 g, 89 % yield). ^{1}H-NMR (THF-d_8): δ = 9.58-9.38, 8.30, 8.11, 7.90, 7.55-7.4, 7.3-7.1, 5.70, 5.21, 4.1-3.8, 2.4-2.3, 1.8-0.7; FT-IR (NaCl, cm^{-1}): 3058, 2959, 2927, 2869, 1737 (ν_{C-O}), 1504, 1464, 1414, 1385, 1351, 1260, 1205, 1027, 970, 862, 800; SEC (THF) M_w = 3.0 x 10^5 g/mol (PD = M_w/M_n = 4.0). UV-Vis λ_{max} = 509 nm (THF).

(MDMO-Pc)-PPV 28 "click" Cu(I)I (n/m = 9). Copolymer **23** (0.050 g, 0.018 mmol triple bond functionalities) was dissolved in dry, degassed THF (10 mL) under N_2 atmosphere. The azide-functionalized reagent, *i.e.* Pc-azide (0.038 g, 0.043 mmol) and 2,6-lutidine (0.0003 g, 0.0036 mmol) were added. The solution was purged with N_2 for 5 min and Cu(I)I (0.008 g, 0.043 mmol) was added under a continuous N_2 flow. After 42 h stirring at reflux temperature, THF was evaporated under reduced pressure and the crude product was redissolved in CH_2Cl_2 (50 mL). The reaction mixture was extracted with NH_4OH (2 x 20 mL) and H_2O (2 x 20 mL). Subsequently, the amount of CH_2Cl_2 was reduced to 10 mL by evaporation. This dark blue solution was precipitated drop wise in cold MeOH (200 mL). The resulting dark red-blue copolymer was filtered off and washed extensively with cold

MeOH and acetone and dried at room temperature under reduced pressure, giving a dark red-blue, fibrous polymer (0.055 g, 82 % yield). ^{1}H-NMR (THF-d_8): δ = 9.58-9.38, 8.30, 8.11, 7.90, 7.55-7.4, 7.3-7.1, 5.70, 5.21, 4.1-3.8, 2.4-2.3, 1.8-0.7; FT-IR (NaCl, cm^{-1}): 3059, 2959, 2927, 2870, 1736 (ν_{C-O}), 1504, 1464, 1414, 1385, 1352, 1260, 1206, 1027, 971, 863, 800; SEC (THF) M_w = 2.1 x 10^5 g/mol (PD = M_w/M_n = 3.2). UV-Vis λ_{max} = 509 nm (THF).

♦ DCC/DMAP-esterification method

Model compound - Pc DCC 29. 9 (0.020 g, 0.084 mmol) was dissolved in dry CH_2Cl_2 (5 mL) and cooled down to 0 °C. The alcohol-functionalized reagent, *i.e.* Pc-alcohol (0.071 g, 0.084 mmol) and N,N'-dicyclohexylcarbodiimide (DCC) (0.019 g, 0.092 mmol) were added. Subsequently, 4-(N,N'-dimethylamino)pyridine (DMAP) (0.002 g, 0.017 mmol) in dry CH_2Cl_2 was added drop wise over a period of 15 minutes under N_2 atmosphere. The reaction was allowed to proceed for 1 h at 0 °C and for an additional 24 h at room temperature. Filtering off dicyclohexylurea (DCU) gave the crude product. The pure product was obtained by column chromatography (SiO_2, eluent THF/hexane 1/4) as a dark blue solid (0.070 g, 78 % yield). ^{1}H-NMR (THF-d_8): δ = 9.55 (m, 3H), 9.37 (m, 3H), 8.44 (m, 3H), 8.30 (m, 3H), 8.18 (dd, 2H), 7.69 (dd, 2H), 6.77 (s, 4H), 5.30 (s, 2H), 3.91 (t, 2H), 3.62 (s, 3H), 2.45 (t, 2H), 1.80 (t, 27H), 1.59-1.78 (m, 4H), 1.44 (m, 2H); FT-IR (NaCl, cm^{-1}): 2959, 2932, 2862, 1736 (ν_{C-O}), 1615, 1508, 1488, 1449, 1392, 1364, 1332, 1153, 1090, 1047, 920, 827, 764, 748.

(MDMO-Pc)-PPV 30 DCC (n/m = 9). (MDMO-CPM)-PPV **8 (n/m = 9)** (0.050 g, 0.018 mmol carboxylic acid functionalities) was dissolved in dry CH_2Cl_2 (12 mL) and cooled down to 0 °C. The alcohol-functionalized reagent, *i.e.* Pc-alcohol (0.018 g, 0.022 mmol) and N,N'-dicyclohexylcarbodiimide (DCC) (0.004 g, 0.022 mmol) were added. Subsequently 4-(N,N'-dimethylamino)pyridine (DMAP) (0.003 g, 0.022 mmol) in dry CH_2Cl_2 was added drop wise over a period of 15 minutes

under N_2 atmosphere. The reaction was allowed to proceed for 1 h at 0 °C and for an additional 24 h at room temperature after which the solution was precipitated drop wise in cold MeOH (200 mL). The resulting red copolymer was filtered off, washed extensively with cold MeOH and acetone and dried at room temperature under reduced pressure, giving a dark red-blue, fibrous polymer (0.057 g, 86 % yield). ^{1}H-NMR (THF-d_8): δ = 9.58-9.38, 8.30, 8.13, 8.00, 7.90, 7.60-7.4, 7.3-7.1, 5.28, 4.1-3.8, 2.4-2.3, 1.8-0.7; FT-IR (NaCl, cm^{-1}): 3058, 2953, 2926, 2868, 1733 (ν_{C-O}), 1503, 1464, 1413, 1384, 1351, 1256, 1204, 1092, 1038, 968, 920, 860, 801; SEC (THF) M_w = 3.1 x 10^5 g/mol (PD = M_w/M_n = 4.4). UV-Vis λ_{max} = 510 nm (THF).

4.6.4. Device preparation and measurement

Photovoltaic devices were made by spin coating a 50 nm PEDOT:PSS layer (Clevios™ P VP Al4083 from H. C. Starck) (60 seconds at 3000 rpm) onto pre-cleaned, patterned indium tin oxide (ITO) substrates (65 nm, 15 Ω per square) (Naranjo Substrates). On top of the PEDOT:PSS layer, the active layer was spin coated. The active layer solution (PPV derivative/PCBM 1/4 in chlorobenzene at a concentration of 5 mg/mL of the PPV derivative) was spin coated at different speeds to obtain different thicknesses of the active layer. As a cathode, a metal top contact consisting of LiF (1 nm) and aluminum (100 nm) was deposited by vacuum evaporation (3 x 10^{-7} mbar). Current *versus* voltage characteristics were measured under 100 mW/cm^2 white light from a tungsten-halogen lamp, filtered by a Schott GG385 UV filter and a Hoya LB120 daylight filter, using a Keithley 2400 source meter. Short circuit currents under AM 1.5 G conditions were obtained from the spectral response and convolution with the solar spectrum. Spectral response was measured under operation conditions using bias light from a 532 nm solid state laser (Edmund Optics). Monochromatic light from a 50 W tungsten halogen lamp (Philips focusline) in combination with monochromator (Oriel, Cornerstone 130) was modulated with a mechanical chopper. The response was recorded as the voltage over a 50 Ω resistance,

using a lock-in amplifier (Stanford research Systems SR830). A calibrated Si cell was used as reference. The device was kept behind a quartz window in a nitrogen filled container.

4.7. References

[1] Winder, C.; Sariciftci, N. S. *J. Mater. Chem.* **2004**, *14*, 1077.

[2] Dhanabalan, A.; van Duren, J. K. J.; van Hal, P. A.; van Dongen, J. L. J.; Janssen, R. A. J. *Adv. Funct. Mater.* **2001**, *11*, 255.

[3] Van Duren, J. K. J.; Dhanabalan, A.; van Hal, P. A.; Janssen, R. A. J. *Synth. Met.* **2001**, *121*, 1587.

[4] Brabec, C. J.; Winder, C.; Sariciftci, N. S.; Hummelen, J. C.; Dhanabalan, A.; van Hal, P. A.; Janssen, R. A. J. *Adv. Funct. Mater.* **2002**, *12*, 709.

[5] Colladet, K.; Nicolas, M.; Goris, L.; Lutsen, L.; Vanderzande, D. *Thin Solid Films* **2004**, *7*, 451.

[6] Wienk, M. M.; Kroon, J. M.; Verhees, W. J. H.; Knol, J.; Hummelen, J. C.; van Hall, P. A.; Janssen, R. A. J. *Angew. Chem. Int. Ed.* **2003**, *42*, 3371.

[7] Arici, E.; Sariciftci, N. S.; Meissner, D. *Adv. Funct. Mater.* **2003**, *13*, 165.

[8] Leznoff, C. C.; Lever, A. B. P. *Eds. Phthalocyanines: Properties and Applications* **1989**, **1993**, **1996**.

[9] McKeown, N. B. *Ed. Phthalocyanine Materials. Synthesis, Structure and Function* **1998**.

[10] de la Torre, G.; Nicolau, M.; Torres, T. *In Supramolecular Photosensitive and Electroactive Materials* **2001**, 1.

[11] Kadish, K. M.; Smith, K. M.; Guillard, R. *Eds. The Porphyrin Handbook* **2003**.

[12] Torres, T. *Angew. Chem. Int. Ed.* **2006**, *45*, 2834.

[13] de la Torre, G.; Claessens, C. G.; Torres, T. *Chem. Commun.* **2007**, 2000.

[14] Engelkamp, H.; Middelbeek, S.; Nolte, R. J. M. *Science* **1999**, *284*, 785.

[15] Elemans, J. A. A. W.; van Hameren, R.; Nolte, R. J. M.; Rowan, A. E. *Adv. Mater.* **2006**, *18*, 1251.

[16] Thordarson, P.; Nolte, R. J. M. *In The Porphyrin Handbook* **2003**.

[17] Kobayashi, N. *Coord. Chem. Rev.* **2002**, *227*, 129.

[18] Gregory, P. *Plenum Press* **1991**.
[19] Law, K.-Y. *Chem. Rev.* **1993**, *89*, 2652.
[20] Emmelius, M.; Pawlowski G.; Vollman, H. *Angew. Chem., Int. Ed. Engl.* **1989**, *28*, 1445.
[21] de la Torre, G.; Vázquez, P.; Agulló-López, F.; Torres, T. *J. Mater. Chem.* **1998**, *8*, 1671.
[22] Brédas, J. L.; Adant, C.; Tackx, P.; Persoons A.; Pierce, B. M. *Chem. Rev.* **1994**, *94*, 243.
[23] André, J.-J.; Simon, J. *Molecular Semiconductors* **1985**.
[24] Rosanthal, I. *Photochem. Photobiol.* **1991**, *53*, 859.
[25] Pandey, P. K.; Herman, C. K. *Chem. Ind.* **1998**, 739.
[26] Tang, C. W. *Appl. Phys. Lett.* **1986**, *48*, 183.
[27] Whitlock, J. B.; Panayotatos, P.; Sharma, G. D.; Cox, M. D.; Sauer, R. R.; Bird, G. R. *Opt. Eng.* **1993**, *32*, 1921.
[28] Wöhrle, D.; Meissner, D. *Adv. Mater.* **1991**, *3*, 129.
[29] Nazeeruddin, M. K.; Humphry-Baker, R.; Grätzel, M.; Murrer, B. A. *Chem. Commun.* **1998**, 719.
[30] Deng, H.; Mao, H.; Lu, Z.; Zu, H. *Thin Solid Films* **1998**, *315*, 244.
[31] Lever, A. B. P.; Hempstead, M. R.; Leznoff, C. C.; Liu, W.; Melnik, M.; Nevin, W. A.; Seymour, P. *Pure Appl. Chem.* **1986**, *58*, 1467.
[32] Parton, R. F.; van Kelecom, I. F. J.; Bezoukhanova, M. J. A.; Jacobs, P. A. *Nature* **1994**, *370*, 541.
[33] Mortimer, R. J. *Electrochim. Acta* **1999**, *44*, 2971.
[34] Mortimer, R. J. *Chem. Soc. Rev.* **1997**, *26*, 147.
[35] Chen, C. H.; Shi, J.; Tang, C. W. *Macromol. Symp.* **1997**, *125*, 1.
[36] Leznoff, C. C.; McArthur, C. R.; Qin, Y. N. *Can. J. Chem.* **1993**, *71*, 1319.
[37] Triska, J.; Vrchotova, N.; Safarik, I.; Safarikova, M. *J. Chromatogr.* **1998**, *793*, 403.
[38] Jinno, K.; Kohrikawa, C.; Saito, Y.; Haiginaka, J.; Saito, Y.; Mifune, M. *J. Microcolumn Sep.* **1996**, *8*, 13.
[39] Wright, J. D. *Prog. Surf. Sci.* **1989**, *31*, 1.
[40] Dogo, S.; Germain, J. P.; Maleysson, C.; Pauly, A. *Thin Solid Films* **1992**, *219*, 251.
[41] Torres, T. *Journal of Porphyrins and Phthalocyanines* **2000**, *4*, 325.

[42] de la Torre, G.; Torres, T. *Journal of Porphyrins and Phthalocyanines* **2002**, *6*, 274.
[43] Kobayashi, N.; Leznoff, C. C. *Journal of Porphyrins and Phthalocyanines* **2004**, *8*, 1015.
[44] Calvete, M.; Yang, G. Y.; Hanack, M. *Synthetic Metals* **2004**, *141*, 231.
[45] Claessens, C. G.; de la Torre, G.; Torres, T. *Proceedings of the Society of Photo-Optical Instrumentation Engineers* **2005**, *5830*, 379.
[46] Claessens, C. G.; Hahn, U.; Torres, T. *Chemical Record* **2008**, *8*, 75.
[47] Guldi, D. M.; Zilbermann, I.; Gouloumis, A.; Vázquez, P.; Torres, T. *J. Phys. Chem. B* **2004**, *108*, 18485.
[48] Gouloumis, A.; de la Escosura, A.; Vázquez, P.; Torres, T.; Khant, A.; Guldi, D. M.; Neugebauer, H.; Winder, C.; Drees, M.; Sariciftci, N. S. *Org. Lett.* **2006**, *8*, 5187.
[49] de la Escosura, A.; Martínez-Díaz, M. V.; Guldi, D. M.; Torres, T. *J. Am. Chem. Soc.* **2006**, *128*, 4112.
[50] Torres, T.; Gouloumis, A.; Sanchez-Garcia, D.; Jayawickramarajah, J.; Seitz, W.; Guldi, D. M.; Sessler, J. L. *Chem. Commun.* **2007**, *292*.
[51] Guldi, D. M.; Gouloumis, A.; Vázquez, P.; Torres, T.; Georgakilas, V.; Prato, M. *J. Am. Chem. Soc.* **2005**, *127*, 5811.
[52] Loi, M. A.; Neugebauer, H.; Denk, P.; Brabec, C. J.; Sariciftci, N. S.; Gouloumis, A.; Vázquez P.; Torres, T. *J. Mater. Chem.* **2003**, *13*, 700.
[53] Sastre, A.; Gouloumis, A.; Vázquez, P.; Torres, T.; Doan, V.; Schwartz, B. J.; Wudl, F.; Echegoyen, L.; Rivera, J. *Org. Lett.* **1999**, *1*, 1807.
[54] Martínez-Díaz, M. V.; Fender, N. S.; Rodríguez-Morgade, M. S.; Gómez-López, M.; Diederich, F.; Echegoyen, L.; Stoddart, J. F.; Torres, T. *J. Mater. Chem.* **2002**, *12*, 2095.
[55] Guldi, D. M.; Ramey, J.; Martínez-Díaz, M. V.; de la Escosura, A.; Torres, T.; Da Ros, T.; Prato, M. *Chem. Commun.* **2002**, *2774*.
[56] Guldi, D. M.; Gouloumis, A.; Vázquez, P.; Torres, T. *Chem. Commun.* **2002**, *2056*.

[57] El-Khouly, M. E.; Ito, O.; Smith, P. M.; D'Souza, F. J. *Photochem. Photobiol. C: Photochem. Rev.* **2004**, *5*, 79.

[58] Isosomppi, M.; Tkachenko, N. V.; Efimov, A.; Vahasalo, H.; Jukola, J.; Vainiotalo, P.; Lemmetyinen, H. *Chem. Phys. Lett.* **2006**, *430*, 36.

[59] Ballesteros, B.; de la Torre, G.; Torres, T.; Hug, G. L.; Rahman, G. M. A.; Guldi, D. M. *Tetrahedron* **2006**, *62*, 2097.

[60] Kahnt, A. M.; Guldi, D. M.; de la Escosura, A.; Martínez- Díaz, M. V.; Torres, T. *J. Mater. Chem.* **2008**, *18*, 77.

[61] de la Escosura, A.; Martínez-Díaz, M. V.; Torres, T.; Grubbs, R. H.; Guldi, D. M.; Neugebauer, H.; Zinder, C.; Drees, M.; Sariciftci, N. S. *Chem. Asian J.* **2006**, *1*, 148.

[62] Martínez-Díaz, M. V.; Esperanza, S.; de la Escosura, A.; Catellani, M.; Yunus, S.; Luzzati, S.; Torres, T. *Tetrahedron Lett.* **2003**, *44*, 8475.

[63] Shaheen, S. E.; Brabec, C. J.; Sariciftci, N. S.; Padinger, F.; Fromherz, T.; Hummelen, J. C. *Appl. Phys. Lett.* **2001**, *78*, 841.

Chapter 5

Grafting onto PPV derivatives

This chapter presents two different procedures to graft polymer chains onto PPV derivatives, i.e. atom transfer radical polymerization and benzyl dithiocarbamate photoiniferter polymerization. Both methods belong to the class of "pseudo" living radical polymerizations. In this way, a controlled radical reaction can be started from the initiator groups on the PPV chain. For atom transfer radical polymerization reactions, this is tested with isobornyl acrylate and styrene. For the benzyl dithiocarbamate photoiniferter, this is investigated for four vinyl monomers i.e. methyl methacrylate, methyl acrylate, methacrylic acid and styrene. It is demonstrated that grafting onto PPV derivatives is readily possible with the use of the photoiniferter method.

5.1. Introduction

Modifying a (polymeric) surface with polymeric materials with specific chemical properties and a well-defined architecture is a well known method for tailoring interfacial properties such as biocompatibility. In the literature, numerous examples can be found, such as the grafting of different surfaces with (meth)acrylates,[1-6] which can be used to develop advanced materials for chemical sensing, drug delivery, catalysis and micropatterning.[7-9] Grafting can also be performed on conjugated polymers, such as

poly(thiophene),[10-12] PPV,[13,14] and poly(acetylene),[15] *via* atom transfer radical polymerization (ATRP) methods.

In this chapter, a universal method towards grafting onto PPV derivatives is presented. In order to evaluate the best possible strategy for grafting, two types of initiator groups have been introduced in the PPV side-chains, *i.e.* ATRP and benzyl dithiocarbamate initiator groups, as can be seen in **Chapter 2**. They can both initiate radical polymerizations, which belong to the class of "pseudo" living radical polymerizations. In this manner, a controlled radical reaction can be started from the initiator groups of the PPV side chains. This gives the possibility to functionalize the PPV derivative with different oligomeric or polymeric side chains, which can be useful for a variety of applications. Controlled radical polymerizations yield materials of controlled molecular weight[16,17] with low polydispersities.[18] Furthermore, this type of chemistry is applicable to many types of monomers, such as (meth)acrylates, styrene, and acrylonitrile.

5.2. "Pseudo" living radical polymerization

A "pseudo" living radical polymerization (PLRP) reaction is a process in which termination and transfer reactions are absent and each growing chain remains 'living' all along the reaction. In this way PLRP-type reactions comprise a powerful toolbox for the syntheses of polymers with well-defined architectures and narrow polydispersities.[19] Many controlled living radical polymerizations have been developed in recent years, including iniferters,[20] nitroxide-mediated polymerizations (NMP),[21] reversible addition fragmentation transfer (RAFT)[22,23] and atom transfer radical polymerization (ATRP).[17,24] All these types of PLRP enables the control of functionality, topology and composition to a substantial degree.

The main analogy between PLRP's and regular radical polymerizations is the participation of free radicals in the process of chain growth. This leads to the same chemo-, regio- and stereo-selectivity's in both cases. The main difference between a PLRP reaction and a radical polymerization reaction is

that in PLRP the concentration of free radicals is established by typical activation and deactivation processes and in radical polymerizations by initiation and termination processes. In addition, in a PLRP the rates of initiation, activation and deactivation are much higher than those of termination, which allows initiation of all chains simultaneously and therefore gives more control over the polymer architecture. The exchange between active and dormant species enables a longer lifetime of the propagating chains in a PLRP as compared to a conventional radical polymerization. In Scheme 5-1, the general mechanism of a PLRP reaction is depicted.

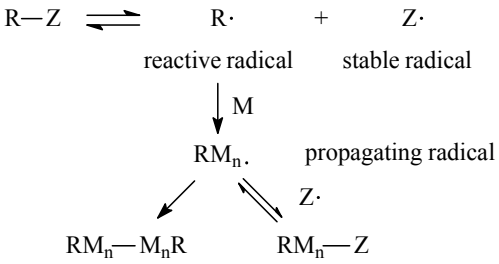

Scheme 5-1 General mechanism of a "pseudo" living radical polymerization (PLRP) reaction

According to the general mechanism, the R-Z initiator undergoes a homolytic cleavage of the R-Z bonding *via* thermal or UV treatment. A reactive and a stable radical are formed. The reactive radical initiates the polymerization, the stable radical on the other hand is not reactive enough to initiate or propagate a polymerization. However, this stable radical is responsible for the reversible termination of the growing chain end. The resulting dormant species are constantly activated thermally or in the presence of UV light. In this way, one gets a radical polymerization with a "pseudo" living character. The concentration of propagating radicals needs to be sufficiently low to eliminate the occurrence of a bimolecular termination RM_n-M_nR. In this work, two types of PLRP reactions are used, which are based on either an ATRP initiator group or a photoiniferter (benzyl dithiocarbamate initiator group).

In ATRP, the atom transfer from an organic halide to a transition-metal complex generates the reacting radicals, followed by a back transfer from the transition-metal complex to a product radical to form the final product. The general mechanism of an ATRP reaction is depicted in Scheme 5-2.

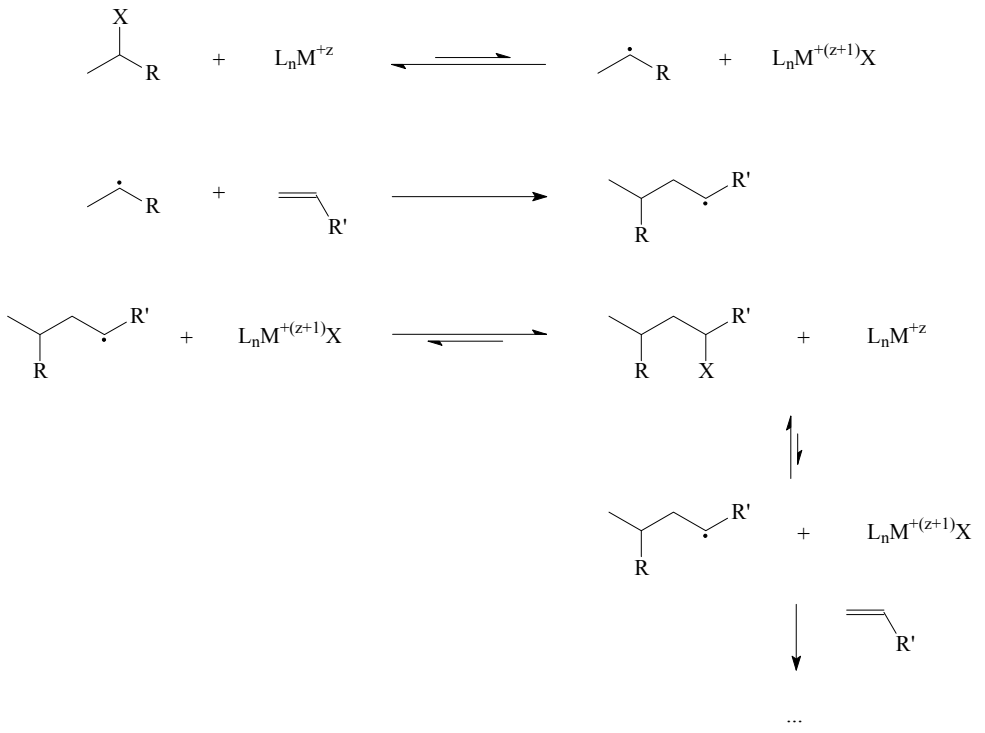

Scheme 5-2 General mechanism of an atom transfer radical polymerization (ATRP) reaction

In the ATRP reaction, the transition-metal complex L_nM^{+z} undergoes a one electron oxidation together with an abstraction of a halogen atom from the substrate. This generates an organic radical and a transition-metal complex $L_nM^{+(z+1)}X$. In order for this reaction to occur, typical substituents are required on the organic halide, which will stabilize the resultant organic radical. This organic radical can add to an unsaturated compound or it can abstract the halogen from the transition-metal complex $L_nM^{+(z+1)}X$ and return to the original dormant organic halide. During this process, the

transition-metal complex L_nM^{+z} is formed again, which completes the catalytic cycle. Due to the low concentration of propagating radicals, the occurrence of other termination reactions is strongly reduced. The substrates for this type of polymerizations are typically chosen such that the radical species, before and after addition of the unsaturated compounds, possess comparable stabilization. The activation-addition-deactivation cycle will repeat until all the unsaturated compounds are consumed. This results in a chain-growth polymerization. Examples of typical transition-metal complex can be found in the literature and include Cu(I),[16,17,25-28] Ni(II),[29,30] Ru(II)/Al(OR_3)[24,31] and Fe(II)[32,33] complexes to catalyze the formation of radicals. In addition, a large variety of ATRP initiator groups can be used, some of which are listed in Figure 5-1.

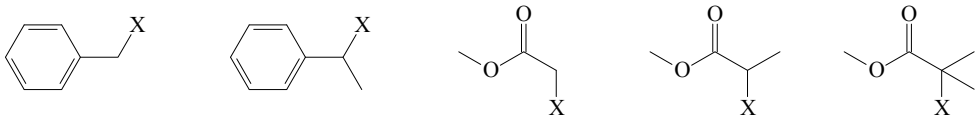

Figure 5-1 Chemical structure of some typical ATRP initiator groups

The second introduced initiator group is a photoiniferter. This iniferter (initiator-transfer agent-terminator) can be activated/deactivated photochemically. A typical representative of this type of initiators is the benzyl dithiocarbamate group (Scheme 5-3). Benzyl dithiocarbamates decompose under UV light into a reactive benzyl radical and a stable dithiocarbamate radical. This type of polymerization reactions have also a "pseudo" living radical character, since chain termination with the stable dithiocarbamate radical is inhibited by the UV light. In the literature, numerous reports can be found on the use of dithiocarbamate photoiniferters.[2,5-9,34]

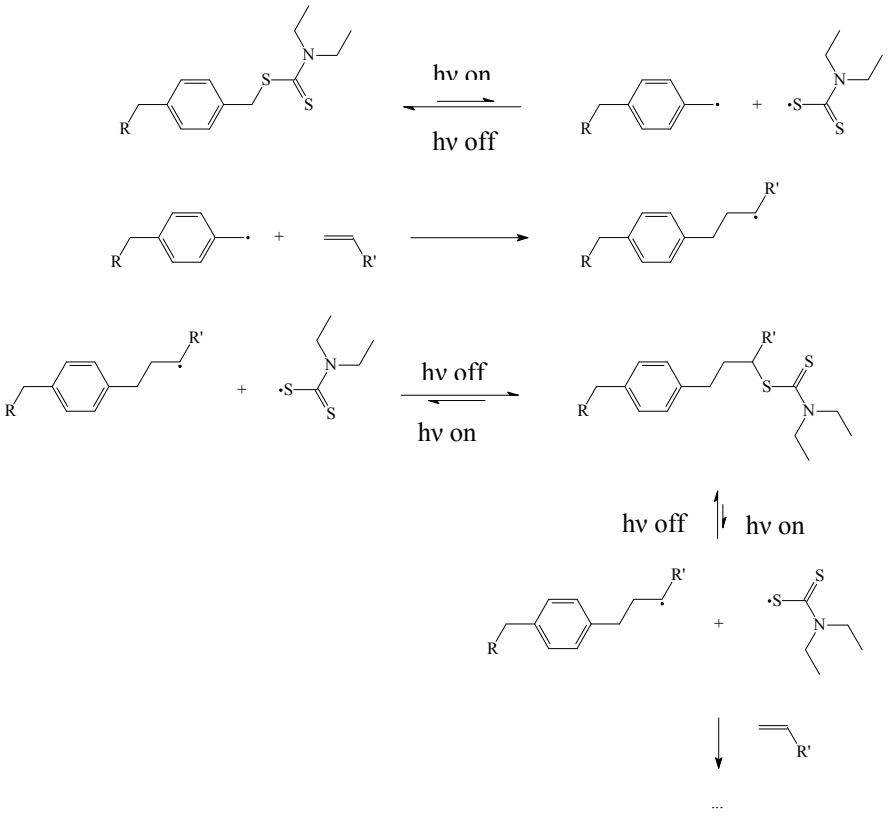

Scheme 5-3 General mechanism of a benzyl dithiocarbamate photoiniferter reaction

5.3. Atom transfer radical polymerization reaction

5.3.1. Influence of ATRP reaction conditions on MDMO-PPV and *vice versa*

To investigate the influence of an ATRP reaction on a PPV derivative and the impact of a PPV derivative on the progress of an ATRP reaction,

isobornyl acrylate (iBA) is polymerized into poly(isobornyl acrylate) (**PiBA**) under ATRP conditions in the presence of MDMO-PPV (Scheme 5-4). As a reference, iBA is also polymerized under the same conditions in the absence of MDMO-PPV.

The ATRP reaction is conducted in degassed THF under nitrogen atmosphere. THF is chosen as solvent due to the good solubility of MDMO-PPV in THF, although it is not a conventional solvent for an ATRP reaction. To a degassed mixture of the vinyl monomer, iBA, and N,N,N',N",N"-pentamethyldiethylenetriamine (PMDETA) (Figure 4-4), degassed THF (with MDMO-PPV) and Cu(I)Br are added. After placing the reaction mixture at 65 °C, the initiator methyl-2-bromopropionate is added to start the polymerization. Samples are withdrawn periodically to monitor the monomer conversion and the average molecular weight. The reaction is allowed to proceed for 4 h at 65 °C. Cu is removed by filtering over Al_2O_3 and purification is done by drop wise precipitating in a non-solvent.

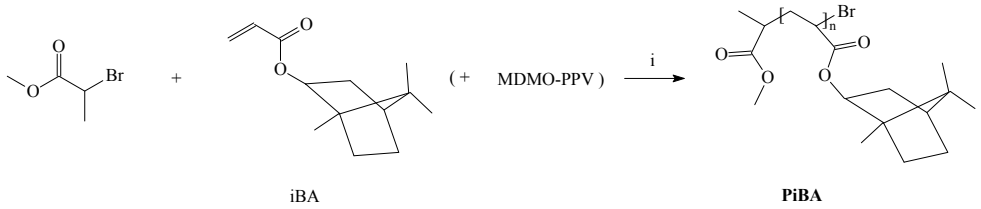

Scheme 5-4 Synthesis of poly(isobornyl acrylate) **PiBA** (in the presence of MDMO-PPV) *via* an ATRP reaction with methyl 2-bromopropionate as initiator (i: PMDETA, Cu(I)Br, THF)

To study the influence of the added MDMO-PPV on the ATRP reaction of iBA, a typical $\ln([M_0]/[M_t])$ *vs.* time curve is plotted in Figure 5-2, for both polymerization reactions. $[M_0]$ represents the concentration of the monomer at the beginning of the polymerization reaction and $[M_t]$ the concentration of the monomer at a certain time after t minutes of polymerization.

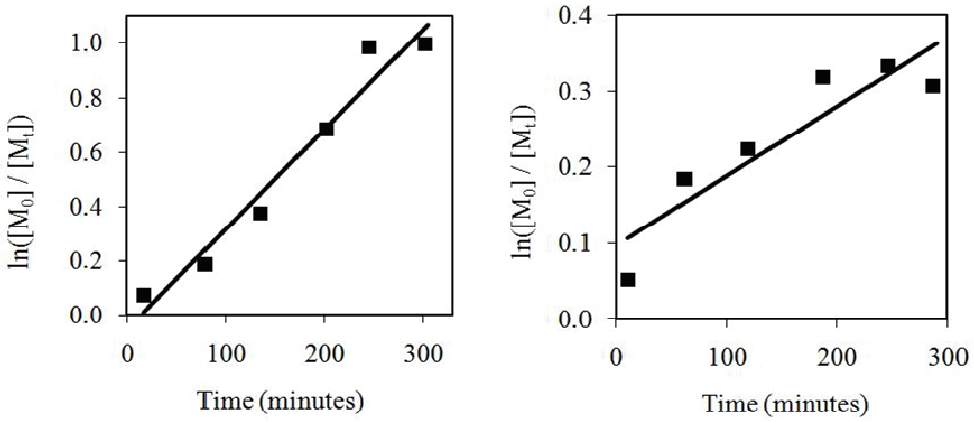

Figure 5-2 $\ln([M_0]/[M_t])$ *vs.* time plot of the ATRP reaction of iBA in THF (left) and the same polymerization reaction in the presence of MDMO-PPV (right)

Both first order kinetic plots show a linear behavior, which indicates the occurrence of a controlled radical polymerization reaction of iBA, *i.e.* the concentration of radicals is constant, although a fit in the absence of MDMO-PPV is better. At longer reaction time, a small deviation is noticeable which indicates a termination of the polymerization. This is already visible at lower conversions for the reaction in the presence of MDMO-PPV *i.e.* at *circa* 200 minutes instead of almost 300 minutes. Furthermore, the number average molecular weight (M_n), the theoretical M_n and the polydispersity (PD) are plotted as a function of the conversion for the ATRP reaction of iBA, with and without MDMO-PPV (Figure 5-3).

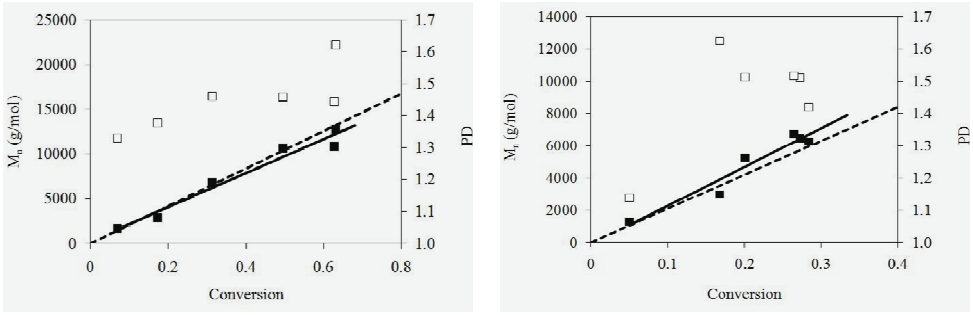

Figure 5-3 Increase of M_n (■) and evolution of PD (□) as a function of conversion for the ATRP reaction of iBA in THF (left) and the same polymerization reaction in the presence of MDMO-PPV (right), also the theoretical M_n (---) is represented

The controlled character of the polymerization reaction is confirmed by the linear increase of M_n as function of the conversion. In both polymerization reactions, M_n is in good agreement with the theoretical M_n. The PD remains reasonably narrow throughout the entire polymerization reaction, with in all cases a value below 1.7. Notwithstanding, there is still a clear influence of the MDMO-PPV visible. The conversion of the polymerization reaction of iBA, in the presence of MDMO-PPV, is much lower as compared to the polymerization reaction of iBA without MDMO-PPV. The polymerization reaction of iBA, in the presence of MDMO-PPV, stops at a conversion of 30 %, whereas the normal polymerization reaction of iBA proceeds to 60 % conversion. As a consequence, M_n of **PiBA** is remarkably lower for the reaction where MDMO-PPV is present.

To investigate the influence of the ATRP reaction of iBA on MDMO-PPV, SEC measurements are performed with a UV-Vis detector. SEC profiles of MDMO-PPV at 500 nm, during the polymerization reaction of iBA, are presented in Figure 5-4.

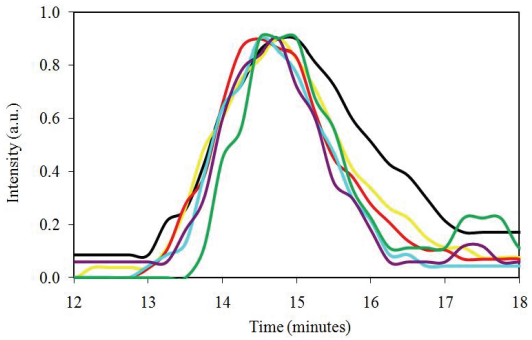

Figure 5-4 SEC profiles of MDMO-PPV at 500 nm after 15, 30, 60, 120, 184 and 240 minutes of polymerization of iBA towards **PiBA** *via* ATRP

From Figure 5-4, it is clear that there is no significant decrease of the molecular weight of MDMO-PPV observable during the ATRP polymerization of iBA. In addition, the λ_{max} of MDMO-PPV, during the polymerization reaction, is investigated. These results are depicted in Figure 5-5.

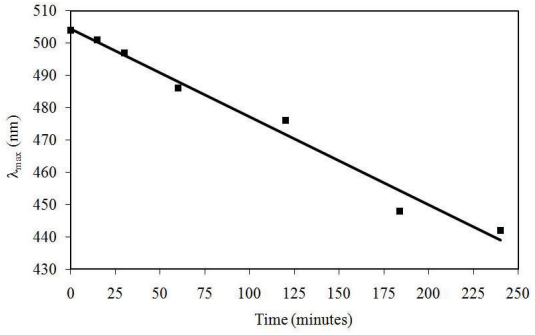

Figure 5-5 λ_{max} of MDMO-PPV as function of polymerization time of iBA towards **PiBA** *via* ATRP

Unfortunately, there is a clear decrease of λ_{max} of the MDMO-PPV visible during the polymerization of iBA. Apparently, the conditions of the ATRP polymerization reaction have a negative influence on the conjugated system of MDMO-PPV. The length of this conjugated system diminishes during the ATRP polymerization reaction. Possibly, the generated radicals will attack the double bonds in MDMO-PPV and in this way conjugation is destroyed. This is already visible after one hour of polymerization, when the initial λ_{max} of 505 nm has decreased to 486 nm.

5.3.2. Initiation of polymerization in solution *via* test molecule 17

After studying the impact of MDMO-PPV, the initiator capacity of the introduced ATRP initiator groups in **17** has been tested for the polymerization of the vinyl monomers isobornyl acrylate (iBA) and styrene towards poly(isobornyl acrylate) (**PiBA**) and poly(styrene) (Scheme 5-5). The ATRP reaction of iBA is conducted in degassed THF under nitrogen atmosphere. To a degassed mixture of the vinyl monomer, iBA, and PMDETA, degassed THF and Cu(I)Br are added. After placing the reaction mixture at 65 °C, initiator **17** is added to start the polymerization. The ATRP reaction of styrene is conducted without solvent, under nitrogen atmosphere. To a degassed mixture of styrene and PMDETA, Cu(I)Br is added. After heating the reaction mixture to 100 °C, initiator **17** is added to start the polymerization. For both reactions, samples are withdrawn periodically to monitor the monomer conversion and the average molecular weight. The reaction is allowed to proceed for 4 h at 65 °C, respectively 100 °C. Cu is removed by filtering over Al_2O_3 and purification is done by drop wise precipitating in a non-solvent.

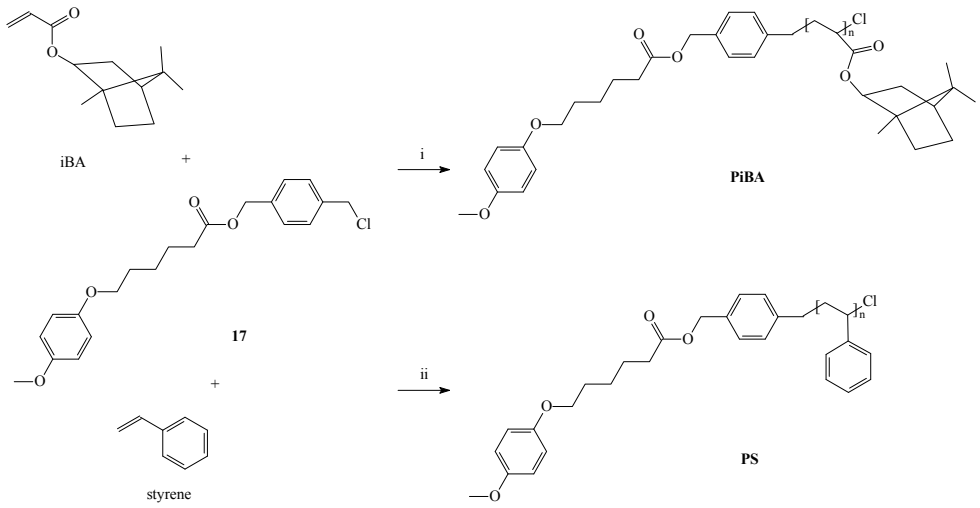

Scheme 5-5 Synthesis of poly(isobornyl acrylate) **PiBA** and poly(styrene) **PS** *via* an ATRP reaction with **17** as initiator (i: PMDETA, Cu(I)Br, THF; ii: PMDETA, Cu(I)Br)

A kinetic study of both ATRP reactions is performed by plotting $\ln([M_0]/[M_t])$ *vs.* time (Figure 5-6) and plots of M_n, the theoretical M_n and PD as function of the conversion (Figure 5-7).

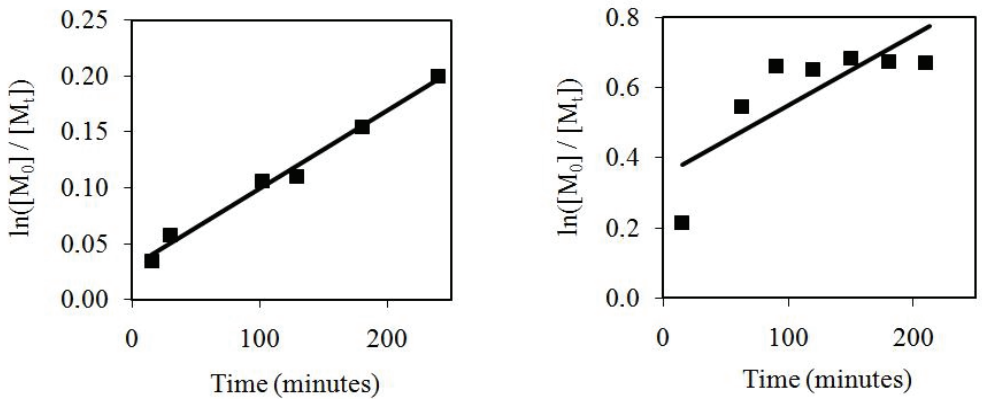

Figure 5-6 $\ln([M_0]/[M_t])$ *vs.* time plot of the ATRP reaction of iBA (left) and styrene (right) with **17** as initiator

For the ATRP reaction of iBA initiated by **17**, the first order kinetic plot shows an excellent linear behavior, which indicates that also in this case a controlled radical polymerization reaction of iBA occurs, *i.e.* the concentration of radicals is constant. In contrast, for the ATRP reaction of styrene initiated by **17**, the first order kinetic plot shows only at the beginning a linear behavior. After 80 minutes, the solution becomes more viscous, which promotes more termination reactions.

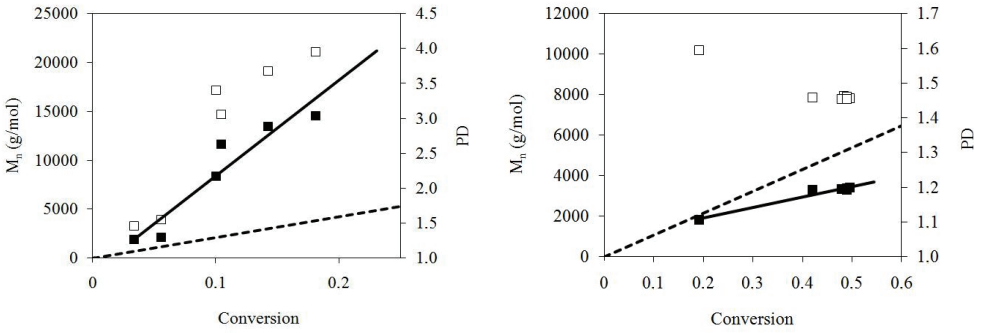

Figure 5-7 Increase of M_n (■) and evolution of PD (□) as a function of conversion for the ATRP reaction of iBA (left) and styrene (right), also the theoretical M_n (---) is represented

In addition, in both cases, M_n increases as function of the conversion, although the observed M_n deviates from the theoretical M_n. For the ATRP polymerization of iBA, this indicates a low efficiency of the initiator group of **17**. For a certain conversion, the observed M_n is higher than theoretically calculated, which suggests that not all the initiators form reactive radicals. In this way, fewer polymers are synthesized, which are, as a result, much longer. For the ATRP reaction of styrene, the observed M_n is lower than the theoretical M_n, which suggests the presence of possible transfer reactions. Furthermore, PD as function of the conversion increases for the ATRP polymerization of iBA. This indicates the somewhat uncontrolled character of the polymerization reaction. Most likely, not all the initiator groups of **17**

initiate a polymerization reaction at the same time, which results in a broad distribution of polymers. In contrast, for the ATRP reaction of styrene, the PD as function of the conversion remains constant at circa 1.5.

Apparently, although the ATRP initiator of **17** can initiate a vinyl polymerization reaction, full control of the polymerization reaction difficulties are not achieved. In addition, the generated radicals will attack the conjugated system of the PPV derivatives, which considerable reduces the opto-electronic quality of these derivatives. Therefore, no further investigations have been done for this type of reactions.

5.4. Benzyl dithiocarbamate photoiniferter

5.4.1. Initiation of polymerization in solution *via* test molecule 18 and copolymer 26

As an alternative for the ATRP reactions, the iniferter method has been optimized. First of all, the initiator capacity of the introduced benzyl dithiocarbamate group in model compound **18** is tested in solution for the vinyl monomers methyl methacrylate (MMA), methyl acrylate (MA), methacrylic acid (MAA) and styrene (Scheme 5-6).

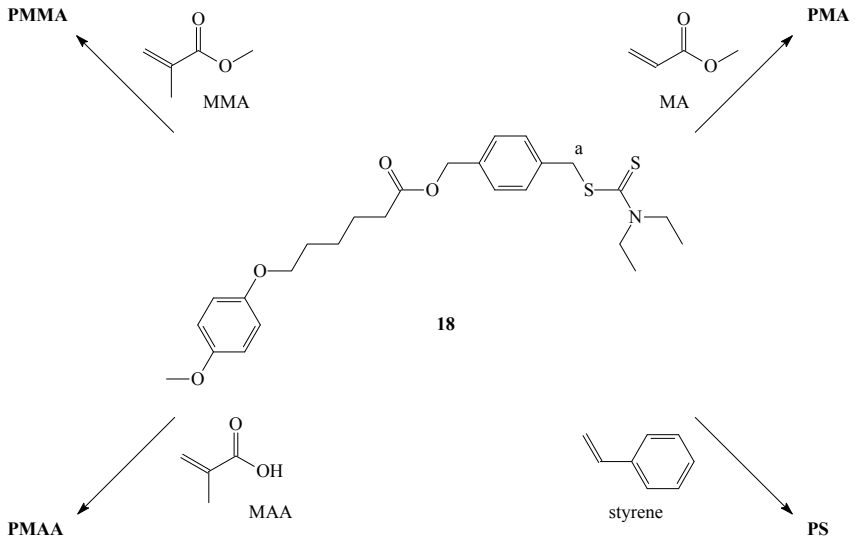

Scheme 5-6 Polymerization of methyl methacrylate (MMA), methyl acrylate (MA), methacrylic acid (MAA) and styrene *via* a benzyl dithiocarbamate photoiniferter molecule **18** under influence of UV light in THF

These iniferter polymerization reactions are conducted in dry, degassed THF under argon atmosphere. To a solution of **18**, the respective vinyl monomer is added and the solution is put under UV light (λ = 365 nm). The polymerization reaction is allowed to proceed for 90 minutes. After the polymerization, purification of **PMMA** and **PMA** is done by precipitating in a non-solvent, followed by filtration, washing and drying under reduced pressure. Purification of **PMAA** and **PS** is done by removing any unreacted monomer by distillation under reduced pressure. Notwithstanding, some monomer remains present in the mixture. **PMMA**, **PMA**, **PMAA** and **PS** are all characterized with ^{1}H-NMR, FT-IR and SEC to verify whether a polymerization has occurred.

^{1}H-NMR and FT-IR spectroscopy indeed confirm the formation of the different expected polymers. In ^{1}H-NMR, the singlet at 4.52 ppm, corresponding to the two protons next to the dithiocarbamate group, which is denoted as a in Scheme 5-6, disappear, whereas the remainder of the protons are still present in the spectrum. Furthermore, all characteristic

peaks for **PMMA**, **PMA**, **PMMA** and **PS** are present in all ^{1}H-NMR and FT-IR spectra. SEC analysis corroborate the polymerization of MMA, MA, MMA and styrene, but for each polymer a broad molecular weight distribution is observed, ranging from 1000 to 10000 g/mol (PD = 2.7). Apparently, not only polymers are formed, but also oligomers. However, one has to take into consideration that SEC analysis is performed relative to polystyrene standards and that the hydrodynamic volume for each polymer may be quite different. In spite of the low molecular weights, it can be concluded that the benzyl dithiocarbamate group, on **18**, is able to initiate polymerizations of MMA, MA, MAA and styrene. The next step is to test the polymerization of the same four vinyl monomers *i.e.* MMA, MA, MAA and styrene, with the benzyl dithiocarbamate initiator located on the side chain of copolymer **26** (Scheme 5-7).

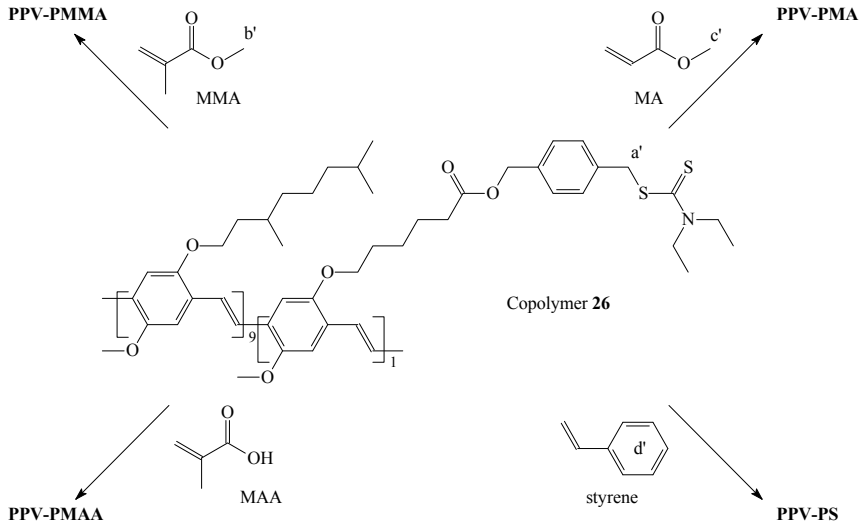

Scheme 5-7 Polymerization of methyl methacrylate (MMA), methyl acrylate (MA), methacrylic acid (MAA) and styrene *via* a benzyl dithiocarbamate photoiniferter PPV derivative **26** under influence of UV light in THF

The same procedure as was utilized for the synthesis of **PMMA**, **PMA**, **PMAA** and **PS** using **18**, is used for the synthesis of **PPV-PMMA**, **PPV-PMA**, **PPV-PMAA** and **PPV-PS**. These polymerization reactions, starting from the side chain of copolymer **26**, are conducted in dry, degassed THF under argon atmosphere. To a solution of copolymer **26**, the respective vinyl monomer is added and the solution is put under UV light (λ = 365 nm). Subsequently, the polymerization reaction is allowed to proceed for 90 minutes. After the polymerization reaction, the solutions are precipitated drop wise in a non-solvent. **PPV-PMMA**, **PPV-PMA**, **PPV-PMAA** and **PPV-PS** are filtered off, washed and dried under reduced pressure. Finally, **PPV-PMMA**, **PPV-PMA**, **PPV-PMAA** and **PPV-PS** are all characterized with ^{1}H-NMR, FT-IR, SEC and UV-Vis absorption spectroscopy to verify the quality of the resulting polymers and to see whether polymerization has occurred.

The successful polymerizations of MMA, MAA and styrene starting from copolymer **26** are clearly visible in FT-IR spectra. All the characteristic vibrations of **PMMA**, **PMAA** and **PS** are also present in the spectra of **PPV-PMMA**, **PPV-PMAA** and **PPV-PS**. The success of the polymerizations of MMA and styrene on copolymer **26** are further confirmed by ^{1}H-NMR spectroscopy. The peak of the methylester group (denoted with b' in Scheme 5-7) in **PPV-PMMA** at 3.58 ppm and the peaks, corresponding to the phenyl group (denoted with d' in Scheme 5-7) in **PPV-PS**, between 6.6 and 6.4 ppm are clearly visible. For **PPV-PMAA**, no further confirmation can be done by ^{1}H-NMR spectroscopy in a straightforward manner, since the characteristic peaks of **PMAA** overlap with those of copolymer **26**. Although, the polymerization of MA on copolymer **26** can be verified by FT-IR, it is not possible to do this using ^{1}H-NMR spectroscopy. This is a result of the fact that there is no peak visible which corresponds to the methylester group (denoted with c' in Scheme 5-7) in **PPV-PMA**. Possibly, not enough MA is polymerized by the benzyl dithiocarbamate group to see a sufficiently large signal with ^{1}H-NMR spectroscopy.

From ^{1}H-NMR spectroscopy, it can also be concluded that not all available initiator groups on copolymer **26** initiate polymerization reactions with the

offered vinyl monomers. In all cases, the singlet at 4.49 ppm, corresponding to the two protons next to the dithiocarbamate group (denoted with a' in Scheme 5-7), reduces in intensity but does not completely disappear. For **PPV-PMMA** only 46 % of the available initiator groups have started a reaction. For **PPV-PMA**, **PPV-PMAA** and **PPV-PS** these numbers are, respectively, 35 %, 79 % and 81 %. Besides the polymerization of vinyl monomers also (an)other unwanted side-reaction(s) occur(s), which may be a result of the presence of the conjugated system of copolymer **26**. This/these side-reaction(s) give(s) rise to extra peaks in the ^{1}H-NMR spectra at 5.13 ppm, 4.94 ppm, 2.79 ppm and 2.60 ppm. Until now, the origin of these peaks remains unclear and further research is needed. The occurrence of this/these side-reaction(s), in the presence of copolymer **26**, is further confirmed using solution UV-Vis absorption spectroscopy of **PPV-PMMA**, **PPV-PMA**, **PPV-PMAA** and **PPV-PS**. The UV-Vis absorption spectra in THF of **PPV-PMMA**, **PPV-PMA**, **PPV-PMAA** and **PPV-PS** are compared to the starting copolymer **26**, depicted in Figure 5-8.

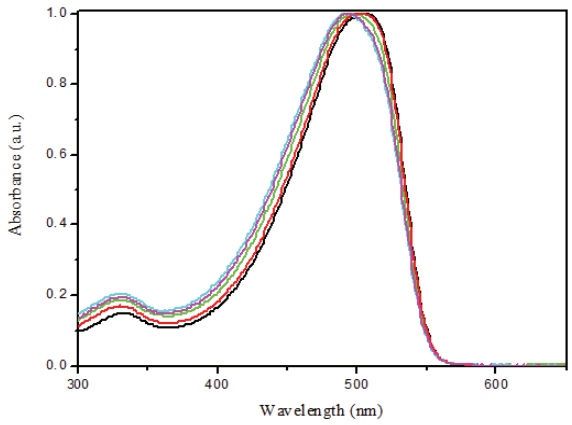

Figure 5-8 Solution UV-Vis absorption spectra of copolymer **26**, **PPV-PMMA**, **PPV-PMA**, **PPV-PMAA** and **PPV-PS** in THF

In these UV-Vis spectra, a blue shift is visible for **PPV-PMMA**, **PPV-PMA**, **PPV-PMAA** and **PPV-PS** as compared to copolymer **26** (Table 5-1). This suggests a degradation of the conjugated system of the PPV derivatives, upon polymerization of the different vinyl monomers *via* a benzyl dithiocarbamate photoiniferter. For the investigated ATRP reaction, a decrease of the initial λ_{max} of 505 nm to 486 nm was found after 60 minutes of polymerization (*cf.* section 5.3.1.). Using the photoiniferter method, also a decrease of the initial λ_{max} of 507 nm was found, but not as large as for the ATRP reaction, even after an additional 30 minutes polymerization. For a polymerization time of 90 minutes, a decrease of λ_{max} is found of *circa* 5 to 10 nm (Table 5-1). In addition, a decrease in molecular weight is observed by SEC analysis (Table 5-1), although it should be taken into account that the hydrodynamic volume for each PPV derivative (methylester, carboxylic acid and phenyl group) is quite different from the original copolymer **26**, which makes it different to compare the obtained values with each other in a detailed manner.

Copolymer	M_w (g/mol)	PD = M_w/M_n	λ_{max} in THF (nm)
26	3.2×10^5	4.6	507
PPV-PMMA	2.4×10^5	4.5	502
PPV-PMA	1.5×10^5	5.3	500
PPV-PMAA	9.4×10^4	3.5	498
PPV-PS	6.1×10^4	5.5	496

Table 5-1 Polymerization results for copolymer **26** and the grafted PPV derivatives **PPV-PMMA**, **PPV-PMA**, **PPV-PMAA** and **PPV-PS**. SEC measurements were preformed *versus* polystyrene standards using THF as eluent

5.4.2. Initiation of polymerization on a surface of copolymer 26

After the initiation of the different vinyl polymerizations in solution, these benzyl dithiocarbamate initiator groups have been "transferred" to a surface to investigate their initiator capacity in heterogeneous systems. To this end, copolymer **26** has been spin-coated on a glass substrate (layer thickness *circa* 60-70 nm). The initiation of a polymerization reaction on a copolymer **26** surface has been studied for the same four vinyl monomers, *i.e.* MMA, MA, MAA and styrene (Scheme 5-8).

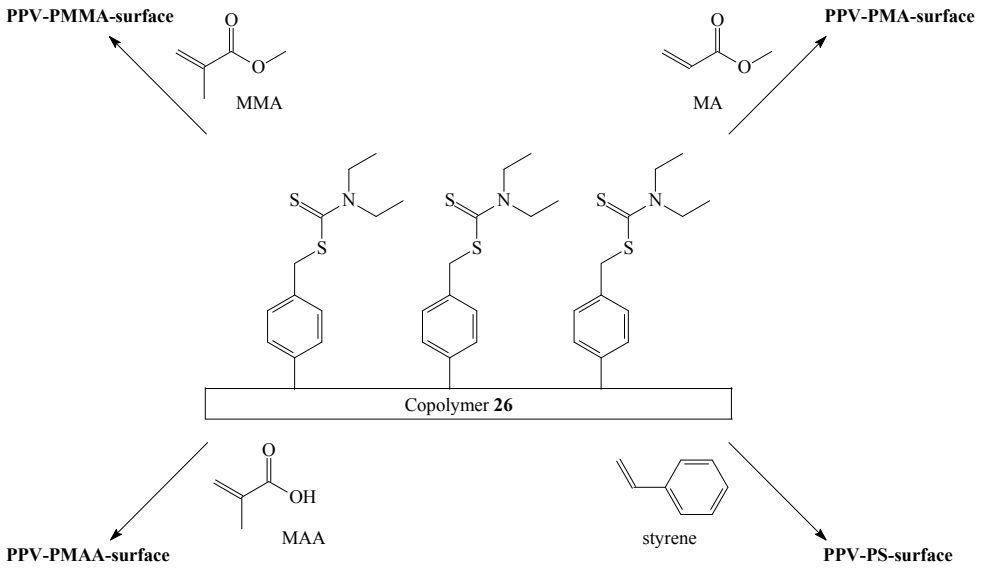

Scheme 5-8 Polymerization of methyl methacrylate (MMA), methyl acrylate (MA), methacrylic acid (MAA) and styrene on copolymer **26** surface, bearing a benzyl dithiocarbamate photoiniferter upon exposure to UV light

The surface initiated polymerization reactions are conducted in the glove box, to avoid external degradation of the PPV derivative. A solution of the respective vinyl monomer is placed on top of the copolymer **26** surface and

the sample is put under UV light (λ = 365 nm) to initiate the polymerization. The actual illumination time is varied from 15, 30, 45, 60 to 75 minutes. After polymerization, each sample is rinsed with acetone and the thickness is measured and compared to the initial thickness of the copolymer **26** surface using a Dektak surface profile measuring system. In Figure 5-9, the thickness of the formed PMMA, PMA, PMAA and PS layer is depicted as a function of the illumination time.

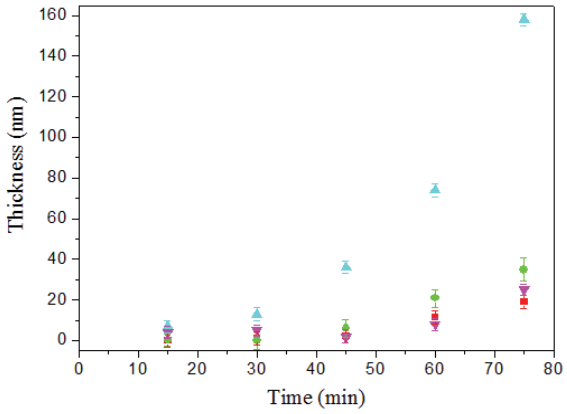

Figure 5-9 Thickness of the formed PMMA (■), PMA (●), PMAA (▲) and PS (▼) as a function of the illumination time of the samples

From Figure 5-9 it can be concluded that grafting of a PPV surface, bearing benzyl dithiocarbamate initiator groups is possible for all of the four investigated vinyl monomers, *i.e.* MMA, MA, MAA and styrene. For these four vinyl monomers, the formation of the respective polymer layer is visible starting at an illumination time of approximately 30 minutes. This time may be associated with the termination of the polymerization process by impurities. Possibly, after these impurities have reacted, the polymerization process can start uninterrupted. The thickness of this polymer layer varies from a few nanometers, for MMA, MA and styrene to almost 20 nanometer for MAA. The continuing growth of polymers at the surface is also observed for longer illumination times. It appears that the

thickness of the formed polymer layer increases exponentially with the illumination time. In the case of MAA, after an illumination time of 75 minutes the thickness of the formed PMAA layer is already 155 nm. For the other three vinyl monomers, the thickness of the formed layers at 75 minutes is between 20 and 35 nm.

5.5. Conclusions

Modifying a (polymeric) surface with polymeric materials of specific chemistry and well-defined architecture can lead to interesting new characteristics. From this point of view, initiator functionalized PPV derivatives have been synthesized. This has been described in **Chapter 2**. These initiator groups are ATRP and benzyl dithiocarbamate initiator groups. Both types can initiate controlled radical polymerizations, which belong to the class of "pseudo" living radical polymerizations. In this way, PPV derivatives can be further functionalized with either oligomers or polymers, with different properties.

The initiator capacity of the introduced ATRP initiator group is tested with the vinyl monomers iBA and styrene. Although a polymerization is readily initiated, both polymerization reactions cannot be fully controlled for a variety of reasons. To optimize the polymerization, it would be better to synthesize PPV derivatives with other ATRP initiator groups. Furthermore, it is found that an ATRP reaction, in the presence of a PPV derivative, has a negative influence on the quality of the conjugated polymer *i.e.* the generated radicals attack the conjugated system, which results in a shorter average conjugation length. This implies that the ATRP reaction times in the presence of a PPV derivative should be kept short.

The initiator capacity of the introduced benzyl dithiocarbamate initiator group is tested with the vinyl monomers MMA, MA, MAA and styrene. Starting at the benzyl dithiocarbamate initiator group on a model compound, the corresponding polymers **PMMA**, **PMA**, **PMAA** and **PS** are readily formed. ^{1}H-NMR, FT-IR and SEC confirm the polymerization of the

different vinyl monomers in solution. However, a large distribution in the molecular weight is observed, *i.e.* not only polymers but also oligomers are formed. In addition, the polymerization reaction is not fully controllable. Notwithstanding, the ability of the benzyl dithiocarbamate initiator groups of the PPV-type copolymer to start a polymerization is tested with the same four vinyl monomers. Polymerization of MMA, MAA and styrene in solution at the PPV chain is confirmed *via* ^{1}H-NMR and FT-IR spectroscopy. The results for MA are inconclusive. In addition, not all available initiator groups start polymerization reactions and (an) unwanted side-reaction(s) is/are observed probably due to the presence of the conjugated system. From solution UV-Vis absorption spectroscopy, a small blue shift is visible for λ_{max} of **PPV-PMMA**, **PPV-PMA**, **PPV-PMAA** and **PPV-PS** as compared to the initial PPV derivative, which suggests that some minor degradation of the conjugated system of the PPV derivatives occurs. Finally, the benzyl dithiocarbamate initiator group is also transferred to a surface, by spin-coating the PPV-type copolymer on a substrate. At the surface the polymerizations of MMA, MA, MAA and styrene are successfully initiated, indicating that for the four different vinyl monomers, grafting of a PPV surface is readily possible.

5.6. Experimental section

5.6.1. Chemical and optical characterization

For the ATRP polymers, SEC analysis was performed on a Waters instrument, using a Waters 1515 isocratic HPLC pump, equipped with Waters Styragel 10^3-10^4-10^5 Å serial columns (5 μm particle size) and a refractive index detector (2410 Waters) at 35 °C. Polystyrene standards were used for calibration and $CHCl_3$ as eluent at a flow rate of 1.5 mL/min.

For the DTC polymers, NMR spectra were recorded with a Varian Inova Spectrometer (^{1}H-NMR 300 MHz). Analytical Size Exclusion Chromatography (SEC) was performed using a Spectra series P100 (Spectra

Physics) pump equipped with a pre-column (5 μm, 50 x 7.5 mm, guard, Polymer Labs) and two mixed-B columns (10 μm, 2 x 300 x 7.5 mm, Polymer Labs) and a Refractive Index detector (Shodex) at 40 °C. THF was used as the eluent at a flow rate of 1.0 mL/min. Molecular weight distributions are given relative to polystyrene standards. FT-IR spectra were collected with a Perkin Elmer Spectrum One FT-IR spectrometer (nominal resolution 4 cm^{-1}, summation of 16 scans). UV-Vis measurements were performed on a Cary 500 UV-Vis-NIR spectrophotometer (scan rate 600 nm/min, continuous run from 200 to 800 nm). The thickness of the polymer layers in the DTC experiments was determined using a Dektak 3ST Surface Profile Measuring System.

5.6.2. Chemicals

Unless stated otherwise, all reagents and chemicals were obtained from commercial sources and used without further purification. PMDETA was distilled under vacuum. Cu(I)Br was purified by stirring in acetic acid for 24 h, to reduce Cu(II) to Cu(I). Subsequently, Cu(I)Br was filtered off and washed with ethanol and diethyl ether to remove $Cu(II)Br_2$ and acetic acid, after which it was dried in a vacuum oven at 75 °C.

5.6.3. Synthesis

- **Polymerization in solution *via* ATRP**

PiBA. A mixture of iBA (6 mL, 28 mmol) and PMDETA (0.089 mL, 0.4 mmol) was purged with N_2 for 1 h to remove oxygen. THF was also purged with N_2 for 1h, after which 3 mL was added to the reaction flask. Cu(I)Br (0.061 g, 0.4 mmol) was added under N_2 atmosphere, and the reaction was placed in an oil bath at 65 °C. When the reaction mixture reached the desired temperature, the polymerization was started by adding methyl 2-

bromopropionate (0.032 mL, 0.3 mmol). Samples were withdrawn periodically to monitor the monomer conversion and the average molecular weight. The reaction was terminated by cooling the reaction mixture in liquid nitrogen. The resulting polymer was dissolved in THF and the Cu catalyst was removed by passing the diluted reaction mixture over a column of neutral Al_2O_3. After evaporating the excess of solvent, the polymer was precipitated in MeOH, filtered off, washed with cold MeOH and dried at room temperature under reduced pressure. The polymer was obtained as a white solid.

PiBA in the presence of MDMO-PPV. This synthesis was performed using a similar procedure as described for **PiBA**. However, MDMO-PPV (2 mg) was first dissolved in THF (5 mL). This dissolved MDMO-PPV in THF was purged with N_2 for 1h, after which 3 mL of this solution was added to the reaction flask instead of pure THF. After polymerization, the polymer was obtained as a white solid.

PiBA using initiator model compound 17. A mixture of iBA (5 mL, 23.6 mmol) and PMDETA (0.074 mL, 0.35 mmol) was purged with N_2 for 1 h to remove oxygen. THF was also purged with N_2 for 1h, after which 2.5 mL was added to the reaction flask. Cu(I)Br (0.050 g, 0.35 mmol) was added under N_2 atmosphere, and the reaction was placed in an oil bath at 65 °C. When the reaction mixture reached the desired temperature, the polymerization was started by adding **17** (0.089 g, 0.23 mmol) in 0.5 mL THF. Samples were withdrawn periodically to monitor the monomer conversion and the average molecular weight. The reaction was terminated by cooling the reaction mixture in liquid nitrogen. The resulting polymer was dissolved in THF and the Cu catalyst was removed by passing the diluted reaction mixture over a column of neutral Al_2O_3. After evaporating the excess solvent, the polymer was precipitated in MeOH, filtered off, washed with cold MeOH and dried at room temperature under reduced pressure. The polymer was obtained as a white solid.

PS using initiator model compound 17. A mixture of styrene (3 mL, 28.4 mmol) and PMDETA (0.059 mL, 0.28 mmol) was purged with N_2 for 1 h to remove oxygen. Cu(I)Br (0.040 g, 0.28 mmol) was added under N_2

atmosphere, and the reaction was placed in an oil bath at 100 °C. When the reaction mixture reached the desired temperature, the polymerization was started by adding **17** (0.107 g, 0.28 mmol) in 0.5 mL of the styrene-PMDETA-Cu(I)Br solution. Samples were withdrawn periodically to monitor the monomer conversion and the average molecular weight. The reaction was terminated by cooling the reaction mixture in liquid nitrogen. The resulting polymer was dissolved in THF and the Cu catalyst was removed by passing the diluted reaction mixture over a column of neutral Al_2O_3. After evaporating the excess of solvent, the polymer was precipitated in MeOH, filtered off, washed with cold MeOH and dried at room temperature under reduced pressure. The polymer was obtained as a white solid.

♦ Polymerization in solution *via* benzyl dithiocarbamate photoiniferter

PMMA using initiator model compound 18. Initiator **18** (0.02 g, 0.04 mmol) was dissolved in dry, degassed THF (3 mL). The vinyl monomer, *i.e.* methyl methacrylate (MMA) (0.408 g, 4.08 mmol) was added. The solution was again degassed for 2 min and sealed from the air. Subsequently, the solution was put under UV light (λ = 365 nm) for 90 min. After polymerization, the solution was precipitated drop wise in cold MeOH (50 mL). The resulting polymer was filtered off, washed with cold MeOH and dried at room temperature under reduced pressure. The polymer was obtained as a white solid. ^{1}H-NMR ($CDCl_3$): δ = 7.2-7.0, 6.78, 5.03, 3.86, 3.73, 3.56, 3.01, 2.34, 1.97-0.80; FT-IR (NaCl, cm^{-1}): 3443, 2993, 2950, 1778, 1729 (ν_{C-O}), 1509, 1484, 1449, 1436, 1384, 1272, 1234, 1192, 1149, 1068, 1039, 988, 967, 826, 749.

PMA using initiator model compound 18. PMA was prepared following a similar procedure as described for **PMMA** using methyl acrylate (MA) (0.352 g, 4.08 mmol) as the vinyl monomer. After polymerization, the solution was precipitated drop wise in cold MeOH (50 mL). The resulting polymer was filtered off, washed with cold MeOH and dried at room

temperature under reduced pressure. The polymer was obtained as a white solid. ^{1}H-NMR ($CDCl_3$): δ = 7.2-7.0, 6.75, 5.01, 3.83, 3.74, 3.60, 3.01, 2.50, 2.29, 1.97-1.18; FT-IR (NaCl, cm^{-1}): 3627, 3541, 3452, 2999, 2953, 2868, 1733 (ν_{C-O}), 1509, 1438, 1381, 1334, 1198, 1165, 1118, 1059, 977, 827, 757.

PMAA using initiator model compound 18. PMAA was prepared following a similar procedure as described for **PMMA** using methacrylic acid (MAA) (0.352 g, 4.08 mmol) as the vinyl monomer. Evaporation of the solvent, under reduced pressure, gave the crude product. After distillation under reduced pressure (75 °C/10^{-2} mbar) a white polymer was obtained. Analysis indicated that some residual MAA remained present in the mixture. ^{1}H-NMR (CD_3OD): δ = 7.2-7.0, 6.80, 5.06, 4.02, 3.84, 3.72, 3.60, 2.50, 2.37, 1.99-1.08; FT-IR (NaCl, cm^{-1}): 3421, 2993, 2944, 2868, 1700 (ν_{C-O}), 1509, 1488, 1452, 1421, 1388, 1272, 1232, 1182, 1038, 967, 933, 826, 747.

PS using initiator model compound 18. PS was prepared following a similar procedure as described for **PMMA** using styrene (0.425 g, 4.08 mmol) as the vinyl monomer. Evaporation of the solvent, under reduced pressure, gave the crude product. After distillation under reduced pressure (75 °C/10^{-2} mbar) a yellow polymer was obtained. Analysis indicated that some residual styrene remained present in the mixture. ^{1}H-NMR ($CDCl_3$): δ = 7.4-7.0, 6.80, 6.6-6.4, 5.05, 4.00, 3.87, 3.74, 2.36, 1.86-1.17; FT-IR (NaCl, cm^{-1}): 3059, 3028, 2928, 2857, 1734 (ν_{C-O}), 1601, 1508, 1493, 1453, 1418, 1380, 1354, 1269, 1231, 1180, 1156, 1108, 1071, 1038, 916, 824, 758.

MDMO-PPV grafted with PMMA. Copolymer **26** (0.005 g, 0.0016 mmol 4-((N,N-diethyldithiocarbamate)methyl)-benzyl functionalities) was dissolved in dry, degassed THF (3 mL) after which methyl methacrylate (MMA) (0.160 g, 1.60 mmol) was added. The solution was again degassed for 2 min and sealed from the air. Subsequently, the solution was put under UV light (λ = 365 nm) for 90 min after which the solution was precipitated drop wise in cold MeOH (50 mL). The resulting red copolymer was filtered off, washed with cold MeOH and dried at room temperature under reduced pressure. The polymer was obtained as a red, fibrous solid. ^{1}H-NMR

($CDCl_3$): δ = 7.6-7.4, 7.31, 7.2-7.1, 5.13, 5.07, 5.05, 4.94, 4.49, 4.1-3.8, 3.58, 2.79, 2.60, 2.4-2.3, 1.9-0.8; FT-IR (NaCl, cm^{-1}): 2953, 2927, 2868, 1732 (ν_{C-O}), 1653, 1505, 1464, 1414, 1384, 1353, 1256, 1205, 1158, 1093, 1037, 969; SEC (THF) M_w = 2.4 x 10^5 g/mol (PD = M_w/M_n = 4.5). UV-Vis λ_{max} = 502 nm (THF).

MDMO-PPV grafted with PMA. MDMO-PPV grafted with PMA was prepared following a similar procedure as described for **MDMO-PPV grafted with PMMA** using methyl acrylate (MA) (0.138 g, 1.60 mmol) as the vinyl monomer. After precipitation in cold MeOH (50 mL), the resulting red copolymer was filtered off, washed with cold MeOH and dried at room temperature under reduced pressure. The polymer was obtained as a red, fibrous solid. ^{1}H-NMR ($CDCl_3$): δ = 7.6-7.4, 7.31, 7.2-7.1, 5.13, 5.07, 5.05, 4.94, 4.49, 4.1-3.8, 2.79, 2.60, 2.4-2.3, 1.9-0.8; FT-IR (NaCl, cm^{-1}): 2953, 2920, 2850, 1738 (ν_{C-O}), 1505, 1464, 1414, 1384, 1353, 1257, 1205, 1158, 1093, 1037, 968; SEC (THF) M_w = 1.5 x 10^5 g/mol (PD = M_w/M_n = 5.3). UV-Vis λ_{max} = 500 nm (THF).

MDMO-PPV grafted with PMAA. MDMO-PPV grafted with PMAA was prepared following a similar procedure as described for **MDMO-PPV grafted with PMMA** using methacrylic acid (MAA) (0.138 g, 1.60 mmol) as the vinyl monomer. After precipitation in cold MeOH (50 mL), the resulting red copolymer was filtered off, washed with cold MeOH and dried at room temperature under reduced pressure. The polymer was obtained as a red, fibrous solid. ^{1}H-NMR ($CDCl_3$): δ = 7.6-7.4, 7.31, 7.2-7.1, 5.13, 5.07, 5.05, 4.94, 4.49, 4.1-3.8, 2.78, 2.60, 2.4-2.3, 1.9-0.8; FT-IR (NaCl, cm^{-1}): 2950, 2922, 2850, 1734 (ν_{C-O}), 1700 (ν_{C-O}), 1505, 1464, 1415, 1384, 1353, 1259, 1205, 1158, 1093, 1033, 968; SEC (THF) M_w = 9.4 x 10^4 g/mol (PD = M_w/M_n = 3.5). UV-Vis λ_{max} = 498 nm (THF).

MDMO-PPV grafted with PS. MDMO-PPV grafted with PS was prepared following a similar procedure as described for **MDMO-PPV grafted with PMMA** using styrene (0.166 g, 1.60 mmol) as the vinyl monomer. After precipitation in cold MeOH (50 mL), the resulting red copolymer was filtered off, washed with cold MeOH and dried at room temperature under reduced pressure. The polymer was obtained as a red,

fibrous solid. ^{1}H-NMR ($CDCl_3$): δ = 7.6-7.4, 7.31, 7.2-7.1, 6.6-6.4, 5.13, 5.07, 5.05, 4.94, 4.49, 4.1-3.8, 2.78, 2.60, 2.4-2.3, 1.9-0.8; FT-IR (NaCl, cm^{-1}): 3060, 3026, 2953, 2922, 2851, 1738 (ν_{C-O}), 1601, 1494, 1454, 1415, 1384, 1353, 1260, 1206, 1158, 1093, 1029, 968; SEC (THF) M_w = 6.1 x 10^4 g/mol (PD = M_w/M_n = 5.5). UV-Vis λ_{max} = 496 nm (THF).

♦ **Polymerization on PPV surface *via* benzyl dithiocarbamate photoiniferter**

All samples for initiation of a polymerization on the copolymer **26** surface were prepared in a glovebox. First a glass substrate, 20 by 10 millimeter, was cut from a microscope slide. The glass substrates were successively cleaned in a soap solution, demineralized water and acetone for 10 minutes each in an ultrasonic bath. This was followed by cleaning in boiling isopropanol for 10 minutes. Afterwards the samples were dried with an N_2 gun. Subsequently, copolymer **26** was spin-coated from chlorobenzene (7 mg/mL of the PPV derivative) solution. The thickness of the polymer layer was determined by the speed and the duration of the spin-coating process. In this way layers of about 60-70 nm were obtained.

Thin films of MDMO-PPV grafted with PMMA. In the glove box, a solution of the vinyl monomer, *i.e.* methyl methacrylate (MMA) (0.3 M) in dry, degassed MeOH (20 mL) was put in a petri dish. Five samples with a copolymer **26** surface were placed in this solution. These samples were put under UV light (λ = 365 nm) and the PPV surface was illuminated for 15, 30, 45, 60 and 75 minutes. After rinsing the samples with acetone, the thickness of the samples was measured and compared to the initial thickness of the copolymer **26** surface.

Thin films of MDMO-PPV grafted with PMA, PMMA and **PS** were prepared following the same procedure using methyl acrylate (MA), methacrylic acid (MAA) and styrene, respectively, as the vinyl monomers.

5.7. References

[1] Quémener, D.; Le Hellaye, M.; Bissett, C.; Davis, T. P.; Barner-Kowollik, C.; Stenzel, M. H. *J. Polym. Sci., Part A: Polym. Chem.* **2008**, *46*, 155.

[2] Luo, N.; Hutchison, J. B.; Anseth, K. S.; Bowman, C. N. *J. Polym. Sci., Part A: Polym. Chem.* **2002**, *40*, 1885.

[3] Morgado, J.; Friend, R. H.; Cacialli, F. *Synth. Met.* **2000**, *114*, 189.

[4] Xu, D.; Deng, Z.; Li, X.; Chen, Z.; Liang, C. *Appl. Surf. Sci.* **2007**, *253*, 3378.

[5] Nagai, D.; Fujii, A.; Ochiai, B.; Sudo, A.; Endo, T. *J. Polym. Sci., Part A: Polym. Chem.* **2008**, *46*, 1990.

[6] Wei, X.; Li, X.; Husson, S. M. *Biomacromolecules* **2005**, *6*, 1113.

[7] Pérez-Moral, N.; Mayes, A. G. *Macromol. Rapid Commun.* **2007**, *28*, 2170.

[8] Sellergren, B.; Rückert, B.; Hall, A. J. *Adv. Mater.* **2002**, *14*, 1204.

[9] Peppas, N. A.; Ward, J. H. *Adv. Drug Delivery Rev.* **2004**, *56*, 1587.

[10] Kim, K. H.; Jo, W. H. *Macromolecules*, **2007**, *40*, 3708.

[11] Costanzo, P. J.; Stokes, K. K. *Macromolecules* **2002**, *35*, 6804.

[12] Economopoulos, S. P.; Chochos, C. L.; Gregoriou, V. G.; Kallitsis, J. K.; Barrau, S.; Hadziioannou, G. *Macromolecules* **2007**, *40*, 921.

[13] Qu, G.; Jiang, F.; Zhang, S.; Usuda, S. *Mater. Lett.* **2007**, *61*, 3421.

[14] Brochon, C.; Sary, N.; Mezzenga, R.; Ngov, C.; Richard, F.; May, M.; Hadziioannou, G. *Journal of Applied Polymer Science* **2008**, *110*, 3664.

[15] Zhang, W.; Shiotsuki, M.; Masuda, T.; Kumaki, J.; Yashima, E. *Macromolecules* **2007**, *40*, 178.

[16] Wang, J. S.; Matyjaszewski, K. *Macromolecules* **1995**, *28*, 7901.

[17] Wang, J. S.; Matyjaszewski, K. *J. Am. Chem. Soc.* **1995**, *117*, 5614.

[18] Patten, T.; Xia, J.; Abernathy, T.; Matyjaszewski, K. *Science* **1996**, *272*, 866.

[19] Braunecker, W.A.; Matyjaszewski, K. *Prog. Polym. Sci.* **2007**, *32*, 93.

[20] Otsu, T.; Yoshida, M. *Makromol. Chem. Rapid. Commun.* **1982**, *3*, 127.

[21] Georges, M. K.; Veregin, R. P. N.; Kazmaier, P. M.; Hamer, G. K. *Macromolecules* **1993**, *26*, 2987.
[22] Chiefari, J.; Chong, Y. K.; Ercole, F. *Macromolecules* **1998**, *31*, 5559.
[23] Barner-Kowollik, C.; Davic, T. P.; Heuts, J. P. A. *J. Polym. Sci. Part A: Polym. Chem.* **2003**, *41*, 365.
[24] Kato, M.; Kamigaito, M.; Sawamoto, M.; Higashimura, T. *Macromolecules* **1995**, *28*, 1721.
[25] Percec, V.; Barboiu, B. *Macromolecules* **1995**, *28*, 7970.
[26] Patten, T. E.; Xia, J.; Abernathy, T.; Matyjaszewski, K. *Science* **1996**, *272*, 866.
[27] Percec, V.; Barboiu, B.; Neumann, A.; Ronda, J. C.; Zhao, M. *Macromolecules* **1996**, *29*, 3665.
[28] Haddleton, D.; Jasieczek, C. B.; Hannon, M. J.; Schooter, A. J. *Macromolecules* **1997**, *30*, 2190.
[29] Granel, C.; Dubois, P.; Jerome, R.; Teyssie, P. *Macromolecules* **1996**, *29*, 8576.
[30] Uegaki, H.; Kotani, Y.; Kamigaito, M.; Sawamoto, M. *Macromolecules* **1997**, *30*, 2249.
[31] Ando, T.; Kato, M.; Kamigaito, M.; Sawamoto, M. *Macromolecules* **1996**, *29*, 1070.
[32] Ando, T.; Kamigaito, M.; Sawamoto, M. *Macromolecules* **1997**, *30*, 4507.
[33] Matyjaszewski, K.; Wei, M.; Xia, J.; McDermott, N. E. *Macromolecules* **1997**, *30*, 8161.
[34] Nagesh, K.; Ramakrishnan, S. *Synth. Met.* **2005**, *155*, 320-323.
[35] Sauerbrey, G. *Zeitschrift für Physik A Hadrons and Nuclei* **1959**, *155*, 206.

Chapter 6

Towards the post-polymerization functionalization of PPV derivatives with natural and artificial receptors

Chapter 6 presents some initial experiments to post-polymerization functionalization of PPV derivatives with natural and artificial receptors. To this end, artificial receptors have been developed for L-nicotine, which have been tested in two different biomimetic sensor set-ups using a PPV-type transducer layer. The actual read-out of both sensor set-ups has been obtained electrochemically, using impedance measurements, and gravimetrically, using quartz crystal microbalance measurements. Furthermore, a strategy has been explored to "click" natural receptors onto PPV surfaces. Therefore, the conditions to "click" a dye onto a PPV surface have been optimized.

6.1. Introduction

A biosensor is a device that uses biological sensing elements to monitor the presence of various analytes in a sample. A commercially viable biosensor should be sensitive, specific for one analyte, low cost, fast and straightforward to operate. In Figure 6-1, a typical built-up of a biosensor is shown.

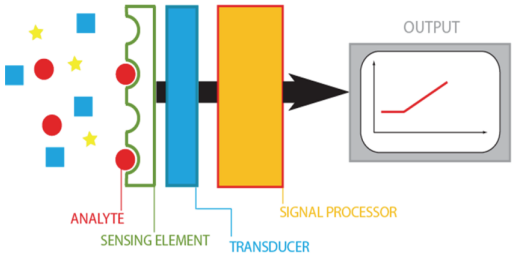

Figure 6-1 Typical built-up of a biosensor

In Figure 6-1, the three main elements of a biosensor are visible, *viz.* the recognition layer, the transducer layer and the read-out system. In the sensor, the recognition or sensing elements are able to recognize specific molecules, *i.e.* the analytes. This recognition is translated *via* the transducer layer into a measurable signal. Depending on the actual type of translation, an electrochemical, optical or piezoelectric readout is achieved.

The recognition layer may consist of enzymes,[1-4] antibodies,[5-7] DNA,[8-10] or synthetic receptors.[11-18] Enzymes are biological catalysts for particular reactions and can bind themselves to specific substrates. Antibodies will specifically bind with the corresponding antigen and DNA can also operate selectively as a result of their base-pairing characteristics. Enzymes, antibodies and DNA are all biological materials and the use of such materials has several restrictions related to the operating conditions. This has inspired researchers to mimic the molecular recognition properties from these biological materials. In this way, synthetic receptors have been developed, which can operate at different conditions and can be custom made for specific analytes. Sensors, based on such type of recognition elements, are usually referred to as biomimetic sensors instead of biosensors.

The working principle of the transducer layer makes is based on a physical change accompanying the binding event between sensing element and analyte. When the binding causes interface changes, the dielectric constant of the surface is influenced. This principle is used for impedance based biosensors. Furthermore, when a signal is produced by changes in mass of

the reactants, the piezo-electric properties of the transducer layer can be influenced and biosensors based on this principle are called microgravimetric biosensors. These are just two examples of translating a binding event into a physical, measurable signal. Depending on the desired transduction, a suitable material can be chosen *e.g.* polymers,[19,20] conjugated polymers,[7,14,21] gold,[6,22-24] silicon,[25-27] silicon oxide,[28] diamond,[29-33] graphite[34,35] and carbon.[36,37]

Immobilization of the natural or artificial receptor to the transducer layer is not always straightforward. The attachment of these receptors has to be stable, reproducible and sufficient coverage of the transducer surface is needed. In the literature, various methods can be found to connect the receptor with the transducer.[38] In this chapter, the results of the first attempts are described to (covalently) link the receptor layer (DNA and molecular imprinted polymers) with a suitable transducer layer (PPV derivatives). This involves a transducer layer, which is tailored with suitable functional groups. The advantage of covalent linking is the certainty that the receptor will not release from the transducer during the sensing. At the same time, it is important to confirm that the covalent attachment does not affect the accessibility of the receptor. In addition, the synthesis of these artificial receptors, molecular imprinted polymers or MIPs, is described in this chapter.

6.2. Molecularly imprinted polymers - "MIPs"

6.2.1. Historical background

Molecular imprinting is based on the theory of Pauling on the formation of antibodies.[39-41] Pauling suggested that antibodies were formed when serum proteins assembled around template antigen molecules. These assembled antibodies were thought to have binding sites, complementary in shape to the antigen molecules. Moreover, the presence of numerous non-covalent interactions, *e.g.* hydrogen bonds, ionic bonds and van der Waals forces,

were expected to result in strong antigen-antibody interactions. Using these basic principles, Pauling and Campbell declared that it should be possible to assemble artificial antibodies.[39] The aim was to obtain materials, possessing sites of which the shape would fit the shape of the molecule to be recognized. These materials could act as an alternative to natural receptors. Although for recognition of specific target molecules, various biological molecules can be used such as microbes, enzymes or antibodies, many difficulties exist due to their intrinsic properties, *e.g.* instability against high temperature, pH and organic solvents. In addition, it is not always easy to find and purify a natural candidate which possesses the desired properties.

Hence, several groups applied Pauling's theory to obtain alternatives.[40,41] Mosbach was the first to synthesize such artificial antibodies, following Pauling's original theory. His group can be credited with the development of the concept of molecular imprinting.[42] Preassembling a non-covalent associated monomer - template complex in solution, prior to the actual polymer formation, was the breakthrough in the formation of molecular imprinted materials. These molecularly imprinted polymers (MIPs) are physical robust, strong, resistant against elevated temperatures and pressures, inert towards acids, bases, metal ions and organic solvents and can be regenerated. They can be used in a variety of applications such as separation science,[43-45]catalysis[46-51] and (bio)sensors.[52-57] As a result, there is a considerable research effort devoted to this field (Figure 6-2).

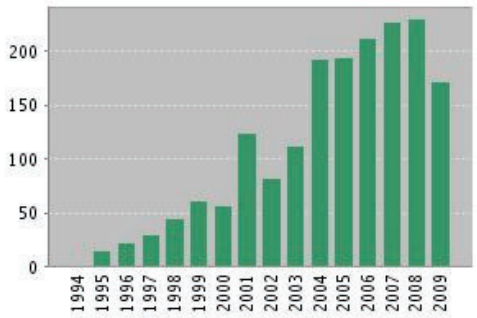

Figure 6-2 Number of publications about molecularly imprinted polymers (MIPs) for each year (source: Web of Science; search term: molecularly imprinted polymer)

6.2.2. General synthesis of MIPs

MIPs can be defined as synthetic polymers with well-defined cavities, also called imprints, created by template molecules. MIPs are able to recognize the template molecule in presence of similar molecules in solution. The general mechanism of the preparation of MIPs is depicted in Figure 6-3.

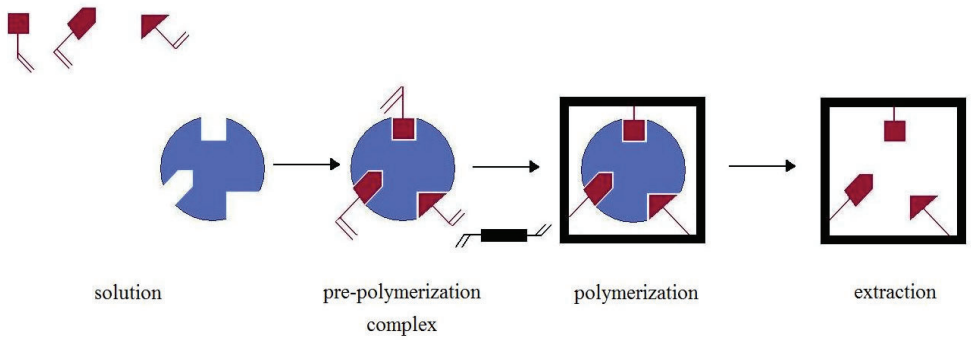

Figure 6-3 General mechanism of the preparation of MIPs

MIPs can be synthesized by the polymerization of appropriate monomers and cross-linkers in the presence of the target molecule (template). The target molecule is allowed to form a pre-polymerization complex in solution with the proposed functional monomers. After polymerization, the target molecule is removed by extraction from the formed solid polymer, leaving cavities complementary in size and shape to the target molecule. Subsequently, the cross-linked polymer or MIP is able to selectively rebind the target molecule.

To synthesize MIPs, usually a bulk polymerization is used. The main drawback of this method is that the resulting MIP particles are irregular in shape and size as a result of the necessary grinding and sieving of the crunched monoliths. This somewhat limits their applicability and reproducibility. Fortunately, there are several techniques for making well-defined imprinted polymers beads, which have a more controlled shape.

Examples include suspension polymerization, which uses liquid perfluorocarbons, mineral oils or water as the continuous phase[58] and dispersion or precipitation polymerization.[59,60] In addition surface modification procedures have been developed to attached MIPs to surfaces, such as grafting of MIPs on silica particles[61] and synthesizing surface-modified imprinted polymers by polymerization methods on seed particles.[62]

The design of MIPs is an interesting interplay between a large number of experimental variables, such as the nature of the template molecule, the functional monomer(s), cross-linker(s), solvent(s), initiator, method of initiation and duration of polymerization. In the following section, these individual components will be discussed in more detail.

6.2.3. Different components for MIP synthesis

The target molecule is of central importance during the MIP synthesis. It directs the organization of the functional groups, which are available on the functional monomers, during the formation of the pre-polymerization complex. Unfortunately, not all target molecules are compatible with the MIP synthesis and some limitations must be taken into account. First of all, the target molecule may not bear any polymerizable groups. Furthermore, it may not inhibit or significantly slow down the free radical vinyl polymerization reaction. Finally, the target molecule must be stable under the applied polymerization conditions (moderately elevated temperatures or UV irradiation). Generally speaking, the target molecule may be any type of molecule, ranging from small molecules such as drug substances, amino acids or steroid hormones to larger molecules such as (poly) nucleic acids or proteins. MIPs can also be developed for large molecular assemblies such as cells and viruses, although for such targets surface imprinting will be more suitable than bulk imprinting. In general, the difficulty of making imprinted materials increases with the size of the selected target molecule.

The functional monomers are responsible for the directional interactions in the imprinted binding sites of the cross-linked polymer. It is of considerable importance for the performance of the MIP to match the functionality of the target molecule, as good as possible, with the functionality of the introduced functional monomers in a complementary fashion. In this way, maximal complex formation and thus a maximal imprint effect is achieved. A selection of suitable functional monomers, used in MIP synthesis, is shown in Figure 6-4.

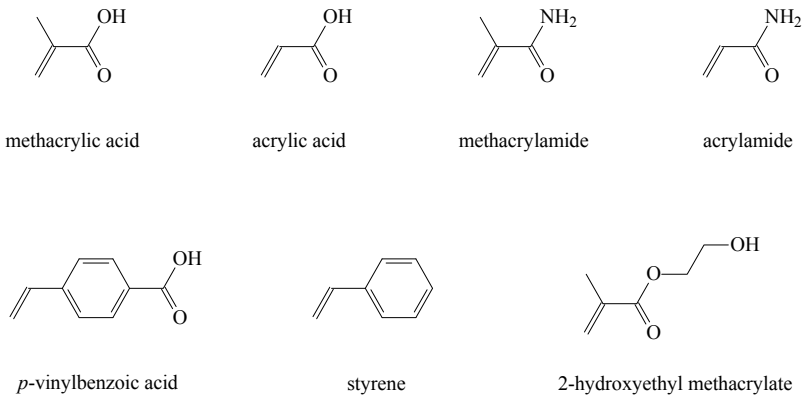

Figure 6-4 A selection of functional monomers, used in MIP synthesis

Cross-linkers are molecules, which are used to stabilize the imprinted binding site, *i.e.* to freeze the pre-polymerization complex. As a result, these molecules bring mechanical stability into the polymer matrix. A selection of cross-linkers, which are used in molecular imprinting, is presented in Figure 6-5. Some of them are also capable of simultaneous complex formation with the target molecule and thus acting not only as cross-linker, but also as functional monomer.

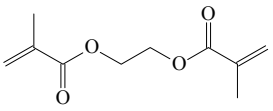

ethylene glycol dimethacrylate

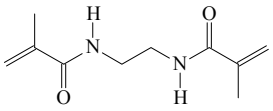

N,N'-ethylene bismethacrylamide

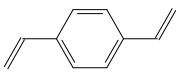

p-divynlbenzene

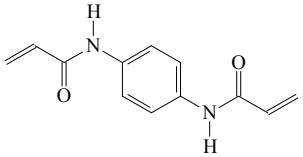

1,4-phenylene diacrylamide

Figure 6-5 A selection of cross-link molecules, used in MIP synthesis

During the MIP synthesis, a solvent is added to bring all the different components for the synthesis into one phase. In addition, the solvent is responsible for the creation of pores in the macro porous cross-linked polymer. In this context, the solvent is quite often referred to as the 'porogen'. The nature and the amount of porogen are used to control the morphology and the total pore volume of the synthesized MIP. Focusing on the non-covalent approach for the synthesis of MIPs (*cf.* section 6.2.4.), the solvent has also an influence on the stability of the pre-polymerization complex, the complex formed by the target molecule and the functional monomer(s). Initiation of the free radical polymerization to synthesize the MIPs, can be done either thermally or photochemically. In Figure 6-6, two typical initiators are depicted.

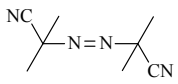

azobisisobutyronitrille

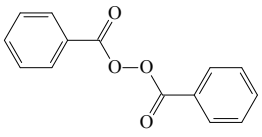

benzoylperoxide

Figure 6-6 Two typical initiator molecules, used in MIP synthesis

6.2.4. Non-covalent approach towards MIPs

Two approaches have been reported for the preparation of MIPs *i.e.* the covalent and the non-covalent approach. However, nowadays, the non-covalent approach is almost exclusively used for MIP synthesis. By using the non-covalent approach, target molecules and functional monomers interact with each other through non-covalent interactions. In an ideal situation, each target molecule should interact with the functional monomer(s) through hydrogen bonds, van der Waals forces, ionic bonds, hydrophobic interactions and/or π-π interactions, leading to a unique pre-polymerization complex with a well-defined stoichiometry. In reality, complexes with different template molecule:functional monomer stoichiometries are formed during the pre-polymerization step, which leads to a variation in the affinities between target molecule and functional monomer(s). As a result, after the removal of the target molecule by breaking the non-covalent interactions, a heterogeneous mixture of binding sites will be present. This together with the different accessibility of binding sites is represented in Figure 6-7.

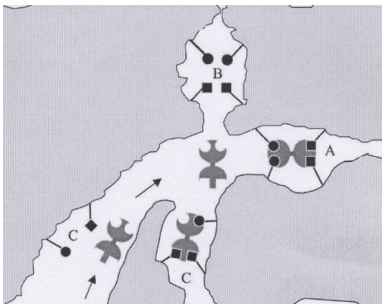

Figure 6-7 Representation of different binding sites present in MIPs (binding site A: high affinity for target molecule and easy accessible; binding site B: high affinity for target molecule but difficult to access; binding sites C: lower affinity for target molecule and easy accessible)[63]

6.3. MIPs for L-nicotine

6.3.1. Synthesis of MIPs for L-nicotine

Nicotine is found in high concentrations in the leaves of the tobacco plant. Two stereo-isomers exist of nicotine, *i.e.* L- and D-nicotine (Figure 6-8), of which L-nicotine is being the naturally occurring stereo-isomer. L-nicotine inhibits the enzyme activity of acetylcholinesterase, which catalyzes the hydrolysis of the neuron-transmitter acetylcholine, and enhances the central nerves system. It has been used as a nerve poison or pesticide. A common source of nicotine is tobacco smoking, since the nicotine adheres to small particles of tar in the smoke. In the body, the nicotine is distributed through the blood and can pass through the blood-brain barrier. After intake, it takes about 7 seconds for nicotine to reach the brain. The most harmful effect of nicotine is addiction. In small quantities, it has a stimulating effect and increases the activity, alertness and memory. It causes an increase of the heart rate and blood pressure and reduces the appetite. High concentrations can produce vomiting and nausea. The LD50 (lethal dosage to kill 50 % of the population) for adult humans is about 50-60 mg, which translates to a concentration of 61.6 μM in the human blood. The concentration of L-nicotine in urine is 0.3 μM for non-smokers and 8.6 μM for cigarette smokers. Sensing of L-nicotine is already been investigated extensively in literature.[64-71] However the current methods require complex operations and are still expensive. In addition, they do not allow for miniaturization, which may be of interest for point of care diagnostics. In the following sections, the first steps towards a fast and straightforward sensing device are presented.

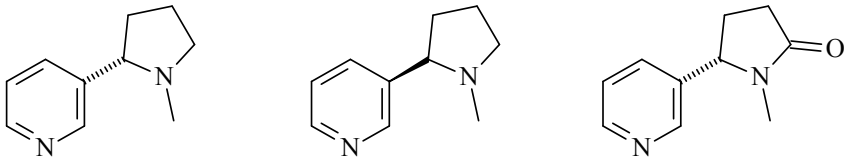

L-nicotine D-nicotine L-cotinine

Figure 6-8 Chemical structure of L-nicotine, D-nicotine and L-cotinine

In the literature, many different methods are found to make MIPs for the target molecule L-nicotine.[72-81] The synthesis, used in this work, is an adapted optimized procedure and is comparable with those found in the literature. The bulk polymerization MIP for L-nicotine is synthesized using methacrylic acid (MAA) as the functional monomer, ethylene glycol dimethacrylate (EGDM) as the cross-linker, azobisisobutyronitrile (AIBN) as the initiator and chloroform as the porogen. The optimized ratio of template molecule:functional monomer:cross-linker is 1:2:4. After dissolving L-nicotine, MAA and EGDM in $CHCl_3$, AIBN is added to the mixture. To exclude oxygen, the mixture is degassed with N_2. Subsequently, the solution is sealed and polymerized, with a UV source (360 nm), at room temperature. After polymerization, the solid MIP is grounded with a mechanical mortar and sieved through a 25 μm sieve. Only particles with a size smaller than 25 μm are used. The last step is the removal of L-nicotine by soxhlet extraction with methanol, followed by a mixture of acetic acid:acetonitrile (1:1) and finally again methanol. In this way, a cross-linked polymer is obtained with cavities, which are complementary in size and shape to the template molecule L-nicotine (Figure 6-9).

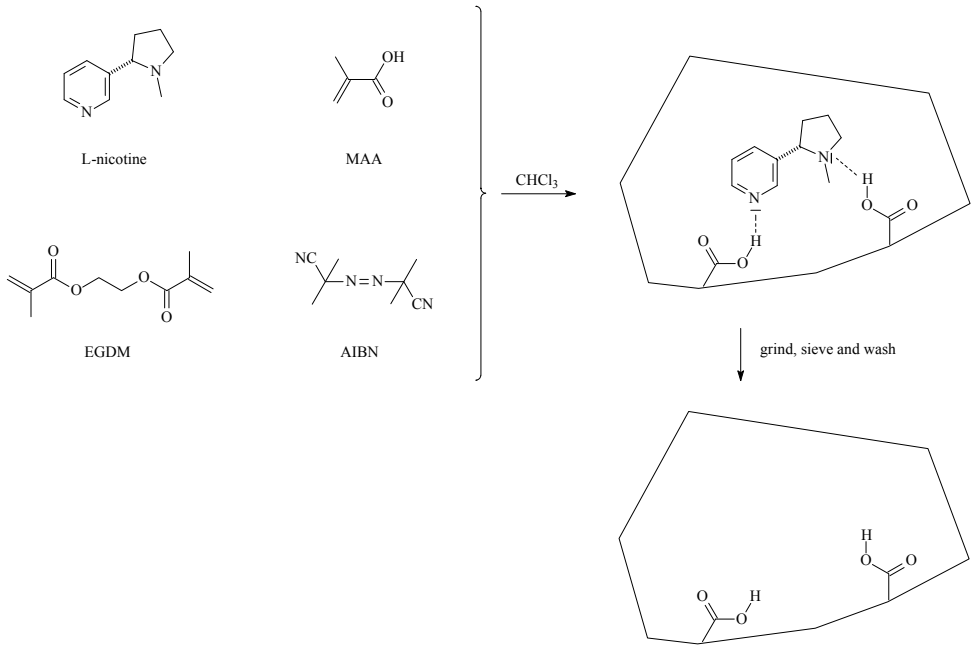

Figure 6-9 Schematic representation of the synthesis of a MIP for L-nicotine

In addition, a non-imprinted polymer (NIP) is synthesized, in the same way as the MIP, but without the presence of the target molecule L-nicotine. This NIP undergoes the same purification steps, after polymerization as the corresponding MIP. In this manner, a reference material is obtained, which can be utilized to verify the working of the actual binding sites in the MIP and to investigate non-specific binding at the surface of the MIP.

6.3.2. Characterization of MIPs for L-nicotine *via* UV-Vis measurements

To assess the quality of the prepared MIPs, the binding constants of the MIPs and corresponding NIPs for L-nicotine have been investigated. To test the specificity of the L-nicotine MIPs, these MIPs have also been exposed to

L-cotinine (Figure 6-8), a byproduct of the human metabolism of L-nicotine. It is very similar to L-nicotine and differs only in one oxygen atom. These batch rebinding experiments are performed using UV-Vis absorption spectroscopy by measuring the L-nicotine optical absorption at 260 nm and the L-cotinine optical absorption at 257 nm.

For the test itself, a fixed amount of MIPs (20 mg) is added to different concentrations of L-nicotine (C_i) in acetonitrile, ranging from 0.2 to 1 mM. After stirring these solutions for one hour at room temperature, the concentration of L-nicotine remaining in solution (C_f) is measured. Subsequently, the concentration of L-nicotine bound to the MIPs (C_b) and the amount of bound L-nicotine molecules per gram MIP (S_b) are calculated. This test is done for the following four systems: MIPs exposed to L-nicotine, NIPs exposed to L-nicotine, MIPs exposed to L-cotinine and NIPs exposed to L-cotinine. Binding isotherms for the four systems are shown in Figure 6-10.

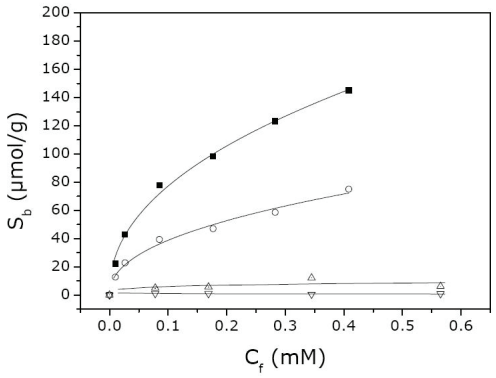

Figure 6-10 Binding isotherms for MIPs exposed to L-nicotine (■) and L-cotinine (Δ) and for NIPs exposed to L-nicotine (○) and L-cotinine (▽)

Due to the specific binding sites in the MIP, the amount of L-nicotine bound to the MIP is higher than to the amount bound to the NIP (Figure 6-10). The amounts of L-cotinine, bound to MIP and NIP, are equal and significantly

lower compared to L-nicotine. It can be assumes that the L-cotinine binding is non-specific.

The binding characteristics of the different binding isotherms can be further analyzed using various models. The simplest model is the Langmuir isotherm.[82] This Langmuir isotherm describes the binding, which takes place at specific homogeneous sites *i.e.* all bindings sites are identical. The Scatchard plot, from this Langmuir isotherm, can be fitted with a straight line according to the following equation.

$$S_b = \frac{NKC_f}{1 + KC_f} \rightarrow \frac{S_b}{C_f} = -KS_b + NK$$

In this equation, N is the total number of binding sites and K is the affinity constant. However, the Scatchard plots of the four different systems do not exhibit a linear relationship between S_b/C_f and S_b (Figure 6-11). This implies a heterogeneous distribution of binding sites, each with different affinities for the added molecule. This is not unexpected in view of the polymerization procedure (*vide supra*).

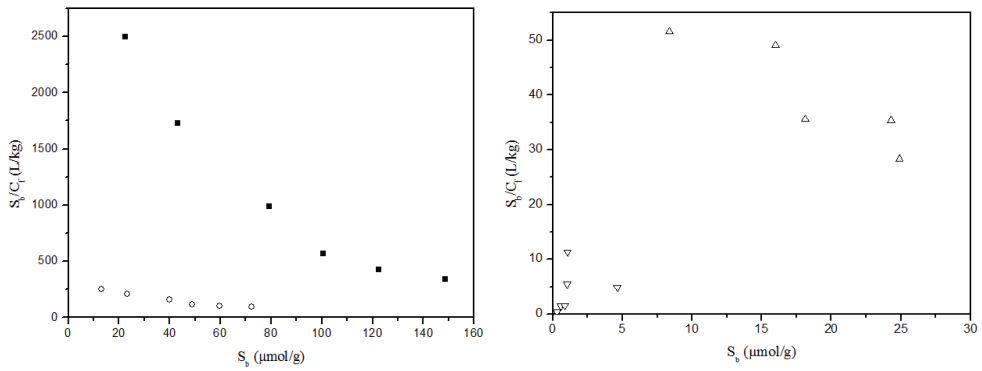

Figure 6-11 The Scatchard plot for MIPs (■) and NIPs (○) exposed to L-nicotine (left) and the Scatchard plot for MIPs (Δ) and NIPs (▽) exposed to L-cotinine (right)

As a result of the different organization of complementary functional groups and different shape-selective cavities, the binding sites in the MIPs have a more heterogeneous character.[83,84] For this type of distribution of binding sites, the binding isotherm can be better studied using, for example, the Freundlich isotherm,[85] according to the following equation.

$$S_b = A \times C_f^{\nu}$$

In this equation, S_b is the amount of bound molecules per gram MIP or NIP, A is the Freundlich constant and ν the Freundlich heterogeneity parameter. ν can vary from 0 to 1. For a homogeneous material ν = 1 and when ν < 1 the material is heterogeneous. The binding isotherms, in Figure 6-10, have been fitted using the Freundlich equation to obtain parameters A and ν, which are listed in Table 6-1, for the four investigated systems.

System	A (µmole/g mM^{ν})	ν
MIP - L-nicotine	217.9	0.45
MIP - L-cotinine	1.6	0.58
NIP - L-nicotine	88.8	0.64
NIP - L-cotinine	0.4	0.68

Table 6-1 Freundlich parameters A and ν for systems MIP - L-nicotine, MIP - L-cotinine, NIP - L-nicotine and NIP - L-cotinine

For the four investigated systems, the value of ν is between 0 and 1 and thus confirms the heterogeneity of the MIPs and NIPS. As expected, the Freundlich constant A has the highest value for the system MIP - L-nicotine, which indicates that the synthesized MIPs have a high affinity for L-nicotine. In addition, the NIP displays some affinity for L-nicotine, but this A value is considerably lower than for the MIP. This is due to non-specific adsorption of L-nicotine on the surface of the polymer material. MIP and NIP do not have affinity for L-cotinine, which results in very low A values.

These parameters, A and ν, can be used to plot the affinity distribution according to the following equation.

$$N(K_i) = A\frac{\sin(\pi\nu)}{\pi}K_i^{-\nu}$$

In this equation, N(K) is the amount of binding sites available for each binding constant K. This affinity distribution is plotted in Figure 6-12, with $K_{min}=1/C_f^{max}$ and $K_{max}=1/C_f^{min}$.

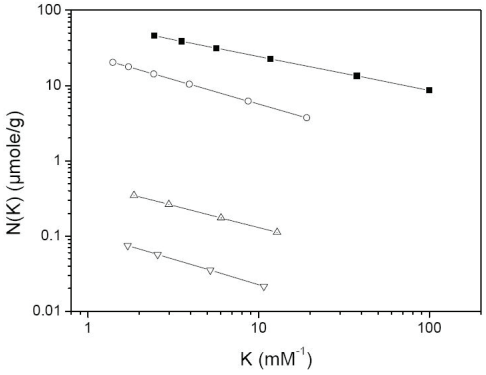

Figure 6-12 The affinity distribution based on the Freundlich model for MIPs exposed to L-nicotine (■) and L-cotinine (Δ) and for NIPs exposed to L-nicotine (○) and L-cotinine (▽)

Using Figure 6-12 and the parameters, A and ν, the total number of binding sites (N_{tot}) for the average binding constant (K_{av}) within the range from 1-100 mM^{-1} can be calculated using the following two equations.[85]

$$N_{tot} = A\frac{\sin(\pi\nu)}{\pi}(K_{min}^{-\nu} - K_{max}^{-\nu})$$

$$K_{av} = \frac{\nu}{1-\nu}\frac{(K_{max}^{1-\nu} - K_{min}^{1-\nu})}{(K_{min}^{-\nu} - K_{max}^{-\nu})}$$

These values are listed in Table 6-2.

System	N_{tot} (µmole/g)	K_{av} (mM^{-1})
MIP - L-nicotine	59.8	10.8
MIP - L-cotinine	0.46	8.7
NIP - L-nicotine	24.3	7.9
NIP - L-cotinine	0.11	7.4

Table 6-2 The total number of binding sites (N_{tot}) for the average binding constant (K_{av}) within the range from 1-100 mM^{-1} for systems MIP - L-nicotine, MIP - L-cotinine, NIP - L-nicotine and NIP - L-cotinine

From Figure 6-12 and Table 6-2, it is obvious that the MIPs have higher affinity for L-nicotine than for L-cotinine. In addition, MIPs have a double amount of binding sites for L-nicotine as compared to the NIPs. These binding sites for L-nicotine in the NIP are a result of non-specific adsorption on the surface of the polymer material.

6.3.3. Sensor built-up and set-up for sensing L-nicotine *via* impedance and QCM measurements

♦ **Sensor built-up for sensing L-nicotine *via* impedance and QCM measurements**

The synthesized MIPs for L-nicotine have been introduced into a biomimetic sensor as the sensing elements. For translating the binding of L-nicotine in the MIPs into a physical, measurable signal, MDMO-PPV is chosen. The actual read-out is electrochemically obtained using impedance measurements and gravimetrically or piezoelectric using a quartz crystal microbalance (QCM).

The electrochemical read-out is based on the interaction between the sensing element and the analyte, which will cause a change in the dielectric properties at the interface, resulting in an impedance change at the interface.[7,8] A piezoelectric read-out is obtained by using QCM. A specifically cut, thin disc of quartz crystal is covered with electrodes. By placing the QCM crystal into an electrical circuit and oscillating the current at a similar frequency to the fundamental mechanical oscillation frequency of the crystal, a resonant oscillation is achieved. This resonant oscillatory frequency is dependent on the chemical structure, density and thickness of the crystal and similar physical properties of the surrounding medium. As a result, this frequency is directly related to the amount or mass of material immobilized onto the surface of the crystal. An interaction between the sensing element and the analyte will result in a change in the oscillation frequency. This change can be related to the mass of the analyte, interacting with the recognition elements.[86-88]

For both read-out methods, impedance and QCM, immobilization of the MIPs, has not been performed directly onto the electrodes, which are present on a glass substrate for impedance measurements or on a quartz substrate for QCM measurements. Direct immobilization would not have provided sufficient adherence. Instead, a transducer layer, consisting of MDMO-PPV, is placed between the electrodes and the MIPs. In this way, immobilization of the MIPs is readily achieved using matrix entrapment.[38] In this method, receptor elements are trapped (partially) inside a polymer layer. Although this can cause barriers to the diffusion of analytes and part of the sensing elements may not be accessible, matrix entrapment remains one of the most straightforward procedures to execute. Hence, as a proof of principle, a modified version of this method has been used to immobilize MIPs onto an MDMO-PPV surface. In addition, special care has been taken to eliminate some of the above mentioned disadvantages. To this end, a polydimethylsiloxane (PDMS) stamp is covered with MIP particles and pressed onto the MDMO-PPV surface during a few seconds. By heating the sample for 10 minutes to 110 °C, which is above the T_g of MDMO-PPV, the MIP particles will partially sink into the MDMO-PPV layer. Cooling down the sample leads to the adherence of the MIPs to the MDMO-PPV surface. After washing away the excess of non-adherent MIPs, the surface coverage

is investigated with optical and scanning electron microscopy (SEM). A total coverage of around 30 % has been observed. The average size of the clusters of the MIP particles ranges from 49.3 μm^2, found by optical microscopy, to 0.047 μm^2, found by SEM. The results show the successfully immobilization of the MIP particles on top of the electrodes, using MDMO-PPV as a semi conductive adhesive layer. However, it should be noted that further improvements to the distribution and uniformity of the MIP particles are certainly desirable, to create a more reproducible surface coverage.

♦ Sensor set-up for sensing L-nicotine

The sensor set-up for sensing L-nicotine *via* impedance measurements is depicted in Figure 6-13. On top of the glass substrates, Pt electrodes are deposited. In the next step, a layer of 200 nm of MDMO-PPV is spin-coated from chlorobenzene. Subsequently, MIPs or NIPs are immobilized in the MDMO-PPV film with the PDMS stamp method. This results in the configuration depicted in Figure 6-13 (left), which contains four sensing sites. The four sensing sites allow for the simultaneous monitoring of a bare Pt electrode, a Pt electrode covered with MDMO-PPV, a Pt electrode covered with an MDMO-PPV-MIP layer and a Pt electrode covered with an MDMO-PPV-NIP layer. Subsequently, this electrode configuration can be positioned onto a sensor chip, after which the contacts are connected to the pads of the chip, using wire-bonding. This chip can be plugged into a slot which is connected to the impedance analyzer. Finally, the measurement cell is closed, which leads to an addition setup as depicted in Figure 6-13 (right). The addition setup allows addition of the analyte by adding a few droplets in the buffer solution to reduce artifacts from replacing the buffer during the measurement.

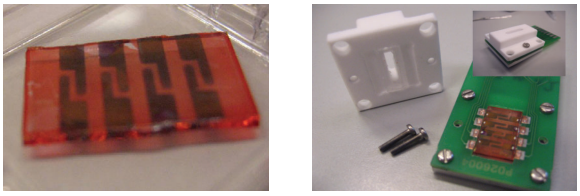

Figure 6-13 Sensor set-up for sensing L-nicotine *via* impedance measurements (left: sensing device with four sensing sites Pt/Pt MDMO-PPV/Pt MDMO-PPV-MIP/Pt MDMO-PPV-NIP; right: addition set-up)

The sensor set-up for sensing L-nicotine *via* QCM measurements is depicted in Figure 6-14. QCM crystals, covered with Au as electrode material, with a resonant frequency of 5 MHz are used. MIPs/NIPs are immobilized in the same way on the Au electrodes as was done for the impedance measurements (Figure 6-14 left). Using this technique, MIP and NIP cannot be measured on one substrate, since each sample contains only one electrode. As a result, MIPs and NIPs have been measured on two different QCM crystals. Finally, the crystal is put in a flow cell (Figure 6-14 right).

Figure 6-14 Sensor set-up for sensing L-nicotine *via* QCM measurements (left: QCM crystal with MDMO-PPV-MIP or NIP; right: flow cell set-up)

6.3.4. Sensing of L-nicotine *via* impedance and QCM measurements

♦ Sensing of L-nicotine *via* impedance measurements

The actual sensing measurements are performed in phosphate buffered saline (PBS) solution. PBS is used to mimic the ionic strength of body liquids and to maintain a constant pH. This is important since L-nicotine is known to have different protonations, depending on the acidity of the solution.[89] To investigate the binding of L-nicotine and L-cotinine (Figure 6-8), the real part of the impedance is tracked in time at the lower frequency regime (213 Hz). At this regime, the signal represents events that take place at the interface between the electrolyte and the sensor surface. Binding of L-nicotine and L-cotinine effects the formation of the double layer at the electrode surface, which is reflected in the capacitive changes in the lower frequency regime. In addition, it influences the charge transfer from the electrolyte to the Pt electrode. In Figure 6-15, the dose-response curves of the four sensing sites of the sensor device are shown, after addition of L-nicotine and L-cotinine to the PBS solution. The impedance change is measured 20 minutes after each addition of L-nicotine and L-cotinine.

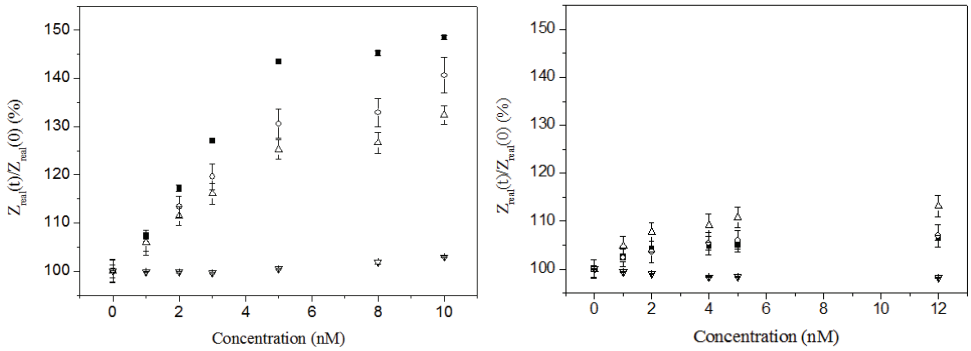

Figure 6-15 Impedance change of Pt (▽)/Pt MDMO-PPV (○)/Pt MDMO-PPV-MIP (■)/Pt MDMO-PPV-NIP (Δ) sensing sites upon addition of L-nicotine (left) and L-cotinine (right) in PBS in an addition set-up

The signal of the MIP coated electrode shows an increase of 45 % when 10 nM of L-nicotine is introduced. At the same time, the signal of the NIP coated electrode only increases with 30 %. The change of the MDMO-PPV coated electrode is in the same order of magnitude as the NIP. Also, the MDMO-PPV and NIP coated electrodes react upon addition of L-nicotine, which is probably due to (non-specific) adsorption at the interface. In the case of the NIP, this adsorption may involve the free acid groups of the monomer MAA, whereas in the case of MDMO-PPV this may be the result of π-π interactions between L-nicotine and the PPV backbone. Subsequently, the influence of L-cotinine is investigated in the same way as was done for L-nicotine. A signal increase is observed due to adsorption of L-cotinine for MDMO-PPV, MIP and NIP coated electrodes. All responses are in the same order of magnitude and markedly lower in comparison to the response observed upon the addition of L-nicotine. It can be expected that this adsorption has a similar origin as for the non-specific adsorption of L-nicotine. To eliminate the contribution of the non-specific adsorption of L-nicotine (and L-cotinine) to the surface of the MIP, the normalized impedance signal of the NIP has been subtracted from the normalized MIP signal (Figure 6-16).

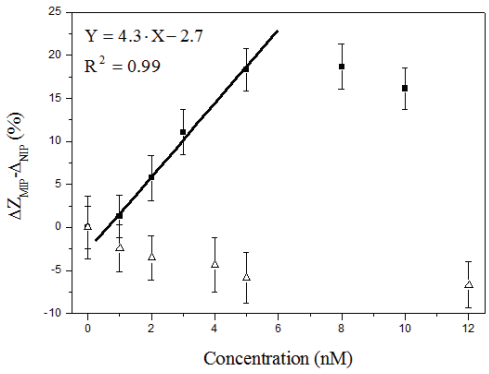

Figure 6-16 Specific impedance change upon addition of L-nicotine (■) and L-cotinine (Δ) in an addition set-up

From Figure 6-16, a clear difference between the binding reaction of the sensor to L-nicotine and L-cotinine is observed. A linear response is found from 2 to 5 nM, with a response of 4.3 % increase of the differential signal per nM. For concentrations above 5 nM, the impedance change is similar for MIP and NIP, due to full occupation of the specific binding places in the MIP. Therefore, MIP and NIP reacts in a comparable way.

♦ Sensing of L-nicotine *via* QCM measurements

In addition to the impedimetric measurements, the sensing properties of the MIPs and NIPs for L-nicotine have been investigated *via* QCM measurements. To this end, preliminary studies are done with the flow cell set-up, depicted in Figure 6-14. These measurements are performed in distilled water and not in PBS solution as for the impedance measurements. In Figure 6-17, a MIP and NIP coated QCM crystal is exposed to an increasing concentration of L-nicotine. After rinsing, the MIP coated QCM crystal is again exposed to an increasing concentration of L-cotinine. The concentrations used are ranging from 50 µM to 300 µM. The change in resonance frequency of the crystal can be correlated with the mass deposited on the crystal, following the Sauerbrey equation.[90]

$$\Delta f = -\frac{2f_0^2}{A\sqrt{\rho_q \mu_q}}\Delta m$$

In this equation, f_0 is the resonant frequency of the crystal (Hz), Δf is the frequency change (Hz), Δm is the mass change (g), A is the piezo-electrically active crystal area (m^2), ρ_q is the density of quartz (2.648 g/cm^3) and μ_q is the shear modulus of a quartz AT-cut crystal (2.947 x 10^{11} g/cm s^2).

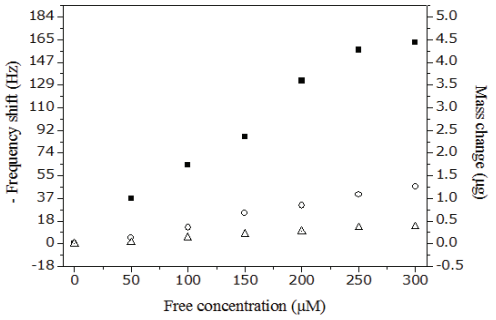

Figure 6-17 Frequency change and corresponding mass change of a MIP and NIP coated QCM crystal exposed to an increasing concentration of L-nicotine and L-cotinine in distilled water flowing at 0.05 mL/min [MIP exposed to L-nicotine (■) and L-cotinine (Δ) and NIP exposed to L-nicotine (○)]

As can be seen in Figure 6-17, the MIP coated QCM crystal binds the largest amount of L-nicotine, which passes through the flow cell set-up. In addition, a response is found for both the NIP with L-nicotine and the MIP with L-cotinine. This response is probably due to non-specific adsorption. Both signals are much lower than those observed for the MIP with L-nicotine, which is in agreement with the observations made using impedance measurements.

6.3.5. Possible improvements for combination of MIPs with PPV derivatives

Despite the good results obtained *via* impedance and QCM measurements, the reproducibility of both sensor types is still not optimal. Although the stamping method is a straightforward technique for immobilizing MIPs onto the sensor surface, the surface coverage and reproducibility of this method remains rather low. A possible solution is trying to grow MIPs directly on top of the transducer layer. This requires the presence of radical initiator groups, directly attached to the conjugated polymer film covering the

electrodes. Since the synthesis of MIPs is a radical polymerization reaction, this initiator group can start such a reaction. In this way the formed structure can be covalently attached to the PPV film. As a result, one can anticipate that the electrodes will be fully covered, which would increase the sensitivity and reproducibility of the sensor considerably. Some preliminary tests to start a polymerization from a PPV covered surface have been described in the previous chapter. It has been shown that vinyl monomers, such as MMA, MAA, MA and styrene can be polymerized on top of a PPV derivative with a dithiocarbamate initiator group under influence of UV light. Although no MIP structures have yet been synthesized in this manner, obviously one of the next steps in the development of a better impedance or QCM sensor is to replace these vinyl monomers with a solution consisting of target molecule, functional monomer(s) and cross-linkers to create a novel efficient sensing architecture.

6.4. Towards post-polymerization functionalization of PPV derivatives with ssDNA

Although as outlined above, synthetic receptors have numerous advantages, interest exist also in the development of conjugated polymer based sensors with natural receptors. Other possible receptors for the use in biosensors are, for example, natural receptors, such as single-stranded DNA (ssDNA). This probe ssDNA is able to specifically recognize target complementary ssDNA. By choosing for the transducer layer also a PPV derivative, the resulting PPV modified ssDNA sample can be implemented in an impedance or QCM sensor set-up in a similar fashion as was done for the MIPs. Subsequently, it should be possible to measure the hybridization of target complementary ssDNA in a straightforward manner. In this section, a series of preliminary tests are presented towards the covalent linking of azido functionalized ssDNA with copolymer **23**, bearing a propargyl group, *via* "click" chemistry (*cf.* section 4.3.2.).

6.4.1. Strategy for post-polymerization of PPV derivatives with ssDNA

In literature, several procedures can be found to attach DNA to glass,[91-98] silicon wafers[99-102] and gold surfaces.[96,103-110] In addition, due to their low cost and versatile chemical, physical and surface properties, metal and polymer surfaces can be used.[111-123] Some important strategies to prepare functional polymer surfaces for quantitative DNA immobilization are surface-initiated ATRP of functional polymer brushes,[116,124] pulsed-plasma polymerization of amino-derivatized polymers,[125] and poly(L-lysine)-*graft*-poly(ethylene glycol) coated onto glass.[126] Recently, the chemoselective "click" chemistry has been applied for the construction of DNA probe surfaces.[123,127-130] This chemistry method is rapid, highly selective and can be performed in aqueous environment. Hence, it is the method of choice to attach ssDNA to conjugated polymers.

To verify the "click" reaction between the surface of copolymer **23** and ssDNA, fluorescence spectroscopy is a powerful tool. This is a result of the fact that ssDNA with a wide variety of dyes with specific fluorescence excitation/emission wavelengths is commercially available. An appropriate dye should be selected based on the fluorescence spectrum of PPV derivatives to exclude, as much as possible, the interference between the dye and the PPV derivative. To this end, a dye with a maximum fluorescence wavelength above 600 nm should be best suitable. Cy^{TM} 5.5 can be excited at a wavelength of 683 nm and the resulting emission is observed in the 700 to 760 nm wavelength range. Excitation of copolymer **23** at a wavelength of 683 nm will not give rise to any emission of the PPV derivative (Figure 6-18). Hence, the dye Cy^{TM} 5.5 has been selected for the study of the "click" reaction between copolymer **23** and ssDNA.

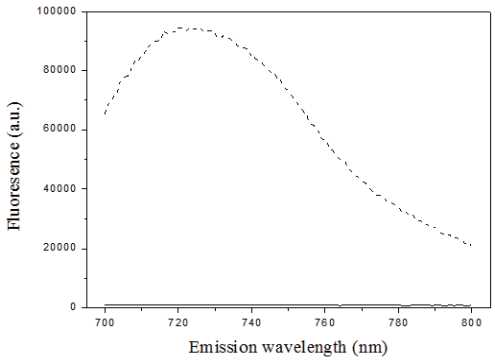

Figure 6-18 Fluorescence emission spectrum of a copolymer **23** spin-coated surface (solid) and a copolymer **23** spin-coated surface with a layer of drop casted Cy™ 5.5 (dashed) at an excitation wavelength of 683 nm

After selection of the dye, the conditions of the "click" reaction should be optimized with azide modified Cy™ 5.5. Subsequently, after positive results, the same conditions can be transferred to the azido functionalized ssDNA, bearing Cy™ 5.5. This is important since optimization of the "click" conditions with the latter would be complex and rather costly. This section focuses on the experiments with Cy™ 5.5. Experiments with ssDNA, bearing Cy™ 5.5 are planned in the near future.

6.4.2. Post-polymerization functionalization of copolymer 23 with azide modified Cy™ 5.5 *via* "click" chemistry

The choice for the active components in the "click" reaction is based on a procedure, found in literature, for "clicking" DNA to non-conjugated polymers.[123] In Figure 6-19, all the components are presented. Sodium ascorbate is needed to prevent oxidation of copper (I) to copper (II), an inactive component in the "click" reaction. However, the use of copper salts with sodium ascorbate is problematic in bio-applications. A solution can be

the use of TBTA, which has been shown to effectively enhance the "click" reaction, without damaging biological scaffolds.[131]

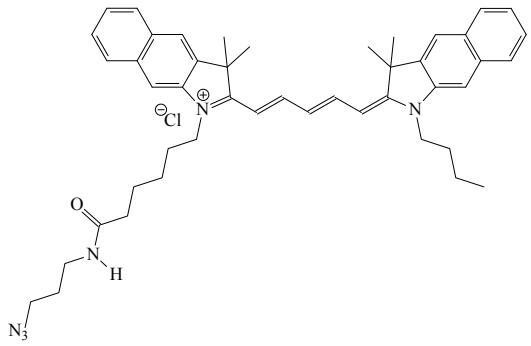

Cy 5.5 azide

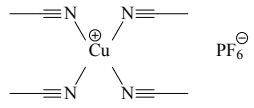

tetrakis-(acetonitrile) copper(I) hexafluorophosphate

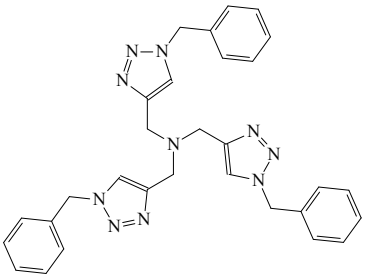

TBTA

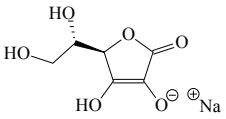

sodium ascorbate

Figure 6-20 Chemical structure of azide modified Cy™ 5.5, *tetrakis*-(acetonitrile) copper (I) hexafluorophosphate, *tris*-(benzyltriazolylmethyl) amine (TBTA) and sodium ascorbate

To perform the "click" reaction, a layer of around 100 nm of copolymer **23** is spin-coated from chlorobenzene. Subsequently, a buffer solution of azide modified Cy™ 5.5, *tetrakis*-(acetonitrile) copper (I) hexafluorophosphate, TBTA and sodium ascorbate in DMSO/H_2O is spotted on top of copolymer **23** (Scheme 6-1). It should be noted that this solution needs to be fresh in order to obtain reproducible results. Subsequently, the sample is placed overnight in a closed chamber. In this way, the concentration of all the components remains constant. As a control, the same treatment has been

done with a film of copolymer **7**, which does not contain any propargyl groups. In addition, a spot, containing only the azide modified Cy^{TM} 5.5 without all the reagents needed for the "click" reaction, is put on top of a copolymer **23** spin-coated surface. Obviously, in both cases no "click" reaction should be observed.

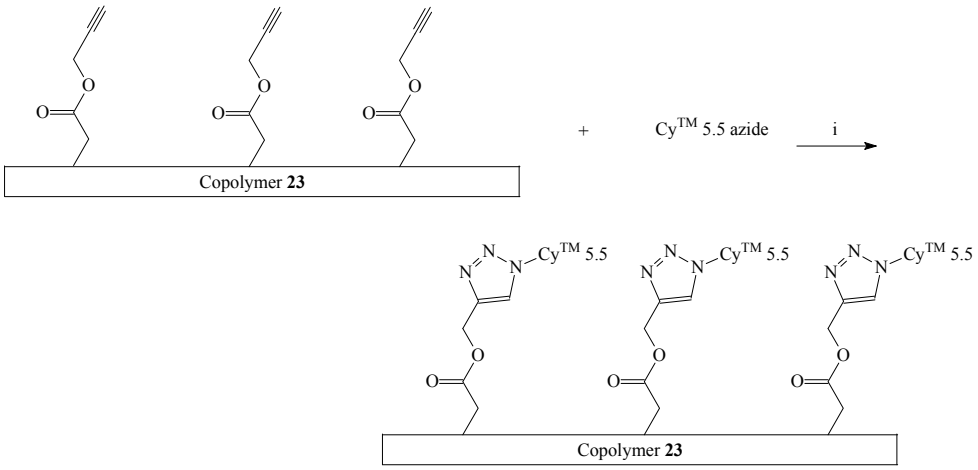

Scheme 6-1 Post-polymerization functionalization of a copolymer **23** surface with azide modified Cy^{TM} 5.5 via "click" chemistry (i: *tetrakis*-(acetonitrile) copper(I) hexafluorophosphate, TBTA, sodium ascorbate, DMSO, H_2O)

After reaction, the sample is washed extensively with DMSO to remove the excess of azide modified Cy^{TM} 5.5, together with all the remaining reagents needed for the "click" reaction. After each washing step, the solution is checked for the presence of residual "dye". It can be assumed that in case there is no "dye" found in the washing solution, the remaining "dye" present on the sample should be covalently "clicked" to the PPV derivative. The presence of the "dye" can directly be checked using fluorescence spectroscopy. The results of the fluorescence measurements on copolymer **7** and **23** are depicted in Figure 6-20.

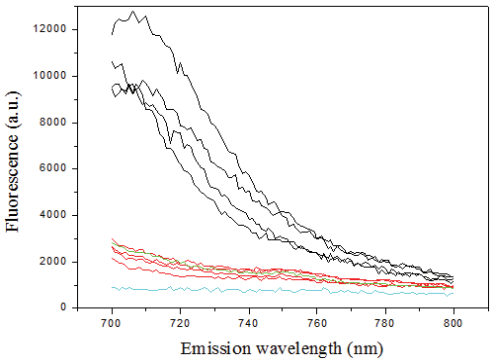

Figure 6-20 Fluorescence emission spectra of copolymer **23** after the "click" reaction (black). As controls also the results are shown for copolymer **23** after exposing to the azide modified Cy™ 5.5 (in the absence of the "click" reagents) (green), for copolymer **7** (red) under "click" conditions and for a copolymer **23** spin-coated surface without any dye as a reference (cyan)

From Figure 6-20, it can be concluded that, as expected, azide modified Cy™ 5.5 gives virtually no reaction with a surface of copolymer **7** under the "click" conditions. In addition, the experiment with copolymer **23** and only azide modified Cy™ 5.5, without the "click" reagents, gives also only a similar minimal fluorescence signal. Comparing both control experiments with a copolymer **23** spin-coated surface, the signal is only somewhat higher, which can be explained by the presence of some non-specific adsorption of the "dye". Apparently, the "dye" cannot be fully washed away under the utilized washing procedures. Notwithstanding, the fluorescence signal of the sample with copolymer **23** is five to six times higher compared to the control experiments and is characteristic for Cy™ 5.5. This demonstrates that Cy™ 5.5 is present on copolymer **23** and cannot be washed away. Hence, it can be concluded that Cy™ 5.5 has to be covalently "clicked" to the copolymer **23** surface. Figure 6-20 demonstrates also the reproducibility of these "click" conditions. After these successful test reactions, the next step in the post-polymerization functionalization of PPV derivatives with ssDNA is to replace the "dye" by azido functionalized

ssDNA, bearing Cy 5.5. These experiments are currently in progress. After a positive outcome of these tests, such a sample can be implemented in impedance or QCM based sensor set-ups after which the hybridization of the target ssDNA should become detectable.

6.5. Conclusions

MIPs, which are polymer based synthetic receptors, have been synthesized for L-nicotine. They have been characterized *via* UV-Vis absorption spectroscopy and the binding properties have been investigated using the Freundlich model. This model indicates the presence of specific recognition sites for L-nicotine and insensitivity of these MIPs towards L-cotinine. The values of the binding parameters are comparable to literature values.[72-81] The actual sensing of L-nicotine has been investigated *via* impedance and QCM measurements. To this end, a good immobilization of the MIPs to the transducer layer, MDMO-PPV, is needed. This has been achieved using a PDMS stamping method. Using this method, about 30 % of the surface is covered with MIPs. Using impedimetric sensing, the synthesized MIPs can be utilized for the specific recognition of L-nicotine. However, it should be noted that a significant amount of non-specific adsorption occurs at both the MDMO-PPV and the NIP. Notwithstanding, impedimetric sensing is able to detect L-nicotine concentrations as low as 10 nM with a response increase of 45 % at a frequency of 213 Hz. This concentration is well below relevant medical concentrations. The reference measurement with L-cotinine indicates a high specificity, *i.e.* no significant sensor response is observed. Similar results and conclusions have been obtained *via* the microgravimetric method. The QCM shows a specific detection of L-nicotine with a detection limit of 50 μM. The QCM MIP sensor also does not significantly react to the addition of L-cotinine. It should be remarked that both sensors can be regenerated by flushing with distilled water.

Other possible receptors for the use in biosensors are natural receptors such as ssDNA. This probe ssDNA can specifically recognize corresponding

target ssDNA. Some preliminary tests have been performed to develop a procedure towards the covalent linking of azido functionalized ssDNA with copolymer **23** *via* "click" chemistry. To this end, it has been demonstrated that it is possible to use "click" conditions to attach an azide modified Cy^{TM} 5.5 dye to a PPV derivative. The transfer of these "click" conditions towards azido functionalized ssDNA, bearing Cy^{TM} 5.5, will be the next step in the post-polymerization functionalization of PPV derivatives with ssDNA, which will ultimately lead to conjugated polymer based ssDNA sensors.

6.6. Experimental section

6.6.1. Chemical and optical characterization, chemicals and materials

UV-Vis measurements were performed on a Cary 500 UV-Vis-NIR spectrophotometer (scan rate 600 nm/min, continuous run from 200 to 800 nm). Unless stated otherwise, all reagents and chemicals were obtained from commercial sources and used without further purification. The stabilizers in MAA and EGDM were removed by filtering over Al_2O_3. Piezo-electric crystals were purchased from Maxtek, Inc., Cypress, USA. They were AT-cut, one-inch diameter crystals, covered with Au, commonly available for liquid work with a resonant frequency of 5 MHz. They were optimized for temperatures around 25 °C, ensuring a minimal influence of temperature on the resonance frequency. The sensitivity factor of the crystal was 0.056 Hz/ng/cm² at 20 °C.

6.6.2. Synthesis

MIP. L-nicotine (1.04 g, 6.41 mmol), MAA (1.07 g, 12.5 mmol), EGDM (5.00 g, 25.2 mmol) and AIBN (0.11 g, 0.66 mmol) were dissolved in 7 mL

$CHCl_3$ in a glass polymerization tube, permeable for UV light. The solution was degassed with N_2 for 10 min and then sealed. Subsequently, the tube was irradiated for 24 h using a UV lamp (360 nm), at room temperature. Following polymerization, the solid MIP was grounded with a mechanical mortar for 24 h and sieved through a 25 μm sieve. Only particles with a size, smaller than 25 μm, were used. This fraction was washed by soxhlet extraction with methanol (48 h), followed by a mixture of acetic acid:acetonitrile (1:1) (48 h) and finally again methanol (48 h).

NIP. The NIP was synthesized in the same way as the **MIP**, but without the presence of L-nicotine. The NIP undergoes also the same purification steps after polymerization.

Copolymer 23 surface with Cy™ 5.5. 50 μL of an 1/1/1/1 *tetrakis*-(acetonitrile) copper(I) hexafluorophosphate/TBTA/sodium ascorbate/azide modified Cy™ 5.5 buffer (15 μL of a 2 mM *tetrakis*-(acetonitrile) copper(I) hexafluorophosphate solution in DMSO, 15 μL of a 2 mM TBTA solution in DMSO, 15 μL of a 2.6 mM sodium ascorbate solution in H_2O, 2.25 μL of a 10 mM azide modified Cy™ 5.5. solution in DMSO and 12.75 μL DMSO) was spotted on the surface of a thin layer of copolymer **23**. The sample was placed overnight in a closed chamber. In a next step, the sample was washed extensively with DMSO to remove the excess of "dye", together with all the other "click" reagents, until no "dye" was found anymore in the washing solution. For this washing procedure, the sample was first three times rinsed with 3 mL DMSO. Next, the sample was placed for one hour in 10 mL DMSO. Finally, the sample was placed again in 10 mL fresh DMSO for four hours. This step was repeated two times. This washing procedure includes thus a seven step washing method. In the last washing step, no "dye" was found anymore in the washing solution. The amount of "dye", which was washed away each time, is depicted in Figure 6-21. In the first step, almost all the excess of "dye" was washed away. In the last washing step, no more "dye" was found anymore in the DMSO washing solution and is therefore not present in Figure 6-21.

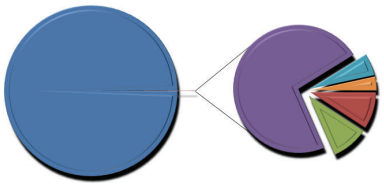

Figure 6-21 Schematic representation of the amount of washed azide modified Cy™ 5.5 for each consecutive washing step (washing step 1, 2, 3, 4, 5, 6 and 7)

Copolymer 7 surface control. Copolymer 7 surface control was prepared following the same procedure described for the **Copolymer 23 surface with Cy™ 5.5** using a thin layer of copolymer **7**.

Copolymer 23 surface control. 50 µL of a solution (15 µL DMSO, 15 µL DMSO, 15 µL H_2O, 2.25 µL of a 10 mM azide modified Cy 5.5. solution in DMSO and 12.75 µL DMSO) was spotted on a thin layer of copolymer **23**. The sample was placed in a closed chamber for 20 h. In a next step, the sample was washed under the same conditions as described for **Copolymer 23 surface with Cy™ 5.5**.

6.6.3. Device preparation and measurement

All sensor samples for impedance and QCM measurements were prepared in a glovebox. The substrates, glass for impedance measurements and piezo-electric crystals for QCM measurements, were successively cleaned for 10 minutes in a soap solution, demineralized water and acetone, in an ultrasonic bath. Subsequently, the substrates were cleaned in boiling isopropanol for 10 minutes. Afterwards the samples were dried with an N_2 gun. For impedance measurements, Pt electrodes of about 70 nm were deposited on the glass substrate, either by evaporation or sputtering using a mask or by etching techniques. For QCM measurements, the piezo-electric crystals were already covered with Au as electrode material. On both

electrodes MDMO-PPV was spin-coated from chlorobenzene (7 mg/mL). The thickness of the polymer layer was controlled by the speed and the duration. In this way layers of 150 to 200 nm were obtained. Subsequently, MIPs or NIPs were immobilized onto the conjugated transducer film. Finally, the sample was mounted in a sensor chip and the contacts were connected to the pads of the chip using wire-bonding.

For the impedance measurements, an 'IVIUMstat electrochemical interface' from Ivium Technologies, the Netherlands, was used. This apparatus was capable of measuring in a frequency range of 10 μHz to 1 MHz with impedance values of 1 Ω to 100 GΩ. The electrochemical impedance measurements were done using homemade electrochemical impedance cells. The different channels were measured subsequently using a multiplexer. The data collection protocol consisted of measuring both Z and the phase shift as function of frequency. This was by done time resolved monitoring. These parameters were fixed at a frequency in the lower range (100 Hz - 1 kHz) upon addition of a certain concentration of target molecules. Data collection software was a self-developed Labview program (National Instruments). After stabilization, the entire spectrum was used to fit according to an equivalent electrical circuit. ZSimpWIN from Princeton Applied Research, USA, was used to fit the data.

For the QCM measurements, a Maxtek PLO-10i phase lock oscillator was used from Inficon, USA. For the phase lock oscillator (PLO), the resonance frequency was found by the hardware. The PLO utilized an internal oscillator to drive the crystal. The crystal current was then monitored and the frequency of the oscillator adjusted until there was zero phase between the crystal voltage and the current. The flow cell was connected to a gradient pump. The volume inside the flow cell was approximately 100 μl.

The substrates for the "click" tests with azide modified Cy^{TM} 5.5 were successively cleaned in a soap solution, demineralized water and acetone, each for 10 minutes in an ultrasonic bath. This was followed by cleaning in boiling isopropanol for 10 minutes. Afterwards the samples were dried with an N_2 gun. Next, the clean glass substrates were silanized by placing in chloromethylsilane at 50 °C for 10 minutes. After washing in ethanol, the

substrates were dried at room temperature under reduced pressure. A 100 nm thick layer of copolymer **7** or **23** was spin-coated on the silanized glass substrates (90 seconds at 2500 RPM). The PPV derivatives were spin-coated from chlorobenzene (8 mg/mL). The fluorescence measurements were performed using a 'Fluorolog® Tau-3 Lifetime System' spectrofluorometer from Horiba Group, USA. The entire system was controlled by DataMax software. The excitation wavelength was kept at 683 nm and the emission was scanned between 700 and 800 nm. The sample was placed at an angle of 22.5°, resulting in the highest fluorescence signal with a minimum of scattering and reflection coming from the glass. The slits of both monochromators were adjusted to 5 nm.

6.7. References

[1] Maines, A. *Analytical Communications* **1996**, *33*, 27.
[2] Marquette, C. A.; Blum, L. J. *Analytical and Bioanalytical Chemistry* **2008**, *390*, 155.
[3] Prodromidis, M. I.; Karayannis, M. I. *Electroanalysis* **2002**, *14*, 241.
[4] Wang, J. *Electroanalysis* **2001**, *13*, 983.
[5] Bonroy, K. *Journal of Immunological Methods* **2006**, *312*, 167.
[6] Frederix, F. *Langmuir* **2003**, *19*, 4351.
[7] Cooreman, P. *Biosensors and Bioelectronics* **2005**, *20*, 2151.
[8] Vermeeren, V. *Langmuir* **2007**, *23*, 13193.
[9] Wenmackers, S. *Functionally Graded Materials VIII* **2005**, *492*, 267.
[10] Schöning, M. J.; Poghossian, A. *Electroanalysis* **2006**, *18*, 1893.
[11] Piletsky, S. A.; Alcock, S.; Turner, A. P. F. *Trends in Biotechnology* **2001**, *19*, 9.
[12] Piletsky, S. A. *Biosensors & Bioelectronics* **2001**, *16*, 701.
[13] Piletsky, S. A. *Analytical Letters* **1996**, *29*, 157.
[14] Thoelen, R. *Biosensors & Bioelectronics* **2008**, *23*, 913.
[15] Ansell, R. J.; Ramstrøm, O.; Mosbach, K. *Clinical Chemistry* **1996**, *42*, 1506.
[16] Cormack, P. A. G.; Mosbach, K. *Reactive & Functional Polymers* **1999**, *41*, 115.
[17] Haupt, K.; Mosbach, K. *Trends in Biotechnology* **1998**, *16*, 468.
[18] Mosbach, K. *Abstracts of Papers of the American Chemical Society* **1994**, *207*, 149.
[19] Marx, K. A. *Biomacromolecules* **2003**, *4*, 1099.
[20] Emr, S. A.; Yacynych, A. M. *Electroanalysis* **1995**, *7*, 913.
[21] Van Severen, I. *Abstracts of Papers of the American Chemical Society* **2006**, *231*, 478.
[22] Frederix, F. *Analytical Chemistry* **2003**, *75*, 6894.
[23] Berggren, C.; Bjarnason, B.; Johansson, G. *Electroanalysis* **2001**, *13*, 173.
[24] Chaki, N. K.; Vijayamohanan K. *Biosensors & Bioelectronics* **2002**, *17*, 1.

[25] Gao, Z. Q. *Analytical Chemistry* **2007**, *79*, 3291.
[26] Letant, S. E. *Sensors and Actuators B-Chemical* **2000**, *69*, 193.
[27] Prieto, F. *Nanotechnology* **2003**, *14*, 907.
[28] Libertino, S. *Applied Surface Science* **2007**, *253*, 9116.
[29] Wang, J.; Carlisle, J. A. *Diamond and Related Materials* **2006**, *15*, 279.
[30] Garrido, J. A. *Applied Physics Letters* **2005**, *86*.
[31] Hartl, A. *Nature Materials* **2004**, *3*, 736.
[32] Christiaens, P. *Biosensors & Bioelectronics* **2006**, *22*, 170.
[33] Wenmackers, S. *Physica Status Solidi a-Applied Research* **2003**, *199*, 44.
[34] Marrazza, G.; Chianella, I.; Mascini, M. *Analytica Chimica Acta* **1999**, *387*, 297.
[35] Marrazza, G.; Chianella, I.; Mascini, M. *Biosensors & Bioelectronics* **1999**, *14*, 43.
[36] Hrapovic, S. *Analytical Chemistry* **2004**, *76*, 1083.
[37] Millan, K. M.; Saraullo, A.; Mikkelsen, S. R. *Analytical Chemistry* **1994**, *66*, 2943.
[38] Eggins, B. *Biosensors An Introduction* **1996**, West Sussex.
[39] Pauling, L.; Campbell, D. *J. Exper. Med.* **1942**, *76*, 211.
[40] Dickey, F. H. *J. Phys. Chem.* **1955**, *59*, 695.
[41] Wulff, G.; Sarhan, A.; Zabrocki, K. *Tetrahedron Lett.* **1973**, *44*, 4329.
[42] Andersson, L.; Sellergren, G.; Mosbach, K. *Tetrahedron Lett.* **1984**, *25*, 5211.
[43] Sellergren, B. *Journal of Chromatography A* **2001**, *906*, 227.
[44] Kempe, M. *Analytical Chemistry* **1996**, *68*, 1948.
[45] Yin, J. F.; Yang, G. L.; Chen, Y. *Journal of Chromatography A* **2005**, *1090*, 68.
[46] Wulff, G. *Chemical Reviews* **2002**, *102*, 1.
[47] Strikovsky, A.; Hradil, J.; Wulff, G. *Reactive & Functional Polymers* **2003**, *54*, 49.
[48] Yamazaki, T. *Analytica Chimica Acta* **2001**, *435*, 209.
[49] Blackwell, A.; Minteer, S. D. *Abstracts of Papers of the American Chemical Society* **2006**, *231*, 1.
[50] Puoci, F. *Drug Delivery* **2008**, *15*, 253.
[51] Schillemans, J. P.; van Nostrum, C. F. *Nanomedicine* **2006**, *1*, 437.

[52] Jenkins, A. L.; Uy, O. M.; Murray, G. M. *Analytical Chemistry* **1999**, *71*, 373.
[53] Percival, C. J. *Analyst* **2002**, *127*, 1024.
[54] Dickert, F. L. *Analytical and Bioanalytical Chemistry* **2004**, *378*, 1929.
[55] Matsui, J. *Analytical Chemistry* **2005**, *77*, 4282.
[56] Rao, T. P. *Critical Reviews in Analytical Chemistry* **2007**, *37*, 191.
[57] Dickert, F. L. *Biosensors & Bioelectronics* **2004**, *20*, 1040.
[58] Tan, C. J.; Tong, Y. W. *Analytical and Bioanalytical Chemistry* **2007**, *389*, 369.
[59] Sellergren, B. *Journal of Chromatography A* **1994**, *673*, 133.
[60] Sambe, H. *Journal of Chromatography A* **2006**, *1134*, 88.
[61] Sulitzky, C. *Macromolecules* **2002**, *35*, 3314.
[62] Haginaka, J. *Journal of Chromatography A* **1999**, *849*, 331.
[63] Turiel, E.; Martin-Esteban, A. *Anal. Bioanal. Chem.* **2004**, *378*, 1876.
[64] Langone, J. J.; Franke, J.; Van Vanakis, H. *Arch. Biochem. Biophys.* **1974**, *164*, 536.
[65] Legros, J. J. *Ann. N. Y. Acad. Sci.* **1975**, *248*, 281.
[66] Robinson, A. G. *Ann. N. Y. Acad. Sci.* **1975**, *248*, 246.
[67] Bush, L. P. *J. Chromatogr.* **1972**, *73*, 243.
[68] Cano, J. P. *Ann. Pharm. Fr.* **1970**, *28*, 581.
[69] Jacin, H.; Slanski, J. M.; Moshy, R. J. *Anal. Chim. Acta* **1968**, *41*, 347.
[70] Blache, D. *Anal. Biochem.* **1984**, *143*, 316.
[71] Pendergrass, S. M.; Krake, A. M.; Jaycox, L. B. *AIHAJ*, **2000**, *61*, 469.
[72] Matsui, J.; Kaneko, A.; Miyoshi, Y.; Yokoyama, K.; Tamiya, E.; Takeuchi, T. *Analytical Letters* **1996**, *29*, 2071.
[73] Andersson H. S.; Koch Schmidt, A.C.; Ohlson, S.; Mosbach, K. *Journal of Molecular Recognition*, **1996**, *9*, 675.Matsui, J.; Takeuchi, T. *Analytical Communications* **1997**, *34*, 199.
[74] Zander, A.; Findlay, P.; Renner, T.; Sellergren, B.; Swietlow, A. *Analytical Chemistry* **1998**, *70*, 3304.
[75] Tan, Y. G.; Yin, J.; Liang, C. D.; Peng, H.; Nie, L. H.; Yao, S. Z. *Bioelectrochemistry* **2001**, *53*, 141.
[76] Liu, Y.; Liu, X. L.; Wang, J. D. *Analytical Letters* **2003**, *36*, 1631.
[77] Liu, Y.; Liu, X. L.; Wang, J. D. *Chinese Journal of Analytical Chemistry* **2003**, *31*, 1202.

[78] Svenson, J.; Karlsson, J. G.; Nicholls, I. A. *Journal of Chromatography A* **2004**, *1024*, 39.
[79] Sambe, H.; Hoshina, K.; Moaddel, R.; Wainer, I. W.; Haginaka, J. *Journal of Chromatography A* **2006**, *1134*, 88.
[80] Yang, J.; Hu, Y.; Cai, J. B.; Zhu, X. L.; Su, Q. D.; Hu, Y. Q.; Liang, F. X. *Food and Chemical Toxicology* **2007**, *45*, 896.
[81] Wu, C. T.; Chen, P. Y.; Chen, J. G.; Suryanarayanan, V.; Ho, K. C. *Analytica Chimica Acta* **2009**, *663*, 119.
[82] Langmuir, I. *Journal of the American Chemical Society* **1918**, *40*, 1361.
[83] Spivak, D. A. *Advanced Drug Delivery Reviews* **2005**, *57*, 1779.
[84] Umpleby, R. J.; Bode, M.; Shimizu, K. D. *Analyst* **2000**, *125*, 1261.
[85] Freundlich, H. *Colloid and capillary chemistry* **1926**, London.
[86] Cosnier, S.; Perrot, H.; Wessel, R. *Electroanalysis* **2001**, *13*, 971.
[87] In'acio, P.; Marat-Mendes, J. N.; Dias, C. J. *Ferroelectrics* **2003**, *293*, 351.
[88] Lucklum, R.; Hauptmann, P. *Analytical and Bioanalytical Chemistry* **2006**, *384*, 667.
[89] Troje, Z. S.; Frobe, Z.; Perovic, D. *Journal of Chromatography A* **1997**, *775*, 101.
[90] Sauerbrey, G. *Zeitschrift für Physik A Hadrons and Nuclei* **1959**, *155*, 206.
[91] Zammatteo, N.; Jeanmart, L.; Hamels, S.; Courtois, S.; Louette, P.; Hevesi, L.; Remacle, J. *Anal. Biochem.* **2000**, *280*, 143.
[92] Taylor, S.; Smith, S.; Windle, B.; Guiseppi-Elie, A. *Nucleic Acids Res.* **2003**, *31*, 87.
[93] Jin, L.; Horgan, A.; Levicky, R. *Langmuir* **2003**, *19*, 6968.
[94] Shen, G.; Francis, M.; Anand, G.; Levicky, R. *Nucleic Acids Res.* **2004**, *32*, 5973.
[95] Conzone, S. D.; Pantano, C. G. *Materials Today* **2004**, 20.
[96] Luderer, F.; Walschus, U. *Top. Curr. Chem.* **2005**, *260*, 37.
[97] Fedurco, M.; Romieu, A.; Williams, S.; Lawrence, I.; Turcatti, G. *Nucleic Acids Res.* **2006**, *34*, 22.
[98] Grainger, D. W.; Greef, C. H.; Gong, P.; Lochhead, M. J. *Methods Mol. Biol.* **2007**, *381*, 37.
[99] Strother, T.; Cai, W.; Zhao, X.; Hamers, R.; Smith, L. M. *J. Am. Chem. Soc.* **2000**, *122*, 1205.
[100] Cavic, B. A.; McGovern, M. E.; Nisman, R.; Thompson, M. *Analyst* **2001**, *126*, 485.

[101] Voicu, R.; Boukherroub, R.; Bartzoka, V.; Ward, T.; Wojtyk, J. T. C.; Wayner, D. D. M. *Langmuir* **2004**, *20*, 11713.
[102] Boecking, T.; Kilian, K. A.; Gaus, K.; Gooding, J. J. *Langmuir* **2006**, *22*, 3494.
[103] Peterson, A. W.; Heaton, R. J.; Georgiadis, R. M. *Nucleic Acids Res.* **2001**, *24*, 5163.
[104] Petrovykh, D. Y.; Kimura-Suda, H.; Whitman, L. J.; Tarlov, M. J. *J. Am. Chem. Soc.* **2003**, *125*, 5219.
[105] Johnson, P. A.; Levicky, R. *Langmuir* **2003**, *19*, 10288.
[106] Petrovykh, D. Y.; Kimura-Suda, H.; Tarlov, M. J.; Whitman, L. J. *Langmuir* **2004**, *20*, 429.
[107] Johnson, P. A.; Levicky, R. *Langmuir* **2004**, *20*, 9621.
[108] Johnson, P. A.; Gaspar, J. M.; Levicky, R. *J. Am. Chem. Soc.* **2004**, *126*, 9910.
[109] Wolf, L. K.; Gao, Y.; Georgiadis, R. M. *Langmuir* **2004**, *20*, 3357.
[110] Sakata, T.; Maruyama, S.; Ueda, A.; Otsuka, H.; Miyahara, Y. *Langmuir* **2007**, *23*, 2269.
[111] Benters, R.; Niemeyer, C. M.; Drutschmann, D.; Blohm, D.; Wohrle, D. *Nucleic Acids Res.* **2002**, *30*, 10.
[112] Miyachi, H.; Ikebukuro, K.; Yano, K.; Aburatani, H.; Karube, I. *Biosens. Bioelectron.* **2004**, *20*, 184.
[113] Sun, H.; Wirsen, A.; Albertsson, A. C. *Biomacromolecules* **2004**, *5*, 2275.
[114] Ivanova, E. P.; Phama, D. K.; Brack, N.; Pigram, P.; Nicolau, D. V. *Biosens. Bioelectron.* **2004**, *19*, 1363.
[115] Senaratne, W.; Andruzzi, L.; Ober, C. K. *Biomacromolecules* **2005**, *6*, 2427.
[116] Tugulu, S.; Arnold, A.; Sielaff, I.; Johnsson, K.; Klok, H.-A. *Biomacromolecules* **2005**, *6*, 1602.
[117] Ameringer, T.; Hinz, M.; Mourran, C.; Seliger, H.; Groll, J.; Moeller, M. *Biomacromolecules* **2005**, *6*, 1819.
[118] Feng, C. L.; Zhang, Z.; Forch, R.; Knoll, W.; Vancso, G. J.; Schonherr, H. S. *Biomacromolecules* **2005**, *6*, 3243.
[119] Kumar, N.; Hahm, J.-I. *Langmuir* **2005**, *21*, 6652.
[120] Zhao, X.; Zhang, Z.; Pan, F.; Ma, Y.; Armes, S. P.; Lewis, A. L.; Lu, J. R. *Surf. Interface Anal.* **2006**, *38*, 548.
[121] Dai, J.; Bao, Z.; Sun, L.; Hong, S. U.; Baker, G. L.; Bruening, M. L. *Langmuir* **2006**, *22*, 4274.
[122] Pu, Q.; Oyesanya, O.; Thompson, B.; Liu, S.; Alvarez, J. C. *Langmuir* **2007**, *23*, 1577.

[123] Chen, L.; Rengifo, H. R.; Grigoras, C.; Li, X.; Li, Z.; Ju, J.; Koberstein, J. T. *Biomacromolecules* **2008**, *9*, 2345.
[124] Bao, Z.; Bruening, M. L.; Baker, G. L. *Macromolecules* **2006**, *39*, 5251.
[125] Zhang, Z.; Chen, Q.; Knoll, W.; Foerch, R.; Holcomb, R.; Roitman, D. *Macromolecules* **2003**, *36*, 7689.
[126] De Paul, S. M.; Falconnet, D.; Pasche, S.; Textor, M.; Abel, A. P.; Kauffmann, E.; Liedtke, R.; Ehrat, M. *Anal. Chem.* **2005**, *77*, 5831.
[127] Chan, T. R.; Hilgraf, R.; Sharpless, K. B.; Fokin, V. V. *Org. Lett.* **2004**, *6*, 2853.
[128] Seo, T. S.; Bai, X.; Ruparel, H.; Li, Z.; Turro, N. J.; Ju, J. *Proc. Natl. Acad. Sci. U.S.A.* **2004**, *101*, 5488.
[129] Seo, T. S.; Bai, X.; Kim, D. H.; Meng, Q.; Shi, S.; Ruparel, H.; Li, Z.; Turro, N. J.; Ju, J. *Proc. Natl. Acad. Sci. U.S.A.* **2005**, *102*, 5926.
[130] Devaraj, N. K.; Miller, G. P.; Ebina, W.; Kakaradov, B.; Collman, J. P.; Kool, E. T.; Chidsey, C. E. D. *J. Am. Chem. Soc.* **2005**, *127*, 8600.
[131] Chan, T. R.; Hilgraf, R.; Sharpless, K. B.; Fokin, V. V. *Org. Lett*. **2004**, *6*, 2853.

Summary

In **Chapter 1**, a general introduction to the field of conjugated polymers is given. Conjugated polymers are unique materials, which combine the electronic and optical properties of semiconductors with the mechanical properties and processability of conventional polymers. Generally, organic and polymeric materials have the advantage of being lightweight, flexible, low-cost and straightforward to process. Nowadays, as a result of the wide variety in available synthetic methods, it is possible to customize the properties of many conjugated polymers for a particular function. In addition, the science of conjugated polymers continues to be of considerable interest for fundamental studies in physics and chemistry. Through the better understanding of structure-property relationships, increasingly sophisticated structures of conjugated polymers can be designed and assembled. Within the broad range of available conjugated polymers, poly(*para*-phenylene vinylene) (PPV) and its derivatives are widely used in a variety of different applications. The focus on this work is on this versatile class of conjugated polymers.

The aim of the research presented in this work is the synthesis and characterization of novel PPV derivatives, which have been prepared *via* the sulfinyl precursor route. Conjugated Polymers made *via* the sulfinyl precursor route have enhanced properties as compared to polymers made *via* other available synthetic routes. For the actual tailoring process of conjugated polymers a wide variety of methods can be found in literature. Hitherto, a significant drawback is the lack of a universal approach, leading to a wide variety of methods and functionalization procedures to obtain specific functional materials. To avoid this drawback, the aim of this work is to develop a universal platform and methodology, which allow for a wide variety of further functionalizations in a uniform manner. A first major objective to achieve is the formation of a PPV derivative with a functional group. From this platform polymer, post-polymerization functionalization of the functional side chain of the PPV needs to be possible *via* a

straightforward, optimized and efficient procedure to obtain the desired final functionalities. It can be anticipated that the resulting novel functionalized PPV derivatives are especially suitable for use in the active layer of photovoltaic devices. Functionalization might lead to stabilization of the morphology and thus a better performance of these devices. Other possible applications are the use in advanced polymer based devices such as (bio)sensors, by functionalizing the PPV derivatives with biological species to enable sensing.

Chapter 2 describes the synthesis of a new copolymer, which can be used as a platform for further post-polymerization functionalization. This copolymer is prepared from the MDMO sulfinyl premonomer as well as an ester sulfinyl premonomer in a ratio of 9/1. After hydrolysis of the ester groups, the side chains of the actual platform copolymer consist of 10 % carboxylic acid functionalities. This platform copolymer has been fully characterized using different analytical techniques. Post-polymerization functionalization of the carboxylic acid group of the platform is done *via* an optimized DCC/DMAP-procedure with the desired alcohol. This procedure is first tested and optimized for model compounds, after which it is utilized to functionalize the platform copolymer. In this way, post-functionalization has been done with a variety of functional groups. PPV-copolymers are prepared with vinyl groups, propenylphenyl groups, propynylphenyl groups, methacrylate groups, atom transfer radical polymerization (ATRP) initiator groups, benzyl dithiocarbamate initiator groups and propargyl groups. The latter group can be utilized to do "click" chemistry, which is demonstrated with an azide-functionalized reagent, *i.e.* azidomethyl phenyl sulfide. In all cases, FT-IR and ^{1}H-NMR are consistent with a quantitative conversion of the functional groups. Furthermore, spectroscopic data and SEC measurements indicate that no substantial degradation of the conjugated system occurs even after consecutive post-polymerization functionalization reactions. This demonstrates the versatility of the developed functionalization methodology.

In **Chapter 3**, the influence of 'modified' MDMO-PPV, with 10 % of different functional groups, is investigated in bulk heterojunction photovoltaic devices. These different functional groups are vinyl groups,

propenylphenyl groups, propynylphenyl groups, acrylate groups and finally propargyl groups. An improvement of the nanoscale morphology of the active layer in bulk heterojunction devices, as compared to devices based on MDMO-PPV, has been found for the devices containing copolymers with vinyl, propenylphenyl and propargyl groups comparing with MDMO-PPV. This results in a better performance of the solar cells, made using the copolymer with propargyl groups, as compared to those made with MDMO-PPV. The thermal stability of the active layer of the copolymer with propargyl groups and MDMO-PPV is comparable. In contrast, thermal annealing of the active layers of the other 'modified' MDMO-PPV copolymers leads to a much faster crystallization of PCBM, which results in a decrease in thermal stability of the active layer. Noteworthy is also the formation of different PCBM crystals, depending on the incorporated functional groups. Finally, the influence of the 10 % 'built-in' functional groups on the T_g is almost negligible.

One of the largest limitations of organic photovoltaic devices is the insufficient absorption of the solar radiation by the active layer. This mismatch with the AM 1.5 solar spectrum limits the efficiency of these kind of devices. Since phthalocyanines (Pc's) absorb strongly in the area where the photon flux of the AM 1.5 solar spectrum is at its maximum, the introduction of these kind of molecules in PPV derivatives can lead to an increased absorption of energy from the sunlight. This has been investigated in **Chapter 4**. To accomplish a covalent connection between Pc's and PPV derivatives, the optimized DCC/DMAP-esterification method as well as "click" chemistry have successfully been used. In addition, the spectroscopic data and SEC analysis indicate that no substantial degradation of the conjugated system occurs. These new materials have been tested in bulk heterojunction devices. In the spectral response curve of the new solar cells, the contribution of the attached Pc's is clearly visible. In this way, the new materials match better with the AM 1.5 solar spectrum as compared to the starting PPV derivatives. However, the built-in of Pc's has a negative influence on the performance of these solar cells, as a result of the poor morphology of the active layers.

Chapter 5 demonstrates the initiator capabilities of the introduced ATRP and benzyl dithiocarbamate initiator groups in a model compound and a functional PPV derivative. In this way, a (polymeric) surface can be modified with polymeric materials of specific chemistry and well-defined architecture, which can lead to interesting new characteristics. The initiator capacity of introduced ATRP initiator group is tested with vinyl monomers isobornyl acrylate and styrene. Although a polymerization is readily initiated, both polymerization reactions cannot be fully controlled. Furthermore, it is found that an ATRP reaction, in the presence of a PPV derivative, results in a shorter average conjugation length, *i.e.* degradation of the conjugated system. This implies that the ATRP reaction times in the presence of a PPV derivative should be kept short. The initiator capacity of the introduced benzyl dithiocarbamate initiator group is tested with the vinyl monomers methyl methacrylate (MMA), methyl acrylate (MA), methacrylic acid (MAA) and styrene. Using a model compound, it has been demonstrated that the corresponding polymers (PMMA, PMA, PMAA and PS) are readily formed, although a large distribution in the molecular weight is observed. Subsequently, the benzyl dithiocarbamate initiator groups of the PPV-type copolymer have been tested with the same four vinyl monomers in solution. Polymerization readily succeeds for MMA, MAA and styrene. However, the results for MA are inconclusive. In addition, not all available initiator groups start polymerization reactions and (an) unwanted side-reaction(s) is/are observed probably due to the presence of the conjugated system. Finally, surface initiation has been tested by spin-coating a thin layer of the PPV derivative with the benzyl dithiocarbamate initiator groups on a surface. It is demonstrated that the surface polymerization of MMA, MA, MAA and styrene is successfully initiated, indicating that for the four different vinyl monomers, grafting of a PPV surface is readily possible.

Chapter 6 focuses on the use of PPV derivatives as the transducer layer in (bio)sensors. To this end, first molecularly imprinted polymers (MIPs) for L-nicotine have been prepared, which can be utilized as synthetic receptors. Characterization shows the presence of specific recognition sites for L-nicotine and insensitivity of these MIPs towards L-cotinine. The actual sensing of L-nicotine has been investigated *via* impedance and quartz crystal microbalance (QCM) measurements. To this end, the MIPs have been

immobilized into the transducer layer, MDMO-PPV using matrix entrapment. However, using this method, only 30 % of the surface has been covered. Notwithstanding, impedimetric sensing is able to detect concentrations as low as 10 nM of L-nicotine with a response increase of 45 % at a frequency of 213 Hz. This concentration is even below the relevant medical concentrations. The reference measurement with L-cotinine indicates a high specificity. Similar results and conclusions can be obtained for QCM sensing. It should be remarked that both sensors can be regenerated by flushing with distilled water. It is anticipated that in the future, an improvement of the sensor performance of the MIP immobilization, and thus an improvement of the sensor performance can be achieved by growing the MIPs directly at the PPV covered electrode surface. Finally, it should be noted that other possible receptors for the use in biosensors are natural receptors like single-stranded DNA (ssDNA). This probe ssDNA can specifically recognize corresponding target ssDNA. Preliminary tests have been performed towards the covalent linking of azido functionalized ssDNA with PPV derivatives *via* "click" chemistry. To this end, it has been demonstrated that it is possible to use "click" conditions to attach an azide modified Cy^{TM} 5.5 dye to a PPV derivative. The transfer of these "click" conditions towards azido functionalized ssDNA, bearing Cy^{TM} 5.5, will ultimately lead to PPV-based sensors with ssDNA receptors.

Samenvatting

In **Hoofdstuk 1** wordt een algemene inleiding gegeven over geconjugeerde polymeren. Dit zijn unieke materialen, die de elektronische en optische eigenschappen van halfgeleiders combineren met de mechanische eigenschappen en verwerkbaarheid van gewone polymeren. Organische materialen en polymeren hebben het voordeel dat ze licht, flexibel, goedkoop en eenvoudig te verwerken zijn. Door de grote verscheidenheid aan synthesewegen is het mogelijk om de eigenschappen van geconjugeerde polymeren aan te passen aan een welbepaalde functie. Geconjugeerde polymeren zijn van groot belang voor de fundamentele studies in de natuur- en scheikunde. Door het beter begrijpen van structuur-eigenschap relaties kunnen steeds geavanceerdere structuren op basis van geconjugeerde polymeren verkregen worden. Binnen het brede gamma aan beschikbare geconjugeerde polymeren worden poly(*para*-fenyleen vinyleen) (PPV)-type polymeren reeds lang gebruikt in verschillende toepassingen. De focus van dit werk ligt dan ook op deze veelzijdige klasse binnen de geconjugeerde polymeren.

Het doel van dit onderzoek is de synthese en karakterisering van verschillende nieuwe PPV-type polymeren. Deze polymeren worden gesynthetiseerd via de sulfinyl precursor route. Geconjugeerde polymeren die bereid zijn door middel van deze route, hebben betere eigenschappen dan polymeren gesynthetiseerd middels andere beschikbare routes. Voor de eigenlijke functionalisatie van geconjugeerde polymeren zijn verscheidene methodes beschikbaar in de literatuur. Het ontbreken van een universele functionalisatie methode is een belangrijk nadeel voor het produceren van gefunctionaliseerde materialen. Om dit te verhelpen is de ontwikkeling van een universeel platform polymeer en een universele postpolymerisatie functionalisatie methode van groot belang voor het verder functionaliseren van polymeren op een eenduidige en uniforme manier. Een eerste belangrijke doelstelling is de synthese van een PPV-type materiaal met functionele groepen. Vanaf dit platform polymeer moet verdere

postpolymerisatie functionalisatie mogelijk worden via een eenvoudige, geoptimaliseerde en efficiënte procedure. Postpolymerisatie functionalisatie van PPV-type polymeren met vrijwel elke functionele groep moet mogelijk zijn, wat kan leiden tot de ontwikkeling van nieuwe toepassingen. Deze nieuwe gefunctionaliseerde PPV-type materialen kunnen bij uitstek gebruikt worden in de actieve laag van organische zonnecellen. Functionalisatie kan leiden tot een stabilisatie van de morfologie en dus een betere efficiëntie van dergelijke zonnecellen. Andere mogelijke toepassingen zijn het gebruik van deze materialen in (bio)sensoren d.m.v. postpolymerisatie functionalisatie van PPV-type polymeren met biologische componenten.

Hoofdstuk 2 beschrijft de synthese van een nieuw copolymeer, dat kan gebruikt worden als platform voor verdere postpolymerisatie functionalisatie. Dit copolymeer is gesynthetiseerd via de sulfinyl precursor route met als premonomeren het MDMO sulfinyl premonomeer en een ester gefunctionaliseerd sulfinyl premonomer in een verhouding van 9 staat tot 1. Na hydrolyse van deze ester groep, bestaan de zijketens van het werkelijke platform copolymeer uit 10 % carbonzuur groepen. Dit platform copolymeer is volledig gekarakteriseerd met behulp van verscheidene analytische technieken. Postpolymerisatie functionalisatie van de carbonzuur groep op het platform wordt uitgevoerd door middel van een DCC/DMAP procedure met het gewenste alcohol. Deze procedure is eerst getest en geoptimaliseerd voor modelverbindingen, waarna het wordt gebruikt voor de postpolymerisatie functionalisatie van het platform copolymeer. PPV-type copolymeren worden op deze manier gesynthetiseerd met dubbele bindingen, dubbele bindingen met een fenylring, drievoudige bindingen met een fenylring, methacrylaat groepen, ATRP initiator groepen, benzyl dithiocarbamaat initiator groepen en drievoudige bindingen. Deze laatste kunnen gebruikt worden voor “click” chemie. Dit is aangetoond met een azide gefunctionaliseerd reagens, azidomethyl fenyl sulfide. Voor alle functionalisaties zijn FT-IR en ^{1}H NMR-spectroscopie in overeenstemming met een kwantitatieve omzetting van de functionele groepen. Bovendien blijkt uit spectroscopische en GPC metingen dat er geen wezenlijke degradatie van het geconjugeerde systeem gebeurt, zelfs na opeenvolgende postpolymerisatie functionalisatie reacties. Dit toont de veelzijdigheid van de ontwikkelde postpolymerisatie functionalisatie methode aan, wat een

ontwikkeling van vele nieuwe toepassingen mogelijk maakt. Dit wordt verder aangetoond in de volgende hoofdstukken.

In **Hoofdstuk 3** wordt de invloed van 'gemodificeerd' MDMO-PPV, met 10 % aan verschillende functionele groepen, onderzocht in organische bulk heterojunctie zonnecellen. Deze verschillende functionele groepen zijn dubbele bindingen, dubbele bindingen met een fenylring, drievoudige bindingen met een fenylring, methacrylaat groepen en tenslotte drievoudige bindingen. Een verbetering van de nano morfologie van de actieve laag in bulk heterojunctie zonnecellen is gevonden bij copolymeren met dubbele bindingen, dubbele bindingen met een fenylring en drievoudige bindingen. Dit resulteert alleen in een betere efficiëntie van de zonnecel gemaakt met behulp van het copolymeer met drievoudige bindingen ten opzichte van het referentie materiaal MDMO-PPV. De thermische stabiliteit van de actieve laag van het copolymeer met drievoudige bindingen is vergelijkbaar met die van MDMO-PPV. Thermische behandeling van de actieve lagen van de andere 'gemodificeerde' MDMO-PPV copolymeren leidt tot een veel snellere kristallisatie van PCBM en dus een verminderde thermische stabiliteit van de morfologie. Opmerkelijk zijn ook de verschillende vormen van ontstane PCBM kristallen, die afhankelijk zijn van de ingebouwde functionele groepen in MDMO-PPV. De invloed van 10 % ingebouwde functionele groepen in MDMO-PPV op de T_g van deze copolymeren is nagenoeg verwaarloosbaar.

Een van de grootste beperkingen van organische zonnecellen is de onvoldoende absorptie van zonnestraling door de actieve laag. Omdat ftalocyanines sterk absorberen in het gebied waar de foton flux van het AM 1.5 zonnespectrum op zijn maximum is, kan de incorporatie van dit soort moleculen in PPV-type polymeren potentieel leiden tot een verhoogde absorptie van energie uit het zonlicht. Dit is onderzocht in **Hoofdstuk 4**. Om een covalente binding tussen ftalocyanines en PPV-type polymeren te bewerkstelligen wordt gebruikt gemaakt van de geoptimaliseerde DCC/DMAP procedure, evenals van "click" chemie. Beide postpolymerisatie functionalisatie methodes geven goede resultaten en uit de spectroscopische en GPC gegevens blijkt dat er geen wezenlijke degradatie van het geconjugeerde systeem plaatsvindt. Deze nieuwe

materialen zijn getest in organische bulk heterojunctie zonnecellen. In de spectrale respons van deze zonnecellen is er een duidelijke bijdrage van ftalocyanines zichtbaar. Op deze manier overlappen de nieuwe materialen beter met het AM 1.5 zonnespectrum dan de oorspronkelijke PPV-type copolymeren. De ingebouwde ftalocyanines hebben echter een negatieve invloed op de efficiëntie van deze zonnecellen. De belangrijkste reden hiervoor is de slechtere morfologie van de actieve lagen.

In **Hoofdstuk 5** wordt de initiator capaciteit van de geïntroduceerde ATRP en benzyl dithiocarbamaat initiator groepen beschreven. Op deze manier kan een (polymeer) oppervlak gemodificeerd worden met verscheidene polymeren, wat kan leiden tot nieuwe interessante eigenschappen van de materialen. Als eerste is de ATRP groep op de modelverbinding getest met de vinylmonomeren isobornyl acrylaat en styreen. Om diverse redenen kunnen deze polymerisaties niet goed worden gecontroleerd. Bovendien reageren de ontstane radicalen waarschijnlijk ook met het geconjugeerde systeem van PPV-type polymeren, wat resulteert in een degradatie van het geconjugeerde systeem. Daarom zal de ATRP reactietijd kort moeten gehouden worden in aanwezigheid van PPV-type polymeren. Vervolgens is de benzyl dithiocarbamaat initiator groep getest met de vinylmonomeren methyl methacrylaat (MMA), methyl acrylaat (MA), methacrylzuur (MAA) en styreen. Gebruik makende van een model verbinding is aangetoond dat er inderdaad polymeren gevormd kunnen worden, hoewel deze polymeren wel een brede moleculegewichtsverdeling hebben. Vervolgens is deze groep op PPV-type polymeren getest. Polymerisatie op deze manier geeft positieve resultaten voor MMA, MAA en styreen in oplossing. Voor MA zijn deze resultaten niet eenduidig. Het blijkt dat er niet vanuit alle beschikbare initiator groepen op de PPV-type polymeren polymerisaties starten en (een) ongewenste nevenreactie(s) word(t)(en) waargenomen. Deze zijn waarschijnlijk te wijten aan de aanwezigheid van het geconjugeerde systeem. Initiatie door de benzyl dithiocarbamaat initiator groep in een dunne PPV film op een oppervlak geeft voor alle vinylmonomeren wel positieve resultaten. Hieruit kan besloten worden dat een polymerisatie starten vanaf een PPV oppervlak mogelijk is voor MMA, MA, MAA en styreen.

Hoofdstuk 6 beschrijft de synthese van moleculair geïmprinte polymeren (MIP's) voor L-nicotine. Deze kunstmatige receptoren zijn gekarakteriseerd met behulp van UV-Vis absorptie spectroscopie. De bindingseigenschappen zijn onderzocht aan de hand van het Freundlich model, wat de aanwezigheid van specifieke herkenningsplaatsen voor L-nicotine bevestigt en een ongevoeligheid van deze MIPs voor L-cotinine aanduidt. De herkenning van L-nicotine is onderzocht via impedantie en kwartsmicrobalans metingen. Hiervoor is een goede verankering van MIPs nodig op de transducer laag, MDMO-PPV. Tot nu toe kan slechts 30 % van het oppervlak worden bedekt met MIPs, wat moet worden verbeterd in de toekomst. Impedantie is tot nu toe in staat om 10 nM L-nicotine te detecteren met een respons van 45 % bij een frequentie van 213 Hz, hetgeen lager is dan relevante medische concentraties. De referentie meting met L-cotinine wijst op een hoge specificiteit van deze MIPs voor L-nicotine. Dezelfde resultaten en conclusies kunnen worden verkregen uit kwartsmicrobalans metingen. Deze metingen tonen een specifieke detectie van L-nicotine aan met een detectielimiet van 50 μM. Ook hier reageert de MIP niet significant op de toevoeging van L-cotinine. Er moet worden opgemerkt dat beide sensoren kunnen geregenereerd worden door spoelen met gedestilleerd water. Een verbetering van de verankering van MIPs op MDMO-PPV zou kunnen worden bekomen door directe MIP groei op het PPV elektrode oppervlak. Tenslotte dient opgemerkt te worden dat typische andere mogelijke receptoren voor gebruik in biosensoren van natuurlijke oorsprong zijn zoals enkelstrengig DNA. Dit enkelstrengig DNA kan specifiek overeenkomstig enkelstrengig ‘doel’ DNA herkennen. Enkele voorbereidende tests zijn gedaan voor het covalent binden van azide gefunctionaliseerd enkelstrengig DNA met PPV-type polymeren via “click” chemie. Eerst en vooral zijn de “click” condities geoptimaliseerd voor de azide gefunctionaliseerde kleurstof Cy^{TM} 5.5. Deze “click” condities kunnen dan gebruikt worden voor de koppeling van azide gefunctionaliseerd enkelstrengig DNA, met Cy^{TM} 5.5, aan PPV-type polymeren.

Publications, conference contributions & awards

♦ Publications

- "Broadening the absorption window in polymer:fullerene solar cells: "Click" functionalization of conjugated polymers with phthalocyanines" Campo, B.; Duchateau, J.; Gilot, J.; Ballesteroz, B.; Oosterbaan, W.; Lutsen, L.; Cleij, T. J.; De la Torre, G.; Janssen, R. A. J.; Vanderzande, D.; Torres, T., in preparation.

- "Versatile post-polymerization functionalization of poly(*p*-phenylene vinylene) copolymers containing carboxylic acid substituents: the development of a universal method towards functional conjugated copolymers" Duchateau, J.; Lutsen, L.; Cleij, T. J.; Vanderzande, D. *Polymer Chemistry*, in preparation.

- "MIP-based sensor platforms for the detection of histamine in the nano- and micromolar range in aqueous media" Horemans, F.; Alenus, J.; Bongaers, E.; Weustenraed, A.; Thoelen, R.; Duchateau, J.; Lutsen, L.; Vanderzande, D.; Wagner, P.; Cleij, T. J. *Biosensors & Bioelectronics*, submitted.

- "A MIP-based impedimetric sensor for the detection of low-MW molecules" Thoelen, R.; Vansweevelt, R.; Duchateau, J.; Vanderzande, D.; Ameloot, M.; Cleij, T. J.; Wagner, P. *Biosensors & Bioelectronics* **2008**, *23*, 913.

♦ Oral conference contributions

- 13th International IUPAC Conference on Polymers and Organic Chemistry (POC '09), Montréal, Canada, 05-08/07/2009, "A universal method for the decoration of conjugated polymers with functional molecules" Duchateau, J.; Lutsen, L.; Cleij, T. J.; Vanderzande, D.

- Biomedica event 2007, Aachen, Germany, 21-22/03/2007, "An impedimetric sensor based on molecularly imprinted polymers for the detection of L-nicotine" Duchateau, J.; Thoelen, R.; Vansweevelt, R.; Horemans, F.; D'Haen, J.; Lutsen, L.; Cleij, T. J.; Vanderzande, D.; vandeVen, M.; Ameloot, M.; Wagner, P.

♦ Poster conference contributions

- BPG annual meeting, De Haan, Belgium, 22-23/05/2008, "Poly(*para*-phenylene vinylene) derivatives as a starting point for "pseudo" living radical polymerizations and "click" chemistry" Duchateau, J.; Dervaux, B.; Vanderzande, D.; Cleij, T. J.

- BPG annual meeting, Houffalize, Belgium, 24-25/05/2007, "An impedimetric sensor based on molecularly imprinted polymers for the detection of L-nicotine" Duchateau, J.; Thoelen, R.; Vansweevelt, R.; Horemans, F.; D'Haen, J.; Lutsen, L.; Cleij, T. J.; Vanderzande, D.; vandeVen, M.; Ameloot, M.; Wagner, P.

- Biomedica event 2007, Aachen, Germany, 21-22/03/2007, "An impedimetric sensor based on molecularly imprinted polymers for the detection of L-nicotine" Duchateau, J.; Thoelen, R.; Vansweevelt, R.; Horemans, F.; D'Haen, J.; Lutsen, L.; Cleij, T. J.; Vanderzande, D.; vandeVen, M.; Ameloot, M.; Wagner, P.

- 10th Bioforum, Bioliège, ULG, Luik, Belgium, 17/05/2006, "Impedance based sensing of low MW molecules using imprinted nanocavities" Thoelen, R.; Vansweevelt, R.; Duchateau, J.; Vanderzande, D.; Lutsen, L.; vandeVen, M.; Ameloot, M.; Wagner, P.; Cleij, T. J.

♦ Awards

- Best Presentation Award, Biomedica event 2007, Aachen, Germany, 21-22/03/2007,

"An impedimetric sensor based on molecularly imprinted polymers for the detection of L-nicotine" Duchateau, J.; Thoelen, R.; Vansweevelt, R.; Horemans, F.; D'Haen, J.; Lutsen, L.; Cleij, T. J.; Vanderzande, D.; vandeVen, M.; Ameloot, M.; Wagner, P.

- Young Scientist Poster Competition Award "Medical Devices", Biomedica event 2007, Aachen, Germany, 21-22/03/2007,

"An impedimetric sensor based on molecularly imprinted polymers for the detection of L-nicotine" Duchateau, J.; Thoelen, R.; Vansweevelt, R.; Horemans, F.; D'Haen, J.; Lutsen, L.; Cleij, T. J.; Vanderzande, D.; vandeVen, M.; Ameloot, M.; Wagner, P.

- BIO TECH Intl Award "From research to industrial application", 10th Bioforum, Bioliège, ULG, Luik, Belgium, 17/05/2006,

"Impedance based sensing of low MW molecules using imprinted nanocavities" Thoelen, R.; Vansweevelt, R.; Duchateau, J.; Vanderzande, D.; Lutsen, L.; vandeVen, M.; Ameloot, M.; Wagner, P.; Cleij, T. J.

Words of thanks - Dankwoord

Zoals bij de meeste belangrijke mijlpalen in iemands leven, was de uitvoering van mijn doctoraatsonderzoek en het schrijven van deze thesis onmogelijk geweest zonder de hulp en steun van velen in mijn omgeving. Een woord van dank is dus wel op zijn plaats. Maar ja, hoe begin je aan een dankwoord? Hoe kan je in een paar zinnen iedereen bedanken die zijn steentje, steen of zelfs rotsblok heeft bijgedragen tot het voltooien van deze thesis? Op deze vier jaar durende reis ben ik tal van mensen tegengekomen die, elk individueel een speciaal woordje van dank verdienen. Ik wil hier dan ook beginnen met het vragen om vergeving aan allen die ik nu niet bij naam noem. Velen hebben ooit wel eens gevraagd: "Hoe gaat het nu?" of "Vordert het een beetje?". En ook al was het niet altijd eenvoudig om uit te leggen hoe het nu werkelijk zat, deze blijk van interesse zorgde voor nieuwe moed om door te zetten en 'alles te geven'!

Laat ik beginnen met die personen te bedanken die meestal pas aan het eind vermeld worden, maar eigenlijk op de eerste plaats komen. Mama en papa, bedankt dat ik de kans kreeg om verder te studeren. Dit lijkt soms vanzelfsprekend, maar ik besef dat dit niet zo is. Zonder jullie nooit-aflatende steun, bezorgdheid en liefde zou ik dit nooit hebben kunnen verwezenlijken. Bedankt voor alles!

Mijn promotor, Prof. Thomas Cleij, wil ik graag bedanken voor de uitstekende wetenschappelijke begeleiding de voorbije jaren. Naast de waardevolle tips, vele discussies en vergaderingetjes met een colaatje wil ik je ook bedanken voor het zorgvuldig doornemen van artikels en presentaties, alsook het leesbaar maken van deze thesis in de Engelse taal. Problemen waren er nooit, alleen maar uitdagingen. Thomas, zonder jouw inbreng was deze thesis nooit hetzelfde geweest. Dank je wel! En ik zou zeggen op naar de vierde Cleij-telg.

Prof. Dirk Vanderzande, mijn copromotor, ben ik erkentelijk voor het aanbieden van de mogelijkheid om te doctoreren aan de Universiteit Hasselt. Het was trouwens mijn eerste sollicitatie zonder 'e pilleke'. Onder zijn toeziend oog en dankzij zijn wetenschappelijke kennis is deze thesis mede ontstaan. Hij beloofde een toffe werksfeer en dat kan ik alleen maar bevestigen.

Prof. Peter Adriaensens en Dr. Laurence Lutsen verdienen hier ook een eervolle vermelding voor het geven van hun deskundige 'raad en daad' tijdens vergaderingen en dergelijke.

Voor de financiële steun heb ik gedurende de voorbije vier jaar mogen rekenen op de Universiteit Hasselt, waarvoor ik natuurlijk zeer erkentelijk ben. De eurokes zijn altijd goed besteed geweest.

Dank ook aan alle juryleden om zich door deze thesis te worstelen, ondanks hun drukke bezighouden. Ik apprecieer dit heel erg!

Mijn IMO-fysica collega's mag ik uiteraard ook niet vergeten. Zonder jullie waren al deze zonnecellen en geavanceerde (bio-)sensoren er nooit gekomen. Bedankt Sabine, Ronald, Rob en Jan. Jaja Ronaldo, een jaar na jou sta ik hier nu ook. En we hebben nog steeds geen MIP spin-off. Maar onze prijzen en het vieren hebben we toch maar mooi gehad, met een waardig BPG congres als slot. Als ik raad nodig heb over fysische problemen dan weet ik jullie nog wel te vinden.

In de laatste maanden van mijn doctoraat was er een intense samenwerking met drie biochemische 'dudes'. Erik, Gunter en 'temptation' Tom hebben werkelijk alles gegeven om die verdomde DNA op mijn polymeertjes gezet te krijgen. Jammer genoeg is dit niet volledig gelukt, maar de aanzet is gegeven dus dat komt volledig in orde, daar ben ik zeker van. Als er nog iets is, jullie weten me te vinden. Hoewel ik me goed kan verstoppen. Die 'Nature' moet eraan komen. Alles 'cava' mannen? Tom, tevens sterspeler van 'Boorsemspor', is zelfs twee keer stagestudent geweest van mij. Ik weet niet over wie dat iets zegt, maar ik was verdomd blij dat ik op hem heb kunnen rekenen!

Daarnaast heb ik binnen de unief dikwijls mensen aan het werk gezet. Omdat ik daar niets vanaf wist en natuurlijk ook omdat ik mensen graag aan het werk zet. Christel, bedankt voor alle bestellingen. Koen en Raoul, bedankt voor het opnemen van de vele NMR's. Jan, bedankt voor het opnemen van alle massaspectra. Huguette, bedankt voor de FT-IR en UV-Vis metingen. Iris en Veerle, mercikes voor de vele GPC analyses.

Ik ben natuurlijk ook een paar keer vreemd gegaan, lees, buiten de universiteit gaan werken. Talloze mensen hebben mij telkens weer uitstekend opgevangen. Bart van de Universiteit Gent, bedankt om je ATRP kennis met mij te delen. Van jou heb ik geleerd hoe belangrijk het is om zo nauwkeurig te werken, er kan zoveel misgaan bij het maken van ATRP polymeren. Jan van de Technische Universiteit Eindhoven, zonder jou kennis waren de zonnecellen bijlange na niet zo goed. Ook aan allen die mij en Bert zo goed hebben opgevangen gedurende ons verblijf aan Universidad Autónoma de Madrid. En daarbij denk ik vooral aan Gema en Beatriz. Vanaf toen was het StuBru en geen ambetante Spaanse radio meer op het labo! Ftalocyanines zijn geweldige beestjes.

De voorbij vier jaar is er altijd een heel toffe en aangename werksfeer geweest bij ons in het labo organische. Ik ben blij dat ik daar deel van heb mogen uitmaken en ben jullie allen dan ook heel dankbaar. Eerst en vooral de 'oude' garde: Kristof (Forza Italia), Jerôme, Lien, Ine, Steven (ik wacht vol ongeduld op de volgende WK quiz), Zarina, Juliette, Jimmy, Fateme en Sofie. Bedankt om mij wegwijs te maken in het labo en ik hoop dat ik jullie voorbeeld kan volgen. De 'recentere' garde: Arne (mijn steun en toeverlaat), Joke (ons bomma die speelt bij de Racing, ...), Fré (MIP T1), Ans (MIP T2), Burak (you funny Belgian people, mmm she is nice, ...), Ayse and Suleyman (the turkish connection), Hanne (HH = housewarming Hanne, ik zal er zijn op jouw verjaardag ...), Sarah (15 mei zal niet snel vergeten worden, alles geven hé Sarah), Lidia, Sylvain (de wereldreiziger), Raoul (bedankt voor alle NMR's, mooie figuurtjes en gesprekken, nog even en jij bent ook aan de beurt) en Wouter (Vlemi, Ros, Julien, Nananana, you're malinwa, stu, protput, Linz, Arsenal, een 'Flogging Mollyke', kortom 'sjowzeg'). Aan de 'recentste' garde: Toon, Brecht (mijn stagestudent en ook wel 'de sikkel' genaamd) en Inge, veel plezier en mooie resultaten

toegewenst. De vrouwen en man die het labo draaiende houden, Iris, Veerle en Wibren. Iris en Veerle, ieder op hun toer want de natuur roept natuurlijk. Jullie stonden altijd klaar om te helpen en dat was een hele geruststelling. Wibren, je bent een kanjer. Ook Gène verdient een speciale vermelding. De man van het 'afronden' stond altijd klaar om te helpen en een praatje te slaan over de voetbal. De laatste in dit rijtje is de heer Campo Bert. Met zo een naam moet je wel naar Spanje en dat hebben we dan ook gedaan. Het was een hele belevenis die twee weken Madrid en ik had het voor geen geld van de wereld willen missen. Bocadillo lomo? Bocadillo tortilla? Bocadillo pepito? Of toch maar jamon of gevulde champignons? Zo vettig, ma zo lekker. De treinrit, bocadillo choco, Real en Atletico, … Ook de rest van de vier jaar hebben we ons goed geamuseerd. Op naar 11 december voor een duo presentatie.

Ook alle overige familie en vrienden wil ik even bedanken voor hun steun en interesse in hetgeen ik allemaal uitgespookt heb. En voor de nodige ontspanning. Oma, opa, ma, oom Co en oom Eddy, bedankt om er altijd te zijn. Hendrik, Dimitri, Tom Corneel en David. Bedankt om altijd met mij mee te gaan naar het voetbal, de concerten, … De voetbalwedstrijdjes en de praatjes aan de toog zullen mij ook altijd bijblijven. Jos (mijn persoonlijk grafisch ontwerper en tevens computerdeskundige, zie vooral de kaft van deze thesis en surf naar www.josv.be), Annie, Leentje, Dieter, Tiesje (ook wel genaamd 'Ties, het machien' en 'kakkertje' bij uitstek), Senna en Cleo, flik(t), flak en flix. Bedankt om mij altijd te steunen en mij een beetje te ontzien de laatste maanden. Als afsluiter van deze paragraaf wil ik gewoon effe heel hard roepen 'komaan KV', 'Peter Maes olé olé' en YNWA!

When you walk through a storm

Hold your head up high

And don't be afraid of the dark

At the end of the storm

There's a golden sky

And the sweet silver song of a lark

Walk on through the wind

Walk on through the rain

Tho' your dreams be tossed and blown

Walk on, walk on

With hope in your heart

And you'll never walk alone

You'll never walk alone

Tot slot rest er mij nog één iemand te bedanken en dan nog wel de belangrijkste persoon in mijn leven, mijn schatteke, mijn Anneke. Telkens ik naar je fotootje keek, kreeg ik weer extra kracht om er tegen aan te gaan, telkens weer zei je na een mislukt experiment "het komt wel goed", telkens weer vond ik bij jou de rust als het schrijven weer eens niet vlotte, telkens weer kon ik op veel begrip en steun van jou rekenen, telkens weer ... was je er voor mij! Woorden schieten mij hiervoor te kort! Bedankt om te zijn wie je bent! Er staat ons nog zoveel moois te wachten en ik ben zo blij dat ik dat allemaal samen met jou mag beleven! 12 juni 2008 was een wonderlijke dag in ons leven, op naar 15 mei 2009 en zoveel meer! Je bent alles voor mij, lieveke!

Ik ben blij dat jullie in mijn team zaten!

Dank aan allen en U in het bijzonder!!!!!